Assessment of fatigue strength of welded steel joints at sub-zero temperatures based on the micro-structural support effect hypothesis

Vom Promotionsausschuss der

Technischen Universität Hamburg

zur Erlangung des akademischen Grades

Doktor-Ingenieur (Dr.-Ing.)

genehmigte Dissertation

von

Moritz Braun

aus

Magdeburg

2021

Vorsitzender des Prüfungsausschusses

Prof. Dr.-Ing. Otto von Estorff

Gutachter

1. Gutachter: Prof. DSc. (Tech.) Sören Ehlers

2. Gutachter: Prof. Dr. Zuheir Barsoum

Tag der mündlichen Prüfung: 9. September 2021

DOI: 10.15480/882.3782

ORCID: 0000-0001-9266-1698

Acknowledgements

This thesis would never have been possible without many bright and loving people.

Sören, thank you for the many years of supervision, mentoring and guidance. I did not expect it to be such a great journey when you asked me to come to Hamburg with you back in early 2014.

I am tremendously grateful to Professor Wolfgang Fricke for the deep conversations and discussions about fatigue theory and the strong support while writing many of the papers that built the basis for this thesis.

I also would like to thank Professor Gunnar Härkegård for sparking my interest in fatigue and fracture mechanics and Professor Zuheir Barsoum for agreeing to act as the second examiner of my thesis.

To all my colleagues at TUHH and in Commission XIII of the International Institute of Welding, thank you for the endless number of funny situations, great conversations, and shared struggles of being a young researcher.

Many thanks to all my students for the many hours that we spent together performing experiments, discussing data and simply talking about everything under the sun.

To my parents, my sister and all friends, thank you for your loving support over all these years.

Esther, thank you for your love, your support and for being the driving force that helped me finish this thesis. You know best how it sometimes feels. I am incredibly lucky to have you by my side.

When a writer of fiction lays the scene of his story on Mars, he recognizes that differences in environment must be met by different materials. He not only describes the Martians themselves and the flora and fauna of the planet as oddly different from the living things we are accustomed to on Earth, but he also supplies the Martian engineer with materials of construction of an entirely different character, fitted to withstand new conditions.

— *H.W. Gillet et al.*, Symposium on Effect of Temperature on the Properties of Metals, ASTM International: West Conshohocken, PA,1932

I | Motivation and general scope

For years, merchant shipping has been increasing in Arctic regions, and there is an increasing number of offshore structures such as oil rigs and wind turbines being set up in areas with seasonal freezing temperatures. In recent years, fatigue of welded joints at sub-zero temperatures has been identified as a major knowledge gap for such structures. Although it is known that the material properties of steel and their welded joints change with decreasing temperatures, the effects on fatigue strength have, so far, rarely been researched. Consequently, the design curves and methods for room temperature are also applied to sub-zero temperatures.

In particular, stress–life data—which is the basis for fatigue design of ships and offshore structures—at sub-zero temperatures is scarce; available data for sub-zero temperature fatigue is based on fatigue crack growth rate tests. These tests showed that fatigue crack growth rates decreased above and increased below the fatigue ductile-brittle transition temperature. Despite this known fatigue transition behaviour, design standards for ships and offshore structures focus almost exclusively on Charpy and fracture toughness properties for material qualification and selection. Therefore, the overall goal of this thesis is to investigate the fatigue strength of welded joints in terms of stress–life curves and how to include temperature effects in fatigue assessment.

By fatigue testing different structural steels and weld details, a database for the fatigue strength of welded structural steels at sub-zero temperatures is created. For this purpose, welded structural steel joints are fatigue tested down to −50 °C. This database is complemented by performing other material tests typically used to qualify materials, which permits a comprehensive assessment of material behaviour of welded steel joints at sub-zero temperatures.

Typical fatigue assessment methods for welded joints are not capable of taking influencing factors such as temperature into account; however, in recent years methods that are based on the micro-structural support effect hypothesis have become much less cumbersome. These methods can relate the fatigue behaviour to general material properties such as strength and grain structure, and are thus expected to be able to take sub-zero temperature effects into account. In this thesis, novel fatigue design concepts—based on the micro-structural support effect hypothesis—for welded joints are extended to sub-zero temperatures.

To assess the relevance of the proposed methods to account for temperature effects within fatigue assessment, a comparison with state-of-the-art methods is performed. Moreover, guidance on the application of fatigue assessment methods for welded steel joints at temperatures below freezing is presented for the first time.

To achieve the overall goal, the following objectives are identified:

1. Determination of static and cyclic material behaviour at room temperature down to temperatures representative for Arctic regions minus a safety margin (i.e. −50 °C) of welded structural steel.

2. Statistical and numerical determination of the fatigue behaviour based on the experiments to create a benchmark for the extension of fatigue design methods to sub-zero temperatures.

3. Review and expansion of fatigue assessment methods—based on the micro-structural support effect hypothesis—for welded joints to sub-zero temperatures.

These objectives form the basis for the determination and evaluation of fatigue behaviour of welded structural steel joints at sub-zero temperatures. Hence, this thesis seeks to help to gain knowledge on the safety margins of weld details in ships and offshore structures operating in Arctic regions and on fatigue design of such structures by accounting for temperature effects within fatigue assessment.

II | List of publications with authors' contributions

This thesis is based on a number of publications published in peer-reviewed journals and conference proceedings. These publications are categoriezed as follows: review of the state of the art [P1], data acquisition and evaluation [P2–P4], application of state-of-the-art fatigue assessment methods to the obtained data [P5], and extension of fatigue assessment methods to cover temperature effects based on a sound physical basis [P6, P7]. Additional publications that fall out of the main scope but contributed to the thesis are [P8–P11].

List of peer-reviewed publications by the author related to this thesis:

[P1] Bock und Polach RUF von, Klein M, Kubiczek J, Kellner L, Braun M, Herrnring H (2019). State of the Art and Knowledge Gaps on Modelling Structures in Cold Regions. ASME 2019 38th International Conference on Ocean, Offshore and Arctic Engineering. Vol. 8: Polar and Arctic Sciences and Technology; Petroleum Technology. DOI: 10.1115/OMAE2019-95085

Each co-author wrote one section of the paper. Braun contributed with a section on fatigue at sub-zero temperatures.

[P2] Braun M, Scheffer R, Fricke W, Ehlers S (2020). Fatigue strength of fillet-welded joints at subzero temperatures. Fatigue & Fracture of Engineering Materials & Structures 43(2):403–416. DOI: 10.1111/ffe.13163

Braun performed the experiments and the assessment of the test results as well as the writing of the paper. Scheffer performed the laser scans of the welded specimens and the post-processing of the laser scans. Fricke and Ehlers contributed with valuable comments and guidance.

[P3] Braun M, Milaković AS, Ehlers S, Kahl A, Willems T, Seidel M, Fischer C (2020). Sub-Zero Temperature Fatigue Strength of Butt-Welded Normal and High-Strength Steel Joints for Ships and Offshore Structures in Arctic Regions. ASME 2020 39th International Conference on Ocean, Offshore and Arctic Engineering. Vol. Volume 3: Materials Technology. DOI: 10.1115/OMAE2020-18892

Braun performed the experiments, the assessment of the test results as well as the writing of the main part of the paper. Kahl, Seidel and Fischer assisted with writing sub-sections on ship classification rules, standards for design of Arctic offshore structures, and material selection for ships and offshore structures operating in Arctic regions. Milaković, Willems and Ehlers contributed with valuable comments and guidance.

[P4] Braun M, Kahl A, Willems T, Seidel M, Fischer C, Ehlers S (2021). Guidance for Material Selection Based on Static and Dynamic Mechanical Properties at Sub-Zero Temperatures. Journal of Offshore Mechanics and Arctic Engineering 143(4):1–45. DOI: 10.1115/1.4049252

This paper is an extension of paper [P3]. Braun performed additional material tests and the assessment of the test results as well as the writing of the paper. Kahl, Seidel and Fischer contributed in the same way as for [P3]. Willems and Ehlers contributed with valuable comments and guidance.

[P5] Braun M, Milaković AS, Renken F, Fricke W, Ehlers S (2020). Application of Local Approaches to the Assessment of Fatigue Test results obtained for Welded Joints at Sub-Zero Temperatures. International Journal of Fatigue 138 DOI: 10.1016/j.ijfatigue.2020.105672

Braun performed the fatigue assessment of the test results based on local approaches as well as the writing of the paper. Milaković helped building the finite element models. Renken assisted with the development of an improved tool for post-processing

of laser scans and performing a new post-processing of the weld scan data. Fricke and Ehlers contributed with valuable comments and guidance.

[P6] Braun M, Milaković AS, Ehlers S (2021). Fatigue Assessment of Welded Joints at Sub-Zero Temperatures by means of Stress Averaging Approach. Ships and Offshore Structures 16 DOI: 10.1080/17445302.2021.1906194

Braun developed the fatigue assessment tool for the stress averaging, did the analysis, and wrote the paper. Milaković helped building the FE models for the application of the stress averaging approach. Ehlers contributed with valuable comments and guidance.

[P7] Braun M, Fischer C, Fricke W, Ehlers S (2020). Extension of the strain energy density method for fatigue assessment of welded joints to sub-zero temperatures. Fatigue & Fracture of Engineering Materials & Structures 43(12):2867–2882. DOI: 10.1111/ffe.13308

Braun built the FE models for the application of the strain energy density method, did the analysis, and wrote the paper. Fischer assisted on the fatigue assessment and during the development of the FE models. Ehlers and Fricke contributed with valuable comments and guidance.

[P8] Braun M, Milaković AS, Andresen-Paulsen G, Fricke W, Ehlers S (2020). A novel approach to consider misalignment effects in assessment of fatigue tests. Ship Technology Research submitted for publication.

Braun wrote the paper and developed the theoretical model presented in this paper. Braun and Milaković developed the FE model that is applied for the misalignment assessment together. Andresen-Paulsen, Fricke and Ehlers contributed with valuable comments and guidance.

[P9] Braun M, Müller AM, Milaković AS, Fricke W, Ehlers S (2020). Requirements for stress gradient-based fatigue assessment of notched structures according to theory of critical distance. Fatigue & Fracture of Engineering Materials & Structures 43(7):1541–1554. DOI: 10.1111/ffe.13232

Braun developed the theoretical basis for the paper. Braun and Müller developed the models and wrote the paper together. Milaković assisted while building the FE

model, which was later adopted for [P6]. Fricke and Ehlers contributed with valuable comments and guidance.

[P10] Schubnell J, Jung M, Le CH, Farajian M, Braun M, Ehlers S, Fricke W, Garcia M, Nussbaumer A, Baumgartner J (2020). Influence of the optical measurement technique and evaluation approach on the determination of local weld geometry parameters for different weld types. Welding in the World 64(2):301–316. DOI: 10.1007/s40194-019-00830-0

Baumgartner, Braun, Garcia and Jung performed the optical measurements and post-processing of data for their measurement method. Schubnell and Jung wrote the paper. All co-authors contributed with comments or guidance.

[P11] A.-S. Milaković, M. Braun, T. Willems, H. Hendrikse, C. Fischer, S. Ehlers, Methodology for estimating offshore wind turbine fatigue life under combined loads of wind, waves and ice at sub-zero temperatures. International Conference on Ships and Offshore Structures ICSOS 2019, Cape Carnival, USA. (2019).

Milaković wrote the majority of the paper. Braun developed the theoretical idea and wrote the section related to the theoretical idea. Willems, Hendrikse, Fischer and Ehlers contributed with valuable comments and guidance.

III | Structure of the thesis

The thesis consists of three main parts that are listed in Figure 1 together with the corresponding papers. The first part reviews the current state of the art on fatigue, and the effect of temperature on fatigue and builds the foundation for both the experimental and the computational parts of the thesis. The experimental work—including the data acquisition and the evaluation—is summarized in Chapters 3, 4, and 5. Based on the first-of-its-kind database on different welded connections tested at room and sub-zero temperatures, two novel methods for including temperature effects in fatigue assessment of welded joints are derived in Section 6.3 and 6.4. These are compared to results obtained with state-of-the-art fatigue assessment methods in Section 6.6. Finally, the applicability of the two novel methods to assess fatigue at sub-zero temperatures and the experimental results are discussed; an outlook with possible directions for further research is given.

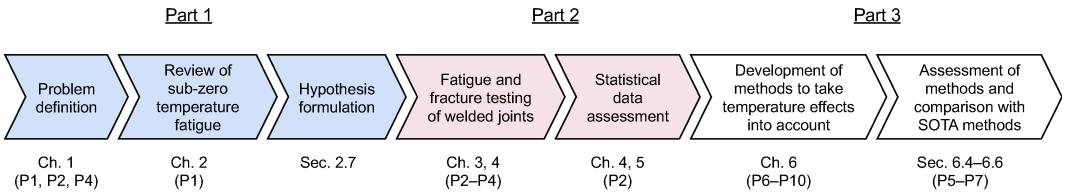

Figure 1. Structure of this thesis

IV | Original contributions

The contributions of this thesis and the corresponding peer-reviewed papers to the current state of the art which are believed to be original are listed below.

[C1] A database of fatigue test results for different types of welded joints, steel types, and welding techniques at room and sub-zero temperatures relevant for Arctic conditions [P2, P3, P4].

[C2] A systematic investigation of temperature effects on fatigue strength, and comparisons with empirical correction functions in current fatigue standards and recommendations and with temperature effects on other material properties [P2, P3, P4].

[C3] An investigation of temperature effects on fatigue strength of welded joints based on statistical methods.

[C4] A study on the limitation of state-of-the-art stress-based fatigue assessment methods for fatigue assessment of fillet-welded joints with weld toe and root failure, and on the deviation caused by sub-zero temperatures [P5].

[C5] Extension of the strain-energy density method for fatigue assessment of welded joints at sub-zero temperatures [P7].

[C6] Proof of the capability of the stress averaging and strain energy density methods to account for temperature-related changes of the micro-structural support effect based on a sound physical basis [P6, P7].

[C7] Derivation of temperature modification factors and functions for weld toe and weld root fatigue assessment for a wide range of fatigue assessment methods [P5, P7].

[C8] The first thorough assessment of differences in prediction of different effective stress methods based on the micro-structural support effect hypothesis in conjunction with a sensitivity study regarding mesh refinement, assumed strength hypothesis and material behaviour [P9].

[C9] A comparison of different measurement methods and systems for local weld geometry assessment based on optical systems [P10].

Notation

Abbreviations

bcc	Body-centred cubic
BS	British Standard
CDF	Cumulative distribution function
CV	Coefficient of variation
DBTT	Ductile–brittle transition temperature
DVS	German Welding Society (in German: *Deutscher Verband für Schweißen und verwandte Verfahren e. V.*)
EN	European Standard
FAT class	Fatigue design class (i.e. the reference fatigue strength at $\mathrm{N} = 2 \times 10^6$ cycles with $\mathrm{P_s} = 97.5\%$ survival probability)
FCAW	Flux-cored arc welding
fcc	Face-centred cubic
FCG	Fatigue crack growth
FDBT	Fatigue ductile–brittle transition
FE	Finite element
FTT	Fatigue transition temperature
HAZ	Heat-affected zone
IIW	International Institute of Welding
ISO	International Organization for Standardization
LAST	Lowest anticipated service temperature
N-SIF	Notch stress intensity factor
PCHIP	Piecewise cubic hermite interpolating polynomial

continued on next page

continued from previous page

PDF	Probability density function
RT	Room temperature
SD	Standard deviation
SE	Standard error
SED	Strain energy density
SIF	Stress intensity factor
S–N	Stress–life
TCD	Theory of Critical Distances
WM	Weld metal
WPS	Welding procedure specification
WR	Weld root
WT	Weld toe

Symbols

a, a_i	[mm]	Crack length and initial crack length at the fatigue limit
$a^{'}$	[mm]	El Haddad-Smith-Topper parameter
$a^{N'}$	[mm]	Characteristic length parameter of V-notched component
a_{th}	[mm]	Weld throat thickness
AD, AD^{*}		Test value and critical value of the Anderson-Darling test
b		Slope parameter of linear fit of correlated data
B, L, t, H	[mm]	Specimen's width, length, and thickness; and stiffener height
d_1, d_2	[mm]	Undercut depths
da/dN	[mm/cycle]	Crack growth rate
dev		Logarithmic deviation between the experimental and the predicted cycles to failure

continued on next page

continued from previous page

E	[GPa]	Young's modulus
e	[mm]	Axial misalignment
e_f	[%]	Elongation at fracture
e_1, e_2		SED stress-strain field correction factors
$f(R)$		Mean stress correction factor
H_w	[mm]	Weld height
k, $\overline{k}$		Slope exponent of the stress-life curve and mean slope exponent
K_C, K_{IC}	[MPa mm$^{0.5}$]	Fracture toughness and plane strain fracture toughness
k_m, $k_{m,e}$, $k_{m,a}$		Total stress magnification factor, stress magnification factors for axial and angular misalignment
K_t		Stress concentration factor
K_1, K_{max}	[MPa m$^{0.5}$]	Stress intensity factor for mode I and maximum stress intensity factor
K_1^N, K_2^N, ΔK_1^N, ΔK_2^N	[MPa mm$^{1-\lambda_1}$, MPa mm$^{1-\lambda_2}$]	Notch-stress intensity factors for mode I and II, as well as corresponding ranges
L	[mm]	Material characteristic length
$M(T)$		Temperature modification formula
m		Slope of fatigue crack growth curves
n		Number of specimens
N_f, $N_{f,exp}$, $N_{f,pred,97.5\%}$, $N_{f,pred,97.7\%}$		Number of cycles to failure, experimental number of cycles to failure, and number of cycles to failure for 97.5% and 97.7% survival probability
p-value		Probability value
P_s		Survival probability
$Q(T)$		Notch sensitivity function

continued on next page

continued from previous page

R, $\widetilde{R}$		Stress ratio (Ratio between lower and upper stress) and nominal load ratio (Ratio between lower and upper applied loading)
R^2		Coefficient of determination
R_C, $R_{C,WT}$, $R_{C,WR}$	[mm]	Control radius, control radius at weld toe, and at weld root
r_{xy}, Δr_{xy}		Pearson correlations coefficient and difference between two dependent correlations coefficient
$\overline{r}^*_{xy}$		Estimate of the correlation coefficient of the real population (mean of bootstrapped estimates)
r_0	[mm]	Distance between the V-notch tip and the origin of the local coordinate system
s		Support factor of notch stress approach
S, S_c	[Nmm/mm^2]	Strain energy density factor and critical strain energy density factor
SD_x, SD_y		Standard deviation about x- and y-axes
T	[°C]	Temperature
T_s		Scatter ratio (1/ ($\Delta\sigma_{R,10\%}/\Delta\sigma_{R,90\%}$))
V_R, $V_{R,97.7\%}$		Fatigue strength ratio between subzero and room temperature, and fatigue strength ratio between experimental results and corresponding FAT class
W	[mm]	Weld width
$\overline{W}$, $\Delta\overline{W}$, $\hat{W}$	[Nmm/mm^3]	Averaged strain energy density, strain energy density range, and normalized strain energy density

continued on next page

continued from previous page

W_c	[Nmm/mm^3]	Critical absorbed energy up to fracture per unit volume
Y		Crack geometry function
z_1, z_2	[mm]	Leg lengths
a		Significance level
2α, γ	[°]	Notch opening angle and bisector
α'_ξ		Non-dimensional shape coefficient of the generalized Kitagawa-Takahashi diagram
$\alpha_\xi^{1/\xi} a$	[mm]	Effective dimension of the generalized Kitagawa-Takahashi diagram
β		Geometrical correction factor of mode I N-SIF threshold value
ΔK_{th}, $\Delta K^N_{1,th}$	[MPa m$^{0.5}$, MPa m$^{1-\lambda_1}$]	Fatigue crack growth threshold for long cracks and mode I N-SIF threshold value
$\Delta K_{th,norm}$, $k_{\Delta K_{th,norm}}$	[MPa m$^{0.5}$, MPa m$^{0.5}$/°C]	Normalised fatigue crack growth rate threshold of ΔK_{th} vs. T data and mean slope of $\Delta K_{th,norm}$
$\Delta\sigma_{eff}$	[N/mm^2]	Effective stress range
$\Delta\sigma_R$	[N/mm^2]	Reference fatigue strength
$\Delta\sigma_{R,FAT}$	[N/mm^2]	Reference fatigue strength given by the FAT class
$\Delta\sigma_{R,50\%}(T)$, $\Delta\sigma_{R,50\%}(T = 20°C)$	[N/mm^2]	Mean fatigue strength and mean fatigue strength at room temperature (i.e. 20 °C)
$\Delta\sigma_{R,97.7\%}$	[N/mm^2]	Fatigue strength at $N = 2 \times 10^6$ cycles for a probability of survival of $P_s = 97.7\%$
$\Delta\sigma_0$	[N/mm^2]	Fatigue limit of smooth base material specimen
θ_1, θ_2	[°]	Weld flank angles

continued on next page

continued from previous page

λ_1, λ_2		Eigenvalues of the Williams' stress field solution for the N-SIF K_1 and K_2 for modes I and II
μ_{WT}, μ_{WR}		Mean deviation for specimens showing weld toe and weld root failure
ν		Poisson's ratio
ξ		Degree of singularity of the Williams' stress distributions
ρ^*	[mm]	Micro-structural support length
ρ_{real}	[mm]	Real notch radius
ρ_{ref}	[mm]	Reference radius
ρ_1, ρ_2	[mm]	Weld toe radii
$\overline{\sigma}$	[N/mm^2]	Averaged stress
$\sigma_{b,w}$	[N/mm^2]	Bending stress
σ_{eff}, $\sigma_{eff,max}$, $\sigma_{eff,norm}$	[N/mm^2]	Effective stress, maximum effective stress, and normalized effective stress
σ_{max}, σ_{min}	[N/mm^2]	Maximum and minimum stress
$\sigma_{m,w}$	[N/mm^2]	Membrane stress
σ_n, $\Delta\sigma_n$	[N/mm^2]	Nominal stress and nominal stress range
σ_{rr}, $\sigma_{r\Theta}$, and $\sigma_{\Theta\Theta}$	[N/mm^2]	Stress components in polar coordinates (r, Θ)
σ_s	[N/mm^2]	Structural stress
$\sigma_{s,w}$	[N/mm^2]	Structural weld stress ($\sigma_{m,w} + \sigma_{b,w}$)
σ_{UTS}, σ_{YS}, $\sigma_{Y0.2}$	[N/mm^2]	Ultimate tensile strength, yield strength, and 0.2% offset yield strength
$\sigma_x(y)$	[N/mm^2]	Stress normal to the leg section
σ_1	[N/mm^2]	First principal stress
$\sigma_1(x)$	[N/mm^2]	First principal stress gradient in x-direction
τ	[N/mm^2]	Shear stresses in the base plate

continued on next page

continued from previous page

τ_w	[N/mm^2]	Shear stresses in the fillet weld
φ	[°]	Angular misalignment
χ_i		Auxiliary parameter for mode i

Contents

CONTENTS

1 | Background

1.1 | Material behaviour at sub-zero temperatures

For years, shipping traffic in the Arctic areas has been increasing considerably; in addition, offshore structures such as oil rigs and wind turbines have been set up in areas with seasonal freezing temperatures. These structures and their materials face severe environmental requirements that must be addressed during design. Several knowledge gaps have been identified in the assessment of structures in Arctic regions in recent years. Among these the most challenging might be ice mechanics, including ice-structure interaction (Jordaan 2001), wave mechanics in ice-covered regions (Hartmann et al. 2020), and material behaviour at sub-zero temperatures (Horn and Hauge 2011; Hauge et al. 2015; Østby et al. 2015). The latter is divided into static and cyclic material properties, related to static or cyclic loads. Among these topics, fatigue behaviour at low temperatures is a crucial aspect with regard to structural safety and a known cause of incidents (Necci et al. 2019). Not surprisingly, the importance of considering fatigue as a driving design factor for ships (Bridges et al. 2006; Zhang et al. 2011; Suyuthi et al. 2013; Kim and Kim 2019) and offshore structures (Zhang et al. 2018a; Hendrikse and Nord 2019; Panin et al. 2019) has led to increased fatigue testing and analysis at sub-zero temperatures. Although it is known that lower temperatures change the material properties of steel and its welded joints, the resulting effects are still only partly understood, in particular regarding fatigue behaviour at sub-zero temperatures (Alvaro et al. 2014; Walters et al. 2016).

Fatigue testing at sub-zero temperatures dates back to the beginnings of aerospace exploration and the storage and transport of liquefied gases (Gillett et al. 1932; McClintock and Gibbons 1960; Reed et al. 1971; Kaufman 1975); however, due to increased shipping and interest in oil and gas exploration in polar regions an increase of studies on

fatigue strength at sub-zero temperatures has recently been noted. Yet, while adverse effects caused by high temperatures (such as creep, see Mannan and Valsan (2006)) are well covered in the literature and in international standards, there are few publications on the fatigue properties of welded joints at sub-zero temperatures, e.g. (Liaw et al. 1985; Shulginov and Matveyev 1997; Baek et al. 2001; Kang et al. 2009; Bridges et al. 2012; Jung et al. 2013; Jeong et al. 2015a; Feng and Qian 2018; Kim et al. 2018; Li et al. 2018; Liao et al. 2018; Viespoli et al. 2019; Zhao et al. 2020a; Zhao et al. 2020b; Wang et al. 2021). Furthermore, most studies on sub-zero temperature fatigue focus on linear elastic fatigue crack growth (FCG) rate testing for cryogenic applications. Stress–life (*S*–*N*) data for welded structural steel joints exposed to temperatures relevant to Arctic conditions are particularly scarce and, with the exception of Bridges et al. (2012), Li et al. (2018), and Wang et al. (2021), who tested different fillet-welded joints, have focussed on butt-welded joints.

Despite most studies finding an increase in fatigue strength at sub-zero temperatures, current fatigue design standards and recommendations do not consider adjusting fatigue design curves (cf. (EN 1993–1–9:2005; LR ShipRight; Hobbacher 2016; EN ISO 19906:2019)). Also, sub-zero temperature effects on fatigue are usually not mentioned, but one exception is the International Organization for Standardization (ISO) standard for Arctic offshore structures (EN ISO 19906:2019), which states that 'attention should be paid to the validity of stress–life curves with regard to low temperature application'; nonetheless, recommendations on how to verify the validity of the *S*–*N* curves are not given. Currently, design standards focus almost exclusively on fracture toughness requirements for engineering structures exposed to sub-zero temperatures (Hauge et al. 2015); however, a wide range of parameters should be considered for applications at temperatures below freezing to reduce the risk of brittle failure.

According to the ISO technical specification for material requirements in Arctic operations (ISO/TS 35105:2018), the main parameter categories for design are tensile properties, fracture and arrest toughness, and fatigue. Avoidance of brittle fractures is achieved by demonstrating sufficient fracture toughness at the design temperature (service temperature minus a safety margin). The *lowest anticipated service temperature* (LAST) is often used to define the temperature range for material tests (EN ISO 19902:2018). A realistic short-term service temperature limit is −40 °C (ISO/TS 35105:2018). The resulting

fracture and arrest toughness requirements are difficult to meet. Furthermore, it raises the question of whether fatigue design curves that are based on room temperature tests are applicable to such low temperatures. The reason for this is the fatigue transition behaviour of structural steels at temperatures in the range of the *ductile to brittle transition temperature* (DBTT).

With decreasing temperatures, the mechanism of stable crack growth behaviour changes from plastic blunting and cracking to cleavage-controlled brittle fractures for ferritic materials with body-centred cubic (bcc) crystal structure like structural steels. On the contrary, materials with face-centred cubic (fcc) crystal structures do not show such a transition behaviour. Several test methods have been invented to measure transition temperatures for design purposes; yet, the most commonly applied in many industries are fracture toughness and Charpy V-notch impact tests. These tests are used to confirm that the DBTT is below the expected operating temperatures minus a prescribed safety margin (EN ISO 19902:2018).

Most fatigue tests at sub-zero temperatures in past decades were performed to investigate the FCG rate of fcc base materials for cryogenic applications (Kawasaki et al. 1977; Yarema et al. 1977; Stonesifer 1978; Moody and Gerberich 1979; Stephens et al. 1979; Basinski et al. 1980; Lucas and Gerberich 1981; Tschegg and Stanzl 1981; Esaklul et al. 1985; Liaw et al. 1985; Stephens 1985; Ostash and Zhmur-Klimenko 1987; Ostash et al. 1988; Lü and Zheng 1991; Vogt et al. 1993; El-Shabasy and Lewandowski 2004). Since the ductile striations mechanism defines the crack growth of such materials down to extremely low temperatures (around 4 K (Alvaro et al. 2014)), it is often assumed that low temperatures have no detrimental effect on fatigue properties (Hauge et al. 2015); however, in the 1970s a transition behaviour of FCG rates of bcc-type materials had already been observed and this was related to the DBTT (obtained from fracture toughness tests) by Kawasaki et al. (1975).

As the material undergoes a transition from ductile to brittle fracture mechanism the fatigue crack growth behaviour (described by Paris' law) also changes. A significant change in the slope exponent of Paris' law, is often associated with the fatigue ductile–brittle transition (FDBT), see Figure 2(a). This is further highlighted by a reduction in fatigue crack growth threshold (stress intensity factor corresponding to fatigue crack growth rates $\leq 10^{-7}$ mm/cycle). The relation between the DBTT and the *fatigue transition temperature*

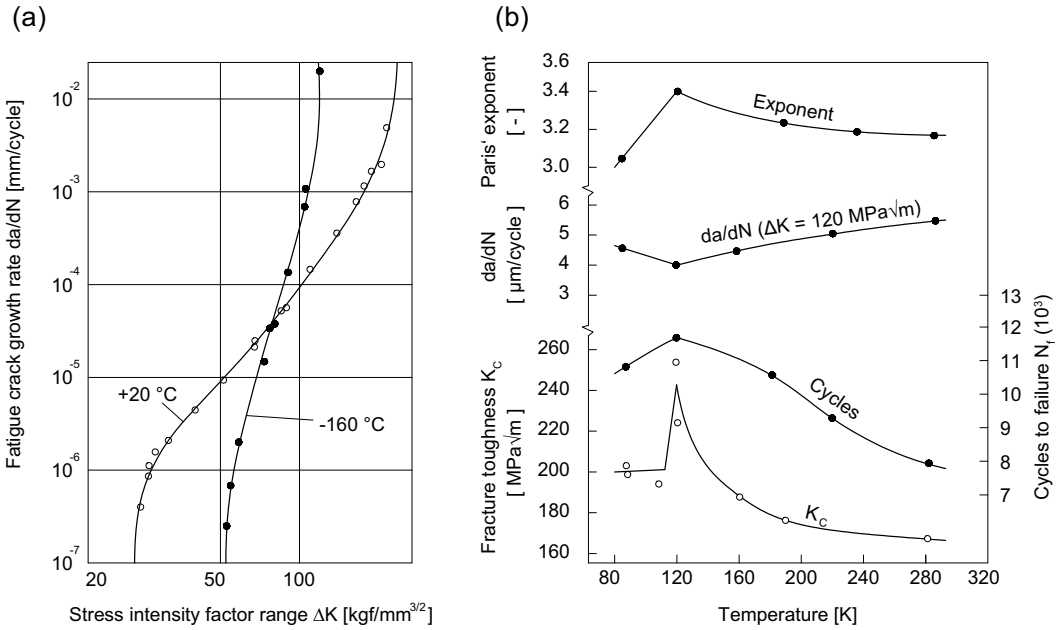

Figure 2. A fatigue crack growth rate (da/dN) versus stress intensity factor range (ΔK) curve for a low-carbon steel above and below the FTT (a) and the effect of test temperature on a number of material parameters of a 5.5% Ni steel (b), based on Yarema et al. (1977) and Kawasaki et al. (1977)

(FTT) is typically confined to a narrow temperature range. This is illustrated by the simultaneous change of fracture toughness K_c, crack growth rate, and slope exponent of Paris' law around 120 K in Figure 2(b).

The first records of the effect of different types of fatigue loading on the DBTT date back to the years following the Second World War (MacGregor and Grossman 1948; Fegredo and Thurston 1966). Also, the effects of both load level (Williams and Lawrence 1962) and loading rate (Harris and Benham 1965) were discovered early; yet, to this day the mechanism of fatigue and fracture transition and the relation between the two are contraversial, see (Alvaro et al. 2016, 2017; Fang et al. 2019; Fang et al. 2020; Zhao et al. 2020a).

By conducting FCG rate tests over a wide temperature range and scanning electron fracture area investigations, Alvaro et al. (2016, 2017) and Fang et al. (2019) and Fang et al. (2020) relate this behaviour to a change in the striation process when ductile crack growth is superimposed by cleavage fractures caused by embrittlement of the material; however, at temperatures below room temperature but above FTT the FCG rate is significantly re-

duced, which extends the life of the structure (Alvaro et al. 2016; Walters et al. 2016; Alvaro et al. 2017; Fang et al. 2019; Fang et al. 2020). The relationship between FTT and DBTT is better understood for various structural steel-based materials due to recent efforts by the above-mentioned research groups. Yet, overall, the influence of temperature on the fatigue properties of welded structures is still poorly understood.

Fracture toughness tests show that the DBTT in the heat-affected zone (HAZ) of welded structures is generally higher than in the surrounding base metal (Anderson and McHenry 1982; Zerbst et al. 2014), which is why such tests must be carried out with the notch tip at the fusion line between the weld metal and the HAZ. Nevertheless, the influence on the fatigue properties of welded structures remains unclear due to the lack of comprehensive investigations on the change in the static and cyclic properties of welded joints at sub-zero temperatures. Thus, this research aims to shed light on the relation between fatigue strength and material parameters that are typically used to qualify materials and welded connections for sub-zero temperatures. In this context, some considerations on the temperature influences on design of ships and offshore structures based on current international standards are given below.

1.2 | Consideration of sub-zero temperature material behaviour in design and standards

It is well known that a wide range of static and cyclic material properties change with temperature, see (Kawasaki et al. 1975; Kawasaki et al. 1977; Outinen and Makelainen 2004; Ehlers and Østby 2012; Wang et al. 2013; Alvaro et al. 2014; Paik et al. 2017; Wang et al. 2020; Zhao et al. 2020a); yet, fatigue is rarely considered in international standards. Only the technical specification ISO/TS 35105:2018 recommends performing FCG rate testing at room temperature and LAST if sufficient Charpy toughness cannot be proven at LAST −18 °C. Even this document does not consider *S–N* approaches. Furthermore, this empirical relation was established based purely on tests of base and welding simulated (Gleeble tests) materials, see (Alvaro et al. 2016; Walters et al. 2016; Alvaro et al. 2017).

Due to the low cost of performing Charpy impact tests, material selection is usually based on empirical Charpy and fracture toughness relationships at design temperatures (according to the Sanz correlation (Sanz 1980)) and DBTT estimates, see (Wallin 1991;

Sedlacek et al. 2008). Depending on the application, different standards must be considered when selecting materials and welding processes for structures operating in Arctic regions or generally at low temperatures. Design standards such as EN ISO 19902:2018 typically specify test temperatures—in relation to the design temperature—depending on steel grade and plate thickness but refer to technical delivery condition standards for minimum toughness requirements. Standards for delivery conditions are, however, not specifically developed for structures exposed to sub-zero temperatures. As a consequence, frequently applied standards for technical delivery condition such as EN 10225-1:2019 and API SPECIFICATION 2W are limited to temperatures above −10 °C and design standards, e.g. NORSOK M101 and IEC 61400-3-1:2019 to temperatures above −14 °C and −15 °C, respectively. Although the latest version of EN 10225-1:2019 includes an informative section on the prequalification of steels for offshore structures in Arctic regions, the requirements are set by agreements between the producer and customer. Nonetheless, these standards are used to set requirements for steel plates and their welded joints which must be fulfilled at the design temperature e.g. LAST (minus a safety margin). For structures in the Barents Sea, design temperature can reach temperatures as low as −40 °C (Horn and Hauge 2011). Due to cost and feasibility aspects, reasonable definitions of material requirements for applications at sub-zero temperatures have become an important topic in recent years, see (Horn and Hauge 2011; Brandt et al. 2012; Horn et al. 2012; Hauge et al. 2015; Østby et al. 2015; Horn et al. 2016); nevertheless, current standards still rely on shifts of toughness requirements with design temperatures well below the intended temperature range of technical delivery conditions. Interestingly, the definition of design temperatures also varies significantly between classification societies and international standards, see (Horn et al. 2016; Ehlers et al. 2018; Kubiczek et al. 2019).

Due to their chemical composition and processing, modern high-strength structural steels are expected to have advantageous mechanical properties at low temperatures compared to mild steels. A high fracture toughness at design temperature is decisive for the selection of materials for Arctic applications. While normal-strength structural steels do not have to meet fracture toughness requirements at temperatures below −20 °C, many higher-strength steels meet these requirements even at temperatures of −50 °C or −60 °C (Thieme and Schröter 2013); however, due to the lack of *S–N* fatigue test data for welded joints it is unclear whether normal-strength steels—which are often used for

ship structures—suffer from a reduced fatigue strength at temperature below the certified operating temperature based on Charpy impact tests.

In the following two sections, the objectives and the scope of this thesis regarding fatigue strength and strength assessment of welded structural steels at sub-zero temperatures as well as the research approach are presented.

1.3 | Specific objectives

As mentioned previously, fatigue of welded joints at sub-zero temperatures has been identified as one major knowledge gap related to design of ships and offshore structures for Arctic regions (Alvaro et al. 2014; Walters et al. 2016). In particular, *S*–*N* data—which is the basis for fatigue design of ships and offshore structures—at sub-zero temperatures is scarce. Hence, the same design curves and methods as for room temperature are applied for sub-zero temperature fatigue assessment of ships and offshore structures. Consequently, the fatigue strength of welded joints in terms of *S*–*N* curves and how to account for temperature effects within fatigue assessment methods are investigated in this thesis.

Fatigue crack initiation and propagation at welded joints as well as actual fatigue assessment are processes that are typically dealt with on a continuum mechanics scale (in the millimetre range and above). As structural materials are not homogeneous, fatigue is, however, inevitably influenced by effects of micro- and meso-scale like crystal phases and grain boundaries. These effects are well known—and have been known for almost a hundred years—to affect crack initiation at notches. In general, the process of crack initiation at notches is not purely governed by the maximum macroscopically derived stress but influenced by the micro-structural features of the material surrounding the notch, see Neuber (1958). This effect is termed the micro-structural support effect hypothesis and is, among others, influenced by the thermally activated plastic deformation process.

By fatigue testing different structural steels and weld details as well as performing other material tests used to qualify materials, both a database for fatigue strength of welded structural steels at sub-zero temperatures is created and the relation to typical material tests is presented. For this goal, welded steel joints of normal and high-strength structural steels are fatigue tested down to -50 °C. On this basis, novel fatigue design concepts—based on the micro-structural support effect hypothesis—for welded joints are

extended and compared to state-of-the-art methods. Typical fatigue assessment methods for welded joints are not capable of taking influencing factors such as temperature directly into account; however, methods based on the micro-structural support effect hypothesis—like the averaged strain energy density method and the stress averaging approach—offer a possibility to overcome this deficiency.

Finally, guidance on the application of fatigue assessment methods for welded steel joints at temperatures below freezing is presented for the first time. To achieve the overall goal (investigating the fatigue strength of welded joints at sub-zero temperatures by *S–N* tests and how to include temperature effects in fatigue assessment), the following objectives are defined.

The first objective is the determination of the static and cyclic material behaviour at room temperature down to temperatures representative for Arctic regions minus a safety margin (i.e. −50 °C) of two welded structural steel types. The fatigue tests build the data basis for the extension of fatigue assessment methods to sub-zero temperatures. Additionally, Charpy V-notch impact tests are performed to relate the change in fatigue behaviour to the properties that are typically applied for material selection.

The second objective is the statistical and numerical determination of the fatigue behaviour based on the aforementioned experimental results. In order to create a benchmark for the novel fatigue design concepts—based on the micro-structural support effect hypothesis—a number of state-of-the-art fatigue assessment concepts are applied to the fatigue test data of welded steel joints.

The third and final objective is the review and expansion of fatigue assessment concepts for welded joints to sub-zero temperatures. To this end, two concepts that are both based on the micro-structural support effect hypothesis are selected and finally compared to state-of-the-art methods.

These objectives form the basis for the determination and evaluation of fatigue behaviour of welded structural steel joints at sub-zero temperatures. Hence, this thesis seeks to further knowledge on the safety margins of weld details in ships and offshore structures operating in Arctic regions and on fatigue design of such structures by accounting for temperature effects within fatigue assessment. In addition to the area of shipbuilding and offshore technology considered here, a transfer of the results to other areas (e.g. civil engineering, general steel construction etc.) is also possible.

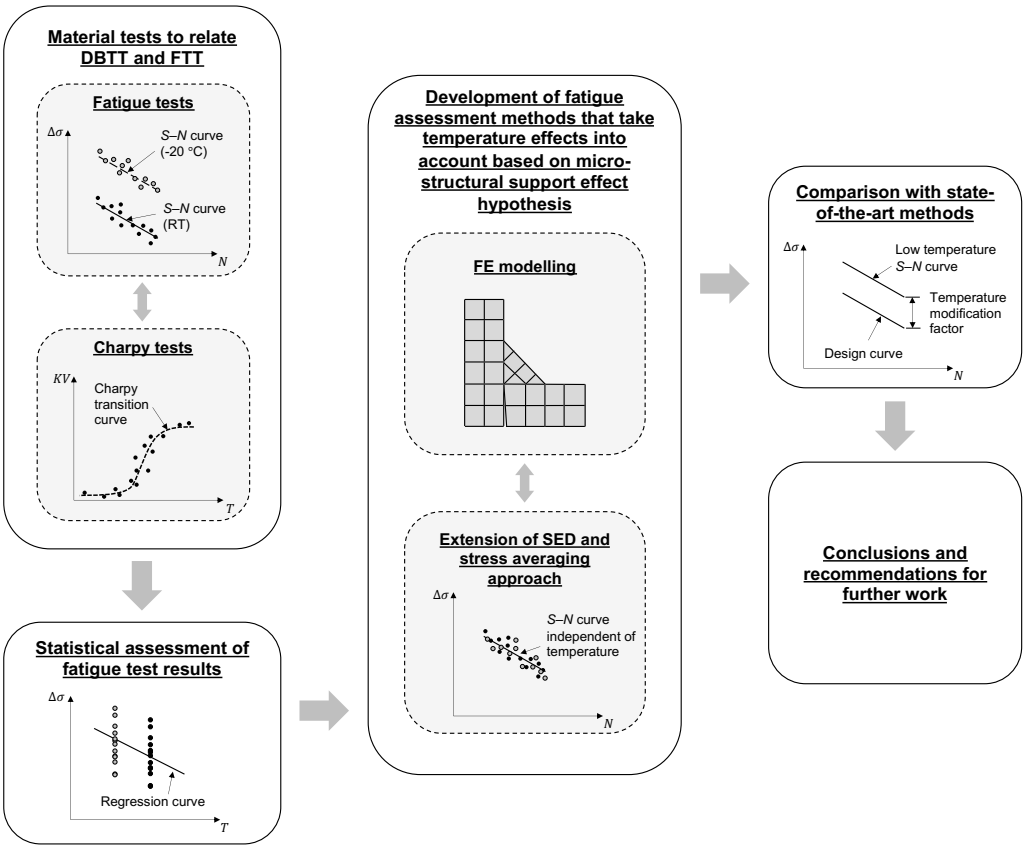

Figure 3. Schematic representation of the research approach

1.4 | Research approach

The main goal of this thesis is to generate a better understanding of the fatigue of welded connections subjected to sub-zero temperatures and to develop ways that enable accounting for temperature effects within fatigue assessment. With the help of experimental, statistical, and numerical investigations, the fatigue behaviour of welded joints at low temperatures is investigated. For this reason, a brief explanation of how the individual objectives will be achieved is given below. To illustrate the research approach a schematical representation is given in Figure 3.

The static and cyclic material tests are carried out on typical weld details like butt- and fillet-welded joints, since these represent the most common forms of welded joints

in the maritime industry. The aim of the experiments is to assess the influence of various parameters on the static and cyclic properties of structural steels and their welded joints at sub-zero temperatures. One focus is on the relationship between the transition temperatures (DBTT and FTT) presented in Section 1.1 and the influence of temperature on the fatigue strength. For this purpose, Charpy impact tests are performed in addition to fatigue tests to measure the DBTT.

To allow comparability with real structures, welding parameters and steel grades are used that would also be used for ships and offshore structures. Consequently, conclusions on the influence of the welding process and weld material on sub-zero temperature fatigue strength and fracture toughness can be drawn that are relevant for practical applications. So far, the relation between DBTT and FTT has primarily been investigated by performing FCG rate tests and either Charpy or fracture toughness tests, because only one specimen is required for each FCG rate test. To derive an *S–N* curve a minimum of 10 specimens are required to yield a statistically verified result for the mean fatigue strength (DIN 50100:2016-12). Regarding the FDBT, a schematic illustration of the *linear elastic fracture mechanics* FCG behaviour above and below the FTT is given in Figure 4(a). As mentioned before, if a distinct effect of FDBT is observed, the slope of the FCG curve changes and the fatigue crack growth threshold is reduced compared to temperatures below room temperature but above the FTT. The corresponding trend of *S–N* curves is expected to look similar to Figure 4(b) due to the relation between both slope parameters (m and k) as well as fatigue limit ($\Delta\sigma_\mathrm{R}$) and threshold stress intensity factor range (also called fatigue crack growth threshold $\Delta\mathrm{K}_\mathrm{th}$). As a result of those two relations, it might be possible to observe a FDBT based on *S–N* tests. On the contrary, the upper regions of fatigue crack growth (Stage III) and stress range (low cycle fatigue regime) are governed by fracture toughness (K_c) and static yield strength (σ_YS).

To avoid biased results related to the chosen steel type, a typical normal-strength shipbuilding steel grade S235J2+N and a higher-strength, thermomechanically rolled fine-grain structural steel S500G1+M were selected for this study. Fine-grain steel is characterized by a high static strength and low-carbon equivalent and is therefore easy to weld. Due to these two properties, a considerable structural weight reduction, compared with conventional structural steels, can be achieved without additional welding requirements like pre-heating. It is therefore frequently used in offshore structures (Thieme and Schröter

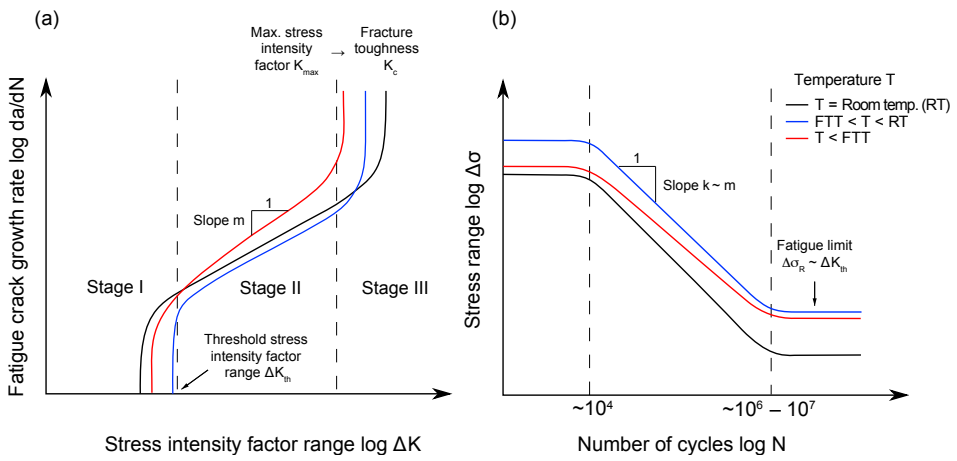

Figure 4. Schematic representation of the effect of low temperature on (a) fatigue crack growth curves based on Alvaro et al. (2014) and (b) expected course effect of temperature on *S–N* curves of welded joints, adopted from Bock und Polach et al. (2019b)

2013). The use of even higher-strength steels (yield strength $\sigma_{YS} > 550$ MPa) in maritime structures is currently restricted by classification societies (DNVGL-RP-0005:2014-06). The reasons for this are that the fatigue strength of welded joints with sharp notch radii is independent of the material strength (Maddox 2002) and high-strength materials typically show higher notch sensitivity (Fricke 2014); nevertheless, such steel types offer significantly better fracture properties at sub-zero temperatures (Walters et al. 2014). By comparing a conventional normal-strength with a high-strength structural steel, conclusions on the effect of steel grade on fatigue strength can be drawn for sub-zero temperature applications.

To reach the aim of this study, two fillet weld details—with the two typical failure initiation sites at weld toes and weld roots—and butt-welded joints are tested at room temperature (RT), −20 °C, and −50 °C. Clearly, more than one different structural weld detail is needed for the development of fatigue assessment concepts for new fields of interest such as sub-zero temperatures. Before the fatigue test data is used as the basis for the development of fatigue assessment methods that take temperature effects into account, a statistical assessment of the test data is performed to verify the effect of temperature on the obtained test results.

State-of-the-art fatigue assessment concepts in international standards and guidelines

are not capable of taking temperature effects into account. Consequently, two novel methods—based on the micro-structural support effect hypothesis—are extended to cover subzero temperature effects on fatigue strength. The two methods are the averaged strain energy density (SED) and the stress averaging approach. For this purpose, finite element (FE) simulations of the different weld details are performed.

This thesis assesses whether the assumption of an effect of yield strength on the micro-structural support effect (Radaj et al. 2006) can be used to account for temperature effects on fatigue strength. The investigation of the micro-structural support length of different materials by Neuber (1968) shows that higher yield strength corresponds to a decrease in the material-related support effect.

Finally, to assess the relevance of the proposed methods to account for temperature effects within fatigue assessment, a comparison with state-of-the-art methods is performed. To reach this goal, well-known fatigue assessment methods such as nominal, structural, and effective notch stress concepts are used for a comparison. The state-of-the-art fatigue methods will be used to investigate how these reflect the temperature effects in the *S–N* curves. It is expected that methods which account for temperature effects lead to higher prediction accuracy than those that do not.

2 | State of the art

2.1 | Fatigue strength at sub-zero temperatures

Due to the increased interest in transarctic shipping and oil and gas exploration in the Arctic, several studies have been conducted in order to ensure the safe operation of ships and offshore structures in Arctic regions (Milaković et al. 2018). The investigated topics span from loading scenarios (Ehlers and Østby 2012; Suyuthi et al. 2013; Zhang et al. 2018a; Hendrikse and Nord 2019) to new welding techniques (Aderinola et al. 2013), and material behaviour at sub-zero temperatures (Alvaro et al. 2014; Hauge et al. 2015; Walters et al. 2016; Akselsen et al. 2017; Panin et al. 2019). There have been a number of recent publications related to fatigue crack growth in structural materials at sub-zero temperatures (Alvaro et al. 2016; Walters et al. 2016; Zhao et al. 2019). Some interesting findings were that fatigue strength increases constantly until a transition temperature is reached. This sudden acceleration of crack propagation below the transition temperature is related to embrittlement of the material (Walters et al. 2016); yet, fatigue strength—in particular of welded structural steel joints—at sub-zero temperatures is a topic which is not yet fully understood due to the lack of available test data (Alvaro et al. 2014; Walters et al. 2016).

In general, in most studies (found in the literature) an increase in fatigue strength with decreasing test temperatures was observed; nonetheless, according to current design guidelines and recommendations, no difference in fatigue strength would be accounted for below RT (EN 1993–1–9:2005; LR ShipRight; DNVGL-RP-0005:2014-06; Hobbacher 2016; EN ISO 19906:2019), which is contradictory to experimental test results. As a consequence, a literature study was performed to gather test results on fatigue crack growth behaviour at sub-zero temperatures. In total 52 datasets were extracted from the literature that report fatigue crack growth rate threshold measurements ΔK_{th} at sub-zero

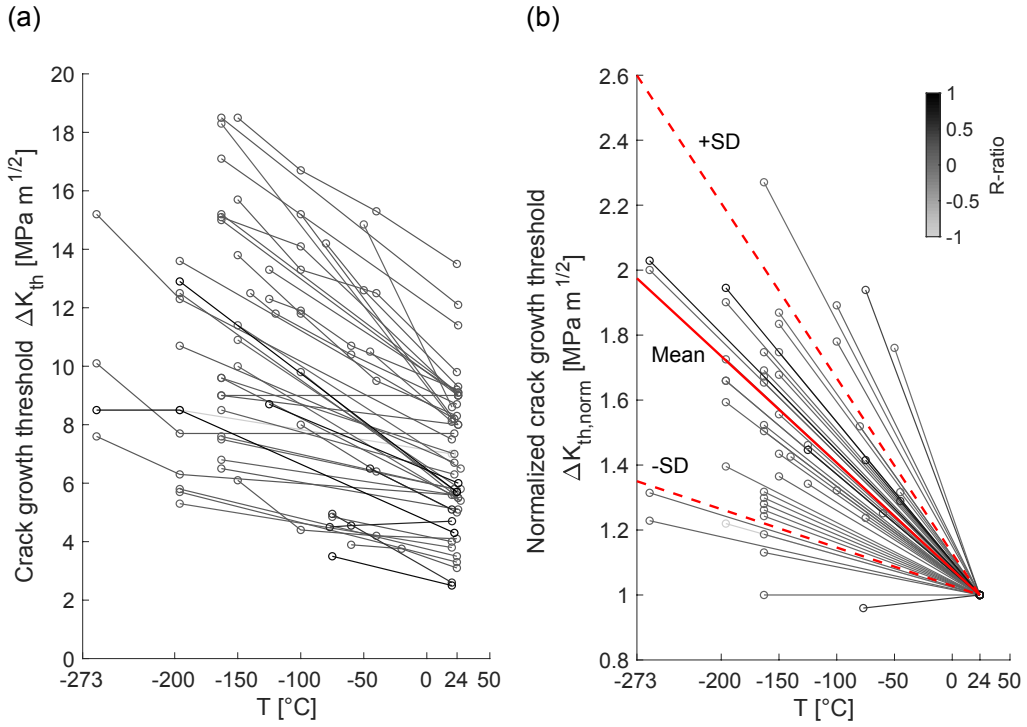

Figure 5. Sub-zero temperatures ΔK_{th} data extracted from the literature (a) and normalized average $\Delta K_{th,norm}$ change at sub-zero temperatures (b) from 50 datasets reported in the literature (Yarema et al. 1977; Lucas and Gerberich 1981; Tschegg and Stanzl 1981; Choi and Schwartz 1983; Yu et al. 1984; Esaklul et al. 1985; Liaw and Logsdon 1985; Liaw et al. 1985; Stephens et al. 1985; Ostash and Zhmur-Klimenko 1987; Aleksenko et al. 1988; Ostash et al. 1988; Lü and Zheng 1991, 1992; Rosenberg 2003; El-Shabasy and Lewandowski 2004; Chai and Johansson 2006; Jung et al. 2013; Jeong et al. 2015a; Jeong et al. 2015b; Walters et al. 2016; Kim et al. 2018; Liao et al. 2018; Thurston et al. 2019), adopted from Braun et al. (2020a)

temperatures. The results are presented in Figure 5(a).

First of all, since a lot of studies focused on the determination of the fatigue transition temperature to brittle material behaviour, only data points which are clearly above the transition temperature were considered for the assessment. By normalizing the extracted data with the fatigue crack growth rate threshold ΔK_{th} at room temperature for each dataset, a normalized mean increase $k_{\Delta K_{th,norm}} = -0.0033$ MPa$\sqrt{m}$/°C is obtained (solid red line in Figure 5(b)) with a standard deviation (SD) of 0.0021 MPa$\sqrt{m}$/°C (dashed red lines). Due to the increase in fatigue crack growth threshold, an increase in fatigue strength is expected at low temperatures, as presented in Figure 4. This is currently not reflected in any international standard for welded engineering structures. Additionally, temperature

effects (except for high temperatures above 100 °C) are also not considered for fatigue assessment of welded joints. The results presented in Figure 5 are later applied to assess the change of fatigue strength of the tested welded joints at sub-zero temperatures as *S–N* fatigue test data of welded joints is scarce.

In general, there are only a few studies that present *S–N* fatigue test data of welded joints at sub-zero temperatures (Shulginov and Matveyev 1997; Kang et al. 2009; Bridges et al. 2012; Li et al. 2018; Viespoli et al. 2019; Zhao et al. 2020b; Wang et al. 2021). More importantly, usually only one type of welded joint was fatigue tested with a limited number of specimens (i.e. less than 10 tests per temperature). This makes the development of fatigue assessment methods for sub-zero temperatures based on literature data impracticable.

DNVGL-RP-C203 recommends performing at least 15 tests for the development of new design curves, preferably on full-scale structures or with high stress ratios R to match the residual stress state of full-scale structures. Studies aiming at the development of new methods or the extension of existing ones often comprise of tests of two or more different structural details (Zhang and Richter 2000; Doerk et al. 2003; Ahola et al. 2017; Ahola 2020; Friedrich 2020; Garcia 2020), sometimes with different failure locations (Eibl 2003; Selle et al. 2011; Fricke and Feltz 2013; Baumgartner 2014; Fischer 2016; Song et al. 2018; Ahola 2020)), different fabrication details (Barsoum 2008; Weich 2009; Selle et al. 2011; Doerk et al. 2012; Lotsberg et al. 2014; Bock und Polach et al. 2019a; Garcia 2020), and different steel types, cf. (Weich 2009; Doerk et al. 2012; Fischer 2016; Ahola 2020; Hensel 2020). As a rule of thumb, typically three different conditions (e.g. specimen type, steel type, or post-weld treatment method) are tested in order to limit statistically uncertainty. There is consequently a need for a systematic investigation into temperature effects on fatigue strength of welded joints as available literature data is limited.

2.2 | Overview of fatigue assessment methods for welded joints considered in this study

In this study, fatigue assessment methods for welded joints are developed that are capable of taking temperature effects into account (stress averaging and strain energy density method); however, in order to assess the relevance of these methods, state-of-the-art

fatigue assessment methods are applied to the same data. These are now introduced.

Among the local state-of-the-art fatigue assessment concepts, the structural hot-spot and effective notch stress concepts are the most commonly applied in industry (Sonsino et al. 2012) and are included in international standards or recommendations for fatigue assessment such as those of the International Institute of Welding (IIW) (Fricke 2012; Hobbacher 2016; Niemi et al. 2018); yet, probably the most commonly frequently fatigue assessment method of all is the nominal stress concept. The global and local fatigue assessment methods that are considered in this thesis are presented in Figure 6.

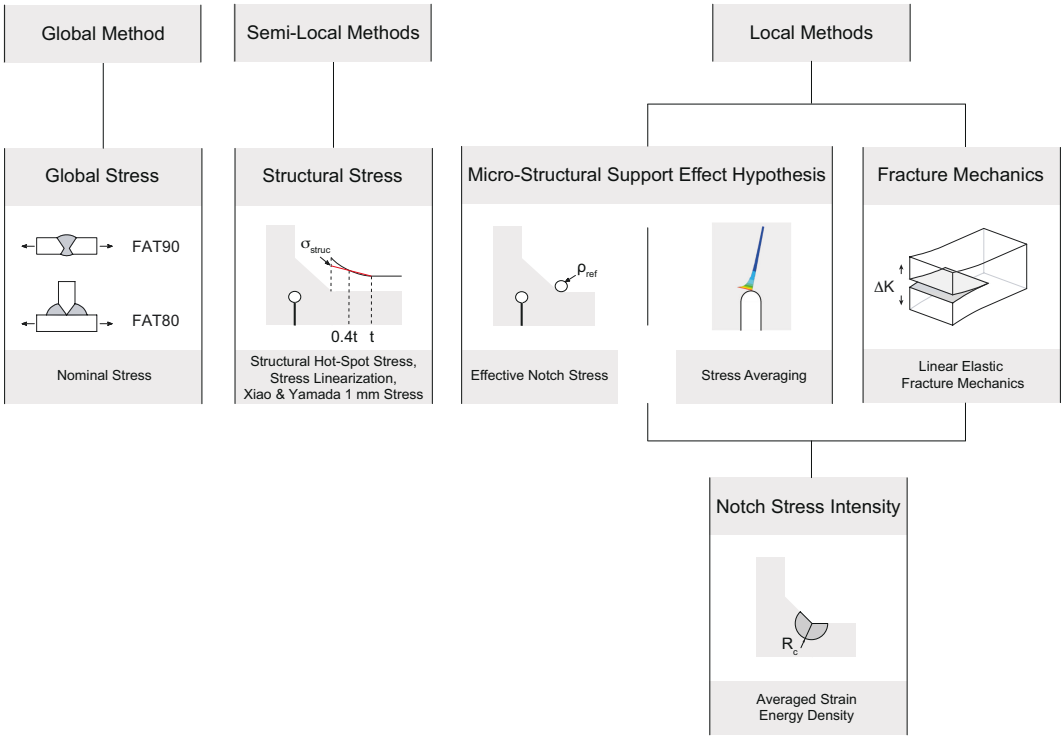

Figure 6. Fatigue assessment methods considered in this study, including their underlying fatigue assessment theory, distinguished by their consideration of local notch effects

In Section 2.3, an introduction to state-of-the-art stress-based fatigue assessment methods for welded joints is given, which is an extension of the review presented in Braun et al. (2020d), and in Sections 2.4 and 2.5 the stress averaging and the strain energy density (SED) methods are introduced, which are later extended to cover sub-zero temperature effects within fatigue assessment. The introduction of these two methods is extended

from initial thoughts presented in Braun et al. (2020a,e, 2021b). Variations of those two methods have been successfully applied to high temperature fatigue of notched components (Berto et al. 2013, 2014; Gallo et al. 2015; Louks and Susmel 2015; Bourbita and Remy 2016; Gallo and Berto 2016) and are thus considered to be suitable for sub-zero temperature fatigue of welded joints.

All methods applied in this thesis have to be understood as fatigue crack initiation methods. Thus, fracture of small-scale fatigue test specimens corresponds to crack initiation in a full-scale structures. Once a crack has developed in a full-scale structure, fracture mechanics method—such as linear elastic fracture mechanics—are best suited to assess the remaining fatigue life or complex structures, see (Barsoum and Barsoum 2009; Baumgartner and Waterkotte 2015; Fischer and Fricke 2016). Fracture mechanics methods are not applied in the context of this thesis, but are, however, closely related to all fatigue assessment methods since in small-scale test specimens a considerable part of the lifetime is also defined by crack propagation, see Maddox (2002).

2.3 | Background on state-of-the-art stress-based fatigue assessment methods for welded joints

There are several methods which are applicable to fatigue assessment of welded joints. They are usually grouped into global methods (nominal stress) and local methods (e.g. structural or notch stress). Nominal stresses are based on cross-sectional quantities (i.e. membrane stress and shell bending) that are calculated using beam theory (Hobbacher 2016). As a result, any local stress-raising effects due to structural details or welds are neglected in stress assessment, but are indirectly considered in the fatigue classes (FAT class). Different types of weld details are thus associated with a particular detail class which defines its nominal stress fatigue strength. The limitations of this are cases where nominal stresses cannot be derived, e.g. for complex structures or dimensional variations (Niemi et al. 2018). Effects related to the structural geometry, but also due to plate misalignment, can be assessed using structural stress methods. This group of methods, however, neglects the local stress increase due to the weld. They can thus be considered as semi-local methods. The local stress increase in the vicinity of a weld is considered in notch stress or other local methods that are not based on fatigue-effective stresses (e.g. strain

or strain energy density).

2.3.1 | Structural stress methods

Different structural stress approaches have been suggested over the years, which can be grouped into three different approaches for taking the structure-related stress concentration into account (Fricke 2013a; Niemi et al. 2018). The three types of structural stress (σ_s) approaches are based on:

- extrapolation of first principal surface stress towards the local weld notch in the area of almost linear stress increase (Figure 7 (a)),
- linearization of membrane (σ_m) and bending (σ_b) stress either through the plate thickness or in a section through the fillet weld (Figure 7 (b)),
- extraction of the stress component in a single point in the vicinity of the notch, but outside the area of non-linear stress increase, e.g. 1 mm according to Xiao and Yamada (2004a,b) (Figure 7 (c)), or 2 mm according to the first structural stress method by Haibach (1968) (Figure 7 (d)).

Further information on the background of the different structural stress methods is given in Braun et al. (2020d). Compared to the nominal stress approach, more complex structures can be assessed by structural stress methods, where a definition of nominal stress is not possible; nonetheless, local stress effects cannot be assessed by these methods and thus have to be covered in fatigue design curves. As a consequence, different design curves are applied for weld toe and root assessment. Such effects can, for example, be covered by notch stress approaches, like the effective notch stress concept according to Radaj (1990).

2.3.2 | Effective notch stress approach

In the effective notch stress concept weld toes and roots are rounded with a fictitiously enlarged reference radius $\rho_{ref} = 1$ mm, see Figure 8. The background of this method is the worst-case assumption of vanishing real notch radii ($\rho_{real} \rightarrow 0$ mm) (Baumgartner

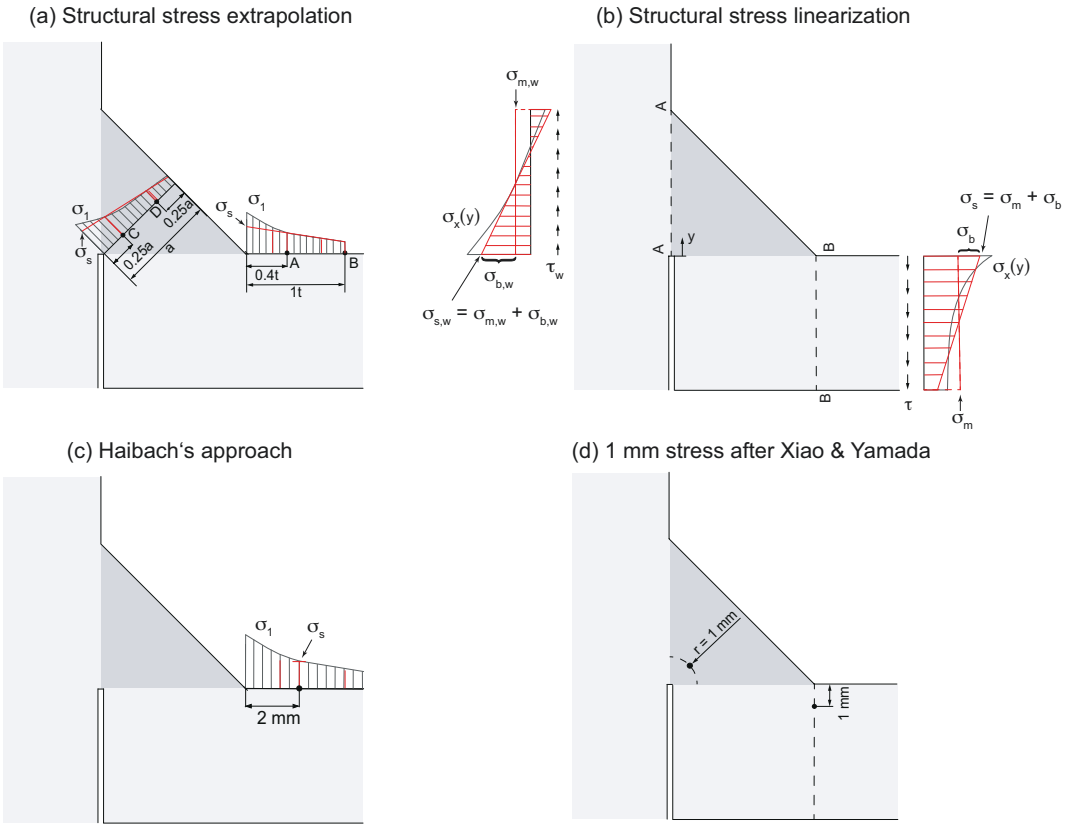

Figure 7. Different structural stress based approaches for fatigue assessment illustrated by a single-sided fillet weld, adopted from Braun et al. (2020d)

2017). Applying the *von Mises stress hypothesis*, an enlargement of the real notch radius ρ_{real} to a reference radius $\rho_{ref} = 1$ mm was introduced as follows:

$$\rho_{ref} = \rho_{real} + s\rho^* \tag{1}$$

with a stress multiaxiality factor $s = 2.5$, and a micro-structural support length of $\rho^* = 0.4$ mm. The factors s and ρ^* were derived assuming plane strain condition and a cast iron-like microstructure in the weld and the fusion line (Baumgartner 2017) with 0.2% offset yield strength of $\sigma_{Y0.2} \sim 300$ MPa (Lazzarin et al. 2004), see Figure 9. In theory, the support factor $s = 2.5$ depends on the notch opening angle for very small notch radii (Radaj et al. 2013); nevertheless, this value, in connection with the micro-structural support length $\rho^* = 0.4$ mm, has proven to be realistic for cracks initiating at weld toes and roots, see

(Radaj 1990; Lazzarin et al. 2004; Radaj et al. 2013; Baumgartner 2017).

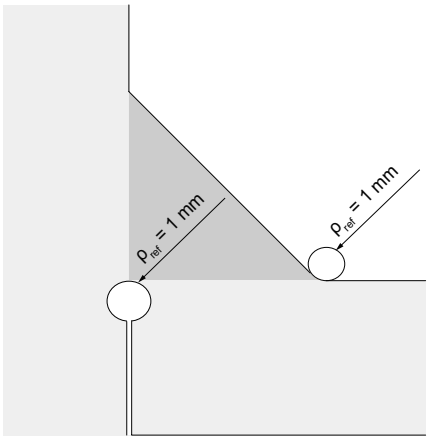

Figure 8. Replacement of the weld toe and root with a reference radius for the effective notch-stress approaches illustrated by a single-sided fillet weld, adopted from Braun et al. (2020d)

The effective notch stress approach has been successfully applied for various tasks including steel, aluminium, and magnesium welded joints, but is most frequently applied for fatigue assessment of joints failing from weld roots, see Fricke (2013a). For thin welded plates (thickness $t < 5$ mm), smaller reference radii (i.e. 0.05 mm and 0.3 mm) in connection with corresponding fatigue design curves have been proposed, see (Zhang and Richter 2000; Eibl et al. 2003; Kranz and Sonsino 2010; Sonsino et al. 2013). Alternatively, the centre of the reference radius may be moved to maintain the correct cross-sectional area; however, this is only applicable for plate thicknesses large enough to enclose the reference radius, see (Fricke 2012, 2013b).

2.4 | Notch stress fatigue assessment based on stress averaging approach and relation to the micro-structural support effect hypothesis

According to Figure 9, the micro-structural support length ρ^* should decrease for higher-strength materials. If the yield strength of the material changes with temperature, a change of support effect and micro-structural support length ρ^* is expected. Hence, changes of support effect with temperature would yield a necessity for different reference radii for varying temperatures, which makes this kind of assessment impracticable.

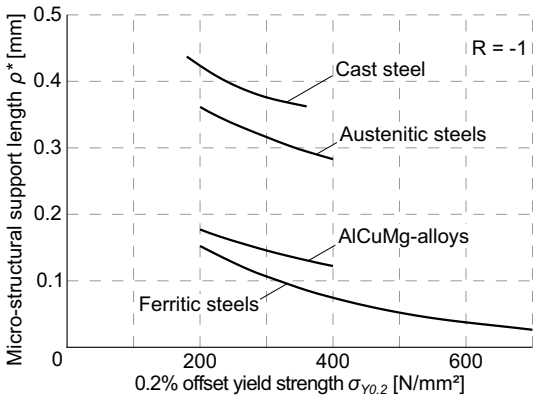

Figure 9. Micro-structural support length of different materials according to Neuber (1968), adopted from Braun et al. (2021b)

The replacement of the weld radii with the fictitious radii of 1 mm is furthermore not recommended for weld details having small stress concentration (K_t < 1.6) and may lead to non-conservative assessment for mild notches with real radii $r_{real} > 1$ mm, see (Pedersen et al. 2010; Fricke 2012; Rother and Fricke 2016; Collmann and Schaumann 2018). An application of real radii would be conceivable for this application, but seems impracticable due to the large range of possible notch radii.

Alternatively, the notch stress concept based on Neuber's stress averaging (Neuber 1958), or critical distance according to Peterson (1959) or Taylor (2007) can be applied, where an effective stress is determined at a certain depth along the expected crack path or the notch bisector. A third possibility suggested by Taylor (2007) or earlier by Kuguel (1961) is the determination of an effective stress by averaging the stress in an area or volume around a stress raiser. Taylor (2007) was not the first to suggest any of the aforementioned approaches; however, he harmonized the three approaches with his *Theory of Critical Distances* (TCD).

The basis of all three TCD methods is the determination of an effective stress σ_{eff}, which takes into account the notch geometry as well as the support effect of the surrounding material. In theory, all three approaches are assumed to yield similar results with an error interval of $\pm$ 20% in the high-cycle fatigue regime of notched components (Susmel and Taylor 2007; Louks and Susmel 2015); however, even higher differences in prediction accuracy between different types of TCD approaches have been reported in the literature

(Susmel and Taylor 2007; Härkegård and Halleraker 2010; Silva et al. 2012; Baumgartner et al. 2015; Louks and Susmel 2015; Yin et al. 2015; Santus et al. 2018; Vedernikova et al. 2019).

In this study, the stress averaging approach is applied in the original sense of Neuber (1958) and based on recent applications of this method (Zhang et al. 2012; Baumgartner et al. 2013, 2015; Schmidt et al. 2015; Karakaş 2017; Marulo et al. 2017; Karakaş et al. 2018; Baumgartner et al. 2019, 2020a,b). Comparing the accuracy of different TCD methods with the later introduced SED method, Hu et al. (2019) found this version of TCD method to be the most accurate for notched components. For this approach, the averaged stress $\overline{\sigma}$ is calculated by averaging the maximum principal stress gradient $\sigma_1(x)$ perpendicular to the surface over the length ρ^* with:

$$\sigma_{eff} = \overline{\sigma} = \frac{1}{\rho^*} \int_0^{\rho^*} \sigma_1(x)\, dx \tag{2}$$

For any given real notch radii ρ_{real}, it can be shown that the stress averaged over ρ^* in Figure 10(a) equals the maximum elastic peak stress obtained by the effective notch stress method for a fictitiously enlarged notch with a reference radius ρ_{ref} in Figure 10(b).

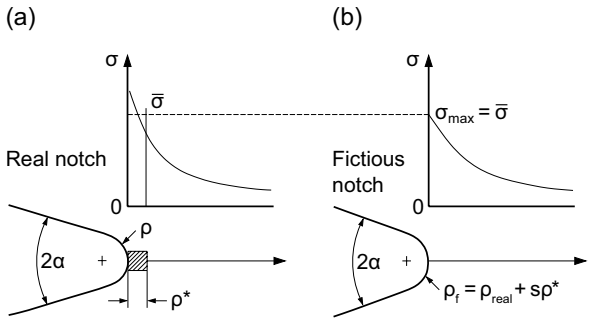

Figure 10. Relation between the stress averaging and the effective notch stress approach based on Radaj et al. (2013)

For the application of TCD methods like the stress averaging approach to welded joints, two different methods for FE modelling were proposed by Baumgartner et al. (2015), i.e. modelling weld toes with the actual notch radii ρ_{real} or with a reference radius ρ_{ref}. Examples in which the actual weld geometry was applied for TCD or similar methods are (Liinalampi et al. 2016; Baumgartner et al. 2019; Niederwanger et al. 2020). The majority of studies, however, applied a reference radius $\rho_{ref} = 0.05$ mm (Zhang et al. 2012;

Baumgartner et al. 2013, 2015; Schmidt et al. 2015; Karakaş 2017; Marulo et al. 2017; Baumgartner et al. 2018; Karakaş et al. 2018; Baumgartner et al. 2020a). No information is available on how this reference radius was derived, but it is assumed that the idea is related to the notch stress approach for thin welded joints, which also applies a reference radius of $\rho_{ref} = 0.05$ mm, see (Zhang and Richter 2000; Eibl 2003; Eibl et al. 2003; Kranz and Sonsino 2010). For the application of the reference radius, a fatigue design curve FAT160 was recommended by Baumgartner et al. (2015) for weld toe and root assessment. This curve is only two reference curves higher than the recommended IIW curve for flush-ground butt joints excluding misalignment effects (FAT130 (Hobbacher 2016)) and is thus thought to be applicable for the case of vanishing notch effect (Baumgartner 2017).

Four different possibilities for applying the stress averaging approach to welded joints are found in the literature (see (Zhang et al. 2012; Baumgartner et al. 2013; Marulo et al. 2017; Baumgartner et al. 2019)), which are:

1. An effective stress is calculated for every possible path along a radius and the maximum effective stress is used, or by
2. Averaging from the point of maximum principal stress, or by
3. Averaging from the weld toe perpendicular to the direction of loading, or
4. Along the notch bisector.

According to Marulo et al. (2017), the first might be more accurate, but is computationally more demanding. This is why, the second is typically applied—as in this study, for reasons of comparability.

At sharp notches such as weld toes and roots, the crack initiation phase is rather short compared to the propagation phase (Maddox 2002). Since crack propagation is dominated by mode I loading (tension crack opening)—which is directly linked to the direction of first principal stress (Richard and Sander 2012)—the averaging path coincides with the crack propagation direction.

In order to perform fatigue assessment of welds or notched components based on effective stresses, values of micro-structural support length can either be taken from Figure 9 or standards such as the German (FKM-Richtlinie). Alternatively, if a TCD method is

applied to a new problem for which no data is readily available, the inverse problem can be solved and ρ^*, for example, is estimated from fatigue test data of various notch shapes (cf. Baumgartner et al. (2015) and Santus et al. (2018)). In that respect, the value ρ^* at which a minimum of the scatter ratio $1/T_S$ of the experimental data occurs is assumed to be representative for the micro-structural support effect of the material. The scatter ratio $1/T_S$ is calculated with

$$1 \,/\, T_S = \frac{\Delta\sigma_{R,10\%}}{\Delta\sigma_{R,90\%}} \tag{3}$$

, where $\Delta\sigma_{R,10\%}$ and $\Delta\sigma_{R,90\%}$ are the fatigue strength at 2 million cycles for a probability of survival P_s of 10% and 90%.

In the literature, scatter ratios of $1/T_s = 1.77$ (Baumgartner et al. 2015) and $1/T_s = 2.2$ (Marulo et al. 2017) are reported for the stress averaging approach. For the effective notch stress with radius $\rho_{ref} = 1$ mm and SED method a scatter ratio of $1/T_s = 1.5$ is stated in (Fischer et al. 2016c); however, a much larger variety and number of specimens were analysed in Marulo et al. (2017) than was used as the basis for the effective notch stress method. Comparing the results for the same dataset assessed by the stress averaging approach and the notch stress method with radius $\rho_{ref} = 0.05$ mm, a lower scatter was obtained for the first method in (Marulo et al. 2017) with $1/T_s = 2.2$ and $1/T_s = 3.1$, respectively.

As mentioned earlier, the micro-structural support length of $\rho^* = 0.4$ mm for welds is based on the assumption that the microstructure of welds resembles cast iron with a yield strength of approximately 300 MPa (Lazzarin et al. 2004); nevertheless, for welds with sharp notches $\rho^* = 0.4$ has been confirmed for a variety of steel strength grades (Baumgartner et al. 2015; Schmidt et al. 2015). It is thus reasonable to assume that the micro-structural support length ρ^* depends not only on the static strength of the material, but also on the notch acuity. Baumgartner et al. (2019), for example, showed a clear material strength dependence for post-weld treated joints with smooth weld transitions described by large weld toe radii.

Interestingly, for welded high-strength thin-walled specimens a similar material strength dependence was observed by Marulo et al. (2017). They observed a lower fatigue strength for higher-strength steels compared to mild steel grades if assessed by the same micro-

structural support length ρ^*, which agrees well with Neuber's theory (see Figure 9).

It is generally assumed that the fatigue strength of welded joints is independent of material strength in as-welded state (Maddox 2002). Thus, in order to yield equal fatigue strength based on effective stresses, the higher-strength steels require a shortened intrinsic micro-structural support length ρ^*. The assumption that the micro-structural support length of ρ^* of non-welded samples should decrease for higher-strength materials is generally agreed upon in the literature, see Radaj and Vormwald (2007).

It is well known, that static strength—typically quantified by yield strength σ_{YS} and ultimate tensile strength σ_{UTS}—increases at low temperatures, see (Ehlers and Østby 2012; Paik et al. 2017). As a result, from the relation between material strength and micro-structural support length ρ^* presented in Figure 9, a decrease of ρ^* is assumed for sub-zero temperatures.

Based on fracture mechanics, Tanaka (1983) showed that the micro-structural support length ρ^* is linked to the transition point between short and long crack growth defined by the fatigue limit of plain specimens $\Delta\sigma_0$ and the fatigue crack growth threshold ΔK_{th}, given by

$$\rho^* \approx \frac{2}{\pi}\left(\frac{\Delta K_{th}}{\Delta\sigma_0}\right)^2 \tag{4}$$

Consequently, if the fatigue limit of plain specimens $\Delta\sigma_0$ and the fatigue crack growth threshold ΔK_{th} at sub-zero temperatures are known it is possible to estimate the micro-structural support effect defined by the micro-structural support length ρ^* or vice versa.

Neuber's hypothesis (Neuber 1958)—that it is not the theoretical peak stress obtained at sharp notches that governs fatigue life, but rather the stress field in the close vicinity of notches—has led to the development of various stress-based fatigue assessment methods but also methods based on other fatigue-driving parameters. Another method that takes the support effect of the material directly into account is the averaged strain energy density method (or just the strain energy density method).

2.5 | Averaged strain energy density method

2.5.1 | Development of the averaged strain energy density method

The size of the fatigue-effective zone surrounding a notch is thought to be about two to five times the grain size and thus ranges from 0.03 mm to 0.50 mm (Berto and Lazzarin 2009). The idea behind this assumption is that this zone defines the border between continuum and micro-mechanics. Due to this, the fatigue-effective zone provides a measure for the area where continuum mechanics analytical solutions are flawed by inhomogeneities such as micro-cracks, dislocations, and grain boundaries (Berto and Lazzarin 2009).

The strain energy density method was initially introduced in order to assess fracture of cracked components. Assuming a pointed notch or crack tip, this leads to a stress singularity. Consequently, in order to solve the problem of stress singularity, the stress intensity factor (SIF) was proposed by Griffith (1921); however, due to the sharpness of notch radius it is incapable of predicting the crack growth direction accurately. As a result, among many other methods, the strain energy density factor S was introduced by Sih (1974) to solve mixed-mode fracture problems. Fractures were expected to happen if the strain energy density factor S (product of the strain energy density by a critical distance from the point of singularity) reached a critical value S_c. Two years later, Gillemot (1976) introduced the critical absorbed energy up to fracture per unit volume W_c as a fracture criterion for tensile tests of notched components and brittle fracture sensitivity. Later, the strain energy density method was extended to fatigue of notched and plain specimens, see Glinka (1985); nevertheless, the strain energy density is also infinite at crack and pointed notch tips.

The breakthrough of the strain energy density method is, however, linked to the development of another concept. In the early 1990s, Nui et al. (1994) introduced the notch stress intensity factor (N-SIF) concept for the assessment of brittle fractures, which was based on William's equations for singular stress fields (Williams 1956). It was later extended to fatigue crack initiation assessment (Boukharouba et al. 1995; Verreman and Nie 1996), similar to the strain energy density method. Compared to the strain energy density method, the N-SIF is asymptotic at crack and notch tips up to a certain radius and opening angle size, see Atzori et al. (2002) and Lazzarin et al. (2009). Moreover, the N-SIF

coincides with the linear elastic fracture mechanics stress intensity factor of a planar crack (with depth equal to the slit half-length) for an opening angle $2\alpha = 0°$ (Lazzarin and Tovo 1998; Fischer et al. 2016c).

Similar to the effective stress methods based on the TCD, the N-SIF method is capable of accounting for scale-effects, see Lazzarin and Tovo (1998) and Atzori et al. (2002)); yet, limitations arise from its requirement for extremely refined FE meshes and inability to take support effects into account. Hence, Lazzarin and Zambardi (2001) suggested using the averaged strain energy density $\overline{W}$ for fatigue and fracture failure assessment. They showed that $\overline{W}$ is finite at a volume surrounding cracks and notches and they linked $\overline{W}$ to the mode I and II N-SIFs.

Instead of analysing the asymptotic stress behaviour in the close proximity of the notch tip to calculate N-SIFs, the strain energy density is averaged in a small volume around the notch tip defined by the control radius R_C. The (averaged) SED method[1] has since then been applied to a variety of fatigue and fracture problems, such as fatigue and fracture strength of notched components at high temperatures (Berto et al. 2013, 2014; Gallo et al. 2015; Bourbita and Remy 2016; Gallo and Berto 2016).

The main advantages of the SED method are the underlying physical relation to the material fracture behaviour via the micro-structural support effect hypothesis and to the N-SIF, as well as the flexibility in FE meshing, see (Lazzarin et al. 2010; Fischer et al. 2016a; Foti et al. 2020; Foti et al. 2021). Contrary to the N-SIF method, the SED method is incapable of predicting crack propagation directions; yet, coupling the SED method with the maximum tangential stress criterion proposed by Erdogan and Sih (1963) solves this problem. Nonetheless, the SED method has to be understood as a crack initiation failure criterion while the N-SIF can be applied in the medium life regime, see (Lazzarin et al. 2008a, 2009; Fischer et al. 2016c).

In the following paragraphs the background of the SED method will be introduced as well as its relation to the micro-structural support effect hypothesis. In Section 2.5.3 the application of the SED method to welded joints is introduced and the link to linear elastic fracture mechanics is presented.

[1] The abbreviation 'SED' hereafter refers only to the averaged strain energy density method according to Lazzarin and co-workers.

2.5.2 | Introduction of the averaged strain energy density method and its relation to the micro-structural support effect hypothesis

Under plain strain condition, the total elastic strain energy density $\overline{W}$ averaged in the area defined by the control radius R_C is calculated by:

$$\overline{W} = \frac{e_1}{E}\left[\frac{K_1^N}{R_C^{1-\lambda_1}}\right]^2 + \frac{e_2}{E}\left[\frac{K_2^N}{R_C^{1-\lambda_2}}\right]^2 \tag{5}$$

where K_1^N and K_2^N are mode I and II N-SIFs, E is the Young's modulus and e_1, e_2 are correction factors, which depend on the infinitesimal strain theory (plane stress/plain strain), notch opening angle 2α, and Poisson's ratio ν. The parameter λ_1 and λ_2 are the eigenvalues of the leading terms of Williams' stress field solution for the mode I and II N-SIFs (K_1^N and K_2^N).[2] The three crack/notch modes used in fracture mechanics are presented in Figure 11(a). Using polar coordinates, the mode I (tension notch/crack opening) and II (in-plane shear crack opening) N-SIFs were defined by Lazzarin and Tovo (1996) as:

$$K_1^N = \sqrt{2\pi}\lim_{r\to 0^+} r^{1-\lambda_1}\sigma_{\Theta\Theta}(r, \Theta = 0) \tag{6}$$

$$K_2^N = \sqrt{2\pi}\lim_{r\to 0^+} r^{1-\lambda_2}\sigma_{r\Theta}(r, \Theta = 0) \tag{7}$$

where σ_{rr}, $\sigma_{r\Theta}$, and $\sigma_{\Theta\Theta}$ are the stress components in polar coordinates (r, Θ) as for Williams' stress field solution around cracks (Williams 1956), see Figure 11(b).

The eigenvalues of the Williams' stress field solution for the N-SIF K_1^N and K_2^N for modes I and II (λ_1, λ_2) are obtained from:

$$\text{Mode I: } \sin(\lambda_1) = -\lambda_1 \sin(\gamma) \tag{8}$$

$$\text{Mode II: } \sin(\lambda_2) = \lambda_2 \sin(\gamma) \tag{9}$$

where $\gamma = 2\pi - 2\alpha$ is the angle between the notch bisector and the notch flanks.

[2] To help distinguishing between crack and notch stress intensity factors, Roman numerals are used for SIFs and Arabic for N-SIFs following Lazzarin's notation.

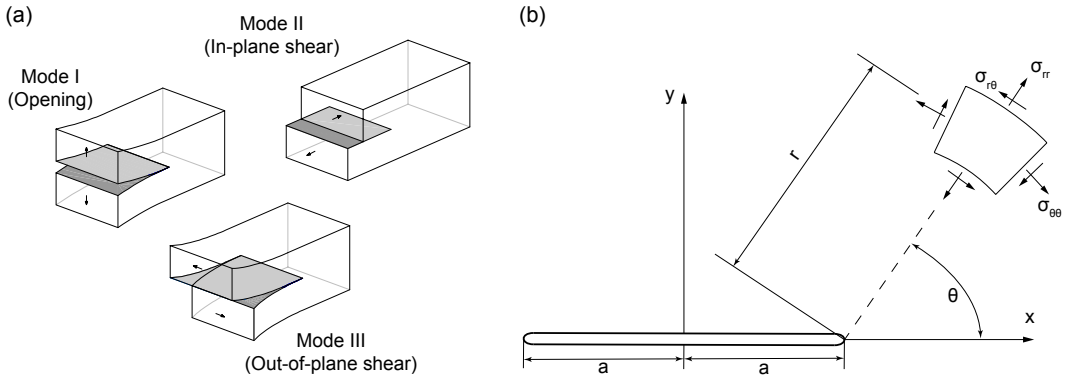

Figure 11. The three crack/notch modes in fracture mechanics (a) and stress components in the vicinity of a through-thickness crack with crack length $2a$ in polar coordinates (b)

Finally, the control radius R_C—for plane strain condition—can be determined using Beltrami's failure criterion from the following expression (Yosibash et al. 2004):

$$R_C = \frac{(1+\nu)(5-8\nu)}{4\pi}\left(\frac{\Delta K_{th}}{\Delta\sigma_0}\right)^2 \tag{10}$$

with ΔK_{th} as the fatigue crack growth threshold for long cracks and $\Delta\sigma_0$ as the fatigue limit of smooth base material specimens. It is important to note that the control radius is thus a material property, which is independent of the opening angle (Lazzarin and Zambardi 2001). For different types of notches (not only welds), different definitions of critical areas have been proposed, which are presented in Figure 12.

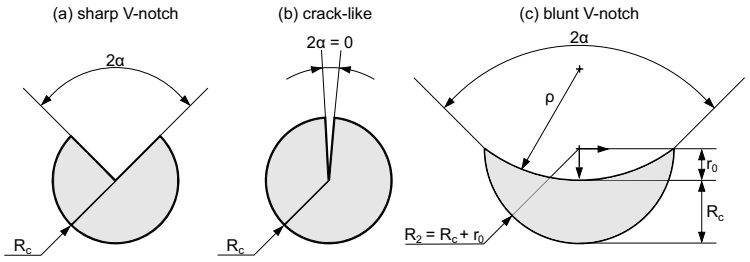

Figure 12. Definitions of the strain energy density method's control area for sharp V-notches (a), crack-like notches (b), and blunt V-Notches with real radius r_0 (c) based on Berto and Lazzarin (2009), adopted from Braun et al. (2020a)

After introducing the El Haddad-Smith-Topper parameter a' (El Haddad et al. 1979), which can be used to predict the transition between short and long fatigue crack arrest,

with:

$$a^{'} = \frac{1}{\pi}\left(\frac{\Delta K_{th}}{\Delta \sigma_0}\right)^2 \tag{11}$$

Eq. (10) becomes:

$$R_C = 0.845 a' \tag{12}$$

under plane strain condition and if $\nu = 0.3$. As a result, the control radius R_C is directly related to the transition behaviour of the material via the El Haddad-Smith-Topper parameter $a^{'}$.

Recalling Eq. (4), a connection between Neuber's micro-structural support length ρ^* and the El Haddad-Smith-Topper parameter $a^{'}$ is unambiguous ($\rho^* = 2a'$). As a consequence, Tanaka (1983) provided a closed-form solution for fatigue strength assessment of deep (crack-like) notches under mode I and mode III (out-of-plane shear notch opening) loading, which was later extended to notches with low notch sensitivity by Lazzarin et al. (1997) and linked to the TCD method by Taylor (1999).

The control radius R_C of the SED method is thus directly related to the micro-structural support length ρ^* through the relation to the El Haddad-Smith-Topper parameter $a^{'}$. Furthermore, it is also directly related to the material characteristic length L of the TCD method based on Taylor and Hoey's assumption (Taylor and Hoey 2009):

$$\rho^* = 2L \tag{13}$$

which yields:

$$a^{'} = L \tag{14}$$

This relation is thought to be limited to stress ratios $R \geq 0$, since crack closure effects are not covered by the El Haddad-Smith-Topper parameter (Radaj and Vormwald 2007); nonetheless, for components loaded in tension, this relation allows derivation of the control radius R_C from either the El Haddad-Smith-Topper parameter $a^{'}$ or material characteristic length L. Interestingly, Silva et al. (2012) showed that Eq. (11) and Eq. (14) can successfully be applied to estimate the fatigue crack growth threshold ΔK_{th} for notch radii $r < 1$ mm and $R = -1$.

Recent research results suggest that Eq. (13) is influenced by the notch geometry and is not universal (Silva et al. 2012; Yin et al. 2015; Santus et al. 2018). The experimental results by Silva et al. (2012), for example, clearly show a lower prediction accuracy for the stress averaging approach and larger notch radii compared to components with sharp notches. This will be of importance for the discussion of results obtained by means of the stress averaging approach for sub-zero temperatures. Furthermore, Radaj and Vormwald (2007) argues that the relation between the material characteristic length L and the El Haddad-Smith-Topper parameter a' (Eq. (14)) can be assumed to be correct as El Haddad et al. (1979) incorporated Peterson's theory of critical distance (Peterson 1959) in their theory and both methods are experimentally validated. In recent years, efforts were made by several authors to prove the equality of the different TCD methods for various relevant fatigue loading cases including torsional and multiaxial fatigue (Susmel 2008; Susmel and Taylor 2013), and under extreme loading conditions such as high temperatures (Louks and Susmel 2015).

Interestingly, a recently published paper by Benedetti and Santus (2020) observed that the normalized coefficient of variation during estimation of L increases with decreasing notch acuity, i.e. increasing notch radius and opening angle. This could explain the increasing difference between various TCD methods and the differences in prediction accuracy obtained by various authors as L is simply more difficult to obtain for larger notch radii. The fact that fatigue datasets are often too small to accurately predict the mean fatigue strength (Martin et al. 2011) and the increasing scatter with decreasing notch acuity (Haibach 2006) supports this hypothesis.

Next, an introduction on the application of the SED method for welded joints is given and its relation to linear elastic fracture mechanics is discussed. This relation will later be used to extend the SED method by incorporating temperature-related changes of the micro-structural support effect in Section 6.4.3.

2.5.3 | Application of the averaged strain energy density method to welded joints

One problem in fatigue assessment methods is the arbitrariness of modelling welded joints due to varying weld shape and the related difficulty in defining representative weld shapes

(Lazzarin et al. 2008a). There are basically two options to generalize weld shapes in state-of-the-art fatigue methods. The first is the rounding of the weld shape with a reference radius, as presented for the effective notch stress method and the stress averaging approach. The alternative is to treat weld toes and roots as pointed notches without a radius.

Assuming V-type notches at weld toe and root radii, Lazzarin and Tovo (1998) showed that N-SIFs can be used as fatigue parameters for the life prediction of cyclically loaded welded joints and derived a N-SIF design curve for welded joints. Although the mode I and II N-SIFs only quantify the magnitude of asymptotic stress distribution based on Williams' stress field solution (Williams 1956), they can be applied for fatigue assessment of sharp corner notches. The reason for this is that a large amount of the crack propagation life of sharply notched components is related to short fatigue crack growth in the zone governed by the V-notch singularity (Lazzarin et al. 2008a). Since the SED method is directly derived from the N-SIF concept, the same assumptions apply to the SED method and so weld toes and weld roots are modelled as V-type notches. Thereafter, the elastic strain energy density $\overline{W}$ is averaged in the volume (area for two dimensional models) around the weld toe and root—defined by the control radius $\mathrm{R_C}$, see Figure 13.

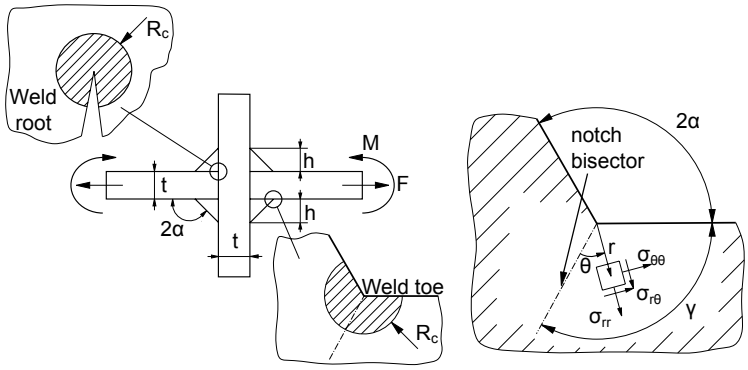

Figure 13. Definitions of the strain energy density method based on Lazzarin et al. (2008b), taken from Braun et al. (2020a)

Assuming a constant flank angle for fillet-welded joints with an opening angle of approximately $2\alpha = 135°$, the mode II contribution becomes non-singular ($1 - \lambda_2 = -0.302$) and thus only mode I N-SIF $\mathrm{K}_1^{\mathrm{N}}$ is required to describe the fatigue strength of welded joints

(Livieri and Lazzarin 2005). Hence, under cyclic loading Eq. (5) becomes:

$$\Delta\overline{W} = \frac{e_1}{E}\left[\frac{\Delta K_1^N}{R_C^{1-\lambda_1}}\right]^2 \tag{15}$$

with the control radius being determined by:

$$R_C = \left(\frac{\sqrt{2e_1}\Delta K_1^N}{\Delta\sigma_0}\right)^{\frac{1}{1-\lambda_1}} \tag{16}$$

where ΔK_1^N is the mode I N-SIF mean reference fatigue strength for fillet-welded joints (i.e. 135° opening angle) and $\Delta\sigma_0$ is the mean reference fatigue strength of butt welds without notch (flush-ground) for welded joints. Both quantities were derived for $R = 0$ and cycles to failure $N_f = 5 \times 10^6$ in the aforementioned study by Lazzarin and Tovo (1998). Assessing fatigue test results from 12 different test series with thicknesses ranging from 13 to 100 mm, they obtained a mode I fatigue strength of $\Delta K_1^N = 211$ MPa mm$^{0.326}$. Combined with fatigue test results on flush-ground butt-welded joints by Atzori and Dattoma (1983) and Taylor et al. (2002) ($\Delta\sigma_0 = 155$ MPa), a control radius $R_C = 0.28$ mm was derived for welded joints, see Livieri and Lazzarin (2005). Based on the so obtained control radius R_C and the data by Lazzarin and Tovo (1998) to derive the N-SIF design scatter band, plus some new fatigue test results, the SED range-life ($\Delta\overline{W}$ – N) design scatter band was derived, see (Lazzarin et al. 2003, 2008a,b) and Figure 14. The underlying idea is that one scatter band represents the fatigue strength of welded joints and all effects that are influencing the local stress state are covered by determining the averaged SED within the control area. This idea follows Haibach's (1968) work on uniform or normalized scatter bands that are independent of notch or weld detail classes and stress ratio (Radaj et al. 2006).

The underlying assumption of a large opening angle for Eq. (16) is violated for weld roots ($2\alpha \approx 0°$); yet, the contribution of mode II is much smaller than the contribution of mode I. Thus, reduced values of ΔK_1^N were reported by Livieri and Lazzarin (2005) for weld root failure, i.e. $\Delta K_1^N = 180$ MPa mm$^{0.5}$. Assuming a crack-like notch shape at weld roots ($2\alpha = 0°$, $\lambda_1 = 0.5$, and $e_1 = 0.133$) and the weld root behaves like a crack ($\Delta K_1^N = \Delta K_{th}$), Eq. (16) becomes:

$$R_C = \frac{0.85}{\pi}\left(\frac{\Delta K_{th}}{\Delta\sigma_0}\right)^2 = 0.85a' \tag{17}$$

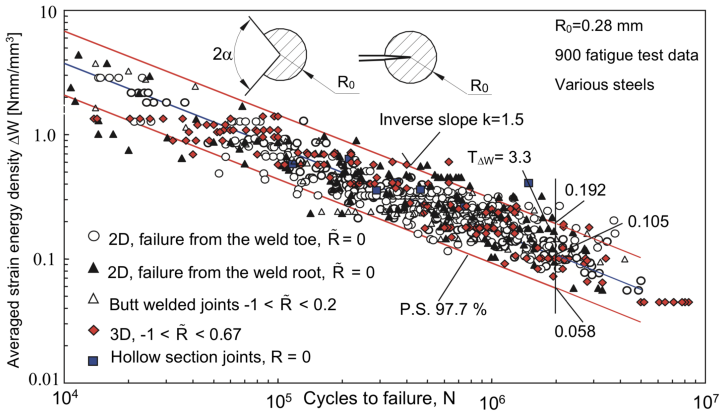

Figure 14. Scatter band of the strain energy density method for a control radius R_C = 0.28 mm (R_0 in the figure) derived from tests of different structural details over a wide range of nominal load ratios $\widetilde{R}$, taken from Berto and Lazzarin (2009) (reproduced with permission from Elsevier)

and similar to notched components, a link to the El Haddad-Smith-Topper parameter a' is obtained. For V-shaped notches at weld toes the relation between both quantities can be derived based on linear elastic fracture mechanics. This will be presented in Section 2.5.4. Before this, however, a small note on recommended control radii is given below.

To derive R_C, fatigue test data of 20 test series on fillet-welded joints was evaluated to obtain ΔK_1^N and fatigue test data of flush-ground butt joints by Atzori and Dattoma (1983) was used for $\Delta\sigma_0$. A recent review of the SED method by Fischer et al. (2016b,c) revealed that the assumed fatigue limit $\Delta\sigma_0$ of flush-ground butt welds of 155 MPa (slope exponent $k = 3.75$) is on the lower end of data found in the literature; yet, this value agrees with recommendations by the IIW (Hobbacher 2016) and Eurocode 3 (EN 1993–1–9:2005), and data by Taylor et al. (2002). While the scatter of the test series on fillet-welded joints in terms of mode I N-SIF (Lazzarin and Zambardi 2001) is rather small (coefficient of variation $CV = SD/mean$ of 8.8%), the scatter of $\Delta\sigma_0$ amounts to $CV = 24.7\%$, see Table 1. The majority of data in the literature is found for a number of cycles to failure of 2×10^6. To avoid an extrapolation that does not match the reported slope exponents k, the scatter is evaluated here for this number of cycles instead of 5×10^6 cycles.

Table 1. Data on fatigue strength of smooth (flush-ground) butt-welded joints $\Delta\sigma_0$ found in the literature, extended from a summary presented by Fischer et al. (2016c)

Reference	Fatigue strength $\Delta\sigma_0$ at $N_f = 2\times10^6$ ($R = 0$, $P_s = 50\%$) in MPa	Slope k	Comments
Atzori and Dattoma (1983)	210	3.75	Obtained by Fischer et al. (2016c) assuming a slope $k = 3.75$
IIW fatigue design recommendations (Hobbacher 2016) and Eurocode 3 (EN 1993–1–9:2005)	153	3	$\Delta\sigma_{50\%} = \Delta\sigma_{97.5\%} \times 1.366$ for FAT112 according to Fricke (2012)
HSE Research Report 090 on flush-ground girth welds (Zhang et al. 2003)	$\approx$ 200	$\approx$ 3	Estimated based on the regression line presented in Figure 4
Olivier and Ritter (1979)	192	3.75	Data statistically reassessed by Fischer et al. (2016c) assuming a slope $k = 3.75$
Reemsnyder (1969)	310	3.75	Data statistically reassessed by Fischer et al. (2016c) assuming a slope $k = 3.75$
Taylor et al. (2002)	207	3	Obtained from reported inverse slope (-0.33)
Mean	212		
Standard deviation (SD)	52.3		
Coefficient of variation (CV)	24.7%		

When Fischer et al. (2016b,c) reassessed the original data, they derived different radii for weld toe and weld root assessment than the initially proposed radius $R_C = 0.28$ mm. The reason for the difference is related to misalignment effects that were not considered while deriving the N-SIF scatter band for weld toe failure. Assuming an additional stress magnification of 5% typically included in *S–N* curves, a difference of about 10% was proposed for the weld toe failures N-SIF scatter band. Hence, control radii of $R_C = 0.32$ mm and $R_C = 0.325$ mm for weld toe and weld root were derived, respectively; however, the scatter band of the SED method (Figure 14) was unchanged.

2.5.4 | Relation of the averaged strain energy density method to linear elastic fracture mechanics

As mentioned earlier, it can be shown that the mode I N-SIF coincides with the linear elastic fracture mechanics SIF of a planar crack with depth equal to the slit half-length for an opening angle $2\alpha = 0°$. Consequently, besides the relation of the N-SIF and the SED

approach to the micro-structural support effect hypothesis, a direct link to linear elastic fracture mechanics exists.

In addition to the equality of the mode I N-SIF and the SIF for $2\alpha = 0°$, Atzori et al. (2008) presented a more general relation between both methods, which is summarized below and extended to present the relation of the SED method and linear elastic fracture mechanics. Furthermore, this relation forms the basis for the verification of the extension of the SED method to sub-zero temperatures.

Starting from Eq. (6) and Eq. (7), Williams' stress field equations can be reformulated in terms of mode I and II N-SIFs. In polar coordinates, the mode I stress distribution becomes (Lazzarin and Tovo 1996):

$$\begin{Bmatrix} \sigma_{\Theta\Theta} \\ \sigma_{rr} \\ \sigma_{r\Theta} \end{Bmatrix} = \frac{1}{\sqrt{2\pi}} \frac{r^{\lambda_1 - 1} K_1^N}{(1+\lambda_1) + \chi_1 (1-\lambda_1)} \times \left[\begin{Bmatrix} (1+\lambda_1)\cos(1-\lambda_1)\Theta \\ (3-\lambda_1)\cos(1-\lambda_1)\Theta \\ (1-\lambda_1)\sin(1-\lambda_1)\Theta \end{Bmatrix} + \chi_1 (1-\lambda_1) \begin{Bmatrix} \cos(1+\lambda_1)\Theta \\ -\cos(1+\lambda_1)\Theta \\ \sin(1+\lambda_1)\Theta \end{Bmatrix} \right] \tag{18}$$

where χ_1 is the auxiliary parameter for mode I, which depends on the notch opening angle 2α.

$$\chi_i = -\frac{\sin[(1-\lambda_i)\gamma\pi/2]}{\sin[(1+\lambda_i)\gamma\pi/2]}, \text{ with } \gamma = 2\pi - 2\alpha \tag{19}$$

Similarly, the stress field for mode II can be written as:

$$\begin{Bmatrix} \sigma_{\Theta\Theta} \\ \sigma_{rr} \\ \sigma_{r\Theta} \end{Bmatrix} = \frac{1}{\sqrt{2\pi}} \frac{r^{\lambda_2 - 1} K_2^N}{(1-\lambda_2) + \chi_2 (1+\lambda_2)} \times \left[\begin{Bmatrix} -(1+\lambda_2)\sin(1-\lambda_2)\Theta \\ -(3-\lambda_2)\sin(1-\lambda_2)\Theta \\ (1-\lambda_2)\cos(1-\lambda_2)\Theta \end{Bmatrix} + \chi_2 (1+\lambda_2) \begin{Bmatrix} -\sin(1+\lambda_2)\Theta \\ \sin(1+\lambda_2)\Theta \\ \cos(1+\lambda_2)\Theta \end{Bmatrix} \right] \tag{20}$$

According to Atzori et al. (2008), the stress intensity factor for mode I (K_I) can be expressed in a closed-form solution by means of Albrecht-Yamada's (1977) simplified method,

assuming a through-thickness crack and crack growth along the Θ-direction (i.e. perpendicular to the maximum tangential stress $\sigma_{\Theta\Theta}$):

$$K_I = Y\sqrt{\pi a}\frac{2}{\pi}\int_0^a \frac{\sigma_{\Theta\Theta}}{\sqrt{a^2-r^2}}dr = Y\sqrt{\pi a}\left[\sigma_{\Theta\Theta}\mid_{r=a} - \frac{2}{\pi}\int_0^a \arcsin\left(\frac{r}{a}\right)\frac{d\sigma_{\Theta\Theta}}{dr}dr\right] \tag{21}$$

with Y as crack geometry factor (1.122 for a through (or edge) crack in a semi-infinite plate). Under the premise of crack growth along the notch bisector of a fillet-welded joint ($2\alpha = 135°$, $\Theta = 22.5°$), the tangential stress component $\sigma_{\Theta\Theta}$ can be expressed as a function of mode I and II N-SIF as follows:

$$\sigma_{\Theta\Theta} = 0.361 r^{-0.326} K_1^N + 0.322 r^{0.302} K_2^N \tag{22}$$

This assumption is generally valid in the early stage of fatigue crack growth. Once the crack leaves the close proximity of the weld toe notch, it tends to grow perpendicular to the plate surface (Atzori et al. 2008). Finally, by inserting Eq. (22) in Eq. (21) one obtains the relation between the stress intensity factor for mode I (K_I) and the mode I and II N-SIFs for fillet-welded joints—with V-shaped notch and $2\alpha = 135°$:

$$K_I\left(\Theta = 22.5°\right) = Y\sqrt{\pi a}\left(0.479 a^{-0.326} K_1^N + 0.269 a^{0.302} K_2^N\right) \tag{23}$$

As the mode II N-SIF K_2^N is non-singular for this opening angle, it does not contribute to the stress field close to the notch tip (below $r/t < 0.1$ (Lazzarin and Tovo 1998)). This fact is of particular importance for non-propagating cracks (i.e. at the fatigue crack growth threshold ΔK_{th}). Since the crack does not leave the asymptotic stress field at the notch tip,[3] it is purely governed by the mode I contribution. Hence, Eq. (23) becomes:

$$K_I\left(\Theta = 22.5°\right) = Y\sqrt{\pi a}\left(0.479 a^{-0.326} K_1^N\right) \tag{24}$$

which clearly shows the linear relation between the stress intensity factor for mode I (K_I) and the mode I N-SIF K_1^N.

Assuming that the SIF value necessary to nucleate a crack at a weld toe or root is equal to the threshold ΔK_{th} of the fatigue crack growth rate at 5×10^6 cycles (Atzori et al. 2008),

[3] Experimental studies showed that cracks initiated at notches may typically be arrested within a region of depth corresponding to one to two times the material characteristic length parameter L (Silva et al. 2012)

the N-SIF threshold value $\Delta K_{1,th}^{N}$ is linearly related to ΔK_{th}. This fact will later be used to relate the change of fatigue crack growth threshold data obtained from the literature (Figure 5) to the proposed extension of the SED method for sub-zero temperatures.

Obviously, such closed-form solutions as Albrecht-Yamada's (1977) simplified method are only valid for a small crack growth increment and require assumptions for initial crack length a_i; nevertheless, as the study by Atzori et al. (2008) has shown, they are well suited to predict the fatigue strength of fillet-welded joints. Furthermore, the assumption of a through-thickness crack is generally only applicable once the crack has reached a significant size; however, as can be seen from Eq. (21) to Eq. (24), it does linearly influence the relation between K_1^N and K_I. Consequently, Atzori et al. (2008) proposed an engineering approach to estimate the initial crack length a_i at the fatigue limit by relating it to the El Haddad-Smith-Topper parameter $a^{'}$ with:

$$a_i = \frac{a^{'}}{Y^2} \tag{25}$$

This assumption seems valid, as it agrees with Härkegård's (1981) extension of the fatigue limit relation for short and long cracks according to El Haddad et al. (1979) for an arbitrary crack geometry factor Y with crack length a:

$$\Delta\sigma_R = \frac{\Delta K_{th}}{Y\sqrt{\pi\,(a + a^{'})}} = \frac{\Delta\sigma_0}{\sqrt{1 + a/a^{'}}} \tag{26}$$

This relation is typically presented in form of the Kitagawa-Takahashi diagram (Kitagawa and Takahashi 1976), see Figure 15. They showed that the fatigue limit of a cracked component $\Delta\sigma_R$ can be determined from the stress intensity factor threshold for long cracks ΔK_{th} with effective crack length $a + a^{'}$. The El Haddad-Smith-Topper parameter $a^{'}$, is thus sometimes referred to as an 'intrinsic' crack length (Wormsen et al. 2008).

For short cracks ($a \ll a^{'}$), the fatigue limit asymptotically approaches the fatigue limit of plain specimens $\Delta\sigma_0$. For physically long cracks ($a \gg a^{'}$), the crack fatigue strength is defined by the fatigue crack growth threshold of long cracks ΔK_{th}.

From the Kitagawa-Takahashi diagram (Kitagawa and Takahashi 1976) and Eq. (26), it can be seen that the fatigue limit is closely related to the initial crack or defect size and the El Haddad-Smith-Topper parameter $a^{'}$. The SED method and in particular the control radius R_C are thus linked to the micro-structural support effect hypothesis through the El

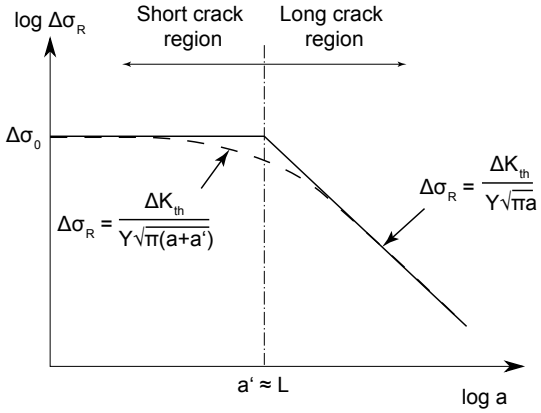

Figure 15. Kitagawa-Takahashi diagram presenting the relation between physically short and long non-propagating cracks and the relation to the micro-structural support effect hypothesis via the El Haddad-Smith-Topper parameter $a^{'}$

Haddad-Smith-Topper parameter $a^{'}$ (Eq. (13) and Eq. (14)) and to linear elastic fracture mechanics through the N-SIF method. Furthermore, Atzori et al. (2008) definition of the initial crack length a_i at the fatigue limit (5×10^6 cycles) has to be understood as a crack length in the order of magnitude of the El Haddad-Smith-Topper 'intrinsic' crack length $a^{'}$. It is thus large enough that linear elastic fracture mechanics can be applied and the assumption of a crack-like notch at the V-shaped fillet weld is reasonable.

To account for the opening angle of sharp V-notches ($2\alpha > 0°$), which behave similarly to crack-like notches, Atzori and co-workers presented a generalized version of the Kitagawa-Takahashi diagram, see Atzori and Lazzarin (2001) and Atzori et al. (2003) and Figure 16. This permits an estimation of the fatigue strength of components weakened by cracks or notches using a single diagram which requires only the El Haddad-Smith-Topper parameter $a^{'}$.

Instead of the crack length a, an effective dimension ($\alpha_\xi^{1/\xi} a$) was introduced, where ξ is the degree of singularity of the Williams' stress distributions[4] ($\xi = 1 - \lambda_1$) (Atzori et al. 2005). For this goal, a non-dimensional shape coefficient $\alpha_\xi^{'}$ was proposed which depends on the component geometry, loading type, and notch opening angle (Atzori et al. 2005). Due to this, a characteristic length parameter of V-notched components $a^{N'}$ (the transition point between short and long fatigue crack growth of V-notched components)

[4]Originally, Atzori et al. (2008) used γ to define the degree of singularity, which is replaced by ξ to avoid confusion with the notch bisector angle.

can be derived for varying V-notch opening angles, which is related to the El Haddad-Smith-Topper 'intrinsic' crack length $a^{'}$ through the shape coefficient α'_{ξ}. The latter can be derived through various methods, e.g. averaged strain energy density, linear elastic fracture mechanics, or the point method (critical distance approach of the TCD methods), see Atzori et al. (2005) for further information.

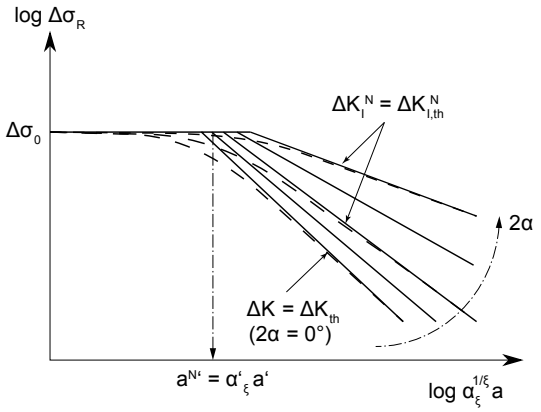

Figure 16. Generalized Kitagawa-Takahashi diagram for V-type notches based on Atzori et al. (2005)

If $a^{N'}$ is determined experimentally, it can be used to obtain the El Haddad-Smith-Topper parameter $a^{'}$ and thereby a measure of the micro-structural support effect around notches (e.g. at weld toe and root notches). The relation between $a^{'}$ and $a^{N'}$ (presented in Figure 16) was introduced in order to keep the El Haddad-Smith-Topper parameter $a^{'}$ a material constant; yet, it is restricted to constant plain specimen fatigue strength $\Delta\sigma_0$.

$$a^{N'} = \alpha'_{\xi} a' \tag{27}$$

If the plain specimen fatigue strength $\Delta\sigma_0$ and the fatigue crack growth threshold of long cracks ΔK_{th} change (assumed for sub-zero temperatures), $a^{N'}$ may be derived similarly to $a^{'}$ from:

$$a^{N'} = \left(\frac{\Delta K_{th}^{N}}{\sqrt{\pi}\Delta\sigma_0} \right)^{\frac{1}{\xi}} \tag{28}$$

where $\Delta K_{1,th}^{N}$ is treated as a material parameter (i.e. V-notch threshold N-SIF) that can be related to the SIF threshold for long cracks ΔK_{th} by matching the experimental conditions

of plain and cracked specimens for various local methods with:

$$\Delta K^{N}_{1,th} = \beta \cdot \Delta\sigma_0^{1-2\xi} \cdot \Delta K^{2\xi}_{th} \tag{29}$$

The geometrical correction factor β depends on the notch opening angle and the chosen local method, see Atzori et al. (2005). Finally, the non-dimensional shape coefficient α'_ξ is related to β in the following form:

$$\alpha'_\xi = \beta^{1/\xi}\pi^{\left(1-\frac{1}{2\xi}\right)} \tag{30}$$

This relation will later be applied to estimate the change of micro-structural support effect in welded connections at sub-zero temperatures.

Almost simultaneously to the proving of the link between the SED method and linear elastic fracture mechanics by Atzori et al. (2008), Berto and Lazzarin (2007) presented a relation of the SED concept to the *J*-integral method by Rice (1968) for elastic-plastic fracture mechanics—thus extending the scope of the SED method to local and global plasticity, which further emphasized its close relation to fracture mechanics. This approach was recently extended to cyclic elastic-plastic fatigue assessment, see Benedetti et al. (2020), which is, however, outside of the scope of this thesis as the SED method is applied to welded joints with sharp notches tested in the high-cycle fatigue regime—where the small-scale yielding condition is fulfilled.

The potential of applying the SED method for fatigue assessment at temperatures different from room temperature has been proven in a number of studies (Berto et al. 2013, 2014; Gallo et al. 2015; Bourbita and Remy 2016; Gallo and Berto 2016). Some of these studies applied modification factors to incorporate temperature effects into the SED method. Indeed, one study by Gallo and Berto (2016) used Eq. (12) and Eq. (14) in conjunction with literature data for fatigue assessment of notched metal specimens at high temperatures; yet, no study has attempted to assess welded joints at temperatures different from room temperature. Nevertheless, these studies prove that fatigue assessment methods that incorporate the micro-structural support effect hypothesis are suitable to assess temperature effects on a sound physical basis. Subsequently, the main findings of the state of the art are summarized before the introduction to the experimental part of this thesis.

2.6 | Summary of the state of the art

The state of the art on fatigue behaviour at sub-zero temperatures and fatigue assessment methods for welded joints was presented in the preceding sections of this chapter. The aim of this chapter was to give an overview of the current understanding of temperature effects on fatigue crack growth behaviour and to introduce the fatigue assessment methods that are applied in this study with the purpose of presenting a physically meaningful way of accounting for temperature effects within fatigue design. For this purpose, typical fatigue assessment methods—included in international standards and guidelines—as well as more advanced methods based on the micro-structural support effect hypothesis were presented. Furthermore, the relation of these methods to linear elastic fracture mechanics was presented, which provides a possibility of linking temperature effects on fatigue behaviour to the support effect at notches. The main conclusions of the state of the art on those two topics are:

- Ferritic steels such as structural steel grades with bcc crystal structure show a transition behaviour of fatigue crack growth rate at low temperatures, sometimes in the range of typical operating temperatures. This transition behaviour is assumed to be related to the ductile–brittle transition typically measured by means of Charpy or fracture toughness tests. This relation is, however, not yet fully understood.

- The fatigue strength of base materials as well as welded joints increases with decreasing temperature as long as the material is above the fatigue ductile–brittle transition temperature.

- Most published studies focus on fatigue crack growth rate measurements or on butt-welded joints, if *S*–*N* tests are performed; nonetheless, the basis for the design of ships and offshore structures are *S*–*N* design curves.

- Typical fatigue assessment methods like the nominal, structural hot-spot, and effective notch stress method, which are included in international standards and guidelines, are not capable of accounting for temperature effects, unless modification factors are applied.

- The micro-structural support effect hypothesis links the thermally activated plastic deformation process that governs crack initiation to a number of fatigue assessment methods.
- Examples of such methods are the averaged strain energy density method and the stress averaging approach, which are both linked to the micro-structural support effect hypothesis and to linear elastic fracture mechanics. Hence, both methods are expected to be able to account for temperature effects on a sound physical basis.
- The relation between these two methods, which will be studied further in this thesis, as well as links to the governing fatigue theories, was discussed in detail.

2.7 | Hypothesis and limitations of this study

This study seeks to improve the accuracy of fatigue design of welded engineering structures exposed to sub-zero temperatures by means of fatigue testing of welded joints and expanding fatigue assessment concepts for sub-zero temperatures. Based on the state of the art the following hypotheses are formulated, which will be investigated in this thesis:

- The fatigue strength of welded joints—in terms of *S*–*N* curves—increases at sub-zero temperatures, as long as the test temperature remains above the fatigue transition temperature.
- The relation of the averaged strain energy density method and the stress averaging approach to the micro-structural support effect hypothesis and to linear elastic fracture mechanics can be used to account for temperature effects within fatigue assessment, without the need for modification factors.

Fatigue and fracture of engineering materials is a complex field, in particular with respect to changes of failure modes (fatigue and fracture ductile–brittle transition), which is affected by various influencing factors. These cannot all be addressed in this study. Consequently, a number of limitations have to be kept in mind while assessing the results and developed methods:

- A number of studies on fatigue crack growth rates have been published in past decades in order to investigate the relation between the ductile–brittle transition

(observed in fracture mechanics tests) and the fatigue ductile–brittle transition; nonetheless, fatigue design is typically performed by means of *S*–*N* approaches. Hence, this thesis does not seek to investigate the effect between these two transition temperatures in detail. The aim of this study is rather to link changes of fatigue strength—measured in terms of *S*–*N* curves—to typical material tests performed for qualification of structural materials, i.e. Charpy impact tests as well as tensile tests.

- Studies by Silva et al. (2012) and others have shown an increase in prediction error for low notch acuities (i.e. large notch radii and opening angles). Furthermore, the relation between different TCD methods based on Taylor and Hoey's assumption (Taylor and Hoey 2009) ($\rho^* = 2L$) has been questioned as notch geometries seem to influence predictions based on this relation. These limitations are not investigated in this study, but are important to keep in mind while applying TCD methods or the SED method as well as during comparisons.

- The aforementioned relation of the strain energy density method to linear elastic fracture mechanics is limited to sharp notch details like fillet-welded joints, since the assumption of V-shaped notches of the N-SIF method is violated for blunt notched components like butt-welded joints with smooth transition radii. As a consequence, only fillet weld details are investigated by means of the strain energy density method.

- This also hinders a direct comparison of the TCD methods and the SED method, as presented in Hu et al. (2019). Therefore, the discussion of the results for both methods is limited to a qualitative comparison.

- As the general fatigue behaviour of welded joints under sub-zero temperature influence is not fully understood, this thesis focusses on fatigue tests under constant amplitude loading. Engineering structures such as ships and offshore structures are, however, exposed to variable amplitude loading.

- Finally, the strain energy density method and the stress averaging approach are compared to state-of-the-art methods. It is expected that these two methods can be extended to sub-zero temperatures without the need for modification factors. Differences in prediction accuracies of all methods are discussed; however, the aim is

not to generally test or recommend particular fatigue assessment methods. A validation based on a large number of different small-scale weld details, and preferably full-scale structures, would be required for this task.

With the help of experimental, statistical, and numerical investigations, the fatigue behaviour of welded joints at low temperatures is investigated in the subsequent chapters. For this purpose, first the experimental study is presented in Chapter 3. The results of the experimental programme are then presented in Chapter 4, and subsequently statistically assessed in Chapter 5 to test the first hypothesis. Based on the so obtained results, the second hypothesis will be analysed by extending the averaged strain energy density method and the stress averaging approach to account for temperature effects in Chapter 6.

3 | Testing methods and experimental procedure

As mentioned before, one aim of this study was to analyse the influence of temperature on fatigue strength of welded joints and to investigate whether these welded joints undergo a change in fatigue and fracture behaviour due to embrittlement of the material. Consequently, a large number of tests were performed for this study in order to investigate the material behaviour and in particular the fatigue strength of welded joints exposed to sub-zero temperatures typical for Arctic regions. To this end, stress–life (*S*–*N*) or Wöhler tests with constant amplitude loading were performed at sub-zero temperatures (i.e. −20 °C and −50 °C) and compared to controls at room temperatures (about 20 °C). EN ISO 19902:2018 requires Charpy impact toughness testing to be performed down to 30 °C below the lowest anticipated service temperature for plate thickness t > 12 mm and at LAST −10 °C for t < 12 mm. As −40 °C is typically used as a temperature limit for Arctic offshore structures (ISO/TS 35105:2018) and the plate thickness of the test specimens is 10 mm, a lower temperature limit of −50 °C was chosen for the fatigue tests in this study to match the Charpy test requirements.

There are other test methods, like crack growth rate measurements, that are more suitable to determine the exact transition temperatures of fatigue and fracture behaviour; nevertheless, the design of ships and offshore structures is mainly based on *S*–*N* approaches. In order to be able to verify the applicability of state-of-the-art fatigue assessment methods included in international standards and guidelines, and newer not-yet-included methods, *S*–*N* test results are thus required.

Beside the investigation of temperature effects on fatigue strength of welded joints,

additional tests to characterize the base material and welded joints were performed. These tests include tensile and Charpy V-notch impact tests. The Charpy V-notch, the tensile test, parts of the misalignment measurement results, and explanations of the performed tests were published in Braun et al. (2020d,f, 2021a); however, they are here presented in a coherent way for the first time. Furthermore, results of the weld geometry measurements are presented, which are later used to build the FE models for fatigue assessment.

3.1 | Welded fatigue test specimens

Three different weld details with two different failure locations made of two different steel types were fatigue tested so as to build a large database for the subsequent study on fatigue assessment methods for sub-zero temperatures. As a result, typical butt and fillet weld details—often found in ships and offshore structures—with fatigue failure initiating at weld toes roots were selected. In welded structures, weld details being prone to weld root failure are usually avoided; nonetheless, such weld details were often used to develop and verify fatigue assessment methods (cf. (Fricke 2012; DNVGL-RP-C203; Fischer et al. 2016b; Niemi et al. 2018)).

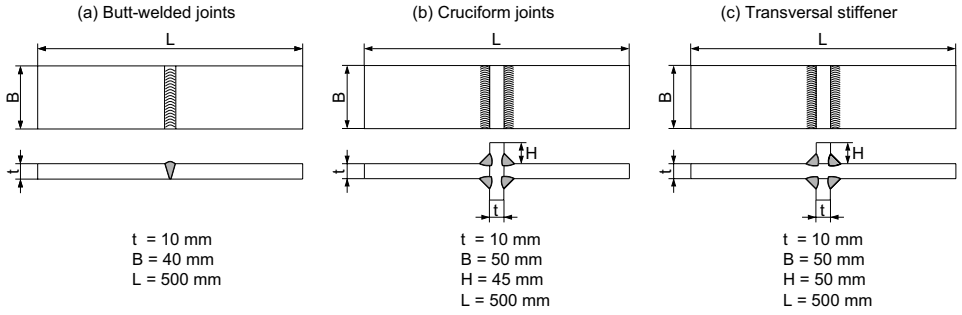

Figure 17. Schematic presentation of fatigue test specimens with dimensions, extended from Braun et al. (2020a)

The selected fillet weld details are a cruciform joint with non-penetrating fillet welds and a two-sided transversal stiffener—leading to weld root and weld toe failure, respectively. The third weld detail is a butt-welded joint with V-groove weld preparation on temporary root backing. The welding procedure specification (WPS) can be found in Appendix A. All three weld details with their respective dimensions are schematically illustrated in Figure 17. In Figure 18, polished and etched macrographs are presented of the three

weld details and both steel types. The orientation of the macrographs is aligned so that the loading direction is in horizontal direction—as for the schematic presentations.

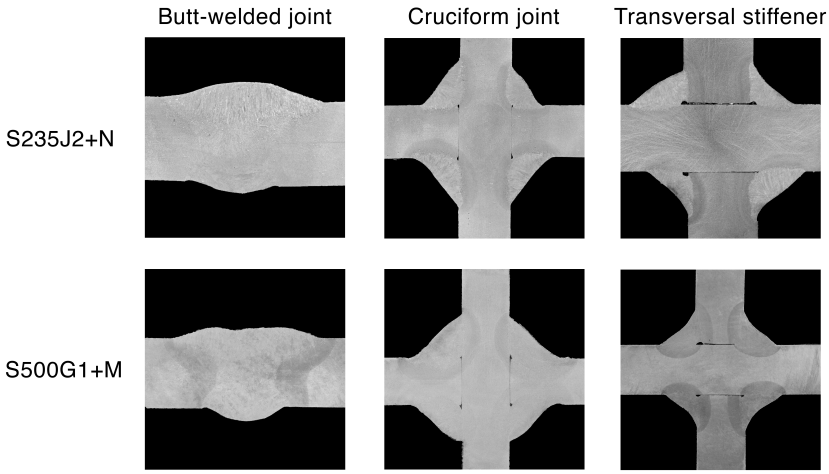

Figure 18. Macrographs of fatigue test specimens

Large welded structures like ships or offshore structures often contain a significant number of stiffeners, which are referred to as transversal stiffeners in fatigue terms if the loading direction is parallel to the continuous plate. In uniaxial fatigue testing, this leads to no load being transfered through the fillet welds, see Figure 19 (a). If the orientation of the welded joint is rotated by 90° and the loading direction is as indicated in Figure 19 (b), the load is transferred through the fillet welds. If the cross-sectional area of the fillet welds is not substantially larger than the cross-section of the base plate (i.e. throat thickness of the fillet weld $\mathrm{a_{th}} > 0.7\mathrm{t}$) the fillet welds exhibit a high risk of weld root failure due to the larger stress concentration at the weld root as compared to the weld toe. In this study, an intentionally low throat thickness of $\mathrm{a_{th}} < 0.7\mathrm{t}$ was chosen to enforce weld root failure of the cruciform joints and to be able to investigate possible differences in the temperature effects on weld toe and root failure.

The specimens of this study were welded by means of flux-cored arc welding (FCAW) process using tack-welded stiffeners to limit angular distortion and are later removed, see Figure 20(a). Later, the 1 m x 0.5 m plates were saw-cut into 500 mm x 50 mm wide (40 mm for the butt-welded joints) x 10 mm specimens. Further details are given in the WPS in

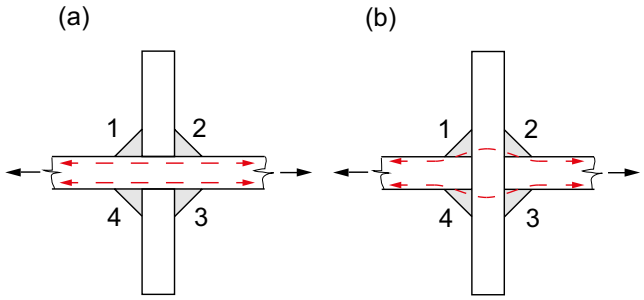

Figure 19. Schematic presentation of load transfer through the fillet welds of non-load-carrying (a) and load-carrying (cruciform joint) fillet-welded joints (b) with sequences of welding, adopted from Braun et al. (2020f)

Appendix A and Braun et al. (2020f).

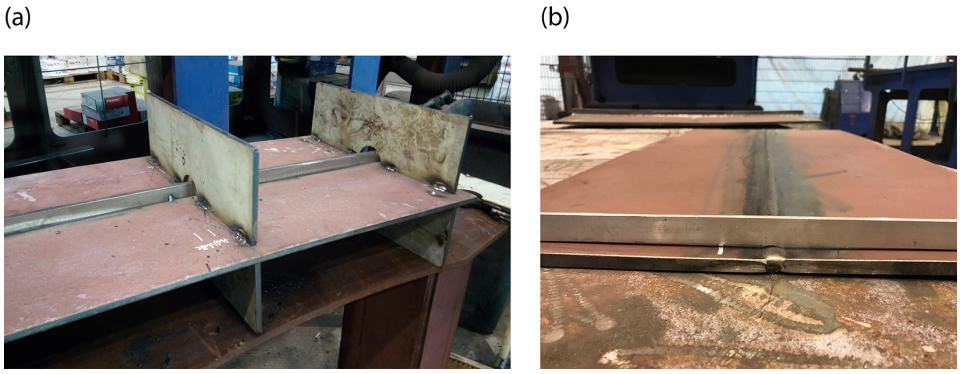

Figure 20. Production of fillet- (a) and butt-welded joint (b) plates for the test programme, taken from Braun et al. (2021a)

3.2 | Material properties of applied steels and welded joints

To rule out material-based uncertainties of the welded joints, two series of each weld detail were produced using two different steel types. The first is a normal-strength S235J2+N normalized steel that is often used in ship structures and the second a S500G1+M thermomechanically rolled, fine-grain structural steel. The chemical composition of the two steels is listed in Table 2. (Braun et al. 2020f)

Table 2. Chemical composition of steels used [w%] (Braun et al. 2020f)

	C	Si	Mn	P	S	N	Cu
S235J2+N	0.107	0.176	1.02	0.014	0.001	–	0.016
S500G1+M	0.056	0.208	1.58	0.012	0.002	0.004	0.273
	Mo	Ni	Cr	V	Nb	Ti	Al-T
S235J2+N	0.002	0.020	0.023	0.001	–	–	0.041
S500G1+M	0.175	0.516	0.056	0.001	0.02	0.001	0.033

'–' means <0.001.

Tensile tests at room and sub-zero temperatures have been performed to characterize the stress-strain behaviour of the material in accordance with (EN ISO 26203-2:2011; EN ISO 6892-3:2015; EN ISO 6892-1:2016); yet, instead of applying the load in a quasi-static manner, a higher loading rate of 10 mm/s was chosen to prevent heating of the pre-cooled specimens and to test the materials at a loading rate in the range of the fatigue tests. The specimens that were tested at sub-zero temperatures were kept in liquid nitrogen for about two minutes and allowed to heat up to the test temperature before the test.

During controls with a quasi-static loading rate, a loading rate dependence of yield strength σ_{YS} and ultimate tensile strength σ_{UTS} was observed; however, the elongations to fracture e_{f} were found to be independent of loading rate, see Braun et al. (2021a) for further details. The following averaged material characteristics were derived for both steel types, see Table 3.

Table 3. Mechanical properties of the base material derived from tests with a loading rate of 10 mm/s, which roughly corresponds to the loading rate of the fatigue tests, data from (Braun et al. 2021a)

Steel	T [°C]	σ_{YS} [MPa]	σ_{UTS} [MPa]	e_{f} [%]
	20	364.5	460.0	27.6
S235J2+N	-20	419.0	492.5	24.9
	-50	472.0	515.5	14.3
	20	506.5	606.0	19.6
S500G1+M	-20	533.5	633.0	15.1
	-50	568.0	659.5	14.1

Charpy V-notch test results confirmed that the base material of both steels has a high longitudinal toughness. From sigmoidal curve fitting, Charpy transition temperatures $\mathrm{T}_{27\mathrm{J}} = -78$ °C and $\mathrm{T}_{27\mathrm{J}} = -119$ °C are obtained for S235 and S500, respectively, which is well below the certified Charpy V-notch impact toughness the steels have to fulfil, see Figure 21.

To correlate possible changes in fatigue behaviour to typical testing methods, Charpy impact testing has also been performed for the middle of the butt weld in the weld metal (WM) in accordance with DNVGL-OS-C401, and the HAZ. The lowest fracture and Charpy impact toughness are often measured along the fusion line between the WM and HAZ; nevertheless, for the present welded joints a higher toughness was measured for the notch location in the HAZ (which intersects the fusion line) than for the WM. For both steels the lowest impact toughness was measured in the WM with Charpy transition temperatures of −28 °C and −64 °C (27J criterion) for the S235 and S500 steel, respectively (Braun et al. 2021a). This is thought to be related to the welding process. FCAW of butt joints with multiple weld layers is expected to lead to detrimental fracture toughness results in the middle of the WM compared to other welding processes (Gubeljak et al. 2002; Vojvodic Tuma and Sedmak 2004; Coronado and Cerón 2010).

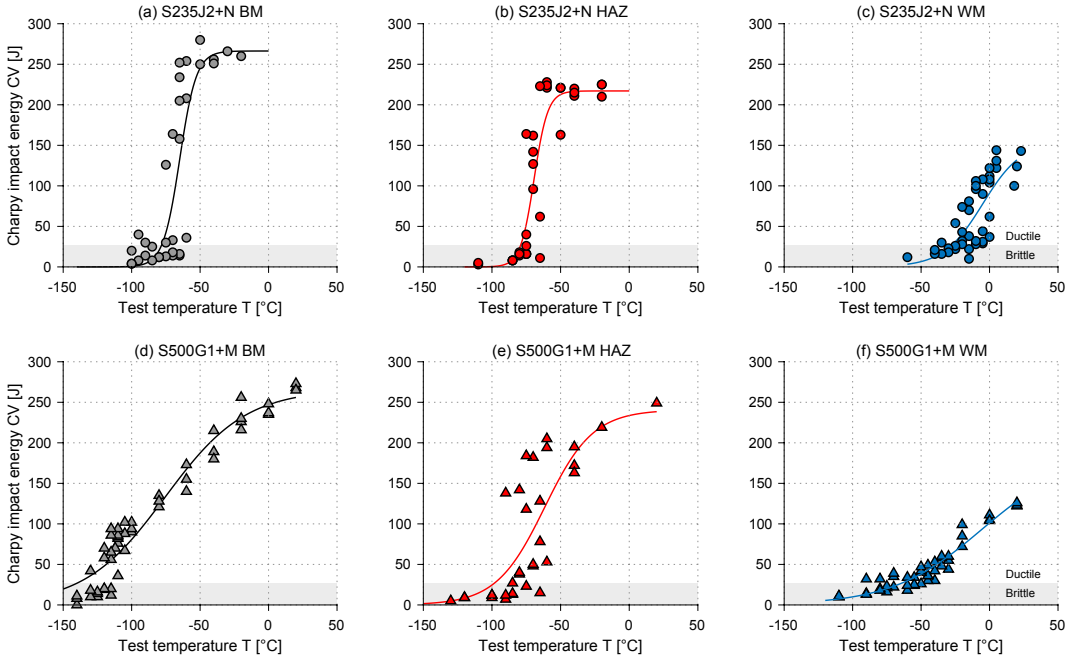

Figure 21. Charpy V-notch impact testing results of S235J2+N and S500G1+M steel with notch location in the base material (BM), the heat-affected zone (HAZ), and the middle of the weld metal (WM), data from (Braun et al. 2021a)

3.3 | Fatigue test setup

Fatigue testing was carried out in a temperature chamber, with a temperature range of −180 °C to +280 °C. A Schenck horizontal resonance testing machine with a maximum load capacity of 200 kN and a frequency of around 33 Hz was retrofitted for this goal (see Figure 22). Cooling is achieved by injecting vaporized nitrogen from a liquid nitrogen tank into the temperature chamber. The temperature of the chamber and the specimen temperatures were monitored during the fatigue test by PT100 platinum measuring resistors. All temperature sensors are calibrated against an additional temperature gauge at room temperature that is positioned in the test lab and experiences only minor variations. As can be seen from Figure 22, a constant temperature within ± 1 °C is achieved. The spikes in specimen temperatures during the tests were caused by injection of nitrogen. Failure of the specimens is defined as full fracture or shortly before if the opening of the fatigue crack exceeds the axial displacement limits of the testing machine. (Braun et al. 2020f)

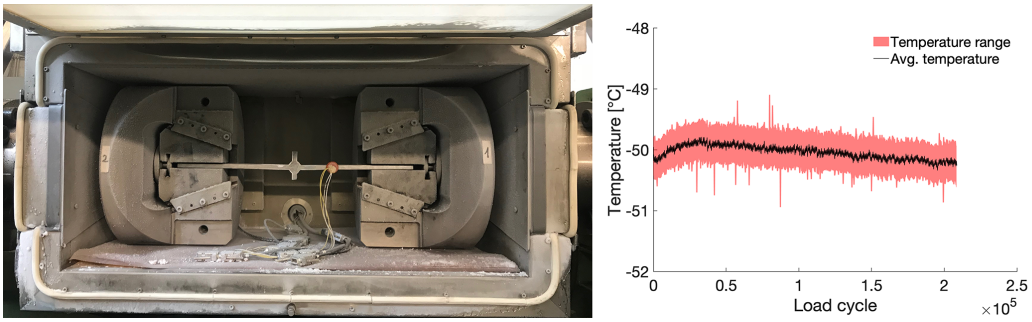

Figure 22. Temperature chamber for sub-zero temperature fatigue tests and temperature variation during fatigue test with mean temperature averaged over 30 seconds, adopted from Braun et al. (2020f)

3.4 | Fatigue test preparation

3.4.1 | Measurement of specimens' misalignment

Fatigue test results of small-scale specimens are known to be directly related to the local weld geometry, i.e. the weld toe transition and secondary bending effects caused by misalignment of test specimens. Thus, the local weld geometry and welding-related misalignment of all specimens was measured prior to fatigue testing. For cruciform and butt

joints, this includes angular (φ) and axial (e) misalignment and for transversal stiffener only angular misalignment, see Figure 23 for the definition of misalignments.

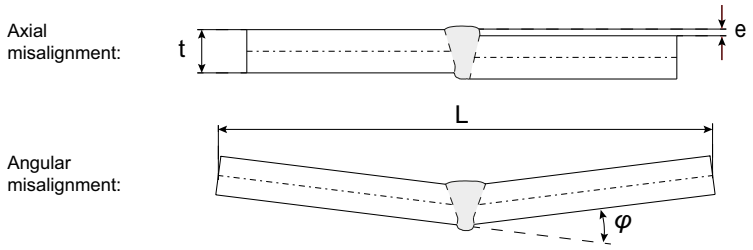

Figure 23. Definition of axial and angular misalignment as illustrated for a butt-welded joint, adopted from Braun et al. (2020b)

Due to the continuous base plate with stiffeners attached on both sides, no axial misalignment arises for transversal stiffener specimens. The misalignment was measured by dial gauges on the test setup presented in Figure 24(a). The specimen location is adjusted within the test setup by variable support beams and fixed supports. Then, the vertical deflection from the horizontal baseline of the specimen is measured at the location indicated by h_2 and h_3 in Figure 24(b). (Braun et al. 2020b)

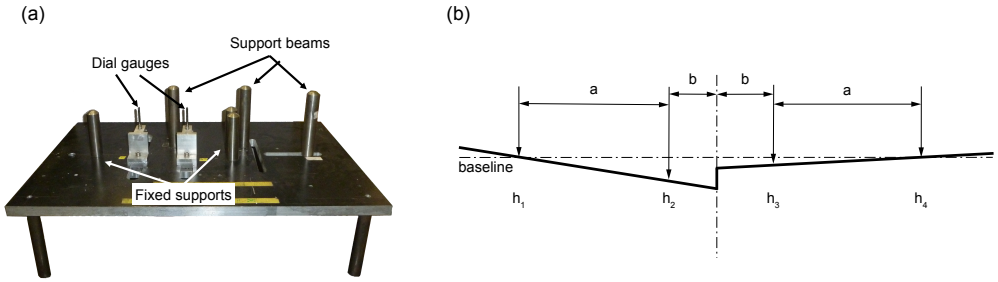

Figure 24. Misalignment measurement setup (a) adopted from Fischer (2016) and principle to determine axial and angular misalignment (b), adopted from Braun et al. (2020b)

During cutting of welded plates (for example into small-scale) residual stresses are relaxed. The level of misalignment of these specimens thus varies from specimen to specimen, due to varying levels of residual stress along the weld seam direction. Moreover, the level of misalignment between specimens of different plates varies even if they are

welded according to the same WPS. Hence, varying levels of misalignment may overlap with other effects, such as temperature. (Braun et al. 2020b)

To separate misalignment from temperature effects, the stress magnification $\mathrm{k_m}$ caused by misalignment was calculated for all specimens according to IIW recommendations (Hobbacher 2016), considering fixed ends. For joint types with angular and axial misalignment, a joint stress magnification $\mathrm{k_m}$ is derived by superposition of stress magnification factors for axial $\mathrm{k_{m,e}}$ and angular misalignment $\mathrm{k_{m,a}}$ with

$$\mathrm{k_m} = 1 + (\mathrm{k_{m,e}} - 1) + (\mathrm{k_{m,a}} - 1) \tag{31}$$

How stress magnification factors are calculated for welded joint with weld toe failure is described in international standards and guidelines (BS 7910:2013+A1:2015; Hobbacher 2016; Niemi et al. 2018). A concept of how a joint stress magnification factor—that takes angular misalignment into account—can be derived for weld root failure of cruciform joints was presented in Braun et al. (2020d). Only the results of the misalignment measurements shall be presented here for each specimen type and separated by steel type, see Figure 25[5]. The bars indicate the mean stress magnification factor of each specimen type and the lines the corresponding standard deviation. As can be seen from Figure 25, the highest stress magnification factors were calculated for the S235 butt-welded joints and the lowest for the transversal stiffener specimens.

A certain degree of misalignment is already covered in fatigue design curves. For local fatigue assessment methods, a general level of stress magnification of 5% is assumed, but for nominal stress methods the level varies with specimen geometry (e.g. 1.15 for butt joints and 1.25 for transversal stiffener). As a consequence, nominal stress results are corrected by an effective stress magnification factor if the level given by the IIW recommendations (Hobbacher 2016; Niemi et al. 2018) is exceeded; yet, no information is given for weld root failure of cruciform joints in the IIW recommendations (Braun et al. 2020d).

3.4.2 | Weld geometry measurement

Besides misalignment and environmental effects, the fatigue strength of a welded joint is largely affected by the local weld geometry. Cracks often initiate at local stress concen-

[5]The codes for creating this figure as well as Figure 28, 29, 38, 41, 43, 46, and 57 are based in part on the plotting tool provided by Urai (2016)

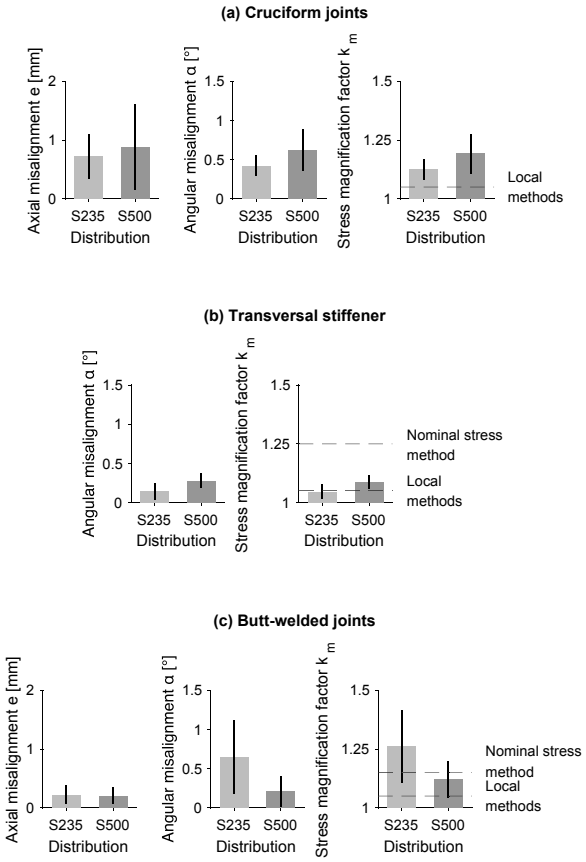

Figure 25. Measured misalignment of the six test series and corresponding stress magnification factors as well as levels of stress magnification included in nominal and local stress design curves, extended for butt joints from (Braun et al. 2020d)

trations along the weld seam or at locations of varying weld shape, see (Hou 2007; Schork et al. 2018; Hultgren and Barsoum 2020; Niederwanger et al. 2020). Moreover, an accurate measurement of the weld geometry is of particular importance for the subsequent FE modelling as the FE models are based on the average geometry obtained by laser triangulation; however, the nominal stress assessment of the cruciform joints also requires a measurement of the throat thickness a of each specimen. An overview of local weld geometry parameters relevant for butt- and fillet-welded joints is given in Figure 26. The main parameters describing weld toes are radius (ρ), local weld toe angle (θ), and undercut depth (d). Additionally, weld height (H_w) and width (W) are measured for butt joints.

According to international standards, nominal stresses σ_n are to be derived in the sec-

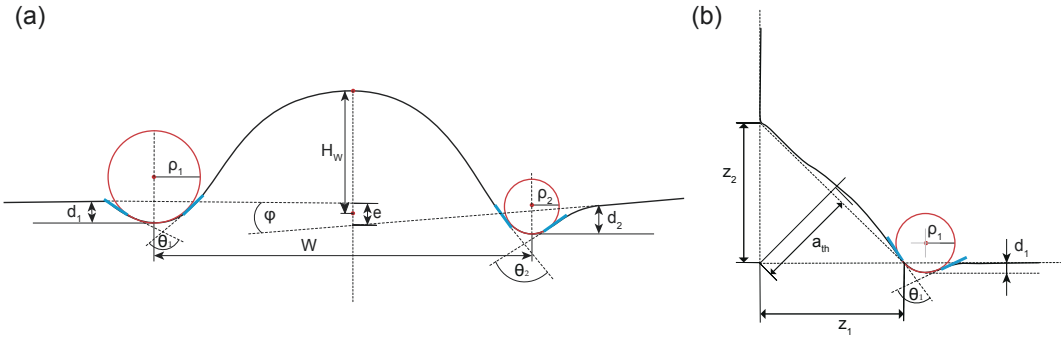

Figure 26. Local weld geometry of butt-welded joints including definition of axial (e) and angular misalignment φ (a) and fillet-welded joints (b), adopted from Braun et al. (2020f)

tional area from membrane and shell bending stresses in the adjacent plates considering macro-geometry effects, e.g. large cut-outs (Hobbacher 2016). For weld root fatigue, the nominal stress is based on averaged stress components in the weld throat instead of the nominal stress acting in the adjacent plate. These stress components are the same that are used for static design of welds (Fricke 2013a; Braun et al. 2020d). In this study, the Eurocode 3 (EN 1993-1-8:2005 + AC:2009) definition of throat thickness a_{th} is applied, which assumes no load transfer through excessive weld overfill. By fitting the largest possible triangle into a fillet weld, the throat thickness is the bisector of the leg lengths (z_1 and z_2), see Figure 26(b).

$$a_{th} = (z_1 + z_2) / \sqrt{z_1^2 + z_2^2} \tag{32}$$

Laser triangulation was used for the local weld geometry measurements, see Figure 27. By doing so, each specimen was scanned after cutting the specimen from welded plates. After assessing the scan quality manually, the post-processing of the point data was then performed using the curvature method developed by Jung (2018), and improved by Renken (2020) and Renken et al. (2021). The curvature method was found to yield consistent results in a comparison to three different weld geometry assessment techniques in Schubnell et al. (2020a).

The obtained weld surface was cut into 10 equidistantly distributed slices during the assessment of the laser scans, as presented in Figure 27(c). Each slice was then evaluated by the curvature method and the results for each slice as well as the mean and standard

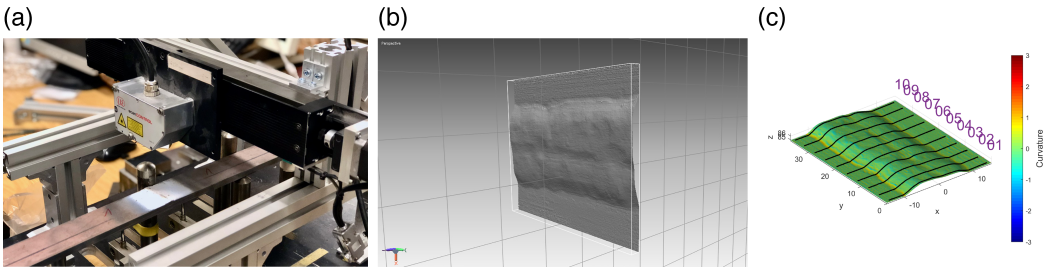

Figure 27. Scanning of the weld geometry of a S500 butt-welded joint (a), visualization to check scan quality (b), and assessment of geometry with 2D weld slices (c)

deviation of each geometry parameter were stored. To investigate whether the assessment was correct, a figure of each slice was exported and later checked manually. The distributions of the averages obtained from the laser scan measurements for a number of important geometry parameters are presented in Figure 28 and Figure 29 for butt-welded and fillet-welded joints, respectively.

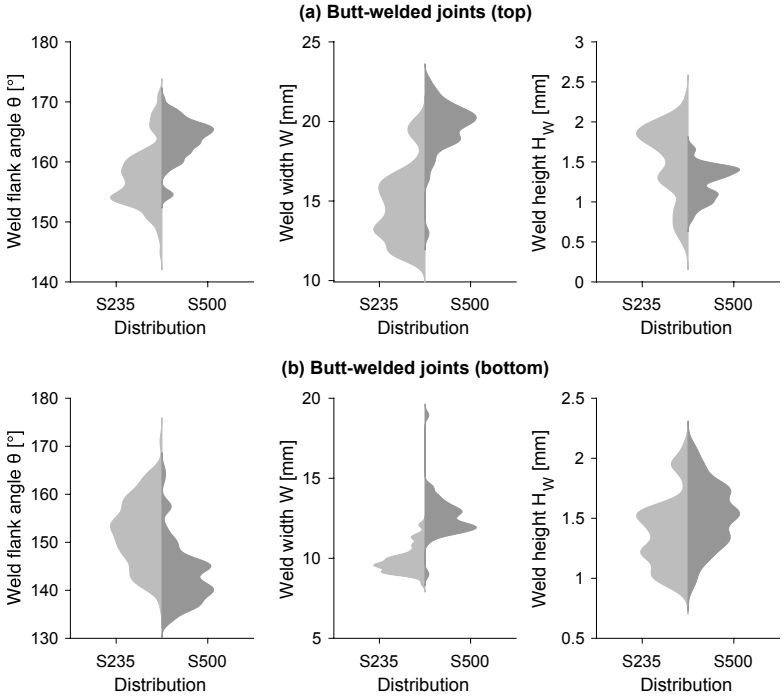

Figure 28. Distributions of measured average geometry parameters of the butt-welded joint specimens' top sides (a) and bottom sides (b)

From the laser scan post-processing, a median throat thicknesses a_{th} of 5.71 mm and

5.85 mm was obtained for the S235 and S500 cruciform joints, respectively (Braun et al. 2020d). These values will later be used to calculate the nominal weld stress acting in the fillet weld cross-section and for the creation of the FE models for fatigue assessment of the experimental test results.

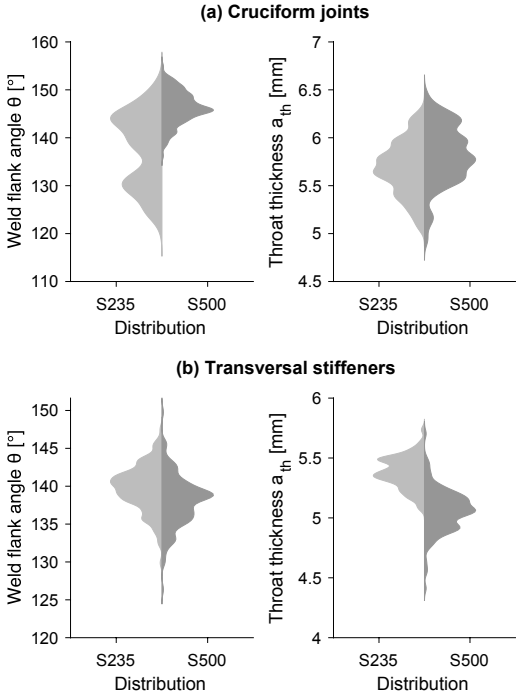

Figure 29. Distributions of measured average geometry parameters of cruciform joints (a) and transversal stiffeners specimens (b)

4 | Results of the experimental test programme

The aim of this study is to analyse the effect of temperature on fatigue strength of welded joints and to develop methods for fatigue assessment that are capable of taking temperature effects into account. For this goal, welded steel joints were *S–N* tested at three different temperatures, i.e. RT, −20 °C, and −50 °C. The fatigue test results are presented in this chapter, including the evaluation approach and a comparison with reference fatigue strength from design standards.

The fatigue test results have been published in Braun et al. (2020c,f, 2021a) including a first comparison with design curves in Braun et al. (2020f); however, the results were reassessed for this thesis for a combined assessment of temperature effects. Furthermore, a comprehensive description of the evaluation approach of the fatigue test data has been included. Finally, an extended assessment of fracture surface investigation was performed to relate the fatigue and fracture behaviour of the welded joints to the Charpy V-notch impact toughness results of the previous Chapter.

4.1 | Evaluation approach for fatigue test data

The fatigue test results of each test series (i.e. for a particular joint type, steel type, and temperature) were statistically evaluated to obtain *S–N* curves with:

$$\mathrm{N_f} = 2 \times 10^6 \left(\frac{\Delta\sigma_\mathrm{n}}{\Delta\sigma_\mathrm{R}} \right)^{-\mathrm{k}} \tag{33}$$

where $\mathrm{N_f}$ is the endured number of cycles to failure on the nominal stress range level $\Delta\sigma_\mathrm{n}$, $\Delta\sigma_\mathrm{R}$ is the reference fatigue strength at 2×10^6 cycles, and k is the slope of the *S–N*

curve. For this purpose, curve fitting based on a least-square algorithm was performed according to the recommendations of the German Welding Society (DVS) (Merkblatt DVS 2403) to derive mean fatigue strength *S–N* curves (i.e. for a survival probability P_s = 50%). By subtracting twice the standard deviation from the mean fatigue strength a reference fatigue strength for survival probability of P_s = 97.7% is obtained. The so obtained reference fatigue strength can then be compared with design curves and reference fatigue strength (FAT class) given in international standards and guidelines, such as the IIW recommendations (Hobbacher 2016). These design values are defined for a probability of survival of 97.5%; yet, the difference is found to be marginal, see Lefebvre et al. (2019). Moreover, the scatter ratio $1/T_s$ between the fatigue strengths for P_s = 90% and 10% is calculated for each data set as a typical measure of variance from Eq. (3).

International standards for welded joints assume that fatigue life of welded joints is predominantly defined by crack propagation. Thus, a fixed slope exponent $k = 3$ for welded joints is the basis of all design curves, see Hobbacher (2016). This assumption holds for large amounts of test data; yet, test data of fatigue studies is often limited to smaller amounts of samples (i.e. specimen number $n < 20$). Consequently, experimental *S–N* curves often deviate from this assumption, which leads to a high uncertainty regarding mean fatigue strength (Martin et al. 2011) and even higher uncertainty for reference fatigue strength. So as to allow a comparison of *S–N* curves obtained for different test temperatures based on mean fatigue strength, all *S–N* curves have been evaluated using a fixed slope exponent $k = 3$ in accordance with international standards and guidelines. Moreover, following international recommendations and standards (DIN 50100:2016-12; Hobbacher 2016) more than 10 tests have been performed for each test series.

Only specimens that failed before reaching 2×10^6 cycles have been included in the statistical assessment of the *S–N* curves, since this number of cycles corresponds to the approximate knee point of *S–N* curves. For higher numbers of cycles, a shallower slope is assumed (see Hobbacher (2016)). Furthermore, tests that reached the assumed knee point were in most cases interrupted (indicated by an arrow in the *S–N* diagrams) and based on the record of test frequency a decision was made whether to re-test the same specimen on a higher stress range level. Stress ranges close to the knee point may initiate fatigue cracks that are non-propagating; nevertheless, if the resonance test frequency remained constant since the test start no fatigue cracks were initiated (cf. Schubnell et al. (2020b))

and specimens were re-tested. To verify the assessment based on test frequency, the data has been statistically assessed for conspicuities between the re-tested run-outs and the remaining data, see Braun and Mayland (2020). One butt joint test result was hence removed from the assessment.

4.2 | Obtained fatigue test results at room and sub-zero temperatures

The results for each specimen type and steel type are presented in the following sections, beginning with the cruciform joints. So as to allow a comparison with design curves of international standards, all *S–N* curves have been assessed using a fixed slope exponent k = 3. Results for free slope exponents are additionally presented in Appendix B. In general, all test specimens, at all test temperatures, fulfil the requirements according to the corresponding FAT weld detail classes in Hobbacher (2016). This is related to the quality of the welded specimens that mainly fulfil class B of EN ISO 5817:2014.

4.2.1 | Cruciform joints

The test results for the cruciform joint specimens of both steel types, are presented in Figure 30 including *S–N* curves for 50% survival probability (dashed lines). The colour scheme for the temperature range is black (room temperature RT), red ($-$20 °C), and blue ($-$50 °C) and filled symbols are used for S500 steel and empty for S235 steel. (Braun et al. 2020d)

First of all, all cruciform joint specimens failed from the weld root due to the chosen throat thickness of $\mathrm{a_{th}} < 0.7\mathrm{t}$. The cruciform joint test series showed a clear improvement of mean fatigue strength (indicated by the numbers at the end of the dashed lines) as test temperature decreased. Interestingly, a slightly larger increase in fatigue strength is observed for the S235J2+N joints compared to the S500G1+M joints, which is thought to be related to differences in misalignment between the test series. This will be assessed further in Chapter 5. More importantly, even though the S235J2+N steel is certified for a temperature of $-$20 °C, the fatigue strength increased even at temperatures as low as $-$50 °C; this is in line with findings of other studies regarding large safety margins on toughness at the certified steel temperatures (Walters et al. 2014). (Braun et al. 2020f)

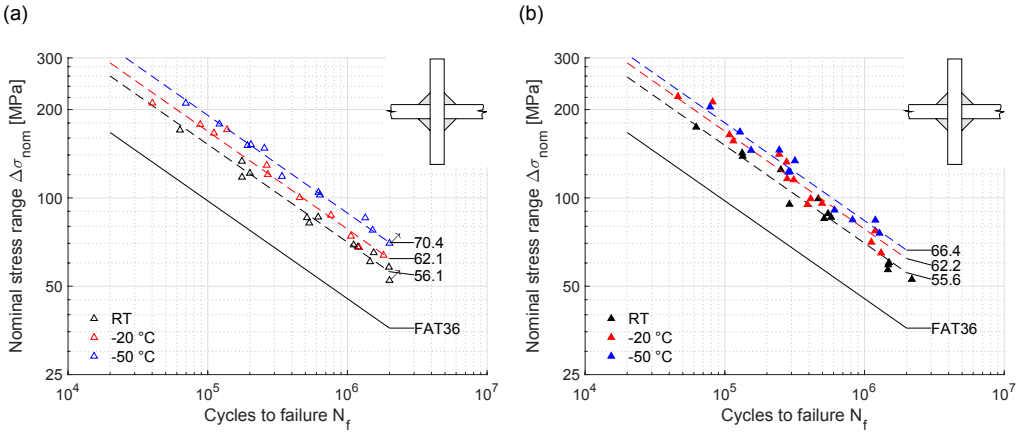

Figure 30. Fatigue test results of S235J2+N (a) and S500G1+M (b) cruciform joints, adopted from Braun et al. (2020a)

4.2.2 | Transversal stiffener

A similar result was obtained for the transversal stiffener test series, presented in Figure 31, with constantly increasing mean fatigue strength at lower test temperatures. The higher scatter of the S235 specimens compared to the S500 specimens is caused by different numbers and locations of crack initiation sites, see Braun et al. (2020f) for further details.

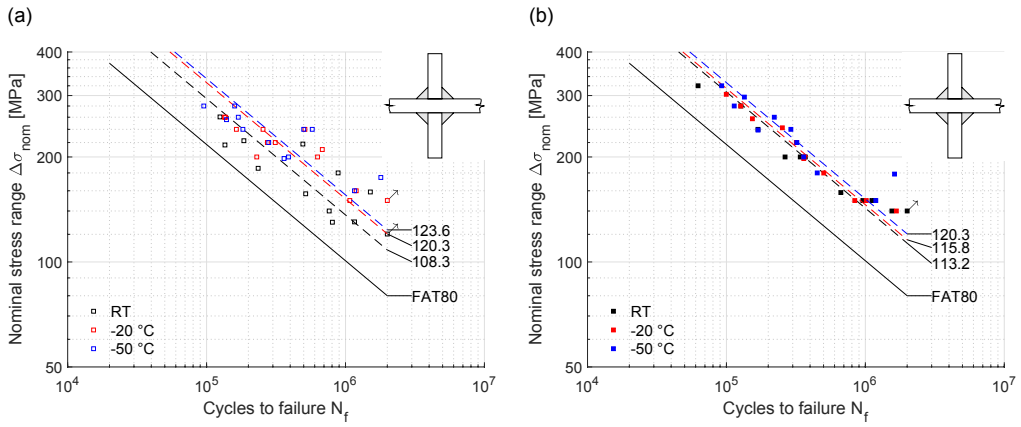

Figure 31. Fatigue test results of S235J2+N (a) and S500G1+M (b) butt-welded joints, adopted from Braun et al. (2020a)

4.2.3 | Butt-welded joints

The fatigue test results of the S235 and S500 butt-welded joints are presented in Figure 32. Again, a constant increase in fatigue strength is observed for lower test temperatures. While the S235 joints are compared with the FAT90 class (weld toe failure, low axial misalignment) according to IIW recommendations (Hobbacher 2016), the S500 joints are compared with the FAT80 curve for weld root failure starting from the side of temporary root backing. The reason for the different failure locations (top and bottom) is related to the sign of angular misalignment that leads to tensile secondary bending stresses on the bottom side for the S500 joints and on the top side for the S235 joints.

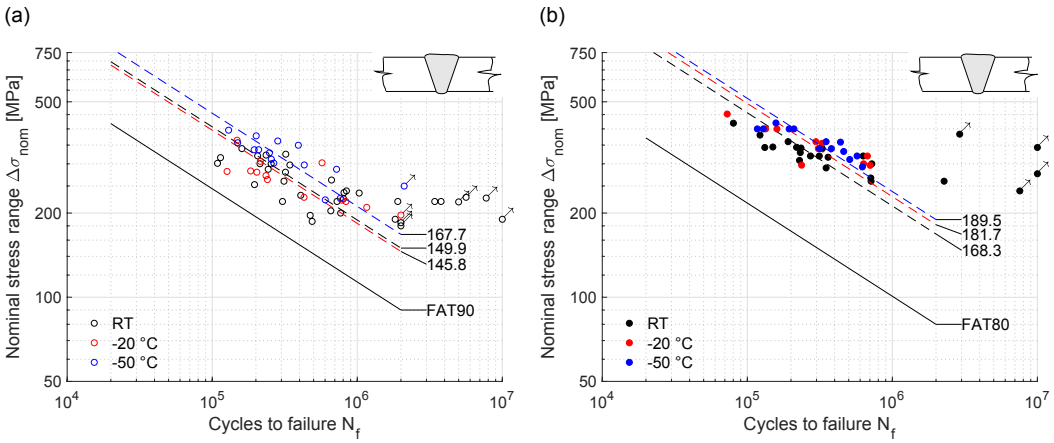

Figure 32. Fatigue test results of S235J2+N (a) and S500G1+M (b) transversal stiffener, adopted from Braun et al. (2020a)

The actual slope exponent of the butt joint *S–N* curves is larger than $k = 3$ due to an extended crack initiation period for high-quality butt-welded joints (large radii and flank angles); however, for these test series a fixed slope of $k = 3$ is also applied to allow a comparison with the other test series (see Braun et al. (2020c) for assessment based on natural slope and best fitting slope exponents). Nonetheless, the results obtained for free slope exponents and the corresponding standard deviation of the slope exponent SD(k) are summarized in Table 4.

Table 4. Summary of obtained slope exponents k, including standard deviation of the slope exponent SD(k)

Weld detail	Temperature	S235J2+N		S500G1+M	
	T	Slope k	SD(k)	Slope k	SD(k)
Cruciform joints	RT	3.11	0.12	2.79	0.13
	−20 °C	2.87	0.13	2.61	0.15
	−50 °C	3.01	0.12	2.81	0.18
Transversal stiffener	RT	3.01	0.73	3.67	0.19
	−20 °C	3.67	0.74	3.33	0.18
	−50 °C	4.20	0.81	3.57	0.50
Butt-welded joints	RT	3.04	0.55	4.80	0.70
	−20 °C	3.51	0.92	4.47	0.91
	−50 °C	2.69	0.52	4.58	0.60

4.3 | Assessment of fracture behaviour based on fracture surface investigation

To investigate the fracture mode of the fatigue test specimens, visual inspection was performed for all specimens. Photographs of exemplary fracture surfaces are presented in Figure 33, Figure 34, and Figure 35 for the cruciform joint, transversal stiffener, and butt-welded joint specimens, respectively.

First of all, almost all fracture surfaces are defined by large areas being related to fatigue crack propagation. Furthermore, except for the S235J2+N butt-welded joint specimen tested at room temperature, most specimens failed due to crack initiation from several small cracks that nucleated after growing one or two millimetres in depth.

At room temperature, the fracture surfaces of the cruciform joint specimens of both steel types show shear lips in the final rupture region, which indicates ductile failure (i.e. plastic collapse). At −20 °C, the fracture surface appearance of the S235J2+N steel is similar to the surface of the RT test; however, at −50 °C a large area of brittle fracture can be seen within the lower fracture fillet weld. Final fracture is, however, related to ductile failure. Also, the S500G1+M cruciform joint fracture surfaces shows a large brittle fracture at −50 °C—with almost no remaining shear lips. This result agrees well with the observed ductile–brittle transition from Charpy V-notch impact testing. For the S235J2+N weld material, a DBTT between −50 °C and 0 °C was observed from the Charpy tests with a $T_{27J} = -28$ °C from sigmoidal curve fitting. The corresponding S500G1+M T_{27J} transi-

tion temperature obtained from curve fitting is below −50 °C; however, a few specimens already showed brittle fracture around −50 °C.

Despite the brittle final fracture behaviour of the cruciform joints at sub-zero temperatures, the fatigue strength increased considerably with decreasing test temperature. This is probably related to the fact that the majority of crack propagation is spent propagating small cracks. Once the crack depth reaches a few millimetres, the remaining fatigue life is rather short.

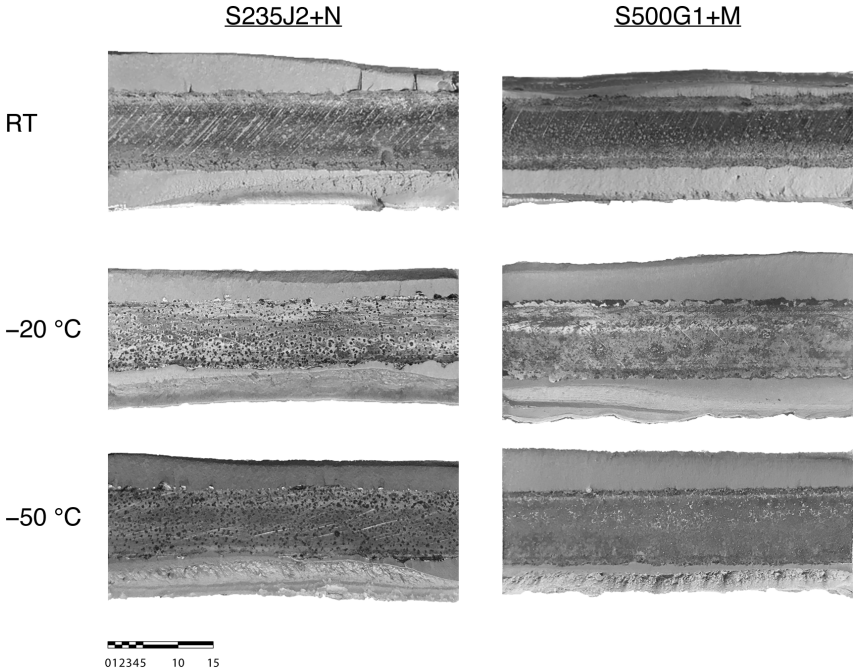

Figure 33. Fracture surfaces of cruciform joint specimens with non-fused plate edge in the middle between the fractured welds (scale in millimetres), adopted from Braun et al. (2020a)

The fracture surfaces of the transversal stiffener specimens in Figure 34 show similar behaviour as the cruciform joints at room temperature; however, the fracture surfaces reveal a different behaviour at sub-zero temperatures. The majority of specimens failed due to plastic collapse. This can be seen from large areas connected to fatigue crack propagation and final fracture which is caused by ductile failure (again, indicated by shear lips, but also some necking for both steel types).

Only the S235J+N fracture surface of the transverse stiffeners revealed a cleavage crack perpendicular to the direction of the applied loading on the right side of the specimen

tested at −50 °C (see Figure 34); this is a clear sign of brittle material behaviour. Interestingly, the lower left corner contains a shear lip, which indicates ductile failure. The reason for this behaviour could be related to the location of final fracture being inside a local brittle zone. This is, however, unlikely as the fracture initiated in the base material. Thus, it is more likely that the base material of this specimen is in the ductile–brittle transition at this temperature and does not fully behave brittle yet. This observation is supported by the fact that the scatter band around the DBTT of the base material begins at about −60 °C. In general, the Charpy transition curve for the S235J2+N base material is quite steep and shows a large scatter. It is hence conceivable that the condition of the fatigue test led to a state of fracture at the transition to brittle fracture. This is exacerbated by the majority of the specimens showing ductile fracture behaviour.

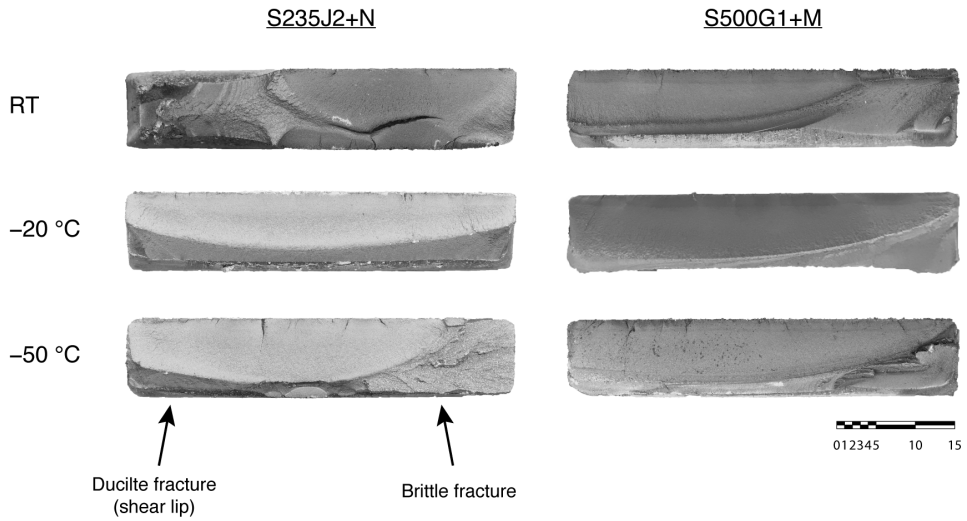

Figure 34. Fracture surfaces of transversal stiffener specimens (scale in millimetres)

The comparisons of fracture surfaces for transversal stiffener and cruciform joint specimens indicate that the DBTT is lower in the weld metal than in the base material. This is supported by the low Charpy impact toughness test results of the weld metal of the butt-welded joints and by the fact that cruciform joint and transversal stiffener specimens were welded with exactly the same welding parameters. Furthermore, the observed partly brittle behaviour of the S235J2+N transversal stiffeners agrees with observations by Alvaro et al. (2017) and Walters et al. (2016), who observed a FTT 15 °C and 12 °C higher than the DBTT for the T_{40J} and T_{27J} value, respectively.

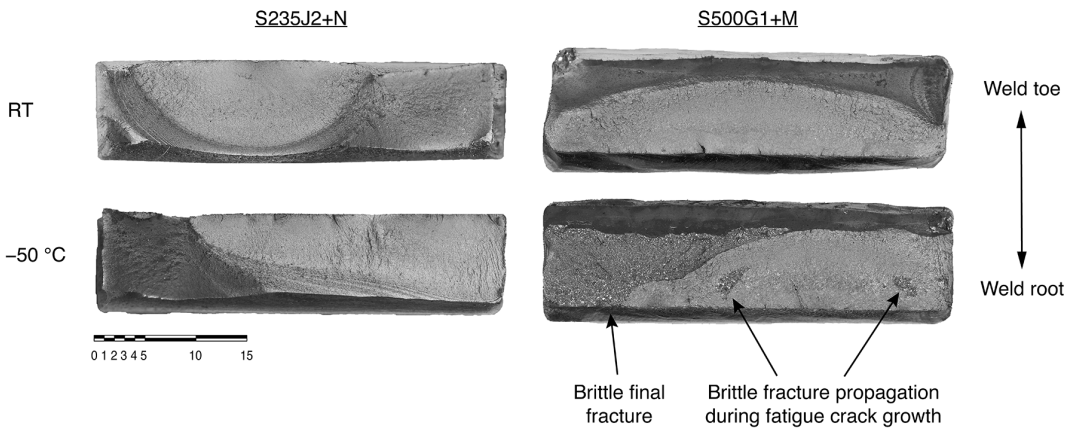

Figure 35. Fracture surfaces of butt-welded joint specimens (scale in millimetres), adopted from Braun et al. (2021a)

The fracture surfaces of the butt-welded joints in Figure 35 show a quite different behaviour for the S500G1+M steel compared with all other test series, with brittle fracture during fatigue crack growth and not only during final fracture. This behaviour was, however, not observed for the S235J2+N butt-welded joints. The reason for this is the difference in fatigue crack initiation location for both steel types. Fatigue cracks initiated in the heat-affected zone for both steel types, but final fracture was either located in the base material (S235J2+N) or the weld metal (S500G1+M) due to the V-shaped welds (Braun et al. 2021a).

While the S235J2+N failed due to plastic collapse at all test temperatures, a number of S500 specimens showed brittle fracture behaviour at −50 °C. Contrary to the cruciform joints and the transversal stiffener, where only final fracture was brittle, the S500G1+M specimens also show some brittle fracture propagation during fatigue crack growth. The brittle cracks, however, seem to be arrested after propagating about 2 mm. This behaviour is revealed by the fatigue crack propagation area between the small brittle fracture areas and the final fracture area. The reason for this is the small difference between the DBTT in the weld metal (−64 °C for the S500G1+M joints) and the fatigue test temperature of −50 °C as well as the large scatter of Charpy test results, see Figure 21. This further explains why some specimens failed in a brittle manor while others did not. Similar to the other tested weld details, the fracture behaviour does not seem to influence fatigue strength as it increases constantly with decreasing test temperature for both steels.

4.4 | Analysis and comparison of fatigue test results

To illustrate the increase of fatigue strength at sub-zero temperatures compared to room temperature, a mean fatigue strength ratio $V_{R,50\%}$ is calculated with

$$V_{R,50\%} = \frac{\Delta\sigma_{R,50\%}\,(T)}{\Delta\sigma_{R,50\%}\,(T = 20°C)} \tag{34}$$

where $\Delta\sigma_{R,50\%}\,(T)$ is the mean fatigue strength and $\Delta\sigma_{R,50\%}\,(T = 20°C)$ the corresponding mean fatigue strength at room temperature (i.e. 20 °C). The results are presented in Figure 36(a) for the different weld details and steel types. In the following sections, abbreviations will be used for the three specimens' types, i.e. 'B' for butt-joint, 'C' for cruciform joint, and 'T' for transversal stiffener.

Compared to room temperature, the fatigue strength of almost all test series increases constantly with decreasing temperature throughout the tested range with an average mean fatigue strength increase of 6.9% at -20 °C and 15.0% at -50 °C. This agrees well with the change in fatigue crack growth threshold data obtained from the literature, see Figure 5. Interestingly, the increase in nominal stress fatigue strength of the cruciform joints matches the change in ΔK_{th} (of about 12% at -20 °C and 21% at -50 °C compared to room temperature) the best. This is related to the sharp notch radii at the weld root. Due to this, the fatigue life of the cruciform joint specimens is almost entirely driven by crack propagation. This also supports the underlying assumption by the SED and N-SIF methods of linear relation between the stress intensity factor for mode I (K_I) and the mode I N-SIF K_1^N.

A second fatigue strength ratio $V_{R,97.7\%}$ for comparison of reference fatigue strength normalizes the fatigue strength $\Delta\sigma_{R,97.7\%}$ at $N = 2 \times 10^6$ cycles for a probability of survival of $P_s = 97.7\%$ with the corresponding IIW design fatigue strength $\Delta\sigma_{R,FAT}$.

$$V_{R,97.7\%} = \frac{\Delta\sigma_{R,97.7\%,\ R=0.5}\,(T)}{\Delta\sigma_{R,FAT}} \tag{35}$$

The results for the fatigue strength ratio $V_{R,97.7\%}$ according to Eq. (35) are presented in Figure 36(b), corrected for the difference in test and design stress ratio R ($R = 0$ in the tests and $R = 0.5$ in the guidelines). Mean stress correction factors $f\,(R) = 1.03$ and $f\,(R) = 1.08$ for the fillet-welded S235 and S500 specimens (cruciform joints and transversal stiffeners),

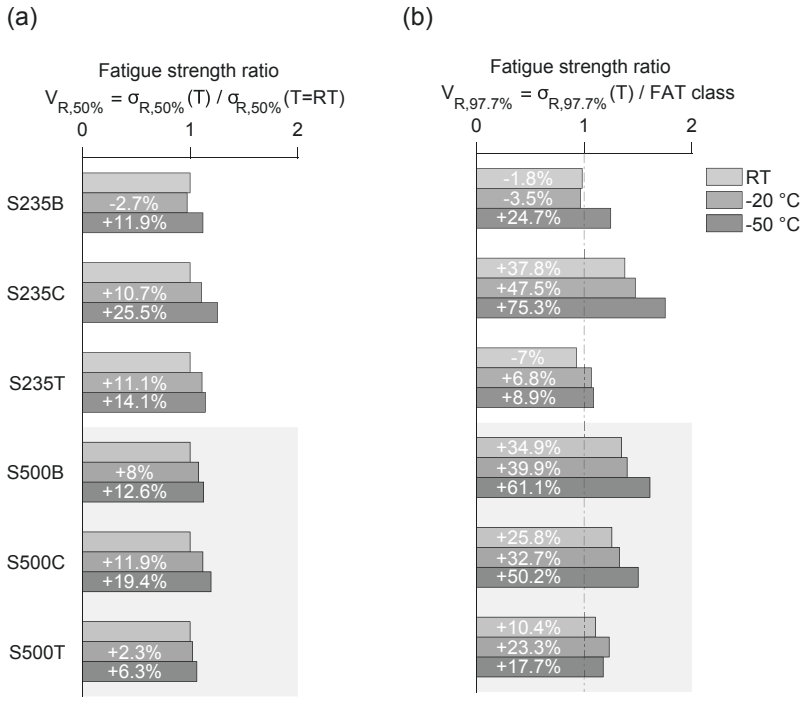

Figure 36. Ratio of experimental mean ($N = 2 \times 10^6$, $P_s = 50\%$) fatigue strength at sub-zero temperatures to room temperature (a) and ratio of experimental to corresponding fatigue strength class (b) ($N = 2 \times 10^6$, $P_s = 97.7\%$), corrected to $R = 0.5$ with the mean stress correction factors $f(R)$ for the fillet weld details derived in (Braun et al. 2020f) and $f(R) = 1.2$ for butt-welded joints

respectively, were derived based on additional tests with stress ratio $R = 0.5$ (see Braun et al. (2020f)). These mean stress correction factors are lower than the usual assumption of the IIW recommendations (Hobbacher 2016) for no remaining residual stresses after small-scale specimen production (i.e. $f(R) = 1.2$) but closer to results of Sonsino (2009), who obtained $f(R) = 1.1$ by analysing a large amount of fatigue datasets. Due to the difficulty of testing normal-strength steel joints at $R = 0.5$, the IIW recommendation (Hobbacher 2016) of $f(R) = 1.2$ is adopted for the butt-welded joints, which is, however, thought to be overly conservative for the S235 steel specimens. Further information concerning the tests and comparisons with temperature modification functions given in current design guidelines and standards is provided in Braun et al. (2020f).

4.5 | Conclusions from the experimental test programme

This chapter investigated the fatigue behaviour of welded normal and high-strength steel joints by means of stress–life tests at room- and sub-zero temperatures. Observations were then assessed using the results of Charpy impact testing presented in Section 3.2. Furthermore, the effect of temperature on the obtained fatigue strength was compared to fatigue design curves and controls at room temperature. The following conclusions are drawn from the investigation:

- Compared to room temperature, the fatigue strength of both steel types increases constantly with decreasing temperature for all three weld details. The average fatigue strength increase in mean fatigue strength compared to room temperature was about 7% and 15% at −20 °C and −50 °C, respectively.
- The highest relative increases in fatigue strength of 25.5% at −50 °C has been found for a steel grade that is only qualified for −20 °C according to the steel type designation.
- The observed increase in fatigue strength of the cruciform joints agree well with estimates based on changing fatigue crack growth rate threshold obtained from the literature data.
- Although fracture surface investigations reveal brittle fracture zones in test specimens that failed from cracks located in the weld metal, the fatigue strength further increases with decreasing test temperatures.
- The ductile–brittle transition behaviour at sub-zero temperatures of the fatigue test specimens agrees well with results obtained by means of Charpy V-notch impact testing.
- Comparison with design curves results in a conservative assessment of fatigue strength of welded joints at sub-zero temperatures.
- Finally, nominal stress fatigue design curves for welded joints derived from tests at room temperature are safe to be applied for temperatures down to −50 °C; nev-

ertheless, the actual fatigue strength at sub-zero temperatures is highly underesti-
mated.

5 | Statistical assessment of test temperature effect on fatigue strength

5.1 | Background on statistical assessment

With regard to the initial research question of temperature effects on fatigue strength of welded joints, an assessment of influencing factors on fatigue strength using statistical methods is of interest. For this purpose, the correlation between test temperature and number of cycles to failure is investigated. Furthermore, as misalignment effects are among the most influential parameters affecting fatigue strength, a comparison against the correlation between fatigue strength and stress magnification factor $\mathrm{k_m}$ of each specimen is performed. Finally, it will be assessed whether the number of test specimens was sufficient to warrant the conclusions drawn from the statistical assessment. The statistical approach is first presented using the fatigue test data for cruciform joints and subsequently applied to the two other weld details.

5.2 | Introduction of the statistical assessment and application to the cruciform joint fatigue test data

First of all, the hypothesis of normally distributed fatigue test data is tested for each specimen and steel type. The assessment is based on the residuals of logarithmic number of cycles to failure $\mathrm{N_f}$ from a linear regression model assuming a similar influence of temperature on all load levels. To confirm this assumption, the residuals are first plotted against the fitted logarithmic number of cycles to failure $\log \mathrm{N_f}$ from the linear regression model (assuming a normal distribution of $\log \mathrm{N_f}$) in Figure 37. Consequenntly, the data for all

temperatures is evaluated jointly.

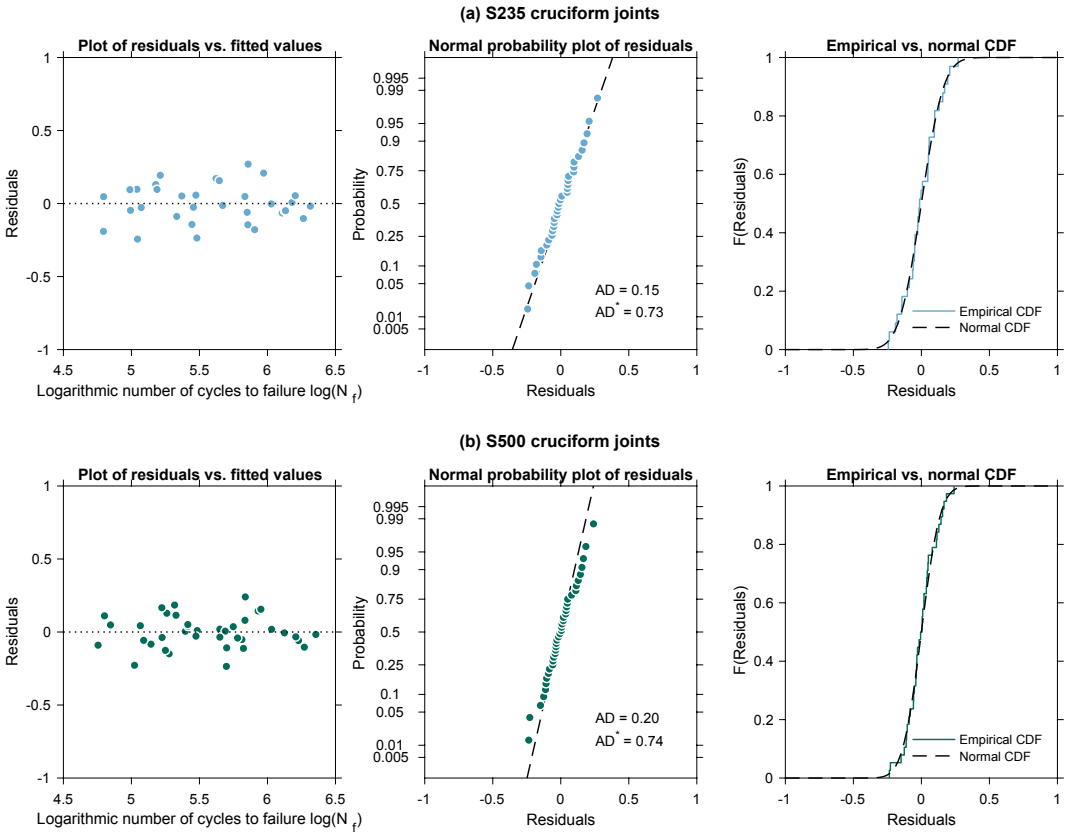

Figure 37. Difference between residuals and fitted normal distribution, normal probability plot of residuals with results of the Anderson-Darling test, and comparison of cumulative distribution functions for S235J2+N (a) and S500G1+M (b) cruciform joints

Notably, the residuals are evenly distributed around the mean (dotted line in left graphs repressing a residual of zero). This is a sign of a symmetrical distribution like a normal distribution. Next, to assess whether the data might stem from a normal distribution, the residuals are plotted against the probability distribution function (PDF) of a normal distribution (dashed line) in the second subplot in Figure 37(a). The closer the data fits the straight line the higher the likelihood it stems from a normal distribution.

To support the graphical assessment, Anderson-Darling tests (Anderson and Darling 1952) for normality were performed for each dataset, which is considered to be the most precise test to analyse whether a sample is drawn from a normal distribution (Wilker 2018). The null hypothesis (data stems from a normal distribution) is confirmed if the test value

AD is smaller than the critical value AD^*—at a given significance level α (here 0.05). A third method for a comparison of test data with an assumed distribution function is typically a comparison of the empirical cumulative distribution function (CDF) with a normal CDF.

Graphical and statistical hypothesis tests—such as the Anderson-Darling test—are not proof that a sample stems from a certain distribution but a good indication. A small uncertainty remains, which is specified by the significance level, e.g. of the Anderson-Darling test ($\alpha = 0.05$). Nonetheless, if all tests indicate a symmetrical distribution similar to a normal distribution and the Anderson-Darling tests confirm the null hypothesis, it can be assumed that the sample is drawn from a normal distribution. Furthermore, if the residuals are assumed to be normally distributed, it can be assumed that the fatigue data follows a log-normal distribution, which is generally assumed for fatigue test results of welded joints, see Haibach (2006).

The residual plots, the normal probability plots, and the comparison of the cumulative distribution functions of the cruciform joint (Figure 37) indicate a symmetrical function and show a good correspondence with the fitted normal distribution for both steel types. This result is backed by the outcomes of the Anderson-Darling tests. The test value AD is much smaller for both samples than the critical value AD^*. Hence, both samples are considered to be normally distributed.

Next, the correlation between the obtained residuals of logarithmic number of cycles to failure and test temperature during the fatigue tests is investigated and compared with the correlation between the residual and the stress magnification factor of each specimen. If the fatigue behaviour is similar (the failure mode is not significantly changed) for all test temperatures, a linear relation between the temperature and residuals is assumed. Thus, the most common type of correlation coefficient (i.e. Pearson correlation coefficients $\mathrm{r_{xy}}$ (Pearson 1895)) is used to assess the correlation, which is typically used to assess linear relations between variables. Furthermore, the probability value (*p*-value) of each fit is the result of a hypothesis test of no correlation against the alternative hypothesis of a non-zero correlation. In other words, if p is small (e.g. $\mathrm{p} < 0.05$) it is assumed that the correlation coefficient is significant.

As previously mentioned, the correlation of residuals of logarithmic number of cycles to failure $\mathrm{N_f}$ against the stress magnification factors $\mathrm{k_m}$ of each specimen is performed to highlight the effect of test temperature on fatigue strength. In Braun et al. (2020b)

it was observed that the formulas to assess stress magnification factors for butt-welded joints overestimate stress magnification factors if fixed clamps are used in fatigue tests; nonetheless, this effect is limited to high stress magnifications and small-scale butt-welded joints. For such scenarios, a non-linear relation can be assumed between misalignment and stress magnification. To enable a direct comparison with temperature effects, however, the same linear correlation coefficient definition (Pearson correlation coefficient r_{xy}) is applied to evaluate the correlation between residuals and stress magnification factors[6].

To evaluate the significance of the two correlation coefficients, Steiger's *Z*-test (Steiger 1980) is performed to test if the two Pearson correlation coefficients (e.g. for stress magnification factor and test temperature) are significantly different. Compared to other popular tests, this test is suitable for small datasets (Meng et al. 1992).

The results of the statistical evaluation of cruciform joint test series are presented in Figure 38. To be able to distinguish results for different test temperatures in the correlation plot of stress magnification factors, different colours are used for each test temperature. Assessing the data of S235 cruciform joints, a strong negative correlation ($r_{xy} = -0.80$) is observed between the residuals of logarithmic number of cycles to failure and test temperature, while there is no correlation between residuals and stress magnification factor. The latter is probably related to the low scatter of stress magnification factors for this weld detail, see Figure 25. The negative correlation between residuals and test temperature is due to the higher obtained fatigue strength at sub-zero temperatures (higher fatigue strength yields a result on the right side of the normal distribution and thus a positive residual).

The line in Figure 38 shows the steepness of the linear relation between test temperature and residuals with the confidence interval being highlighted in grey. The slope of the linear fit b is derived from correlation coefficients with:

$$b = r_{xy} \left(\frac{SD_y}{SD_x} \right) \tag{36}$$

where SD_y and SD_x are the standard deviation about x- and y-axes, respectively. A higher value b represents a stronger influence of temperature on residuals of logarithmic number

[6]Non-linear correlation coefficient formulations (e.g. Spearman's rank correlation) led to almost identical results and were thus not further considered.

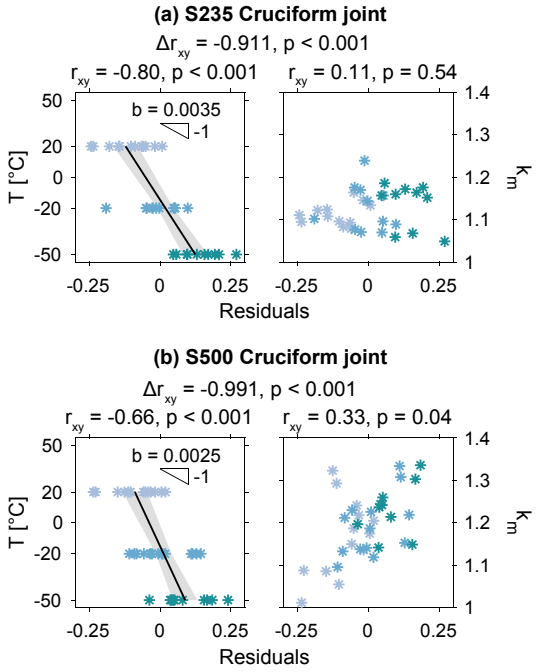

Figure 38. Correlation between test temperature and normal distributed residuals and comparison of correlation with stress magnification factors k_m for S235J2+N (a) and S500G1+M (b) cruciform joints

of cycles to failure. Furthermore, a small probability value p also leads to a small confidence interval.

A correlation is considered strong if $|r_{xy}| > 0.7$ and moderate if $|r_{xy}| > 0.3$ (Ratner 2009). As can be seen from Figure 38, the correlation between test temperature and residuals is strong for the S235 and close to being strong for the S500 cruciform joint test data. Moreover, there is almost no correlation between stress magnification factor k_m and the residuals for the S235 cruciform joints, whereas a moderate correlation is found for the S500 cruciform joints. This could be related to the increased range of stress magnification factors k_m of the latter as compared to the S235 cruciform joint specimens.

For both cases, it can be assumed that the variables are significantly different ($|\Delta r_{xy}| > 0.9$) as the outcome of the Z-test is statistically significant ($p < 0.001$). Interestingly, the two variables account for more than 90% of the variability of residuals in both cases. Consequently, it can be concluded that the two parameters (stress magnification factor and test temperature) are almost solely responsible for the relative fatigue strength, i.e. the

location within the normal distribution of residuals of logarithmic number of cycles to failure. This conclusion seems reasonable given a small variation in the weld throat thickness of the specimens and sharp notch radii at weld roots, see Figure 18. This leads to a fast crack initiation at several locations and similar crack growth behaviour and duration for all cruciform joint specimens. In contrast, specimen types with crack initiation at weld toes typically show larger scatter due to differences in fatigue crack initiation behaviour. Furthermore, the slope of the linear fit of test temperature against residuals of S235 cruciform joints is shallower (higher b) than for the S500 specimen. This is in line with the result of the change of mean fatigue strength presented in Figure 36.

Next, *bootstrapping* of the samples is performed in order to assess the variance of the obtained correlation coefficients. Bootstrapping approaches are a group of statistical methods belonging to the group of random sampling with replacement. Thereby, new samples are created from the original sample without the need to know the exact distribution of the original sample. By repeating this process a sufficient number of times, a probability density of the original sample or a confidence interval of a quantity like the correlation coefficient $\mathrm{r_{xy}}$ can be obtained; the typical number of repetitions is 1000 (Pattengale et al. 2009). An estimate of the correlation coefficient of the real population $\bar{\mathrm{r}}^{*}_{\mathrm{xy}}$ is then obtained by calculating the mean of the bootstrapped probability density estimates presented in Figure 39.

As can be seen from the two figures, the bootstrapped estimates seem to follow a normal distribution (solid line in the histogram). The standard deviation of a bootstrapped distributions is the standard error SE of the investigated quantity (here the correlation coefficient). If the sampling distribution is normally distributed, the 95% confidence interval of the mean value (estimate of the correlation coefficient $\bar{\mathrm{r}}^{*}_{\mathrm{xy}}$) corresponds to $1.96 \times \mathrm{SE}$ (Pham 2006).

The estimate of the correlation coefficient $\bar{\mathrm{r}}^{*}_{\mathrm{xy}}$ is equal to the calculated correlation coefficient of both samples of cruciform joints. More importantly, low standard errors and confidence intervals are obtained for both samples. One principle of bootstrapping is that the real variance of a quantity is approximately equal to the bootstrapped variance (Wu and Thompson 2020). This confirms the correlation between the test temperature and the residuals of logarithmic number of cycles to failure and thereby the high effect of test temperature on fatigue life.

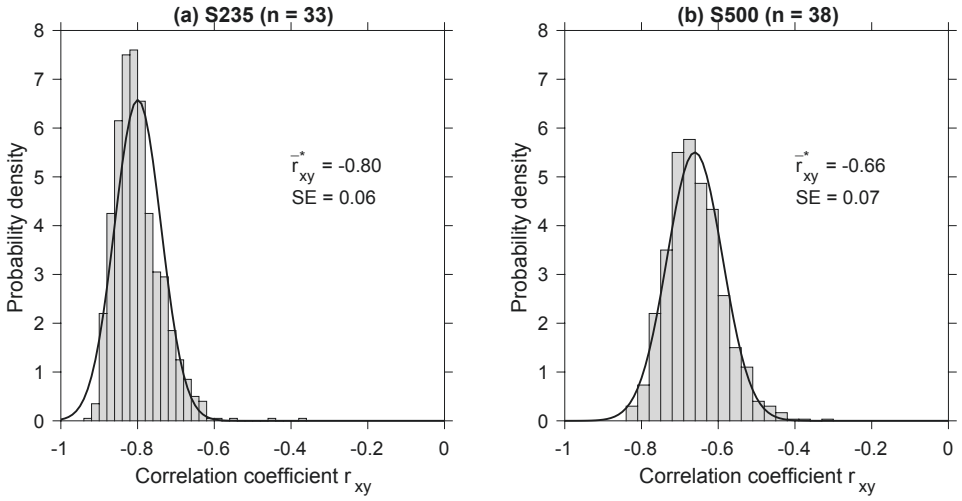

Figure 39. Histograms of probability density of correlation coefficients obtained from 1000 bootstrap samples from the initial sample size of S235 (a) and S500 (b) cruciform joint test data with estimates of the correlation coefficient $\bar{r}^{*}_{xy}$ and the standard errors SE

Next, the effect of the number of test specimens on the obtained correlation coefficient is assessed in order to investigate if the number of test specimens was sufficient to obtained the aforementioned conclusions. For this purpose, an increasing number of test specimens are randomly excluded from the initial dataset and a combination of a bootstrapping and a *jackknife approach* is applied.

Jackknife approaches are a different group of resampling methods—that pre-date bootstrapping approaches—with the aim of assessing the variance of a sample, see Efron (1992). Instead of creating additional samples by means of resampling, one or more observations are removed from the dataset. This process is repeated *n* times, resulting in *n* jackknife means. The estimate of a mean of a sample is then obtained from averaging all jackknife means.

The combination of both approaches allows us to investigate whether the same conclusions would have been obtained with a reduced number of specimens. In this context, the reduction of data is obtained by the jackknife approach, while the confidence interval of the estimates obtained from the reduced sample is assessed by bootstrapping. As a result, histograms of probability density of correlation coefficients obtained from 1000 bootstrapped samples after randomly removing 20 specimens from the S235 (a) and from the S500 cruciform joints (b) are tested for normality, see Figure 40. A minimum specimen

number of $n - 20$ was chosen for the jackknife approach, which is about the number of specimens tested for one test temperature instead of three, and corresponds roughly to the minimum size of specimens required to establish an *S–N* curve (DIN 50100:2016-12).

For the S500 joints, the data seems to follow a normal distribution but not for the S235 joints. This is related to the interval of correlation coefficient, i.e. [−1, 1]. More importantly, the scatter (spread of the distribution) increases for a lower number of specimens n. From a normal distribution fit, confidence intervals of 0.253 and 0.294, respectively, are obtained for the two probability plots presented in Figure 40. Only a small difference in the estimates is obtained for the full and reduced sample size ($n - 20$) of S235 joints. This result is, however, coincidental. A single jackknife assessment is not suitable to assess the variance of the jackknife means as the results are highly dependent on the randomly excluded specimens. The aforementioned procedure—to estimate the correlation coefficient r_{xy}—is thus repeated 1000 times for decreasing number of specimens until $n - 20$.

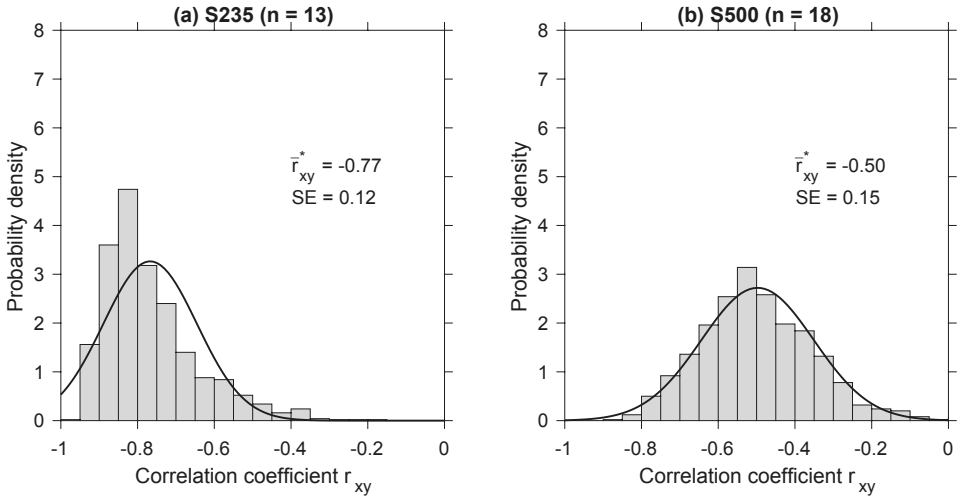

Figure 40. Histograms of probability density of correlation coefficients obtained from 1000 bootstrap samples after randomly removing 20 specimens from the initial sample size of S235 (a) and S500 (b) cruciform joint test data with estimates of the correlation coefficient $\bar{r}^{*}_{xy}$ and the standard errors SE

From the 1000 repetitions, the mean and the confidence band of the mean are consequently obtained for each number of specimens. The result of the assessment of cruciform joint test data is presented in Figure 41. Here, the estimate of the correlation coefficient (mean value) is indicated by the lines and the confidence interval by the shaded area

around the mean. As can be seen from the figure, the confidence interval continuously increases for decreasing number of specimens; yet, the correlation remains moderate to strong even for the lowest number of specimens ($n - 20$). Finally, it can be concluded that for a much smaller sample size ($n - 20$) a correlation between test temperature and fatigue strength of the cruciform joints would have also likely been obtained.

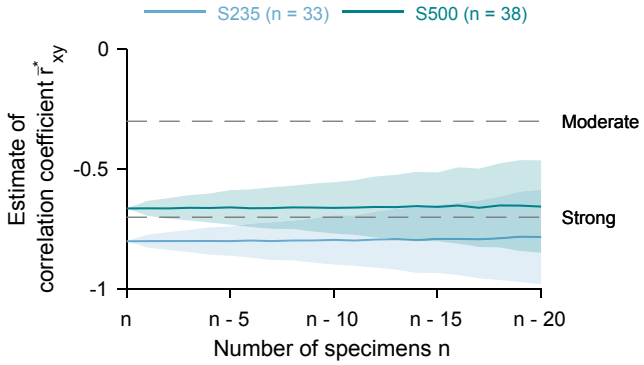

Figure 41. Change of confidence intervals of the estimated correlation coefficients $\bar{r}^*_{xy}$ with number of specimens $n - 20$ of cruciform joint test data; the lines represent the mean of the 1000 bootstrapped samples and the shaded area the confidence intervals

5.3 | Statistical assessment of transversal stiffener fatigue test data

The same statistical assessment is now repeated for the results obtained from testing transversal stiffener specimens. First of all, residuals of logarithmic number of cycles to failure are tested for normality using graphical tests and the Anderson-Darling test. Interestingly, the null hypothesis of normal distributed data is rejected for the S500 steel due to one specimen with exceptional high fatigue strength at the upper right corner of the normal probability plot, see Figure 42(b).

The residual of the assumed outlier is about two and a half times that of the second highest residual. The result was therefore removed from further assessments. As a consequence, the reassessment of the residuals (presented in Figure 42(c)) now leads to an accepted null hypothesis of the Anderson-Darling test and much better graphical agreement between empirical and theoretical normal CDF in the tails.

Compared to the S500 sample, a higher scatter of residuals is obtained for the S235 series and a worse correspondence with the normal distribution fit in the middle and the

tails of the probability plot. This is anticipated as the fatigue test data showed a higher scatter for each test temperature than the corresponding data of the S500 joints.

From the assessment of the correlation between residuals and test temperature as well as stress magnification factor k_m, a moderate correlation is found for both steel types, see Figure 43; however, the significance of the results is much lower than for the cruciform joints. Interestingly, a moderate correlation between stress magnification and residuals is found for the S500 specimens, while no correlation is obtained for the S235 specimens. Moreover, the results from the Steiger's *Z*-test fail to support the hypothesis that both correlations are independent. The reason for this is likely related to other influencing factors affecting fatigue strength of specimens failing from weld toes as compared to weld roots. Clearly, factors like local weld geometry (weld toe radius and angle) affect fatigue strength for transversal stiffeners, while the notch geometry at the weld root is almost identical for all cruciform joint specimens. Nonetheless, based on the confidence intervals of the linear regression of test temperature and residuals, a trend towards higher fatigue strength at lower temperatures is observed.

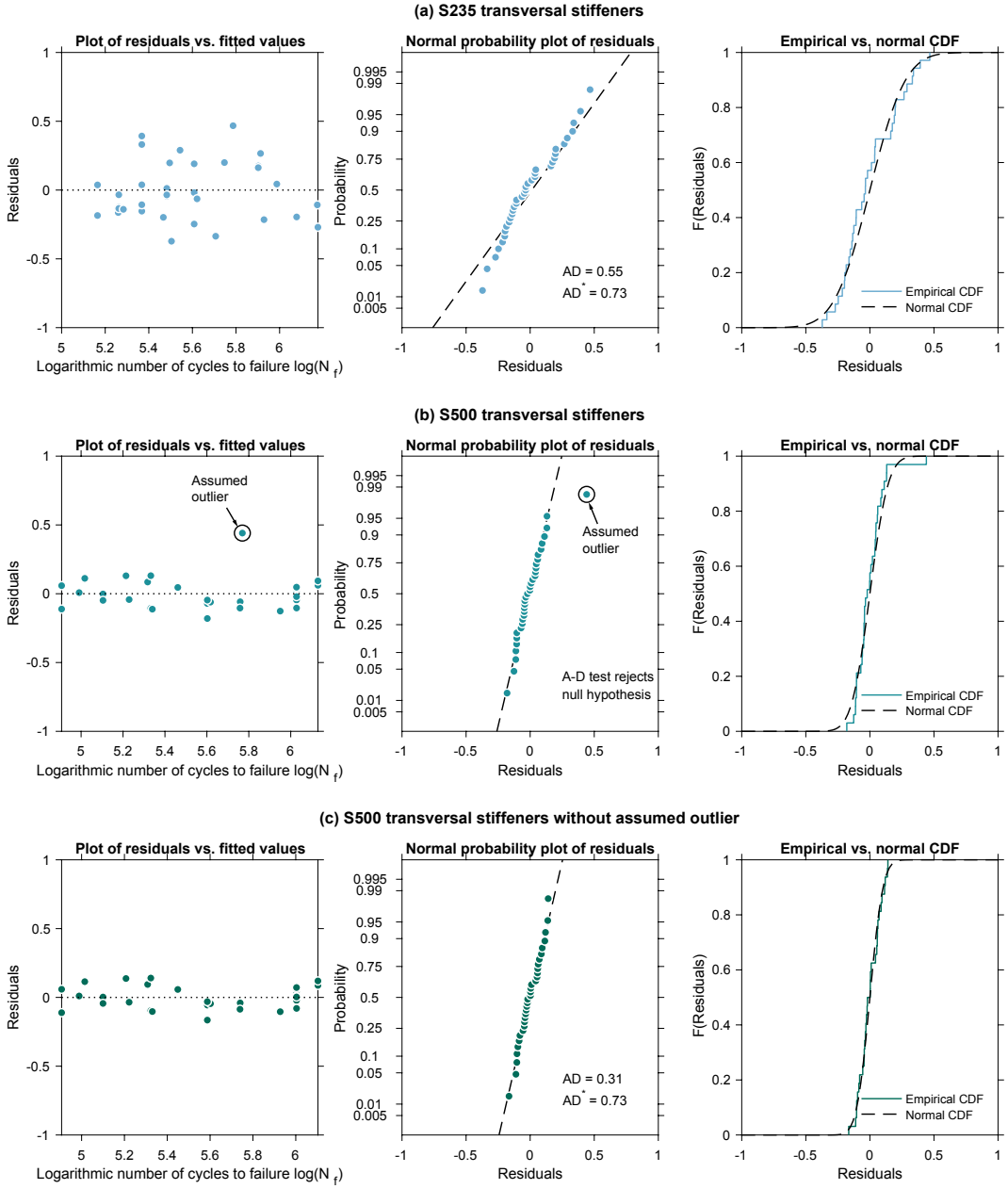

Figure 42. Difference between residuals and fitted normal distribution, normal probability plot of residuals with results of the Anderson-Darling test, and comparison of cumulative distribution functions for S235J2+N (a) and S500G1+M (b) transversal stiffeners, as well as of S500G1+M transversal stiffeners after removing an assumed outlier (c)

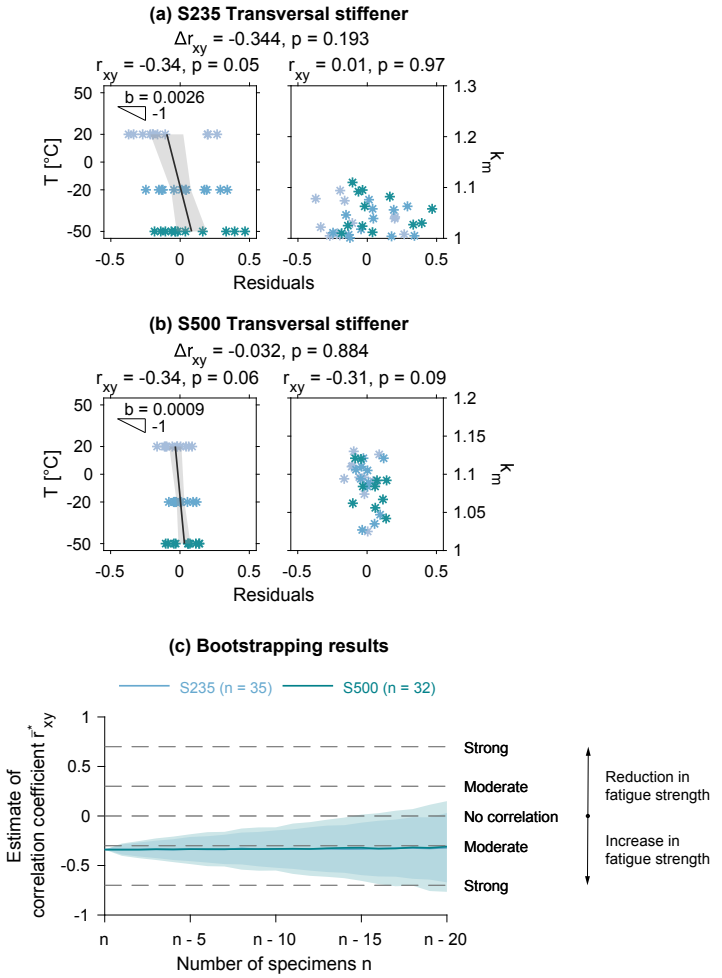

Figure 43. Correlation between test temperature and normal distributed residuals and comparison of correlation with stress magnification factors k_m for S235J2+N (a), S500G1+M (b) transversal stiffener, as well as the change of confidence intervals of the estimated correlation coefficients $\bar{r}^*_{xy}$ with number of specimens (c)

Since the correlation coefficient is similar for both steel types, the confidence interval for reducing the number of specimens of the jackknife assessment is largely overlapping and has a similar range, see Figure 43. For $n - 20$ specimens a confidence interval of about $\pm$ 0.4 around the mean is calculated. It thus ranges from no correlation to a strong correlation. The larger scatter and thereby uncertainty of the obtained correlation coefficient—compared to the cruciform joints—is also confirmed from the assessment of the

bootstrapped probability density estimate of the initial sample of S500 transversal stiffeners (see Figure 44(a)). Here, a standard error of $\mathrm{SE} = 0.17$ is obtained, which corresponds to a confidence interval of $\pm$ 0.33. This is more than twice as much as for the cruciform joint data. For the smallest analysed data set ($\mathrm{n} - 20$), the standard error and confidence interval are significantly increased, see Figure 44. The results of the S235 transversal stiffener specimens are not presented as they are very similar to those of the S500 specimens.

It can be concluded that the number of specimens was sufficient to come to the conclusion that there is a correlation between test temperature and number of cycles to failure, but the data set should not have been much smaller. Earlier studies on welded joints at sub-zero temperatures tested much fewer specimens than were tested for this study. Given the presented result, their conclusions have to be treated with caution.

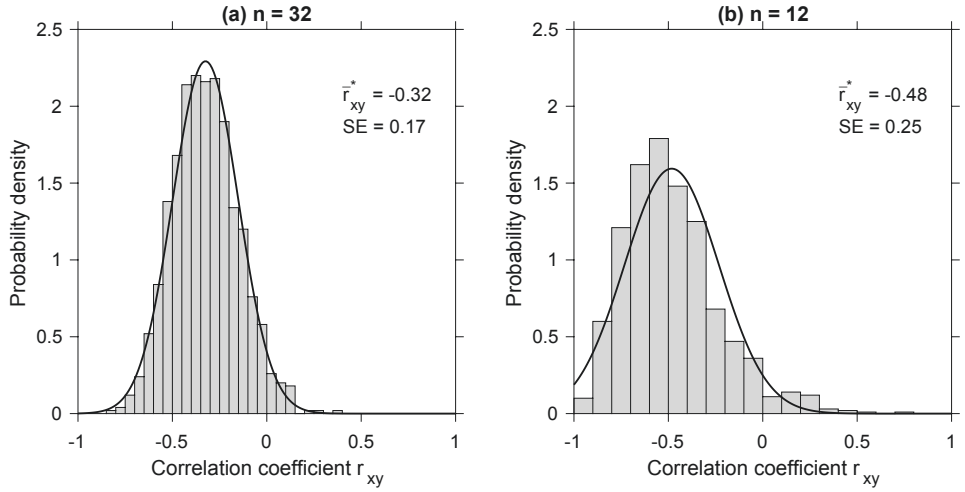

Figure 44. Histograms of probability density of correlation coefficients obtained from 1000 bootstrap samples from the initial sample size of S500 transversal stiffener test data (a) and after randomly removing 20 specimens (b)

5.4 | Statistical assessment of butt-welded joint fatigue test data

Finally, the test data of the butt-welded joints is statistically assessed for temperature effects on fatigue strength. First of all, due to the large scatter for both steel types—which is thought to be related to the high weld quality and corresponding shallow slope of the *S–N* curve—a larger number of fatigue tests have been performed compared to the test series of the other two weld details. Although the scatter of the residuals of logarithmic

number of cycles to failure from the linear regression model (normal distribution) is the highest of all test series, the null hypothesis of the sample being drawn from a normal distribution is not rejected by the Anderson-Darling test, see Figure 45.

From graphical comparison with typical normal probability plots, it appears that the residuals of the S235 butt joints stem from a right-skewed distribution. The discrepancy in the tails of the empirical CDF supports this conclusion; yet, the AD test value is significantly lower than the critical value. Interestingly, the AD test value of the S500 butt-welded joints is identical to the S235 joints; nonetheless, the distribution functions appear closer to a normal distribution function.

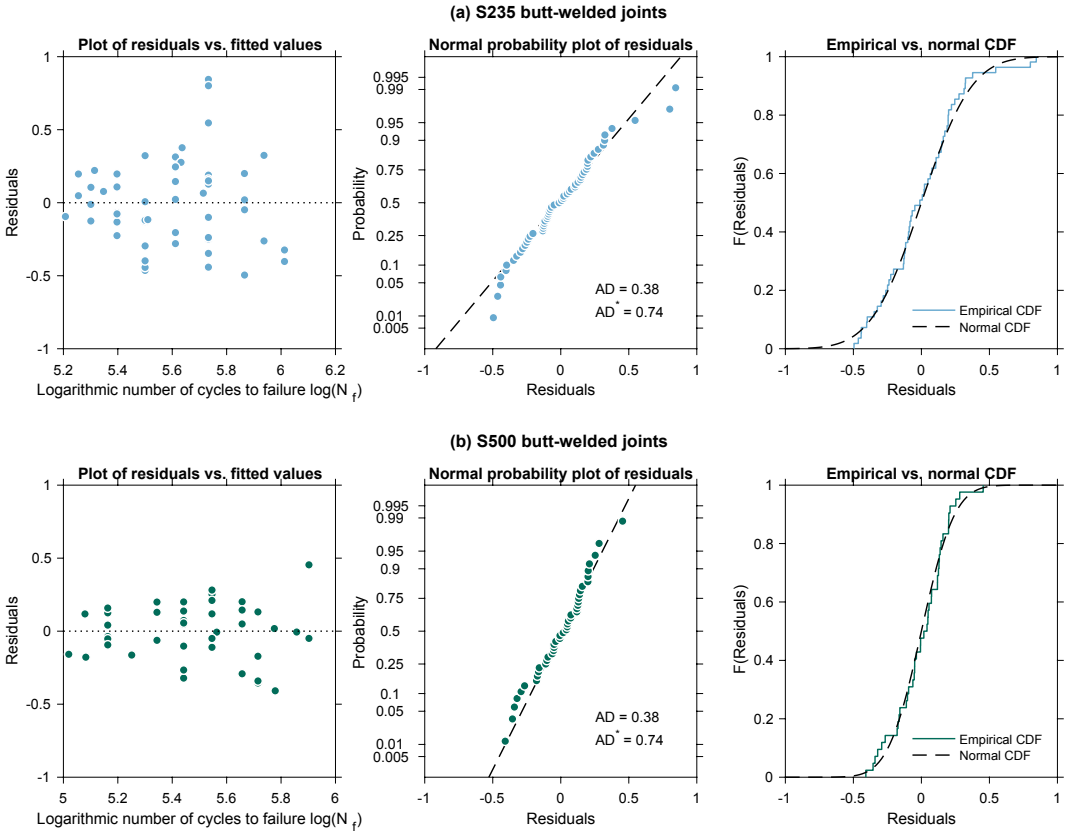

Figure 45. Difference between residuals and fitted normal distribution, normal probability plot of residuals with results of the Anderson-Darling test, and comparison of cumulative distribution functions for S235J2+N (a) and S500G1+M (b) butt-welded joints

Comparing the correlation of residuals and test temperatures as well as stress magnification factors, a higher correlation with stress magnification factors is obtained for both

steel types. Interestingly, the correlation coefficient between test temperature and residuals of the S235 sample is almost zero. This does not mean that there is no temperature effect on fatigue strength of the S235 butt-welded joints but the correlation to the stress magnification factor is much stronger, which is likely to influence the other correlation.

Furthermore, a large number of tests performed at room temperature showed very high fatigue strength (positive residuals). From Figure 46(a) it can be seen that the majority of S235 tests at room temperature were performed using test specimens with a small stress magnification factor, while the tests of other test series (including the tests of the S500 butt joints) had more evenly distributed scatter of stress magnification factors. Thus, the missing correlation to test temperature seems to be influenced by the correlation to the stress magnification factors of the S235 butt joint specimens.

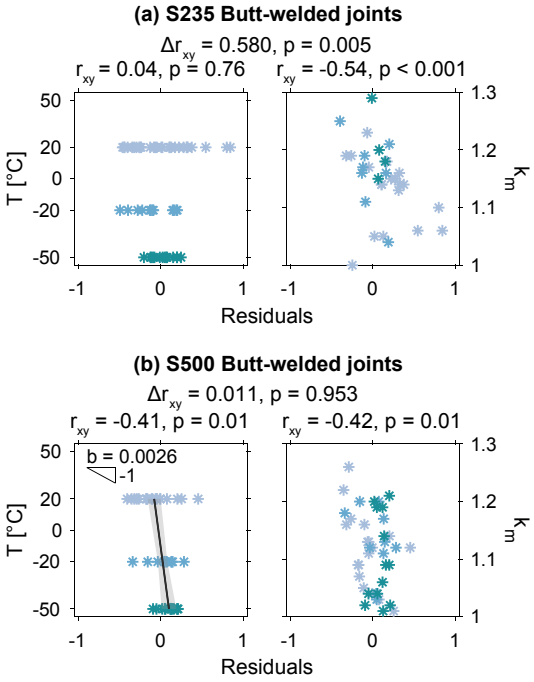

Figure 46. Correlation between test temperature and normal distributed residuals and comparison of correlation with stress magnification factors k_m for S235J2+N (a) and S500G1+M (b) butt-welded joints

Interestingly, a similar correlation coefficient was calculated for the correlation between test temperature and residuals, and test temperature and stress magnification factors for the S500 specimens. As a consequence, Steiger's Z-test rejects the null hypothesis of

independent correlation of test temperatures and stress magnification factors. Notably, the range of residuals at −50 °C is smaller than at −20 °C and room temperature. The reason for this result is not clear; yet, the result might be influenced by other factors such as local weld geometry.

From the bootstrap assessment (Figure 47) of the correlation coefficients, a lower standard error is obtained for S235 and S500 butt joints as for the transversal stiffeners. It can thus be concluded that the missing correlation between residuals of logarithmic cycles to failure to test temperature of the S235 butt joints is not coincidental but evidently related to other influencing factors like the weld geometry. Finally, more tests for the butt-welded joints would likely help the assessment of whether the test temperature has a significant effect on fatigue strength. Hence, no jackknife assessment was performed for the butt-welded joints.

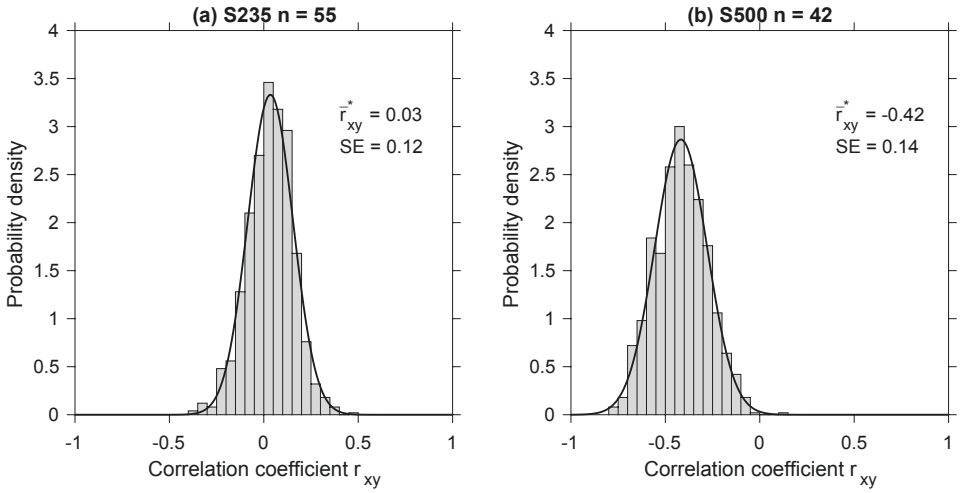

Figure 47. Histograms of probability density estimate of correlation coefficients obtained from 1000 bootstrap samples of S235 (a) and S500 (b) butt-welded joint test data

5.5 | Conclusions from the statistical assessment of the fatigue test results

This chapter investigated the effects of temperature on the obtained fatigue strength results based on statistical methods. The following conclusions are drawn from the investigation:

- First of all, it can be concluded that the residuals of the logarithmic number of cycles to failure for all three weld details and the two steel types are normality distributed, as the Anderson-Darling test does not reject the null hypothesis of the samples being drawn from a normal distribution. This is expected for welded specimens as it means that the fatigue life itself is log-normal distributed, but still it is important to verify as it supports further assessments based on the assumption of normally distributed residuals. The sample of the S235 butt-welded joints shows some deviation from a normal distribution in the tails, but the Anderson-Darling test results still supports the assumption of normally distributed residuals.

- The statistical assessment of the fatigue test data reveals a strong correlation between the test temperature and the residuals of logarithmic number of cycles to failure for the two cruciform joint specimen series. This is thought to be related to the low observed scatter in fatigue test results, which is in turn related to the larger number of crack initiation sites at the sharp notch of the weld root. It is well known that fatigue test specimens with high notch acuity usually show less scatter than mildly notched specimens and scatter in fatigue test results is often associated with variations in crack initiation behaviour.

- A moderate correlation between the test temperature and the resulting number of cycles to failure is observed for the transversal stiffener specimens. This is related to the additional influencing factors for specimens with weld toe failure (larger variation in local notch geometry and thereby in the number of crack initiation sites).

- The missing correlation between residuals of logarithmic number of cycles to failure to test temperature of the S235 butt joints is not coincidental but evidently related to the specimens' misalignment.

- The slope of the linear fit b for the different weld details and steel types cannot be compared directly, since the residuals of each data set are influenced by the general scatter of fatigue test results; yet, it is interesting to note that the absolute values are all in the same order of magnitude. More importantly, if a correlation between residuals of logarithmic number of cycles to failure to test temperature was obtained,

the result always showed a positive effect of decreasing test temperature on fatigue strength.

- Finally, the combined assessment of fatigue test data by means of bootstrapping and jackknife approaches confirm that the number of test specimens of cruciform joints and transversal stiffener was large enough to come to these conclusions. For the cruciform joints, a much smaller number of specimens would have been sufficient to confirm an effect of test temperature on fatigue strength; however, for the mildly notched butt-welded joint specimens, more data might be useful to sufficiently confirm the temperature effect.

6 | Numerical fatigue assessment of welded joints at sub-zero temperatures based on the micro-structural support effect hypothesis

6.1 | Introduction and scope of the numerical fatigue assessment

As the effect of temperature on fatigue strength has been proven statistically in the previous chapter, the following chapter focuses on the development of fatigue assessment methods that are able to account for temperature effects on a sound physical basis.

Currently, state-of-the-art fatigue assessment methods in international standards and guidelines for fatigue design of ships and offshore structures are all based on *S–N* approaches, cf. (EN 1993–1–9:2005; DNVGL-CG-0129; *DNV GL Rules for Classification, Ships, Pt. 3 Hull, Ch. 9 Fatigue* 2019; ABS Guide for the Fatigue Assessment of Offshore Structures); nevertheless, effects that do not directly influence the respective stress can only be incorporated via modification factors. These include thickness (Hobbacher 2017), environmental (Milella 2012), post-weld treatment and special welding techniques (Yildirim et al. 2013; Baumgartner et al. 2019; Hensel et al. 2020), but also temperature effects (BS 7910:2013+A1:2015; Hobbacher 2016). (Braun et al. 2020a)

From the statistical assessment and the comparison of *S–N* curves, it is possible to derive modification factors for typical *S–N* approaches. This was, for example, presented in Braun et al. (2020d) for fillet-welded joints with weld toe and root failure; yet, these

factors are limited to individual fatigue assessment methods and failure locations. The transferability to other methods or joint types is questionable.

In order to develop a general concept to account for temperature effects, two different methods (the averaged strain energy density method and the stress averaging approach) were extended to cover temperature effects within fatigue assessment in Braun et al. (2020a, 2021b). These two methods are thus reapplied in this thesis to study subzero temperature fatigue strength of welded steel joints based on the micro-structural support effect hypothesis in a comprehensive way that links and compares the two different approaches. Furthermore, a comparison of prediction accuracy to state-of-the-art stress-based fatigue assessment methods is presented based on the results obtained in Braun et al. (2020d).

The first is the stress averaging approach that is a method which has gained significant interest in recent years, judging by the variety of applications (Benedetti et al. 2010; Spaggiari et al. 2011; Zhang et al. 2012; Baumgartner et al. 2013, 2015; Louks and Susmel 2015; Schmidt et al. 2015; Li et al. 2016; Liinalampi et al. 2016; Al Zamzami and Susmel 2017; Karakaş 2017; Marulo et al. 2017; Al Zamzami and Susmel 2018; Baumgartner et al. 2018; Karakaş et al. 2018; Santus et al. 2018; Baumgartner et al. 2019; Beber et al. 2019; Braun et al. 2019; Faruq and Susmel 2019; Luo et al. 2019; Muñiz-Calvente et al. 2019; Baumgartner et al. 2020a; Braun et al. 2020e; Justo et al. 2020). The basic idea is that the stress gradient in the vicinity of a stress raiser like a weld toe or root is averaged over a micro-structural support length ρ^* which reflects the support effect of the surrounding material.

The second method is the averaged strain energy density method, which—similar to the stress averaging approach—derives a fatigue-effective quantity by assessing the area or volume around a stress raiser; nonetheless, instead of averaging the stress gradient, the local elastic SED is averaged. This method has already been successfully applied to notch fatigue at high temperatures, see (Berto et al. 2013, 2014; Gallo et al. 2015; Bourbita and Remy 2016; Gallo and Berto 2016).

6.2 | Consideration of misalignment effects within fatigue assessment

Before the assessment procedure and the results of both methods are presented, a short introduction to how misalignment effects have been considered in the assessment shall be given. This is an important aspect when assessing fatigue test results of welded joints, as has previously been shown within the statistical assessment of fatigue test results in Chapter 5.

Welded plates show varying axial (offset e) and angular misalignment (angle φ) along the weld seam, due to the non-uniform heating and cooling process during welding. If a fatigue test specimen containing misalignment is loaded under tension, secondary out-of-plane bending stresses arise due to the non-linear geometry. Such effects are well known to significantly affect fatigue strength and thus fatigue assessment, see (Maddox 1985; Ferreira and Branco 1991; Andrews 1996; Lotsberg 2009; Dong et al. 2019; Ottersböck et al. 2019). To improve fatigue assessment accuracy, all test results are corrected for their misalignment-induced secondary bending stresses as these vary considerably between specimens. (Braun et al. 2020b,d)

In this study, misalignment effects in fillet-welded joints are considered by a raised nominal stress, which is derived from stress magnification factor equations presented in the IIW recommendations (Niemi et al. 2018) and Section 3.4.1. For butt-welded joints a procedure presented in Braun et al. (2020b) is applied. This method takes the reduction of seam sag during specimen clamping into account. Current recommendations do not account for this effect, as it is limited to small-scale specimens and typically only pronounced in thin butt-welded joints (thickness $t \leq 10$ mm); yet, it has been shown to be important for the fatigue assessment of butt-welded joints, see Robert and Fricke (2015) and Ottersböck et al. (2018).

The level of misalignment included in fatigue design curves is sometimes not known or can only be roughly estimated as for the SED method, see Fischer et al. (2016c). For typical stress-based methods, information of included misalignment levels are given in the IIW recommendations (Hobbacher 2016) and for the stress averaging approach in Baumgartner et al. (2015). Typically, design curves (i.e. FAT160 of the stress averaging approach) are derived using specimens with limited misalignment, i.e. all specimens complied to EN ISO 5817:2014 quality level B, or were corrected for misalignment effects. The majority of this

thesis' specimens fulfil quality level B of EN ISO 5817:2014, with the exception of some butt-welded joints. These, however, fulfil level C due to angular misalignment between 1° and 2°. Due to the large range of misalignment levels, and thereby secondary bending stresses, it is important to consider the actual stress state for fatigue assessment. (Braun et al. 2021b)

For local and semi-local methods included in international standards (structural stress and effective notch stress methods), a small constant stress increase due to misalignment (magnification of 1.05) is considered to be covered by the design curves, see Hobbacher (2016). For the SED method, a similar estimation was performed by Fischer et al. (2016c) as the data used to derive these design curves came from the same database; nonetheless, exact values are not known for all methods, e.g. Xiao and Yamada's 1 mm stress approach (Xiao and Yamada 2004a,b). As the level of already covered stress magnification is small compared to the actual stress increase of some specimens of this study, no correction for already covered misalignment is applied.

6.3 | Stress averaging approach

6.3.1 | Model development and averaging of stress gradients

The stress averaging approach based on Neuber's idea of micro-structural support effect (Neuber 1958) is one of the oldest fatigue assessment methods for notched components; nonetheless, until a few years ago, it was rarely applied for welded joints due to computationally demanding FE simulations. With the increasing processing power of modern computers, it can now be fairly easily applied within assessment routines for seam-welded joints. Baumgartner et al. (2015) proposed two different methods of FE modelling for the application of the stress averaging approach to welded joints. The first alternative is modelling weld toes with the actual notch radii ρ_{real} and the second is using a reference radius ρ_{ref}. Both ideas have proven to be successful for certain scenarios; yet, modelling seam welds with the actual notch geometry is hindered by the high variation of weld geometry along the seam as well as difficulties in measuring the local weld geometry (i.e. weld toe radius and weld toe angle), see (Hou 2007; Schork et al. 2018; Hultgren and Barsoum 2020; Niederwanger et al. 2020; Schubnell et al. 2020a; Renken et al. 2021). Thus, the

constant reference radius of $\rho_{ref} = 0.05$ mm is adopted in this study to be able to verify the approach at room temperature based on the FAT160 design curve recommended by Baumgartner et al. (2015).

The FE models of this study are either quarter or half models to make use of the symmetry of the weld details, see Figure 48. Due to small variations of weld geometry between the test specimens, the median weld geometry obtained from Figure 28 was used to build the butt-joint FE model. For the transversal stiffener model, a median weld flank angle of about 138° was measured for both steel types (see Figure 29), which is slightly larger than the typically assumed angle of 135°; still, an angle of 135° was used for the FE model for the sake of comparability. Similarly, the cruciform joint model was built using a flank angle of 135°. Using the correct throat thickness has a much higher impact on the local stress state than the small variation of flank angle for these joints due to crack initiations at the weld roots. Furthermore, the definition of the throat thickness based on Eq. (32) also accounts for the actual flank angle. To simplify the assessment, the median throat thickness was thus used to build the FE models (e.g. $a_{th} = 5.71$ mm for the S235 cruciform joints); nonetheless, the actual throat thickness of each specimen is used to calculate the nominal stress (Braun et al. 2020a).

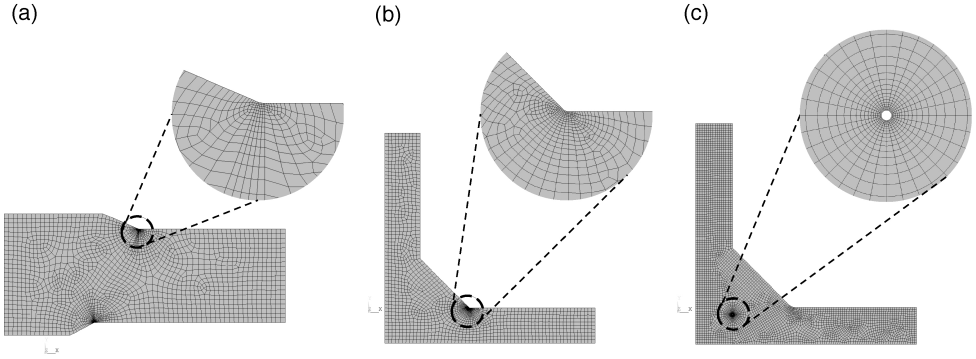

Figure 48. FE models of butt-welded joint (a), transversal stiffener (b), and cruciform joints specimens, with a root gap opening angle of 0.01° to simulate a weld root opening angle of almost zero degrees

The depth of the root gap was estimated to be equal to the plate thickness (i.e. full lack of penetration) based on the macrographs presented in Figure 18. Finally, the root gap opening angle was set to 0.01° to simulate a weld root opening angle of almost zero

degrees. Due to the small angle only the end of the keyhole is visible in Figure 48(c). At some weld roots higher opening angles are observed; nevertheless, it is assumed that the opening angle approaches zero degrees at several locations along the weld root seam.

A similar modelling procedure was adopted in (Baumgartner et al. 2015; Schmidt et al. 2015; Baumgartner et al. 2019); yet, Baumgartner et al. (2015) and Schmidt et al. (2015) based their models on averages of measured geometrical features. The difference in effective stress caused by the difference between mean and median, however, is thought to be negligible relative to the scatter of fatigue test results related to variations in local weld toe radii and angle. Fatigue cracks typically initiate at extreme values (e.g. smallest radius) rather than the mean or median quantities of geometry, see (Hou 2007; Hultgren and Barsoum 2020; Niederwanger et al. 2020). The median was selected over the mean as it is less sensitive to extreme values caused by local variations or incorrect measurements.

For mesh refinement, the recommendations developed in (Braun et al. 2020e) are adopted. In this study, it was concluded that 24 elements per 360° with a quadratic shape function are sufficient for weld toes (135° opening angle) and 32 elements per 360° for weld roots (Braun et al. 2020e). Moreover, typical material parameters for linear elastic FE simulations are applied, i.e. a Young's modulus $\mathrm{E} = 206$ GPa and a Poisson's ratio $\nu = 0.3$. To assess the varying nominal stresses applied to the test specimens, a unit stress is applied to the free edge of the FE model and subsequently scaled in post-processing (including the stress magnification due to misalignment).

Next, the location of maximum stress along the weld toe or root radius is determined and the maximum principal stress is averaged perpendicular to the direction of maximum principal stress. This is performed using scripts in Matlab. Examples of the stress gradients obtained for the S235 specimens are presented in Figure 49. The abbreviation 'WT' denotes the failure location weld toe of the S235 butt-welded joints. Besides recommendations for mesh refinement, an efficient way of curve fitting for steep stress gradients, by piecewise cubic hermite interpolating polynomial (PCHIP) curve fitting, was suggested in Braun et al. (2020e), which is here adopted.

From Figure 49(b), the typical difference in effective stress gradient at weld toes and roots can be observed. Assuming a micro-structural support length of ρ^* = 0.4 mm, a 30% higher normalized effective stress is obtained for transversal stiffener specimens compared to the cruciform joints, see Bruder et al. (2012).

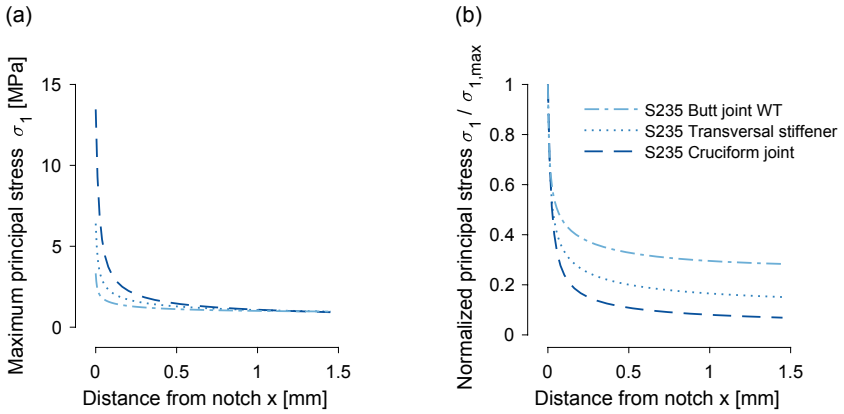

Figure 49. First principal stress gradients of the three analysed S235J2+N weld geometries (a) and normalized by the peak stress for the different specimen types (b), adopted from Braun et al. (2021b)

In order to derive the micro-structural support length ρ^*, the inverse problem is solved as explained in Section 2.4. For this purpose, the stress gradient is averaged according to Eq. (2) over increasing values of ρ^* and plotted into an *S–N* curve. By doing so, ρ^* is varied in the range of 0.05 to 1 mm in 0.025 mm steps. For each micro-structural support length ρ^*, a new *S–N* curve is calculated by linear regression using a fixed slope exponent $k = 3$ (typical for welded joints) as presented in Section 4.1. Finally, the value of ρ^* that leads to the least scatter is assumed to correspond to the micro-structural support length ρ^* (see Baumgartner et al. (2015)).

Baumgartner et al. (2015) and Marulo et al. (2017) applied fixed slopes $k = 4$ and $k = 5.63$ for their assessment since the dataset consisted mainly of thin-walled specimens (thickness $t < 10$ mm). In a more recent study, Baumgartner et al. (2019) again applied a fixed slope $k = 4$, since post-weld treated joints are usually more realistically represented by *S–N* curves with slopes $k > 3$ (cf. (Yıldırım 2015; Braun et al. 2018; Ahola et al. 2021; Braun and Wang 2021)). In the current study, a slope $k = 3$ is chosen since it agrees well with the majority of nominal stress *S–N* curve slopes (mean slope exponent of all S235 test series $\overline{k} = 3.23$, see Table 4). This is furthermore in line with recommendations for welded joints by the IIW (Hobbacher 2016) and only slightly below recent findings by Baumgartner et al. (2020a), who obtained average slope exponents between $k = 3.5$ and $k = 4.1$ for transversal stiffener type specimens and butt-welded joints with thickness $t \geq 10$ mm, respectively.

6.3.2 | Assessment results at room temperature

The results for the S235 specimens tested at room temperature are presented in Figure 50 for ρ^* = 0.475 mm, i.e. the value that yields the minimum scatter ratio $1/T_s$ based on Eq. (3). The notation of Section 4.4 was reapplied to distinguish test series, i.e. 'T' for transversal stiffener, 'C' for cruciform joint, and 'B' for butt-welded joint specimens. On the right side of Figure 50 the change of the scatter ratio $1/T_s$ and reference fatigue strength $\Delta\sigma_{R,97.7\%}$ ($N_f = 2 \times 10^6$ cycles and $P_s = 97.7\%$) are presented for varying values of ρ^*. Furthermore, the shaded area corresponds to the region enclosed by the curves for 10% and 90% survival probability (i.e. the curves that define the scatter ratio $1/T_s$). (Braun et al. 2021b)

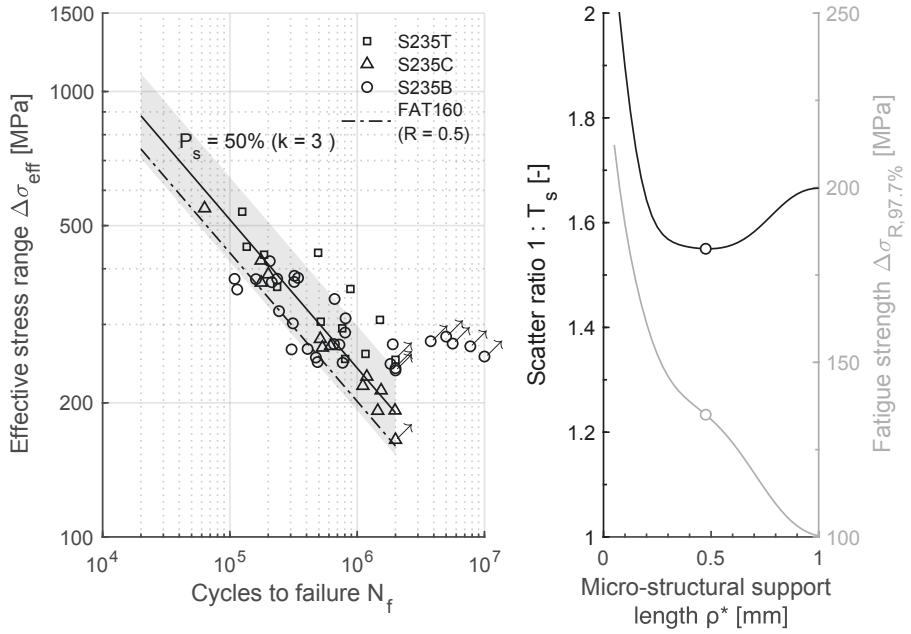

Figure 50. *S–N* curve obtained for stress averaging the S235J2+N room temperature fatigue test data for the minimum scatter ratio $1/T_s$ at ρ^* = 0.475 mm (left) and change of fatigue strength and scatter ratio over micro-structural support length ρ^* (right), for R = 0 and based on Braun et al. (2021b)

First of all, the assessment leads to a plateau of almost equal micro-structural support lengths ρ^* in the range 0.3 to 0.55 mm, thus making it difficult to correctly determine

the micro-structural support length ρ^* at room temperature. The micro-structural support length $\rho^* = 0.475$ mm that led to the minimum scatter ratio ($1/T_s$) is found to be close to the typically assumed value for welded joints of ρ^* = 0.4 mm (cf. (Radaj 1990; Lazzarin et al. 2004; Radaj et al. 2006, 2013; Baumgartner et al. 2015; Baumgartner 2017)). Consequently, to be able to compare the results with results from the literature, the fatigue test results at room temperature are presented in Figure 51 for a micro-structural support length ρ^* = 0.4 mm.

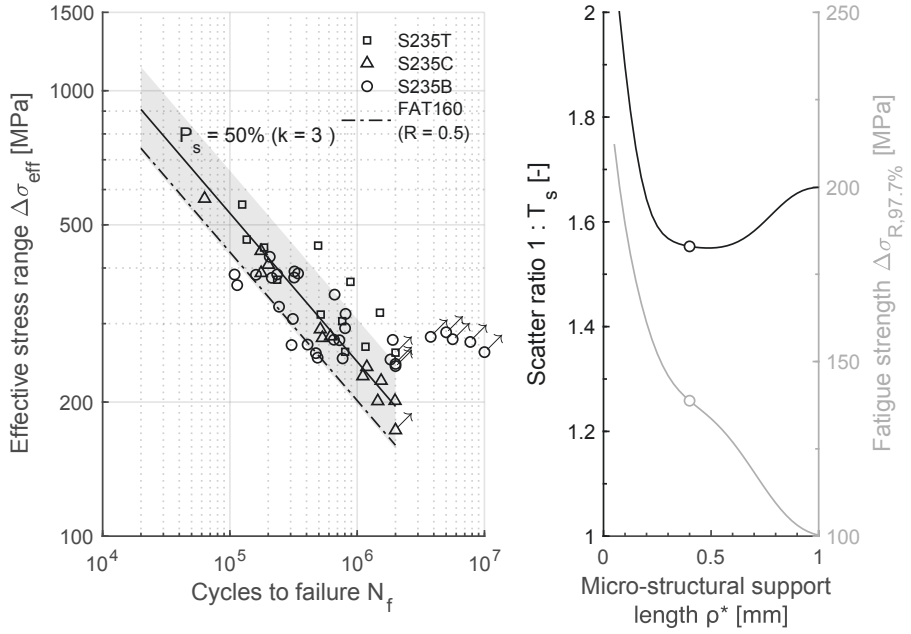

Figure 51. *S–N* curve obtained for stress averaging the S235J2+N room temperature fatigue test data for ρ^* = 0.4 mm (left) and change of fatigue strength and scatter ratio over micro-structural support length ρ^* (right), for R = 0 and based on Braun et al. (2021b)

In general, the majority of test specimens are placed above the recommended design curve FAT160. Only six specimens are found to be below this curve and all of them are butt-welded joints. This is likely to be related to the mild notches at the S235J2+N weld toes (i.e. large weld toe radii and opening angles), see Figure 18. Mildly notched weld details with stress concentration factors (K_t < 1.6) are also known to cause inaccuracies in the effective notch stress method, see (Pedersen et al. 2010; Fricke 2012; Rother and

Fricke 2016; Collmann and Schaumann 2018); nonetheless, the results are only slightly below the reference curve. This agrees well with the expectation by Baumgartner (2017) that even flush-ground butt joints can be assessed by the FAT160 without being overly non-conservative. The butt-welded joints of this study were not ground, but the flux-cored arc welding process produces joints with large weld toe transition radii that yield a fatigue strength similar to ground butt-welded joints, see Figure 32.

6.3.3 | Assessment results at sub-zero temperature

The test results obtained at −20 °C and −50 °C are presented in Figure 52 and Figure 53 for the micro-structural support length ρ^* that leads to the minimum respective scatter ratio $1/T_s$. Similar to the room temperature results, a small number of butt-welded joints lie below the FAT160 reference curve at −20 °C. The majority of specimens are, however, again positioned above the FAT160 design curve.

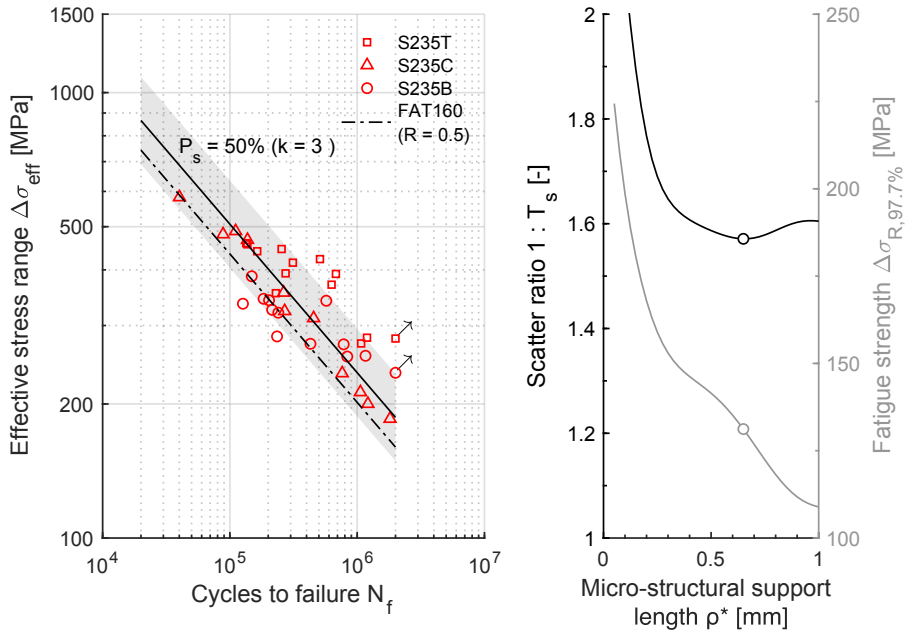

Figure 52. *S–N* curve obtained for stress averaging the S235J2+N fatigue test data obtained at −20 °C for the minimum scatter ratio $1/T_s$ at ρ^* = 0.65 mm (left) and change of fatigue strength and scatter ratio over micro-structural support length ρ^* (right), for R = 0 and based on Braun et al. (2021b)

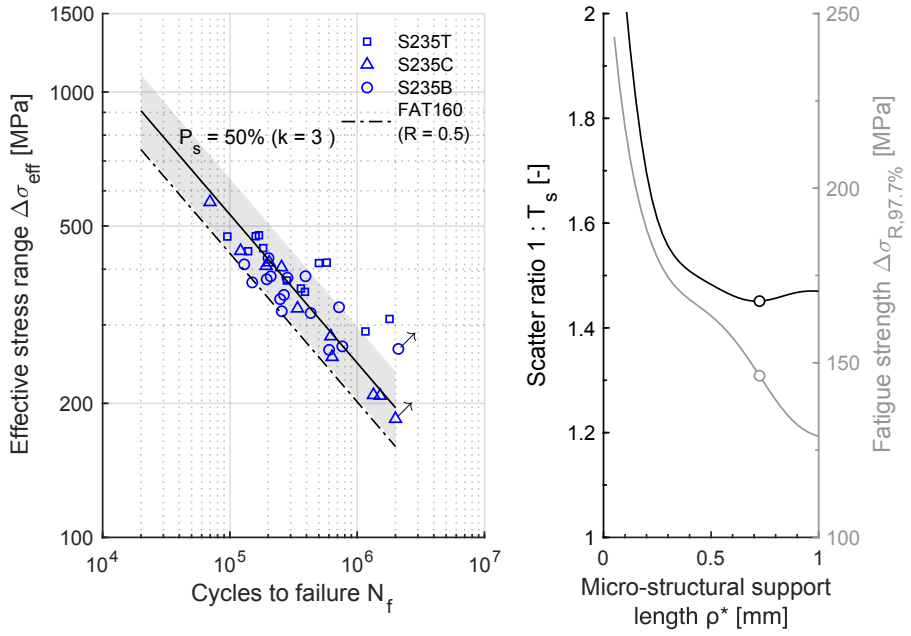

Figure 53. *S–N* curve obtained for stress averaging the S235J2+N fatigue test data obtained at −50 °C for the minimum scatter ratio $1/T_s$ at ρ^* = 0.725 mm (left) and change of fatigue strength and scatter ratio over micro-structural support length ρ^* (right), for R = 0 and based on Braun et al. (2021b)

The welded joints made of S500G1+M have not been included in the assessment by means of stress averaging approach, due to material strength-related differences in fatigue strength. The difference in fatigue strength of between S235 and S500 butt-welded joints, measured between 13% and 25% depending on test temperature. Thus, the material strength of the S500G1+M butt-welded joints has an over-proportional effect on the estimated micro-structural support length ρ^* due to the small number of different test series for each temperature. This can be assessed by including an additional fitting parameter for material strength (see Baumgartner et al. (2019)) or by applying a correction formula (see Braun et al. (2020f)); however, the *S–N* curve assessment of the S500G1+M butt joints using a free slope exponent also led to a slope exponent k which was much higher than for the other weld details, see Table 4. This would lead to a high uncertainty regarding a suitable slope exponent for the assessment by means of the stress averaging approach. These effects are further discussed in Section 7.2.1. Furthermore, assessing

only the data of the fillet weld details was found to result in a high uncertainty of predicted micro-structural support length ρ^*, as the remaining amount of test data was too small to apply the stress averaging approach.

Fatigue test data and the results of fatigue assessment studies are typically presented for a high stress ratio of $\mathrm{R} = 0.5$ to simulate high residual stresses in full-scale structures. Also, the FAT160 curve was defined for this stress ratio. The results of the stress averaging approach are here not corrected to this stress ratio as it was found that the chosen stress ratio correction factor (i.e. according to the IIW recommendations (Hobbacher 2016)) had a significant effect on the estimated micro-structural support lengths ρ^*. Furthermore, it was not possible to determine the stress ratio influence for all test series experimentally, among other reasons, because this is not possible for the S235 butt-welded joints due to the low yield strength and simultaneous high fatigue strength. Accurately determining a suitable correction factor is thus not possible.

Table 5. Summary of stress averaging results for $\mathrm{R} = 0$ and minimum scatter ratio $1/\mathrm{T_s}$

Temperature	Micro-structural support length ρ^* [mm]	Characteristic fatigue strength $\Delta\sigma_{\mathrm{R},97.7\%}$ [MPa]	Scatter ratio $1/\mathrm{T_s}$
RT	0.475	135.0	1.550
-20 °C	0.65	131.2	1.571
-50 °C	0.725	146.3	1.451

The results of the stress averaging approach are summarized in Table 5. Interestingly, the estimated micro-structural support lengths ρ^* that lead to the minimum respective scatter ratio $1/\mathrm{T_s}$ increase with decreasing test temperature. This is in contradiction to the prediction based on Neuber's diagram for yield strength effect on micro-structural support lengths ρ^* for various metallic material (Figure 9). Clearly, the yield strength of the steels increases with decreasing temperature, see Table 3. Hence, the assumption was made that an increase in yield strength should lead to a decrease in micro-structural support lengths ρ^*. In fact, the opposite behaviour is observed from the fatigue tests at -20 °C and -50 °C. As a consequence, Neuber's diagram is not applicable to relate temperature induced variations of static material properties to the micro-structural support effect. By means of fatigue assessment based on the SED method, it will be investigated whether this effect is systematic or observed by coincidence.

6.4 | Averaged strain energy density method

6.4.1 | Model development for the averaged strain energy density method

There are a number of studies available in the literature that applied the SED method to mildly notched components, but only a few that investigated mildly notched welded joints, see Foti and Berto (2020a,b). The typical field of application are weld details with sharp V-type notches—as they formed the basis for the development of the N-SIF method, which later laid the foundation for the SED method. As the butt-welded joints of this study violate the underlying assumption of the N-SIF method (i.e. sharp notches with small weld toe radii, see Berto and Lazzarin (2009)), they have been excluded from the assessment based on the SED method; nonetheless, the data for both steel types was assessed together since the material strength does not influence the fatigue strength of weld details with sharp notches (see Maddox (2002)).

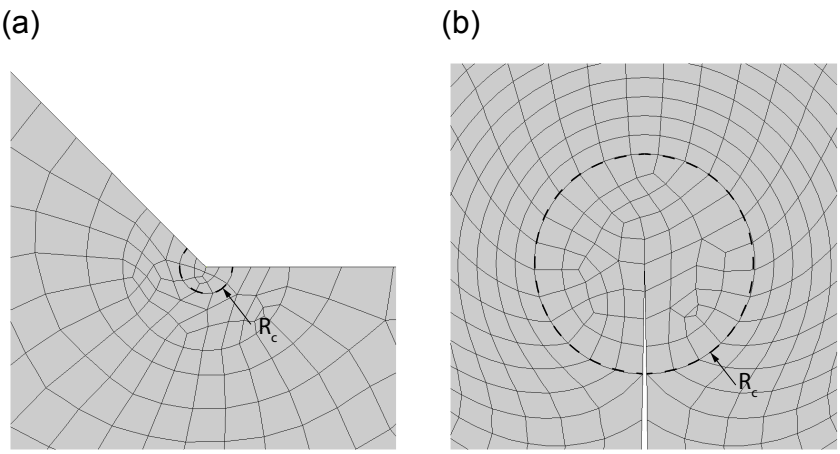

Figure 54. Mesh at weld toe (a) and weld root (b) of a fillet-welded joint generated by free mesh algorithm; root gap opening angle is enlarged for visualization purposes

The FE models for the application of the SED method are based on recommendations by Fischer et al. (2016a). Initially, a fixed mesh pattern was proposed, however, they showed that the approximation error is negligible (below 3%) even for relatively coarse meshes (Fischer et al. 2016a). Two recent studies by Foti et al. (2020) and Foti et al. (2021) support this result. The local FE meshes for the assessment of transversal stiffeners and cruciform joints with weld toe and weld root failure, respectively, are presented in Fig-

ure 54. The size of the control radii R_C is based on the aforementioned reassessment by Fischer et al. (2016b,c), i.e. 0.32 mm at the weld toe and 0.325 mm at the root, considering an increased $\Delta K_1^N = 231$ MPa mm$^{0.326}$ and $\Delta\sigma_0 = 1.05 \times 155$ MPa which aims to account for misalignment effects. The parameters that are used to calculate the control radii according to Eq. (16) are summarized in Table 6.

Table 6. Calculation of control radii R_C for room temperature based on Fischer et al. (2016c) and taken from Braun et al. (2020a)

	Weld toe	Weld root
2α	135°	0°
e_1	0.118	0.133
λ_1	0.6736	0.5
ΔK_1^N	231 MPa mm$^{0.326}$	180 MPa mm$^{0.5}$
$\Delta\sigma_0$	1.05 $\times$ 155 MPa	1.05 $\times$ 155 MPa
R_C	0.32 mm	0.325 mm

Axial and angular misalignment effects were considered in the same way as for the stress averaging approach, i.e. by multiplying the applied nominal stress with a stress magnification factor k_m obtained according to IIW recommendations (Niemi et al. 2018). To accurately represent the nominal stress state in the throat section, the median weld throat thickness is used in the FE models of the cruciform joints (i.e. $a_{th} = 5.71$ mm and $a_{th} = 5.85$ mm for S235 and S500 cruciform joints, respectively). Before the SED method is extended to sub-zero temperatures, parameters derived from tests at room temperature are applied to quantify the deviation between room temperature and sub-zero temperature results. For this goal, the typical material parameters for steels with Young's modulus of 206 GPa and Poisson's ratio $\nu = 0.3$ are applied again.

6.4.2 | Assessment based on parameters derived at room temperature

The results in terms of averaged strain energy density $\Delta\overline{W}$ are shown in Figure 55. To distinguish between failure location, abbreviations are used, i.e. 'WT' for weld toe failure (transversal stiffeners) and 'WR' for weld root failure (cruciform joints). Furthermore, the steel grades are differentiated by filled symbols for S500 steel and empty symbols for S235 steel. The colour scheme for the three test temperatures is adopted from earlier chapters, i.e. black for room temperature, red for -20 °C, and blue for -50 °C.

First of all, the majority of fatigue test results fit nicely into the scatter band for welded joints proposed by Lazzarin et al. (2003); nevertheless, the fatigue strength of the tests at sub-zero temperatures approach and partially exceed the upper limit of the scatter band. Interestingly, a higher fatigue strength is observed for transversal stiffeners compared to cruciform joints. This is in line with results obtained by Fischer et al. (2016b,c) and thought to be related to the difference in the crack initiation to propagation ratio of both joint types.

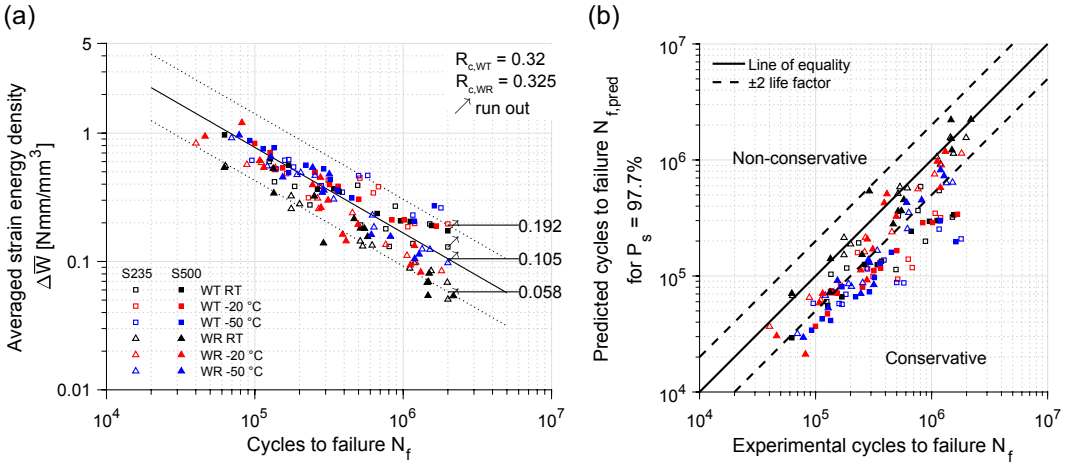

Figure 55. Results for sub-zero temperatures with room temperature control radii for weld toe and root failure ($R_{C,WT}$ = 0.32 mm and $R_{C,WR}$ = 0.325 mm) (a) and comparison of experimental and predicted cycles to failure (b), adopted from Braun et al. (2020a)

Next, a measure of the goodness-of-fit between the experimental N_f and the predicted cycles to failure $N_{f,pred}$ is derived to quantify the increase in deviation for decreasing test temperature. Pearson correlation coefficients r_{xy}, which were applied in Chapter 5, but also the coefficient of determination R^2, are not suitable to determine the quality of the model as they standardize the variance of data (Legates and McCabe 1999). To compare experiments and model predictions, root-mean-square error or mean absolute error based on the difference from the line of equality are well suited, see Legates and McCabe (1999). The results for deviation between the experimental $N_{f,exp}$ and the predicted cycles to failure based on the lower bound of the scatter band ($N_{f,pred,97.7\%}$) are displayed in Figure 55(b).

As the fatigue life is log-normal distributed, the logarithmic deviation (dev) is applied

in this study to further quantify the difference. Contrary to the stress averaging approach, a different approach is chosen here as it permits an easy comparison with state-of-the-art fatigue assessment methods. The logarithmic deviation (dev) is calculated with:

$$dev = \log N_{f,exp} - \log N_{f,pred,97.7\%} \tag{37}$$

The distributions of the logarithmic deviations are presented in Figure 56 for the three different test temperatures and separated by failure locations. The reason for this is the large difference between predicted and experimental number of cycles to failure for both failure locations and thereby deviation parameters (dev). The parameters μ_{WT} and μ_{WR} refer to the mean deviation for specimens showing weld toe and weld root failure, i.e. the peak of the fitted normal distributions. (Braun et al. 2020a)

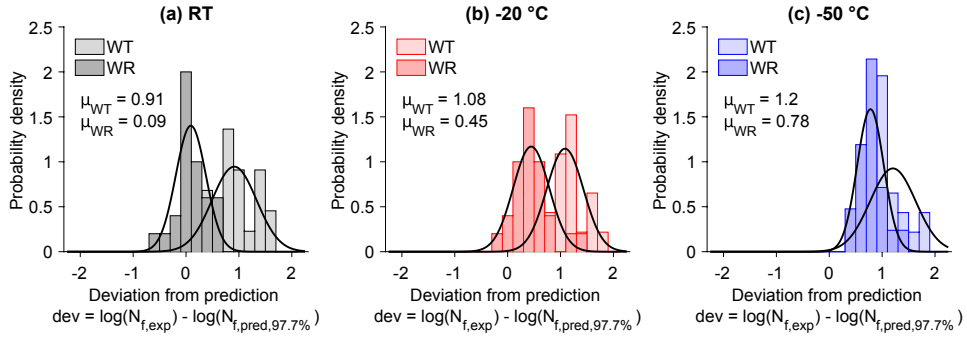

Figure 56. Deviation between experimental and predicted cycles at room temperature (RT), 20 °C, and 50 °C for the two different failure locations and control radii ($R_{C,WT}$ = 0.32 mm and $R_{C,WR}$ = 0.325 mm), taken from Braun et al. (2020a)

The distributions of the logarithmic deviations, presented in Figure 56, further highlight the difference in fatigue strength assessment for cruciform joint (WR failure) and transversal stiffener (WT failure) specimens. Interestingly, the difference between both specimen types and the corresponding failure locations (weld toe and weld root) decreases with decreasing temperature. This is related to the higher increase in fatigue strength with decreasing temperature for the cruciform joints, cf. Figure 36.

Except for a small number of cruciform joints, the majority of the fatigue test results of transversal stiffeners and cruciform joints can safely be assessed with the original standard scatter band of the SED method; yet, the increasing deviation between the experimental $N_{f,exp}$ and the predicted cycles to failure $N_{f,pred,97.7\%}$ leads to unnecessary conservatism.

Hence, the following section will present a concept to include temperature effects based on material parameters for sub-zero temperatures. This concept is subsequently linked and assessed by means of the micro-structural support effect hypothesis and the sub-zero temperature fatigue crack growth threshold data presented earlier. The need for modification factors or new scatter bands is therefore avoided.

6.4.3 | Extension of the strain energy density method to sub-zero temperatures

In Section 2.5.2, the relation between the SED method and the micro-structural support effect hypothesis was presented. This relation is based on the El Haddad-Smith-Topper parameter $a^{'}$, which describes the transition between short and long fatigue crack arrest. Recalling Eq. (11), the El Haddad-Smith-Topper parameter $a^{'}$ is related to the fatigue strength of physically short cracks and is defined by the fatigue limit of smooth specimens $\Delta\sigma_0$ and threshold of fatigue crack growth rate ΔK_{th}. It is well known that ΔK_{th} increases with decreasing temperature as long as the temperature remains above the fatigue transition temperature (see Figure 5); nonetheless, the fatigue limit of smooth specimens $\Delta\sigma_0$ is also expected to increase with decreasing temperature as weld details with mild and sharp notches showed an increase in fatigue strength, see Chapter 4. This agrees with the results of the majority of studies for base materials and mildly notched butt-welded specimens at sub-zero temperatures, see (Liaw et al. 1985; Shulginov and Matveyev 1997; Kang et al. 2009; Jung et al. 2013; Kim et al. 2018; Zhang et al. 2018b; Viespoli et al. 2019; Wang et al. 2021).

How much each of the two parameters changes decides whether the El Haddad-Smith-Topper parameter $a^{'}$ increases, decreases, or remains the same. An experimental determination of the El Haddad-Smith-Topper parameter $a^{'}$ for different temperatures would require a tremendous amount of fatigue tests, see (El Haddad et al. 1979; Wormsen 2007; Wormsen et al. 2008). The change of micro-structural support effect at sub-zero temperatures is consequently assessed by estimating the El Haddad-Smith-Topper parameter $a^{'}$ from the fatigue test data of welded joints presented in this study. The relation between the size of the SED control radius R_C and the El Haddad-Smith-Topper parameter $a^{'}$ will be applied for this aim.

Similarly to solving the inverse problem of the stress averaging approach, control radii R_C are derived that fit the sub-zero temperature fatigue data the best. The control radii R_C that lead to the same mean deviations (μ_{WT}, μ_{WR}) as for room temperature, based on Eq. (37), are expected to reflect the change of support effect at sub-zero temperatures. A similar attempt was presented by Berto et al. (2014). They have shown that fatigue test data of notched components at room temperature and high temperatures (up to 500 °C) can be summarized in one scatter band for one control radius by introducing a notch sensitivity function $Q(T)$. As the notch sensitivity changed at 650 °C, a separate scatter band with a different slope had to be proposed for this temperature. This was attributed to the change in material behaviour due to the test temperature being above the heat-treatment temperature, see Berto et al. (2014).

Although the fracture surface investigation of the current study revealed brittle fracture behaviour for some weld details at sub-zero temperatures, it is here assumed that the chosen approach is feasible, since the majority of fatigue life is dominated by early crack growth in the vicinity of the weld toe and root notch. Once brittle fracture occurred, the remaining fatigue life would have been rather short even without brittle failure. It is thus assumed that the original scatter band for welded joints can also be applied for sub-zero temperatures, including specimens which showed brittle final fracture.

Besides the control radius, the Young's modulus E also affects the averaged elastic strain energy density. In this study it is assumed that the Young's modulus changes by 10 GPa for every 100 °C of temperature change (cf. (Outinen and Makelainen 2004; Wang et al. 2013; Paik et al. 2017; Wang et al. 2020; Zhao et al. 2020a)), which agrees with data for high temperatures below the creep limit in international standards and supporting documents (BS 7910:2013+A1:2015; ASME BPVC Section II D - Properties). Interestingly, these standards assumed a smaller change for sub-zero temperatures than for high temperatures; however, the reason for this is not apparent and does not agree with data by Paik et al. (2017) and Wang et al. (2020). Therefore, a Young's modulus of 202 GPa is adopted for the assessment at -20 °C and 199 GPa for -50 °C.

To highlight the increasing deviation between the experimental $N_{f,exp}$ and the predicted cycles to failure $N_{f,pred,97.7\%}$ with decreasing test temperature, the logarithmic mean deviations (μ_{WT}, μ_{WR}) are presented in Figure 57(a) for the two failure locations (weld toe and root). The vertical lines around the mean value represent the standard de-

viation obtained from the distributions in Figure 56. Clearly, an almost linear increase is observed for both failure locations as the test temperature decreases. Hence, an averaged deviation relative to room temperature is shown in Figure 57(b)—including the change per temperature (illustrated by the slope triangle). (Braun et al. 2020a)

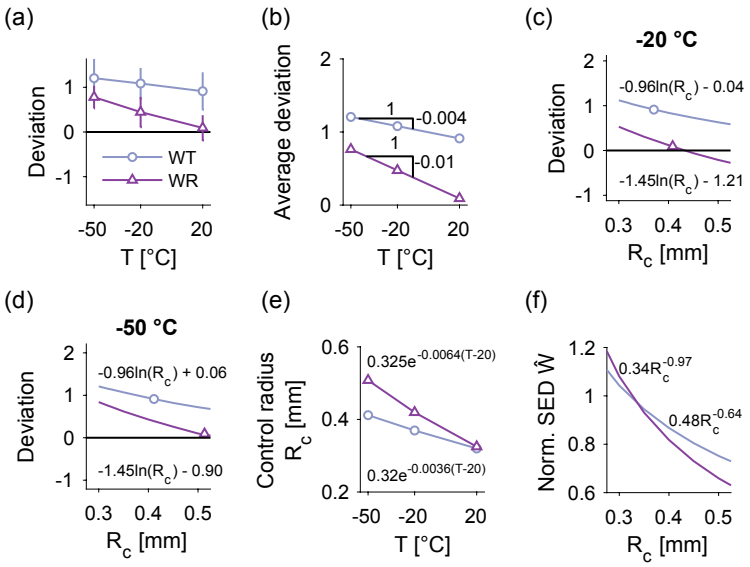

Figure 57. Deviation between experimental and predicted cycles to failure (a), average deviation relative to room temperature (b), deviation as a function of control radius R_C for -20 °C (c) and -50 °C (d), control radii as a function of temperature (e), and normalized elastic strain energy density $\hat{W}$ as a function of the control radii (f), adopted from Braun et al. (2020a)

Next, control radii R_C suitable for SED-based assessment at sub-zero temperatures are derived by finding the radii that yields the same mean deviation (μ_{WT}, μ_{WR}) as for room temperature. This is achieved by varying the control radii R_C for weld toe and root assessment from 0.3 to 0.53 mm and calculating the corresponding mean deviation, which is presented in in Figure 57(c) and (d) for -20 °C and -50 °C, respectively. The symbols (circle and triangle) mark those radii that match the mean deviation observed at room temperature. Assessing the results for various control radii, a logarithmic relation between mean deviation and control radii is observed (also included in the figures). Next, the resulting control radii are presented as a function of temperature in Figure 57(e) and curve fitted considering the control radii at room temperature as fixed points. The so obtained radii are summarized in Table 7.

Table 7. Control radii $\mathrm{R_C}$ for both failure locations and all three test temperatures

Temperature T	Weld toe control radius $\mathrm{R}_{\mathrm{C},WT}$	Weld root control radius $\mathrm{R}_{\mathrm{C},WR}$
RT	0.32 mm	0.325 mm
-20 °C	0.37 mm	0.41 mm
-50 °C	0.41 mm	0.51 mm

These control radii can be used to generate a general description of control radii for welded joints with weld toe and root failure as a function of temperature in °C:

$$\text{Weld toe failure } (2\alpha = 135^\circ) : \mathrm{R}_{\mathrm{C},WT} = 0.32e^{-0.0036(\mathrm{T}-20)}\text{, for T in °C} \tag{38}$$

$$\text{Weld root failure } (2\alpha = 0^\circ) : \mathrm{R}_{\mathrm{C},WR} = 0.325e^{-0.0064(\mathrm{T}-20)}\text{, for T in °C} \tag{39}$$

; nevertheless, varying the control radii during fatigue assessment for the various design temperatures a structure will be exposed to is rather time consuming. Thus, a modification function is derived, which reflects the effect of varying the control radii. Contrary to empirical modification factors for stress-based fatigue assessment methods, this modification function can be linked directly to the micro-structural support effect hypothesis. This is achieved by using the control radius size effect on the averaged strain energy density, i.e. the percentage change of $\overline{W}$ with respect to $\mathrm{R_C}$ ($\overline{W}\left(\mathrm{R_C}\right)$). By doing so, a normalized elastic strain energy density $\hat{W}$ is introduced by dividing $\overline{W}\left(\mathrm{R_C}\right)$ with the corresponding averaged strain energy density for control radii $\mathrm{R}_{\mathrm{C},WT} = 0.32$ mm and $\mathrm{R}_{\mathrm{C},WR} = 0.325$ mm. This relation is presented for the weld toe and root control radii in Figure 57(f). Finally, the temperature modification function $\mathrm{M}\left(\mathrm{T}\right)$ for SED-based fatigue assessment of weld toe and weld root failure is obtained by inserting Eq. (38) and Eq. (39) in the respective equation given in Figure 57(f):

$$\mathrm{M}\left(\mathrm{T}\right) = \begin{cases} \left(e^{-0.0036(\mathrm{T}-20)}\right)^{-0.64} & : \text{if } 2\alpha = 135^\circ \\ \left(e^{-0.0064(\mathrm{T}-20)}\right)^{-0.97} & : \text{if } 2\alpha = 0^\circ \end{cases}\text{, for T in } ^\circ\mathrm{C} \tag{40}$$

This temperature modification function allows a fatigue assessment of welded joints at sub-zero temperatures with the same scatter band as proposed for room temperature. By

modifying averaged strain energy density ranges ($\Delta\overline{W}\,(\mathrm{T} = \mathrm{RT})$)—calculated using parameters for room temperature—with $\mathrm{M}\,(\mathrm{T})$, corresponding $\Delta\overline{W}$ for temperatures different from room temperature are obtained with:

$$\Delta\overline{W}\,(\mathrm{T}) = \mathrm{M}\,(\mathrm{T}) \times \Delta\overline{W}\,(\mathrm{T} = \mathrm{RT})\,, \text{ for T in °C} \tag{41}$$

In Figure 58, the results for the adjusted control radii, together with the original $\Delta\overline{W}-\mathrm{N}$ scatter band, are presented, but using the temperature modification function would have yielded the same results. As can be seen from the results, no visible difference between test temperatures can be noted.

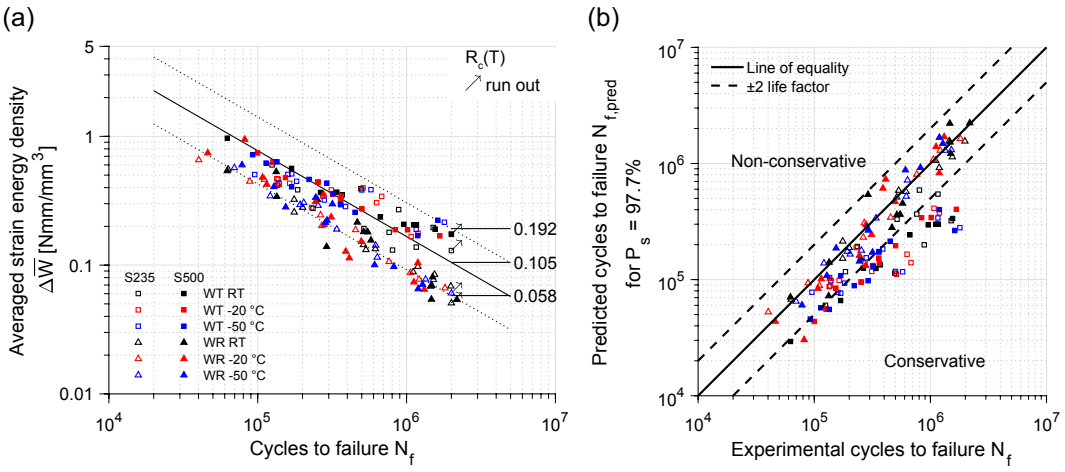

Figure 58. Results for sub-zero temperatures with control radius $\mathrm{R_C}\,(\mathrm{T})$ adjusted to sub-zero temperatures, adopted from Braun et al. (2020a)

Contrary to the results obtained using control radii, which are based on fatigue tests performed at room temperature (see Figure 55), the majority of fatigue test results are now inside the proposed scatter band for welded joints; however, the results for cruciform joints are partially below the scatter band, i.e. below the $\Delta\overline{W}-\mathrm{N}$ curve for 97.7% survival probability. This, however, is expected as the room temperature results are already scattered around the lower boundary of the scatter band and in line with results by Fischer et al. (2016b,c) for the same specimen type and same plate thickness ($\mathrm{t} = 10$ mm).

Table 8. Comparison of the mean deviations of weld toe and root data for fatigue assessment with control radii obtained from room temperature data and with radii $R_C\,(T)$ adjusted for sub-zero temperatures

Temperature	SED $R_C\,(T = RT)$				SED $R_C\,(T)$			
T	μ_{WT}	Difference	μ_{WR}	Difference	μ_{WT}	Difference	μ_{WR}	Difference
RT	0.91	–	0.09	–	0.91	–	0.09	–
−20 °C	1.08	18.9%	0.45	389%	0.92	0.3%	0.09	−6.5%
−50 °C	1.20	31.9%	0.78	756%	0.91	−0.1%	0.07	−28.1%

In summary, the SED method was extended to capture temperature effects on fatigue strength, due to the link between the size of the control radius R_C and the change in mean deviation between experimental $N_{f,exp}$ and predicted cycles to failure $N_{f,pred,97.7\%}$ for decreasing temperatures. Using control radii $R_C\,(T = RT)$ obtained from room temperature data, a steady increase in mean deviation is observed for sub-zero temperatures, see Table 8. By adjusting the control radii to sub-zero temperatures, the difference in mean deviation—between room and sub-zero temperatures—for weld toe failure (transversal stiffener specimens) is reduced from 18.9% at −20 °C and 31.9% at −50 °C to 0.3% and −

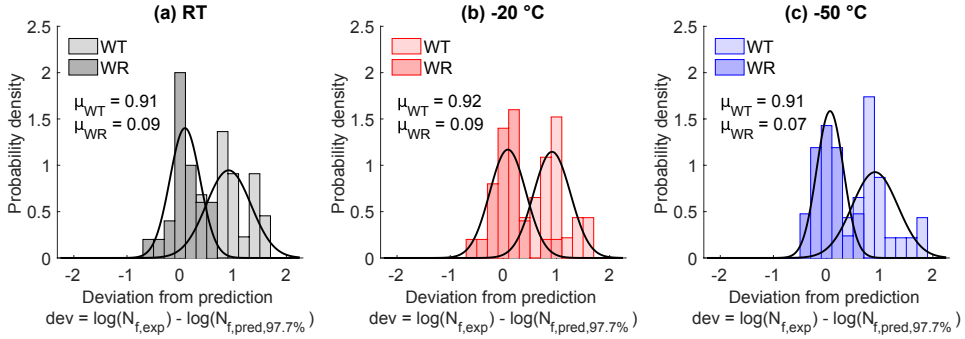

Figure 59. Deviation between experimental and predicted cycles at room temperature (RT), 20 °C, and 50 °C for the two different failure locations and modified control radii $R_C\,(T)$ for sub-zero temperatures

6.4.4 | Assessment of the results using data of material fatigue

Next, 1) the feasibility of the adjusted control radii $R_C\,(T)$ and the temperature modification function for sub-zero temperatures and 2) the link of the control radii R_C to the micro-structural support effect hypothesis via the El Haddad-Smith-Topper parameter a' are investigated.

Recalling Section 2.5.2, the control radius $\mathrm{R_C}$ for welded joints was originally derived for room temperature data of mode I N-SIF fatigue strength for notched component $\Delta \mathrm{K_1^N}$ and the fatigue limit of flush-ground butt welds $\Delta\sigma_0$, see Eq. (16). Deriving representative data for sub-zero temperatures would be a challenging task, given the typically high scatter in fatigue strength of ground welded joints, and is outside the scope of this thesis; yet, in order to evaluate the results a comparison is performed in this thesis. For this goal, the fatigue limit of flush-ground butt welds at sub-zero temperatures $\Delta\sigma_0\,(\mathrm{T})$ is estimated using previously presented data and compared to fatigue test data of the S500 butt-welded joints. The reason for this is the comparable fatigue strength of the S500 butt joints with flush-ground butt joints found in the literature. Furthermore, the free slope exponents k were larger than four for all three test temperatures, see Table 4.

In Section 2.5.4, the relation between the SED method and linear elastic fracture mechanics was presented. As can be seen from Eq. (24), a linear relation between the stress intensity factor for mode I ($\mathrm{K_I}$) and the mode I N-SIF $\mathrm{K_1^N}$ exists. As a consequence, it can be assumed that the N-SIF threshold value $\Delta \mathrm{K_{1,th}^N}$ (usually referred to as mode I N-SIF fatigue strength for notched component $\Delta \mathrm{K_1^N}$ at 5×10^6 cycles) is also linearly related to the long fatigue crack growth threshold $\Delta \mathrm{K_{th}}$. This permits an estimation of the change of $\Delta \mathrm{K_1^N}$ with temperature from the threshold of fatigue crack growth rate $\Delta \mathrm{K_{th}}$ at sub-zero temperatures.

Based on the data presented in Figure 5(b) and normalized mean slope $\mathrm{k_{\Delta K_{th,norm}}} = -0.0033$ MPa$\sqrt{\mathrm{m}}$/°C, an increase of $\Delta \mathrm{K_1^N}$ of about 12% at -20 °C and 21% at -50 °C is estimated relative to room temperature. From the change of $\Delta \mathrm{K_1^N}$, the corresponding change in fatigue limit of flush-ground butt welds $\Delta\sigma_0\,(\mathrm{T})$ is estimated that fulfils the micro-structural support effect hypothesis, under the assumption of the correct estimation of changing control radii $\mathrm{R_C\,(T)}$. This is achieved by rearranging Eq. (16):

$$\Delta\sigma_0\,(\mathrm{T}) = \frac{\sqrt{2e_1}\Delta \mathrm{K_1^N}\,(\mathrm{T})}{\mathrm{R_C\,(T)}^{1-\lambda_1}} \tag{42}$$

The estimated plain specimen fatigue strength (by inserting the calculated control radii $\mathrm{R_C}$ and mode I N-SIF fatigue strength for notched component $\Delta \mathrm{K_1^N}$) is presented in Table 9. As expected, the estimated fatigue strength of smooth (flush-ground) butt-welded joints $\Delta\sigma_0\,(\mathrm{T})$ increases at sub-zero temperatures, which is in line with the obtained test

results for all weld details in Chapter 4.

Table 9. Estimates of fatigue strength of smooth (flush-ground) butt-welded joints $\Delta\sigma_0\,(\mathrm{T})$ at sub-zero temperatures at $\mathrm{N_f} = 5 \times 10^6$ ($\mathrm{R} = 0$, $\mathrm{P_s} = 50\%$), according to Eq. (42)

Temperature	Weld toe ($e_1 = 0.118$, $\lambda_1 = 0.6736$)				Weld root ($e_1 = 0.133$, $\lambda_1 = 0.5$)			
T	$\Delta K_1^N\,(\mathrm{T})$ MPa mm$^{0.5}$	$R_{C,WT}\,(\mathrm{T})$ mm	$\Delta\sigma_0\,(\mathrm{T})$ MPa	Deviation to RT	$\Delta K_1^N\,(\mathrm{T})$ MPa mm$^{0.5}$	$R_{C,WR}\,(\mathrm{T})$ mm	$\Delta\sigma_0\,(\mathrm{T})$ MPa	Deviation to RT
RT	210	0.32	155.0	–	180	0.325	155.0	–
−20 °C	1.12 × 210	0.37	158.0	+2%	1.12 × 180	0.41	162.4	+5%
−50 °C	1.21 × 210	0.41	165.1	+7%	1.21 × 180	0.51	157.3	+1%

As mentioned earlier, determining the El Haddad-Smith-Topper parameter a' for sub-zero temperatures experimentally (see (El Haddad et al. 1979; Wormsen 2007; Wormsen et al. 2008)), and in particular the fatigue testing of plain butt-welded specimens, would be a complex and costly task (see Fischer (2016) and Fischer et al. (2016c)). Instead, the results of the S500 butt-welded joints are used to evaluate the estimates of fatigue strength of smooth (flush-ground) butt-welded joints $\Delta\sigma_0\,(\mathrm{T})$ at sub-zero temperatures presented in Table 9.

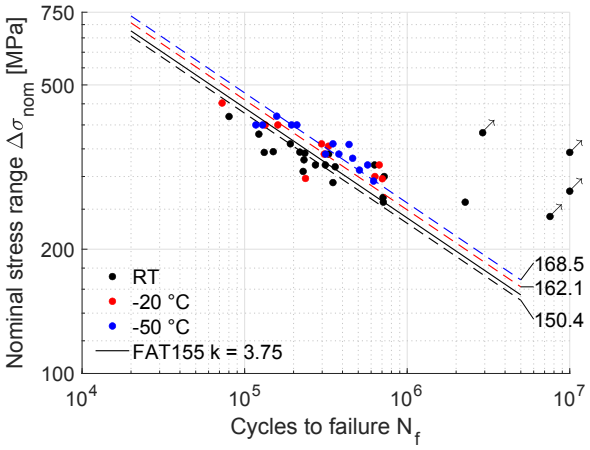

Figure 60. *S-N* results of S500 butt-welded joints assessed with a fixed slope exponent of $\mathrm{k} = 3.75$, adopted from Braun et al. (2020a)

Due to the large weld toe radii (up to 3 mm) and flank angles (130° to 170°), the fatigue strength of this test series is quite close to the fatigue strength of ground-flush butt-welded joints presented in Table 1. The fatigue test results of the S500 butt-welded joints shown and discussed in Chapter 4 are thus re-evaluated using a fixed slope exponent $\mathrm{k} = 3.75$ (according to the recommendation by Atzori and Dattoma (1983)), see Figure 60. Besides

the experimental data, the curve with reference fatigue strength of 155 MPa is included as reference. The results match the estimates—presented in Table 9—well, in particular for weld toe failure at −20 °C and −50 °C (2.6% and 2.1%, respectively) and weld root failure at −20 °C (-0.2%). A slight deviation from the prediction is obtained for weld root failure at −50 °C (7.1%). For this temperature, a reduction in plain specimen fatigue strength is predicted. This is in contrast to the general trend of increasing fatigue strength at sub-zero temperatures. The reason for this is related to the large estimated control radius. Compared to the estimated weld root radius, the radius for weld root failure increases almost twice as much from room temperature down to −50 °C. This will be discussed in more detail in Chapter 7. Nonetheless, given the uncertainty of the various influencing factors, and in particular the change of fatigue crack growth rate threshold ΔK_{th} at sub-zero temperatures, the deviation between the estimates and the fatigue strength of the S500 butt-welded joint reference seems marginal. (Braun et al. 2020a)

The derived sub-zero temperature control radii $R_C\,(T)$ can be further used to estimate the El Haddad-Smith-Topper parameter a' at sub-zero temperatures. Recalling Eq. (12) and Eq. (17), both parameters are assumed to be linearly related. Hence, from the increase of control radii a subsequent increase of the El Haddad-Smith-Topper parameter a' with decreasing temperature would be expected. This assumption is based on the idea that one SED scatter band should be representative for fatigue data under different conditions.

In general, the estimated increase of control radii agrees with the general understanding of the SED method for fracture assessment. Lazzarin et al. (2003) states that R_C is smaller for more brittle materials. The fatigue strength of bcc materials increases with decreasing test or operating temperature, as long as the temperature is above the fatigue transition temperature. Consequently, an increase of the El Haddad-Smith-Topper parameter a' with decreasing temperature agrees well with the fatigue behaviour of materials that show a fatigue transition behaviour.

6.5 | Estimation of the change of micro-structural support effect based on the generalized Kitagawa-Takahashi diagram

Another possibility to estimate the change of micro-structural support effect based on the control radii of the SED method is given by the generalized Kitagawa-Takahashi diagram.

As has been shown in Section 2.5.4, the El Haddad-Smith-Topper 'intrinsic' crack length a_0 can also be derived from the characteristic length parameter of V-notched component $a_{0,V}^{N'}$ for varying V-notch opening angles through the shape coefficient α_ξ'. Recalling Eq. (11) and Eq. (28), $a_{0,V}^{N'}$ and a_0 are similarly determined and both depend on the SIF threshold for long cracks ΔK_{th} and the plain specimen fatigue strength $\Delta\sigma_0$. Thus, their relation will be used to estimate the change of micro-structural support effect at sub-zero temperatures.

By inserting the relation between the N-SIF threshold $\Delta K_{1,th}^{N}$ and the SIF threshold for long cracks ΔK_{th} (Eq. (29)) into Eq. (28), the characteristic length parameter of V-notched component $a_{0,V}^{N'}$ can be determined with:

$$a_{0,V}^{N'} = \pi^{\frac{-1}{2\xi}} \frac{\Delta K_{th}^2}{\Delta\sigma_0^2} \beta^{\frac{1}{\xi}} \tag{43}$$

where ξ is the degree of singularity of Williams' stress equation for mode I and β a geometrical correction factor depending on the notch opening angle 2α that was calibrated for different local fatigue assessment methods.

Atzori et al. (2005) proposed three different methods to derive $a_{0,V}^{N'}$ by determining β. Here, the values reported for the SED method are applied to enable a comparison with more recent results by Atzori et al. (2008). Alternatives are mentioned in Section 2.5.4, but will not be considered as the difference between them is marginal for opening angles between 90° and 150° (Atzori et al. 2005). Following Atzori et al. (2008), a long fatigue crack threshold $\Delta K_{th} = 180$ MPa mm$^{0.5}$ (5.7 MPa m$^{0.5}$) is applied (cf. Radaj (1990) and Livieri and Lazzarin (2005))[7] in conjunction with the fatigue strength of the S500 butt-welded joints at $N_f = 5 \times 10^6$ ($R = 0$, $P_s = 50\%$, $k = 3.75$), and $\xi = 0.5$ and $\xi = 0.3264$ for 0° and for 135°, respectively. The estimates for the characteristic length parameter of V-notched component $a_{0,V}^{N'}$ based on Eq. (43) are presented in Table 10.

[7] This value refers to a reported lower bound value of SIF threshold for non-welded structural steel for R = 0 in Radaj (1990). Interestingly, Livieri and Lazzarin (2005) found that the mean mode I N-SIF fatigue strength at $N_f = 5 \times 10^6$ ($R = 0$, $P_s = 50\%$, $k = 3.2$ equals the same value.

Table 10. Estimates of characteristic length parameter of V-notched component $a^{N'}$ and El Haddad-Smith-Topper parameter a' at sub-zero temperatures from fatigue test data at $N_f = 5 \times 10^6$ ($R = 0$, $P_s = 50\%$) and estimates for the change of long fatigue growth threshold stress intensity factor

Temperature	Assumed plain specimen fatigue strength	Long fatigue crack threshold	Weld toe ($2\alpha = 135°$)				Weld root ($2\alpha = 0°$)		
T	$\Delta\sigma_0$	ΔK_{th}	ξ	β	$a^{N'}$	a'	ξ	β	$a^{N'} = a'$
RT	150.4 MPa	180 MPa mm$^{0.5}$	0.3264	1.345	0.615	0.456	0.5	1	0.456
-20 °C	162.1 MPa	1.12 $\times$ 180 MPa mm$^{0.5}$	0.3264	1.345	0.664	0.492	0.5	1	0.492
-50 °C	168.5 MPa	1.21 $\times$ 180 MPa mm$^{0.5}$	0.3264	1.345	0.717	0.531	0.5	1	0.532

To estimate the change of the El Haddad-Smith-Topper parameter a' at sub-zero temperatures, a' is determined using the shape coefficient α'_ξ (Eq. (27)). Again, applying the values reported for β and α'_ξ for the SED method by Atzori et al. (2005), an increase in micro-structural support effect (here defined by a') is determined for sub-zero temperatures, see Table 10.

This result confirms the outcome of Section 6.4.3, i.e. the control radii of the SED method should increase with decreasing temperature (cf. Eq. (12) and Eq. (17)). Moreover, the assumption that one SED scatter band should be representative for fatigue data under different conditions (e.g. different temperatures) is supported.

Finally, the estimated increase of the El Haddad-Smith-Topper parameter a' at sub-zero temperatures agrees well with the trend of increasing micro-structural support lengths ρ^* at sub-zero temperatures obtained from the stress averaging approach. It can thus be concluded that the micro-structural support effect hypothesis is well suited to perform fatigue assessment of welded joints at sub-zero temperatures.

6.6 | Comparison of analysed fatigue assessment methods

To assess the relevance of the proposed methods to account for temperature effects within fatigue assessment, a comparison with state-of-the-art methods from Section 2.3 is performed. The results for the state-of-the-art methods is taken from Braun et al. (2020d). Due to the large exceedance of the design curves by the butt-welded joints, which is typical for high-quality butt-welded connections (see Maddox (2002)), only the results of the fillet-welded joints are subsequently compared. As a consequence, the results of the stress averaging approach are also excluded from the comparison since they included the butt-welded joints in the assessment. Nonetheless, results for the application of the SED

method with the standard control radii $R_C\,(T = RT)$ derived from room temperature tests are included as a reference.

In Figure 61, a comparison of mean deviations from the predictions (fatigue design curves for $P_s \approx 97.5\%$) is presented—including error margins for the standard deviation. Both quantities are derived similar to the results for the SED method (Figure 56) by using Eq. (37), see Braun et al. (2020d). Each resulting value is further listed in Table 11.

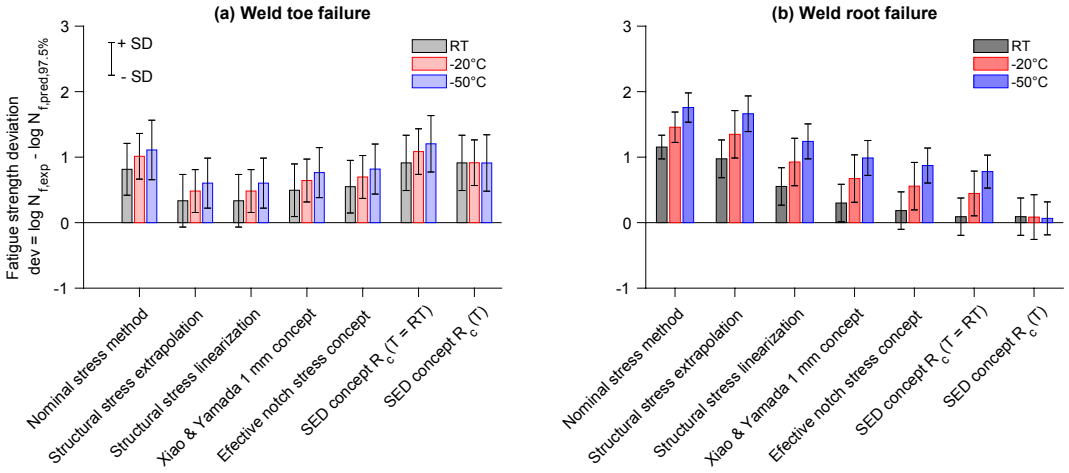

Figure 61. Deviation between experimental and predicted fatigue strength ($P_s \approx 97.5\%$ for (a) weld toe failure and (b) weld root failure, extended from Braun et al. (2020d) for the results of the SED method. Stress ratio $R = 0$ for ASED method and $R = 0.5$ for the other methods.)

Table 11. Summary of mean deviations for fatigue assessment of weld toes and roots at sub-zero temperatures

Fatigue assessment concept	RT		−20 °C		−50 °C	
	WT	WR	WT	WR	WT	WR
Nominal stress	0.81	1.15	1.01	1.46	1.11	1.76
Structural hot-spot stress extrapolation	0.33	0.97	0.48	1.35	0.60	1.66
Structural stress linearization	0.33	0.55	0.48	0.93	0.60	1.24
Xiao & Yamada 1mm	0.49	0.30	0.64	0.67	0.76	0.99
Effective notch stress	0.55	0.18	0.70	0.56	0.82	0.87
SED $R_C\,(T = RT)$	0.91	0.09	1.08	0.45	1.20	0.78
SED $R_C\,(T)$	0.91	0.09	0.92	0.09	0.91	0.07

The prediction accuracy seemingly varies between failure locations (weld toe and root) and fatigue assessment methods. The structural hot-spot stress extrapolation and linearization, for example, fit well for weld toe failure. On the contrary, the deviation is among

the largest for weld root failure. In general, the deviation of the stress-based methods is highest for the nominal stress approach; yet, this comparison is slightly biased since the nominal stress design curves account for higher levels of misalignment. In addition, the effective notch stress method and Xiao and Yamada's 1 mm stress approach give the least over-conservatism of the stress-based methods for weld root failure (smallest bars), but lead to a greater deviation in weld toe fatigue compared to the other local methods. In contrast, it should be noted that the differences are smaller for all methods of assessing weld toe failure. While a small number of samples tested at room temperature are below the corresponding design curves of all local fatigue assessment methods, none are below the design curves of the nominal stress methods. This agrees with a recent study by Rohani Raftar et al. (2021), who found that the effective notch stress approach is less conservative than the nominal stress approach for weld root fatigue. Furthermore, the calculated standard deviation of all stress-based methods is almost identical due to the scaling of the nominal stress results with different stress concentration factors. (Braun et al. 2020d)

Interestingly, a comparably large deviation between the SED results and the design curve is found for weld toe failure; nonetheless, at the same time the smallest deviation between experimental and predicted results is obtained for weld root failure. It is, however, important to note that a number of cruciform joint test results lie below the design curve for this concept. More importantly, while the mean deviations significantly increase for all state-of-the-art methods (that are not capable of accounting for temperature effects), they remain constant if temperature effects are considered by adjusting the control radii and Young's modulus of the averaged SED method. For the state-of-the-art methods, the mean deviation for weld toe failure changes by about 0.15 and 0.27 for -20 °C and -50 °C, respectively, and by 0.36 and 0.69 for -20 °C and -50 °C, respectively, when assessing weld root failure.

From the mean deviations between the experimental and predicted number of cycles to failure, modification factors usable for the common fatigue approaches can be determined, see Table 11. The deviations are, however, not suitable for modifying the design curves directly as they refer to the deviation from the lower end of the scatter band ($P_s \approx 97.5\%$); however, if a fixed deviation or safety level is determined, these factors could be used to correct the design curves of various fatigue assessment concepts for a

given temperature. Furthermore, modification functions could be derived by curve fitting in order to assess varying temperature ranges, but this is not part of this thesis, as the goal was to develop methods that are capable of taking temperature effects into account.

In summary, the fatigue assessment results for stress-based concepts can only account for temperature effects by means of temperature modification factors. The benefit of the two methods based on micro-structural effect hypothesis is that no correction factors need to be applied, as the temperature effect is directly accounted for due to the relation between temperature and micro-structural support effect.

7 | Discussion

This thesis had three objectives. First, the determination of the static and cyclic material behaviour at room temperature down to temperatures representative for Arctic regions (i.e. −50 °C) of two welded structural steel types. These tests built the basis for the extension of fatigue assessment methods to sub-zero temperatures. Additionally, Charpy tests were performed to relate the change in fatigue behaviour to the properties that are typically applied for material selection. Second, the fatigue behaviour of the aforementioned experimental results was statistically and numerically assessed. Finally, fatigue assessment concepts for welded joints—based on the micro-structural support effect hypothesis—were extended to sub-zero temperatures and the results compared to the results obtained from the state-of-the-art stress-based concepts.

In the two subsequent sections, first the fatigue results obtained at sub-zero temperatures, and second the results obtained from the extended fatigue assessment concepts, are discussed.

7.1 | Discussion of fatigue test results obtained at sub-zero temperatures

From the experimental fatigue test results presented in this study, a clear increase in fatigue strength is observed at sub-zero temperatures compared to room temperature. This increase is evidently related to the effect of temperature, as statistical methods verified a correlation between test temperature and fatigue life for the majority of weld details and steel types. Thereby, results of earlier studies on FCG rate testing of base materials, recent systematic investigations (e.g. Walters et al. (2016) and Alvaro et al. (2016)), as well as *S–N* fatigue tests of welded joints at sub-zero temperatures (Kang et al. 2009; Bridges

et al. 2012; Li et al. 2018; Viespoli et al. 2019; Zhao et al. 2020b; Wang et al. 2021) are confirmed.

The increase in relative fatigue strength was found to be in the same order of magnitude for all weld details and both steels. Interestingly, the highest relative increase was obtained for the weld detail with the highest notch acuity (cruciform joint), but the highest absolute increase was obtained for the weld detail with the lowest notch acuity (butt-welded joint).

In the cruciform joints and the S500 butt-welded joints, the fatigue cracks either had already initiated in or grew into the weld metal, which was found to behave in a brittle manor at −50 °C. This was confirmed by Charpy V-notch impact testing and fracture surface investigations. Nonetheless, the fatigue strength of these test series further increased below the ductile–brittle transition temperature of the weld metal. This is a beneficial effect for fatigue design; yet, unacceptable from a fracture toughness perspective due to the risk of brittle failure of the engineering structure. The integrity of a structure could, for example, be at risk due to welding defects in the weld metal. Interestingly, not all international standards and classification societies require testing for the middle of the weld metal. For example, EN 10225-1:2019 does not require such tests, but DNVGL-OS-C401 does.

The low fracture toughness of the weld metal is thought to be related to the welding procedure (here flux-cored arc welding). In comparisons between flux-cored and submerged arc welded joints with multiple weld layers, several studies found that flux-cored arc welding leads to detrimental fracture toughness results in the middle of the weld metal compared to other welding processes (Gubeljak et al. 2002; Vojvodic Tuma and Sedmak 2004; Coronado and Cerón 2010). Interestingly, in some butt-welded joints, brittle cracks were found to arrest before final fracture, which is a desirable material property for structures exposed to low temperatures, see Hauge et al. (2015).

In general, welded joints can be assumed to possess better fatigue properties at temperatures typical for Arctic regions as long as the temperature remains above the ductile–brittle transition temperature. In this study, fatigue tests were performed down to a temperature of −50 °C, which is lower than the design temperature defined by Hauge et al. (2015) (−40 °C); however, the definition of suitable design temperature is an ongoing debate, see (Horn et al. 2016; Ehlers et al. 2018; Kubiczek et al. 2019). Still, in order to exploit

the full potential of increased fatigue properties, steels and welding processes need to be chosen so that high fracture toughness properties can be ensured in all material zones.

Interestingly, a larger relative increase in fatigue strength was found for cruciform joints with root failure compared to transversal stiffener and butt-welded joints with weld toe failure. Although transversal stiffener specimens and butt-welded joints show a longer crack initiation period for which a higher temperature effect would be expected, the increase in relative fatigue strength for these weld details was smaller than for the cruciform joint detail. This confirms the expectation that the crack initiation and propagation are affected differently by temperature effects. From FCG rate measurements by Walters et al. (2016) and Alvaro et al. (2016), a stronger decrease in FCG rate was found in the low stress intensity factor range than in the intermediate and higher region of the Paris-curve at sub-zero temperatures. This might explain the different increase in fatigue strength as the ratio between crack initiation and propagation varies significantly with notch acuity. In welded joints with sharp notches, such as cruciform joints, the majority of the lifetime is defined by crack propagation of gradually increasing crack length and stress intensity factor. On the contrary, for mildly notched weld details like butt-welded joints, a large fraction of the lifetime is spent initiating a crack and propagating it the first micrometres (Maddox 2002; Lazzarin et al. 2008a). Once the crack has initiated it grows rapidly due to the relatively high applied load level. In order to assess the effect of temperature on crack initiation at mildly notched weld details, different fatigue assessment methods (e.g. the notch strain approach) are better suited than stress-based methods or linear elastic fracture mechanics, see Radaj et al. (2006).

Although the mean fatigue strength of the S500 transversal stiffener at RT is almost the same as the S235 transversal stiffener specimens, the latter experienced a higher fatigue strength increase at sub-zero temperatures. On the other hand, the fatigue strength increase is much higher for the S500 butt-welded joints compared to the S235 butt-welded joints. These observations could be coincidental as the statistical assessment of the S235 transversal stiffener test results has revealed that the correlation between test temperature and residuals of logarithmic number of cycles to failure (assuming they follow a normal distribution) has a significantly larger confidence interval than the S500 transversal stiffener test results. Furthermore, the confidence interval of the estimate of correlation coefficient quickly increases for reduced smaller sample sizes of transversal stiffeners—obtained from

the combined bootstrapping and jackknife approach.

While the confidence interval varies between moderate to strong correlation for the smallest number of cruciform joints ($n - 20$), it varies from no correlation to strong correlation for about the same number of transversal stiffeners. For the S235 butt-welded joints no correlation was observed at all. This highlights two important aspects. Firstly, other influencing factors such as local weld toe geometry significantly affect fatigue strengths, and thereby the number of specimens required to confirm a correlation between fatigue life and test temperature. This effect does not affect the correlation of cruciform joints as there is no significant variation of notch geometry of weld roots. Secondly, the number of specimens was more than sufficient to verify the effect of test temperature for cruciform joints with a very small scatter in fatigue test results, but was the minimum required for transversal stiffeners and was not enough to investigate the temperature effect for butt-welded joints. It is here assumed that they should also be affected by test temperature, as this was proven for the other weld details and confirmed by the majority of literature.

The majority of studies available in the literature tested fewer specimens than have been tested for this thesis and also fewer than typically recommended to derive *S–N* curves, cf. (DIN 50100:2016-12; DNVGL-RP-C203; Hobbacher 2016). Typically, only one type of weld detail was tested in most studies. Additionally, some studies performed tests on base material specimens; however, none presented results for different weld details. As has been seen in this study and is generally known in fatigue theory, specimens with lower notch acuity often show a higher scatter of fatigue test results (Haibach 2006). Consequently, more test data is required for mildly notched specimens in comparison to specimens with sharp notches. This leads to the question of whether the amount of *S–N* test data was the main reason why some studies did not observe a pronounced effect of test temperature on fatigue strength. In some studies (e.g. Kang et al. (2009), Bridges et al. (2012), and Wang et al. (2021)), the scatter in fatigue strength is much larger than the change in mean fatigue strength; still, only a few studies assessed their fatigue test results statistically for a temperature effect on fatigue strength (e.g. Kang et al. (2009) and Wang et al. (2021)).

Interestingly, the majority of studies—for which *S–N* test of welded joints has been performed—chose to investigate the fatigue strength of butt-welded joints. Butt-welded joints are one of the most common weld types in ship and offshore structures and are,

for example, used in the outer hull of ships to join block sections. From a fatigue strength perspective, these types of welds are often less critical than fillet-welded joints due to their higher fatigue strength and typically higher plate thickness based on ultimate strength requirements. There is a small number of studies on fatigue behaviour of non-load-carrying fillet-welded joints and longitudinal stiffeners available in the literature (Bridges et al. 2012; Li et al. 2018; Wang et al. 2021), but no studies are known to investigate the fatigue behaviour of joints showing weld root failure. This is, however, not surprising as weld details that are prone to weld root failure are typically avoided in ships and offshore structures. On the other hand, the benefit of performing tests on cruciform joints that fail from the weld root is related to the small scatter of fatigue strength results and the low susceptibility to angular misalignment effects—compared to joints that show weld toe failure. In that regard, *S–N* tests of cruciform joints with weld root failure seem to be almost as well suited to investigating particular influencing factors as fatigue crack growth rate tests, but are easier to perform.

As initially stated, temperature effects on fatigue behaviour are more often investigated using fatigue crack growth rate testing than *S–N* testing due to the smaller differences between individual specimens; nevertheless, fatigue design of engineering structures typically relies on stress-based fatigue assessment methods and thus on *S–N* data. Hence, this thesis presented the first comprehensive study on *S–N* fatigue testing of welded joints at sub-zero temperatures by means of three different weld details and for two different steel types.

The positive effect of decreasing test temperature (above the fatigue transition temperature) on fatigue strength reported in the literature was experimentally and statistically confirmed for the majority of weld details in this study; yet, further investigations are required to explain the smaller relative increase observed for the transversal stiffeners' and butt-welded joints' fatigue strength. For example, tests with artificially notched specimens could help to fully assess the temperature, geometry, and material effects on fatigue strength increase at sub-zero temperatures—similar to other studies investigating fatigue influencing factors, see (Atzori et al. 2005; Berto et al. 2013; Baumgartner 2014; Berto et al. 2014; Gallo et al. 2015; Louks and Susmel 2015; Fischer et al. 2016b).

The specimens of this study failed due to cracks either initiating in the heat-affected zone (butt-welded joints and transversal stiffeners) or the weld metal (cruciform joints).

The local microstructure is well known to affect fatigue crack initiation, but fatigue crack propagation is known to be almost independent of microstructure within one group of materials (Maddox 2002); nonetheless, local brittle zones in welded joints can have a strong effect if the test temperature is below their fatigue transition temperature (Zerbst et al. 2014). While fatigue cracks of the cruciform joint weld detail initiate in the weld metal, they initiate in the heat-affected zone of the transversal stiffener and butt-welded joints. Furthermore, residual stresses can vary significantly within welded connections, even in small-scale specimens (cf. (Barsoum 2008; Barsoum and Barsoum 2009; Friedrich 2020; Hensel 2020)) and are well known to affect the ductile–brittle transition temperature, see (Anderson and McHenry 1982; Horn and Hauge 2011; Horn et al. 2012; Zerbst et al. 2014; Østby et al. 2015; Horn et al. 2016).

Despite the steady increase in fatigue strength at sub-zero temperatures—even below the ductile–brittle transition temperature obtained from Charpy V-notch testing—in this study, adverse effects of temperature on fatigue strength of full-scale structures cannot completely be ruled out. In their fatigue crack growth rate tests, Walters et al. (2016) and Alvaro et al. (2017) found fatigue transition temperatures of 15 °C and 18 °C, respectively, above the ductile–brittle transition temperature from Charpy V-notch impact testing (T_{27J}). Both measured only a small increase of the threshold stress intensity factor range below the FTT, but the likelihood of hitting local brittle zones rises with increasing weld seam length, see Zerbst et al. (2014).

Typically, the highest ductile–brittle transition temperature is found in the coarse-grained and intercritically reheated coarse-grained heat-affected zones (Brandt et al. 2012; Zerbst et al. 2014; Alvaro et al. 2016; Horn et al. 2016). This could possibly have led to smaller fatigue strength increases for the specimens failing from the weld toe (butt-welded joints and transversal stiffeners) compared to the cruciform joints. This seems contradictory to the obtained Charpy V-notch impact test results—with higher ductile–brittle transition temperatures in the middle of the weld metal than in the heat-affected zone. The reason for this might be related to the weld shape of the butt-welded joints. The notch tip intersects only a small area of the heat-affected zone in the Charpy V-notch specimens. The likelihood of hitting a local brittle zone is consequently lower than in a fatigue specimen where sometimes multiple cracks initiate along the heat-affected zone; nevertheless, such effects would still be confined to a small area and only influence a fraction of the fatigue

crack growth. If such an effect occurred it would be difficult to identify it based on visual examination of the fracture surfaces, as the depth to crack initiation is only a few tenths of a millimetre. The observed brittle fracture zones (during fatigue crack growth) all appeared during later stages of the fatigue crack growth, when a significant fatigue crack had already formed. Furthermore, the increase in fatigue crack growth rate below the FTT was found to be less pronounced for lower stress intensity factor ranges (see Walters et al. (2016) and Alvaro et al. (2016, 2017)); this would explain why the fatigue strength at −50 °C is higher than at −20 °C.

In summary, the fatigue strength of welded joints—in terms of *S*–*N* curves—was found to increase at sub-zero temperatures, even below the assumed fatigue transition temperature of different zones of the welded connections. The reason is assumed to be related to the likelihood of hitting local brittle zones during early fatigue crack growth as this phase dominates fatigue life of the specimens tested for this study. For large scale structures, the likelihood of hitting local brittle zones increases with increasing weld length; still, a high ductile–brittle transition temperature and static fracture toughness might be more important for the integrity of a structure in such a scenario than a decreased fatigue strength below the fatigue transition temperature.

In general, a significant fatigue strength increase was observed for welded joints at sub-zero temperatures for all three weld details and both steel grades. While there is no distinct difference in fatigue strength between normal and high-strength steel for the fillet-welded test series, a higher increase was found for the S500 butt-welded joints compared to the S235 test series. This is, however, not surprising as the fatigue strength of weld details with sharp notches is typically independent of material strength, see Maddox (2002). More importantly, international standards and guidelines do consider adverse effects of high temperature (typically above 100 °C) on fatigue strength, but neglect similar effects at temperatures below room temperature, see (EN 1993–1–9:2005; LR ShipRight; BS 7910:2013+A1:2015; Hobbacher 2016; EN ISO 19906:2019). To approach the design of engineering structures at sub-zero temperatures in a more holistic way, this aspect should be considered in future generations of guidelines and standards.

7.2 | Discussion of extended fatigue assessment methods applied to sub-zero temperature fatigue test data

To allow fatigue assessment of welded joints for sub-zero temperature environments, seven different fatigue concepts have been applied to assess the obtained fatigue test data. Except for the stress averaging approach and the SED method, which are expected to be able to cover temperature effects on fatigue strength based on the micro-structural support effect hypothesis, all other methods rely on modification factors to take temperature effects into account.

7.2.1 | Discussion of the extension of the stress averaging approach

Currently, the application of the stress averaging approach or other effective stress methods for the general assessment of welded joints at sub-zero temperatures is less feasible than, for example, the SED method due to some general questions on the comparability of different effective stress methods; yet, the biggest obstacle is the large number of test data required to calibrate the method for particular applications by means of inverse estimation of the micro-structural support length ρ^* (estimation by minimization of scatter according to the proposal by Baumgartner et al. (2015)). Furthermore, problems arise with the assessment of mildly notched weld details.

First, the shallower slope of the *S–N* curves for butt-welded joints makes it difficult to find a suitable slope for the inverse procedure to determine ρ^*. Second, the wide scatter compared to fillet-weld details decreases the accuracy of the method if a reference fatigue strength is determined by means of curve fitting and third, mild notches experience a material strength effect, which has a significant effect on the estimated value of ρ^*. The last effect can be accounted for by means of a material strength correction as in (Baumgartner et al. 2019; Braun et al. 2019); however, all three effects decrease the accuracy of the inverse procedure or require a large amount of data to be mitigated. On the contrary, the direct procedure of estimating the characteristic length parameter (El Haddad-Smith-Topper parameter a_0 or characteristic length parameter of V-notched component $a_0^{N'}$) can be achieved more easily using data for the two typical weld shapes assumed by the SED method (0° and 135° opening angle) in combination with either own material tests or

literature data.

More reliable results for ρ^* could probably be obtained by limiting the results to sharp notch details like fillet-welded joints like for the SED method; nonetheless, this would significantly affect the estimates for the micro-structural support length ρ^* in this study, as the amount of data is reduced by one third. A reduction of specimen number in this range would significantly influence the estimate for ρ^*, as can been seen from the statistical assessment of fatigue test results in Chapter 5. Another possible approach is the application of the localized weld toe geometry in FE models instead of using the assumption of a reference radius $r_{ref} = 0.05$ mm as recommended when the actual geometry cannot be determined, see Baumgartner et al. (2015). The reference radius might be suitable for sharp notches at weld toes and roots of fillet welded joints, but is probably less suitable for large transition radii at the weld toes of butt-welded joints made by flux-cored arc welding.

Interestingly, the application of the actual weld geometry in the microscale, also seems to affect the estimate of the micro-structural support length ρ^*, see Liinalampi et al. (2016). Applying the stress averaging approach to laser-hybrid welds made from thin plates, they obtained a micro-structural support length much smaller than typically reported for welded joints ($\rho^* = 0.05$ mm). This approach seems certainly promising; yet, the measuring accuracy and resolution of laser profile sensors is known have a strong effect on the determined weld geometry, see Schubnell et al. (2020a). Therefore, it seems likely that more research is required until actual weld geometries can reliably be modelled and used for fatigue assessment based on the stress averaging approach or other TCD methods.

In general, it is difficult to compare the SED's direct method for the determination of the material characteristic length L to the inverse method of the stress averaging approach. Both methods rely on large datasets to determine either ρ^* or the reference fatigue strength parameter that form the basis of the SED method (plain specimen fatigue strength $\Delta\sigma_0$ and mode I N-SIF fatigue strength ΔK_1^N). Despite the large scatter in the normalized mean increase of threshold stress intensity factor range at sub-zero temperatures ($k_{\Delta K_{th,norm}}$) presented in Section 2.1, the uncertainty of mode I N-SIF fatigue strength ΔK_1^N at sub-zero temperatures is expected to be smaller than the uncertainty of plain specimen fatigue strength $\Delta\sigma_0$. While the coefficient of variation of the data used to determine ΔK_1^N is rather small ($CV = 8.8\%$), the variation of $\Delta\sigma_0$ found for room temper-

ature results in the literature amounts to $\mathrm{CV} = 24.7\%$, see Table 1. It is thus assumed that the plain specimen fatigue strength $\Delta\sigma_0$ is also the main source of uncertainty at sub-zero temperatures.

Comparing the estimates of material characteristic length parameter from the stress averaging (ρ^*) and SED method ($a^{N'}$ or a') directly is not feasible. Both (material characteristic length L of the TCD method and the El Haddad-Smith-Topper parameter a') are considered to be material constants, but the procedure to determine them varies significantly. Furthermore, it still has to be investigated whether the application of the inverse procedure of determining ρ^* is suitable to estimate L. Originally, a' and L did not include any geometrical effects. Eq. (11) was later extended for arbitrary crack geometry function Y by Härkegård (1981). This relation is mentioned by Taylor (2007); however, he specifically acknowledges that both parameters lead to different predictions due to the consideration of the crack shape ($Y \neq 1$)—expect for the cases of long cracks ($a' \ll a$) and plain specimens ($a \approx 0$ mm). He further elaborates that the difference between both becomes largest for crack lengths in the range of the material characteristic length L. It is thus assumed that it is not possible to estimate L by means of the inverse procedure, due to the aforementioned strong influence of the notch geometry on the estimates of the micro-structural support length ρ^*. Furthermore, a strong deviation between effective stresses obtained for the two most commonly applied TCD methods was observed in Braun et al. (2020e) for different notch shapes and material behaviour (plane stress and plane strain). Similar deviations were obtained by Hu et al. (2019) for a large number of experimental results of notched components obtained from the literature. Interestingly, the highest deviation was found for blunt notches and short material characteristic lengths $L < 0.3$ mm. This agrees with an investigation by Silva et al. (2012) and by Benedetti and Santus (2020), who observed an increase in prediction error for low notch acuities.

Assuming that the initial crack length a_i at the fatigue limit is of the order of the El Haddad-Smith-Topper parameter (a'/Y^2) according to the engineering approach by Atzori et al. (2008) (Eq. (25)), a large deviation between actual and estimated L can be assumed if L is estimated from fatigue test data of welded joints according to the inverse procedure. The reason is that most welded joints are neither similar to plain specimens nor fulfil the long crack requirement (except for cruciform joints failing from a non-penetrating weld root). One possibility could be to account for the notch shape by correcting the stress

gradient or the effective stress for various micro-structural support lengths ρ^* during stress averaging; nevertheless, this would significantly increase the effort needed to applied the stress averaging approach and can thus be considered infeasible.

An alternative could be to extend a more recent formulation of the TCD methods by Susmel and Taylor for the medium-cycle fatigue regime, see Susmel and Taylor (2007, 2013). In their work, they treated the material characteristic length L as a parameter dependent on number of cycles to failure and obtained it by equating the fatigue strength of plain and notched specimens. Thereby, differences in slope exponent of fatigue data of components with blunt and sharp notches can also be accounted for. Consequently, this approach has proven to be successful for various loading scenarios of notched components (Susmel and Taylor 2007, 2013; Louks and Susmel 2015; Faruq and Susmel 2019; Luo et al. 2019), as it takes the notch geometry directly into account. A similar procedure was proposed by Susmel and co-workers for welded joints, see (Susmel 2008; Al Zamzami and Susmel 2017, 2018). To account for the scatter of fatigue test results of welded joints, the TCD method was linked to the N-SIF scatter band and estimates for the plain specimen fatigue strength of flush-ground butt-welded joints—using data by Livieri and Lazzarin (2005). Interestingly, Atzori et al. (2005) suggested a similar approach for the determination of the generalized Kitagawa-Takahashi diagram for V-notched components.

As an alternative to the estimation of the notch shape opening angle effect by means of the SED method, they proposed an assessment based on the point method of the TCD methods. Rearranging Eq. (6) so that the tangential stress of Williams' stress equation becomes a function of the mode I N-SIF with:

$$\sigma_{\Theta\Theta}\left(r, \Theta = 0\right) = \frac{K_1^N}{\sqrt{2\pi} r^{\xi}} \tag{44}$$

and assuming the stress to be equal to the fatigue strength at a critical distance ($r = L/2$) along the notch bisector ($\Theta = 0$) offers a possibility to estimate L for sharp notches. As a result, it is possible to estimate L separately for different notch geometries; yet, similarly to the previously discussed approaches, Atzori et al. (2005) and Susmel and co-workers' (Susmel 2008; Al Zamzami and Susmel 2017, 2018) approaches are strictly limited to sharp notches that fulfil the requirements of the N-SIF method. Consequently, identical estimates from TCD methods and the SED method can be obtained from data of sharply

notched specimens. The material characteristic length L, however, equals the El Haddad-Smith-Topper parameter a_0 only for a through crack in an infinite plate ($Y = 1$) (Taylor 2007; Taylor and Hoey 2009).

In summary, there are a number of problems related to the application of the stress averaging approach for welded joints which are still to be answered before it seems feasible to estimate the material characteristic length L under different conditions like sub-zero temperatures; nonetheless, a general trend is certainly obtainable from fatigue test data using the approach proposed by Baumgartner et al. (2015). Thus, it is not surprising that the trend of increasing micro-structural support lengths ρ^* with decreasing test temperature was confirmed by the SED method. Nonetheless, compared to including temperature effects into the stress averaging approach, the application of the SED method appears to be more straightforward; nevertheless, the SED method also has certain limitations, which are subsequently discussed.

7.2.2 | Discussion of the extension of the SED method

Two different approaches based on the averaged strain energy density method were applied to estimate the change of micro-structural support effect at sub-zero temperatures compared to room temperature.

- The first idea was based on an optimization approach similar to the inverse procedure of the stress averaging approach; nonetheless, instead of finding a set of parameters that minimizes the fatigue scatter, control radii $R_C\,(T)$ for sub-zero temperatures were calculated that led to the same mean deviation of fatigue life from the design curve for all three test temperatures.

- The second is based on the generalized Kitagawa-Takahashi diagram for V-notched components by Atzori et al. (2005) and the relation of the characteristic length parameter of a V-notched component $a^{N'}$ to the El Haddad-Smith-Topper parameter a_0, and thereby to the control radius R_C.

Both approaches are subsequently discussed—starting with the approach based on a uniform scatter band for SED-based assessment of welded joints. To extend the SED

method for welded joints to sub-zero temperatures, the assumption that one fatigue design curve can be representative for the assessment of various notch or weld details under different condition was adopted for this study. This assumption was in the past not only applied to welded joints, but also for notched components made of the same material but tested at different temperature (e.g. room temperature and high temperatures of several hundred °C). The only requirement is that support effects are covered on the load-side, for example, by varying the control radius R_C. The same assumption is the basis for the FAT160 curve of the stress averaging approach or other local fatigue assessment methods and is based on normalized *S–N* curve concept by Haibach, see Haibach (1968).

Assuming the control radii and scatter band to be correct for room temperature, radii were estimated separately for weld toe and weld root failure. The basic idea of the first SED-based approach relates to the relation between control radii R_C and the El Haddad-Smith-Topper parameter $a^{'}$ (Eq. (12)). This relation is frequently applied to assess the fracture behaviour of various materials (e.g. Lazzarin and Zambardi (2001) and Berto and Lazzarin (2007, 2009)), but is also regularly applied for the fatigue assessment of notched components, see (Berto et al. 2013, 2014; Gallo et al. 2015; Gallo and Berto 2016; Hu et al. 2019). For welded joints, the initially proposed control radius R_C has been changed a number of times since the first application of the SED method to assess the fatigue strength of welded joints in (Lazzarin and Zambardi 2001). This process is related to reassessment of the underlying assumptions; yet, the range of suggested radii remained within 0.26 to 0.36 mm. In this study, the radii proposed by Fischer et al. (2016b,c) were applied for the room temperature fatigue test data. These radii were obtained by reassessing the original data, which was used to establish the SED method for welded joints, and by performing new tests on artificially notched welded joints.

Recalling Eq. (16), the control radii R_C for welded joints are a function of the mode I N-SIF (ΔK_1^N) and the fatigue limit of flush-ground butt-welded joints ($\Delta\sigma_0$). Relating the initial defect at weld toes to $a^{'}$, Atzori et al. (2005, 2008) showed that the micro-structural support effect at weld toes is also related to the El Haddad-Smith-Topper parameter $a^{'}$.

Next, control radii for weld toe and root failure at sub-zero temperatures were derived using the fatigue test data of transversal stiffeners and cruciform joints, following the master *S–N* curve assumption. By doing so, the mean deviation between experimental and estimated number of cycles to failure was calculated for both failure locations at room

temperature. This mean deviation was then used to find the control radii that led to the same deviation at −20 °C and −50 °C. Consequently, an assessment of fatigue strength of welded joints is possible without introducing a correction of the proposed $\Delta\overline{W} - \mathrm{N}$ scatter band as is required for stress-based concepts, see Braun et al. (2020d). The novelty of this approach is that fatigue test data at different temperatures is synthesized by finding radii that fit the data best. This is achieved by a adjusting the radii until the same deviation from the design curve is achieved as for room temperature test data. A similar approach was presented by Berto et al. (2014) for notched and unnotched 40CrMoV13.9 steel specimens; however, they introduced an empirical temperature sensitivity function $\mathrm{Q}\,(\mathrm{T})$ instead of adjusting the radius to reflect the change in micro-structural support effect.

Verifying this concept by performing tests for $\Delta\sigma_0$ and $\Delta\mathrm{K}_1^{\mathrm{N}}$ at sub-zero temperatures is practically infeasible, as it requires a large amount of data to be tested at equal conditions and due to the large inherent scatter in fatigue test results of flush-ground butt-welded joints. Hence, three assumptions were introduced.

First, in Chapter 4 and literature results, it was assumed that $\Delta\sigma_0$ and $\Delta\mathrm{K}_1^{\mathrm{N}}$ are a function of temperature based on the fatigue test results of weld details with sharp and mild notches. Second, the assumed linear relation between $\Delta\mathrm{K}_1^{\mathrm{N}}$ and stress intensity factor threshold for long cracks $\Delta\mathrm{K}_{\mathrm{th}}$ (according to Atzori et al. (2005, 2008)) was applied to estimate the change of $\Delta\mathrm{K}_1^{\mathrm{N}}$ at sub-zero temperatures. Third, the change of fatigue strength of the S500 butt-welded joints was used as an estimate for the change of $\Delta\sigma_0$ with temperature. The first assumption can be considered true based on the assessment of correlation between test temperature and fatigue test results in Chapter 5. The second can be applied as long as the fatigue life is mainly governed by fatigue crack propagation and the mode II N-SIF is non-singular (i.e. fatigue strength is defined only by the mode I contribution). The third is based on the fact that a fatigue strength similar to those reported for flush-ground butt-welded joints was obtained for the S500 butt-welded joints. The reason for the high fatigue strength is the large weld toe radii of up to 3 mm.

Using this relation an increase in control radii at sub-zero temperatures is estimated, which agrees with the assumption of the master *S–N* curve approach. The reason for this is the larger increase of mode I N-SIF ($\Delta\mathrm{K}_1^{\mathrm{N}}$) compared to the fatigue limit of flush-ground butt-welded joints ($\Delta\sigma_0$). This result agrees with the higher relative increase in fatigue

strength of weld details with sharp notches compared to the mildly notched butt-welded joints.

More importantly, an increase in control radii simultaneously leads to an increase of the El Haddad-Smith-Topper parameter $a^{'}$ or material characteristic length L according to Eq. (12). This result agrees well with the results presented for the stress averaging approach. Clearly, it cannot be considered proof, as both approaches are based on the same data, but if Berto et al. (2014) had adjusted the control radius for their data instead of introducing the temperature sensitivity function $Q\,(T)$, they would have obtained a decreasing control radius for increasing temperature.

Next, the second approach based on the generalized Kitagawa-Takahashi diagram for V-notched components by Atzori and Lazzarin (2001) and Atzori et al. (2003) will be discussed. Again, the relation between control radii R_C and the El Haddad-Smith-Topper parameter $a^{'}$ was applied to assess the change of micro-structural support effect at sub-zero temperatures. By extending the original diagram for a shape coefficient α_ξ', a characteristic length parameter of V-notched component $a^{N'}$ for varying V-notch opening angles was introduced. Using different local fatigue assessment methods, they showed that α_ξ' is only dependent on the notch opening angle (2α). As a result, the El Haddad-Smith-Topper parameter $a^{'}$ can directly be determined if the mode I N-SIF (ΔK_1^N) and the fatigue limit of flush-ground butt-welded joints ($\Delta\sigma_0$) are known. Again, the aforementioned assumptions were applied to estimate ΔK_1^N and $\Delta\sigma_0$ in order to estimate the change of micro-structural support effect at sub-zero temperatures.

Following Atzori and Lazzarin (2001) and Atzori et al. (2003) hypothesis, $a^{N'}$ is considered to be representative for the micro-structural support effect at weld toes and roots of the specimens tested for this thesis; nevertheless, the relation between control radii R_C and the El Haddad-Smith-Topper parameter $a^{'}$ (Eq. (12) and Eq. (17)) is used to compare the two approaches presented in this study. Comparing the estimates of control radii obtained by means of the generalized Kitagawa-Takahashi diagram with the ones obtained by adjusting the mean deviation, a reasonably good agreement is obtained (see Table 12).

Interestingly, the highest deviation is obtained at room temperature. Indeed, the control radii obtained using the generalized Kitagawa-Takahashi diagram are closer to the original proposed radii for the SED method. The reason is probably related to the slight difference between the fatigue limit of flush-ground butt-welded joints ($\Delta\sigma_0$) and the fa-

Table 12. Comparison of the estimated control radii $R_C\,(T)$ obtained by adjusting the mean deviation based on Eq. (37) and from the generalized Kitagawa-Takahashi diagram using the estimates of El Haddad-Smith-Topper parameter $a^{'}$ at sub-zero temperatures

Temperature	Generalized Kitagawa-Takahashi diagram				Adjusting the mean deviation based on Eq. (37)		Deviation between both approaches	
	Weld toe		Weld root		Weld toe	Weld root		
T	$a^{'}$ [mm]	$R_{C,WR}$ [mm]	$a^{N'} = a^{'}$ [mm]	$R_{C,WR}$ [mm]	$R_{C,WT}$ [mm]	$R_{C,WR}$ [mm]	Weld toe	Weld root
RT	0.456	0.385	0.456	0.388	0.32	0.325	17.0%	16.2%
−20 °C	0.492	0.416	0.492	0.418	0.37	0.41	11.0%	2.0%
−50 °C	0.531	0.449	0.532	0.452	0.41	0.51	8.6%	−12.8%

tigue strength of the S500 butt-welded joints at room temperature; still, two important aspects can be seen from this comparison. First, both methods simultaneously estimate an increase of control radii R_C and the El Haddad-Smith-Topper parameter $a^{'}$ at sub-zero temperatures based on the available test data and literature results. Second, a small variation in the parameters used to estimate the micro-structural support effect can have a significant effect on the estimated fatigue parameter. The reason is that small changes of control radii have strong effect on the averaged strain energy density ($\Delta\overline{W}$). This, and the general application of local fatigue assessment methods for welded joints using the micro-structural support effect hypothesis to account for fluctuating temperatures, will be discussed in the subsequent section.

7.3 | Applicability of local fatigue assessment methods based on the micro-structural support effect hypothesis for welded joints at room and sub-zero temperatures

While the aim of the preceding two sections was to discuss particular aspects related to the extension of the stress averaging approach and the SED method to sub-zero temperatures, the aim of this section is to discuss the application of local fatigue assessment methods based on the micro-structural support effect hypothesis for problems like fluctuating temperatures.

To this day, there is a limited number of studies related to the fatigue of welded joints under the influence of fluctuating temperatures and, in general, temperatures different from room temperature. Furthermore, the majority of available studies focus on temperatures high enough to cause creep, see Mannan and Valsan (2006). Although it is well

known that temperature effects cause changes of the micro-structural support effect at notches, studies investigating this effect for sub-zero temperatures are not known; yet, there are a number of related studies on fatigue of notched components at high temperatures. Among those, Gallo and Berto (2016) applied both the SED method and TCD methods for fatigue assessment based on the micro-structural support effect hypothesis. They showed that temperature effects on fatigue strength can be accounted for on a sound physical basis without the need for modification factors. Their work motivated the application of those methods for fatigue assessment of welded joints at sub-zero temperatures; however, a couple of basic questions remain that were not investigated in this study, but are important for the application of both methods.

One example of such questions is the recommended SED control radii for welded joints. Lazzarin et al. (2003) stated that as long as only mode I stress distribution is singular, small variations of R_C have limited effect on the fatigue life predictions. Otherwise, the influence of varying R_C is significantly increased. In more recent studies by Fischer et al. (2016a,b,c) and Hu et al. (2019), this assumption was refuted; nevertheless, the determination of suitable radii in connection with the proposed scatter band is still unresolved.

The application of the control radii according to Fischer et al. (2016b,c) led to a non-conservative assessment for weld root failure of cruciform joints. The reason is that the scatter band for welded joints was originally established for a control radius of 0.28 mm. This result agrees with the observations by Fischer et al. (2016b,c). Therefore, it is recommended to adjust the scatter band, e.g. by accounting for misalignment effects. This can be easily be achieved by adjusting the scatter band by the same factor as the data that was used to derive the larger control radii. Alternatively, the control radii proposed by Lazzarin et al. (2003) may be applied; yet, this would lead to more conservative results for other joints details.

Interestingly, Taylor et al. (2002) reported analytical—based on Radaj's effective notch stress method (Radaj 1990)—and experimental values of the El Haddad-Smith-Topper parameter a' for welded joints equal to 0.31 mm and 0.43 mm, respectively. This leads to control radii R_C of 0.26 mm and 0.36 mm according to Eq. (17), cf. Lazzarin et al. (2003). As the fatigue test results of the fillet-welded joints match well both the design curve of the effective notch stress method (see Braun et al. (2020d)) and the SED scatter band, it can be assumed that the El Haddad-Smith-Topper parameter a' for welded joints reported

by Taylor and the control radii in this range are likely representative for the fatigue test at room temperature.

In this study, an extension of the SED method to sub-zero temperatures was presented by adjusting the control radii. This approach allows an accurate assessment based on the micro-structural support effect hypothesis; nonetheless, adjusting the radius to fluctuating temperatures might be impractical. In order to overcome the disadvantage of adjusting the control radii for various temperatures, a temperature correction formula $M(T)$ was introduced to ease SED-based assessment for temperatures different from room temperature. The difference to the empirical modification factors for stress-based methods is that changes of Young's modulus E and the micro-structural support effect hypothesis are accounted for in this formula.

Comparing the results of the SED method with other fatigue assessment methods, a good agreement between experimental and predicted fatigue life at RT is achieved for most local stress-based fatigue assessment methods except, for the structural stress extrapolation method applied to weld root failure. For the nominal stress approach, a significantly higher deviation is found, which is partially due to the higher level of misalignment considered in the design curves of the nominal stress approach. Interestingly, a high deviation is also found for the SED method and weld toe failure. This comparison shows that there is still work required to improve fatigue assessment of welded joints at room temperature, but also at sub-zero temperatures.

Finally, comparing the results obtained for the averaged SED method with control radii and Young's modulus adjusted to sub-zero temperatures, the advantage of methods that account for the micro-structural support effect becomes clearly visible. While the mean deviations significantly increase for all state-of-the-art methods, they remain constant if temperature effects are considered by adjusting the control radii and Young's modulus of the averaged SED method. This plainly shows the relevance of methods based on the micro-structural support effect hypothesis and the importance of including temperature effects within fatigue assessment.

8 | Summary and conclusions

This study investigated the fatigue strength of welded steel joints at room and at sub-zero temperatures by means of *S–N* tests. To confirm observed trends, experimental results were statistically assessed regarding temperature effects and compared with international standards. Furthermore, Charpy V-notch impact and tensile testing was performed in order to characterize the material behaviour at sub-zero temperatures and to relate changes of fatigue strength to material tests typically required by international standards.

In regard to the first research hypothesis and objective, the fatigue strength of welded joints was found to increase at sub-zero temperatures, even below the assumed fatigue transition temperature of different zones of the welded connections.

Next, the applicability of local fatigue assessment methods for welded joints exposed to sub-zero temperatures was analysed. Two fatigue assessment methods based on the micro-structural support effect hypothesis were extended to be able to account for temperature effects on fatigue strength.

With respect to the second research hypothesis as well as the second and third objective, fatigue assessment methods based on the micro-structural support effect hypothesis have proven to be suitable to account for temperature effects based on their relation to the El Haddad-Smith-Topper parameter α' and linear elastic fracture mechanics. The following conclusions are drawn from the experimental test programme and the statistical assessment of the fatigue test results:

- On average, the fatigue strength of the welded steel joints tested in this study increased constantly with decreasing temperature throughout the tested range. The average fatigue strength increase in mean fatigue strength compared to room temperature was about 7% at -20 °C and 15% at -50 °C, respectively. This trend was

statistically confirmed by an assessment of the correlation between test temperature and the number of cycles to failure using bootstrapping and a jackknife approach.

- Fatigue design curves for welded joints derived from tests at room temperature can safely be applied to temperatures as low as −50 °C, but highly underestimate the actual fatigue strength at sub-zero temperatures; this is in particular true for cruciform joints.

- Comparing the increase in fatigue strength at sub-zero temperatures, the highest relative increase was obtained for the weld detail with the highest notch acuity (cruciform joint with weld root failure), but the highest absolute increase was observed for the weld detail with the lowest notch acuity (butt-welded joint).

- The highest increase in mean fatigue strength, of approximately 25.5%, has been found at −50 °C for the cruciform joints made of a normal-strength steel grade that is only qualified for −20 °C (based on fracture toughness properties). This extends the findings of Walters et al. (2014) that steel grades not aimed for particular low temperature toughness properties often fulfil fracture toughness requirements at lower temperatures.

- The correlation between test temperature and number of cycles to failure is influenced by the number of other influencing factors (i.e. misalignment and local weld geometry). As a result, the strongest correlation was observed for the weld detail with the lowest number of factors (cruciform joints with weld root failure). Furthermore, the statistical evaluation has shown that the amount of data was generally adequate to draw these conclusions; nevertheless, the lower the notch acuity the larger the amount of data required to confirm a temperature effect. Hence, previous studies that did not confirm a pronounced effect of temperature on fatigue strength might not have tested enough specimens.

- Welded joints produced by FCAW exhibit a low fracture toughness in the middle of the weld zone after undergoing several heat cycles; however, fatigue cracks usually initiate in the heat-affected zone and not in the weld metal (with the exception of cruciform joints showing weld root failure). As a consequence, the low fracture toughness does not seem to decrease the fatigue strength of the specimens in this

study. In large welded structures this could, however, lead to brittle fracture of the structure, if the crack advances along a weld seam through the weld metal.

- Although visual inspections of the fracture surfaces reveal brittle fracture areas in some specimens, the fatigue strength increases even below the assumed fatigue and ductile–brittle transition temperature. The reason is that the fatigue strength of small-scale specimens is dominated by early fatigue crack propagation; the likelihood of hitting local brittle zones at this stage of fatigue crack propagation is low compared to latter stages when a line-type crack has formed along the weld toe.

The following conclusions are drawn from the extension of fatigue assessment methods for welded joints based on micro-structural support effect hypothesis to sub-zero temperatures, and the comparison with state-of-the-art fatigue assessment methods:

- In general, fatigue assessment methods based on the micro-structural support effect hypothesis are well suited for the fatigue assessment of welded joints at sub-zero temperatures. Both applied methods (stress averaging approach and averaged strain energy density method) are capable of accounting for changes of support effect based on their underlying relation to material characteristic length parameters like the El Haddad-Smith-Topper parameter.

- Using both methods and two different approaches based on the averaged strain energy density method, an increase in micro-structural support effect (defined by the material characteristic length parameter) is estimated for decreasing test temperatures.

- It is possible to assess the fatigue strength of welded joints at different temperatures using the SED scatter band—that was derived using room temperature fatigue data—by adjusting the control radii and Young's modulus. The need for modification factors as for stress-based methods is thereby avoided.

- Comparing the SED method and its extended version for sub-zero temperatures with state-of-the-art fatigue assessment methods, large differences in prediction accuracy are found for weld toe and weld root failure. In general, all methods lead to conservative results for weld toe failure; yet, the results of cruciform joints showing

weld root failure are non-conservatively assessed by some local fatigue assessment methods.

- Finally, all fatigue assessment methods are applicable at sub-zero temperatures as they lead to more conservative assessment results compared to room temperature; nevertheless, methods based on micro-structural support effect hypothesis help to avoid over-conservatism.

9 | Outlook

Knowledge about the fatigue behaviour of welded structures under extreme temperature conditions is decisive for their safety in Arctic environments. This study has confirmed an increasing fatigue strength of welded joints with decreasing temperature; yet, the majority of current standards and guidelines do not consider temperature effects on fatigue strength below room temperature. Furthermore, no guidance is given regarding material and welding process selection to achieve an optimal combination of fatigue strength and fracture toughness in structures exposed to sub-zero temperatures. In consultation with classification societies, the basis for the approval of steels and welded structures under extreme conditions should be extended to approach this topic from a more holistic perspective. This applies to the assessment of fatigue strength as well as design concepts for ships and offshore structures in general; nevertheless, the obtained insights are useful for other engineering structures as well.

The results demonstrated the general applicability of normal and high-strength steels under these conditions. Furthermore, the use of high-strength steels, with careful consideration of application criteria and production processes, offers considerable advantages to improve the design of ship and offshore structures exposed to sub-zero temperatures. For the future, however, optimized welding procedures will facilitate the consideration of increased fatigue strength at sub-zero temperature. To reach both high fatigue strength and fracture toughness, further research is required, since butt joints with multiple weld layers made by flux-cored arc welding are known to suffer low fracture toughness compared to joints made by submerged arc welding processes, in particular in the middle of the weld metal. From a fracture mechanics perspective, the required toughness at low temperatures in the weld metal is not fulfilled by the flux-cored arc welded joints in this

study. Contrary to this, *S–N* testing does not show any decrease in fatigue strength due to embrittlement of the weld material and the heat-affected zone. Indeed, joints made by flux-cored arc welding often possess smoother weld toe transition radii than other welding processes, thus explaining the higher fatigue strength of flux-cored arc welded compared to submerged arc welded joints. To meet fracture toughness properties at low temperatures in all zones of welded joints and to exploit the high fatigue strength of flux-cored arc welded high-strength steel joints, welding materials with very high fracture toughness properties are required. If this is not followed, the toughness in the weld metal is far below that of the base material and in the heat-affected zone.

Further research is necessary to cover all aspects of fatigue assessment to enable the consideration of increased fatigue strength under sub-zero temperatures within the design of ships and offshore structures. Major open points are seen in the behaviour under variable amplitude loading and fatigue strength of thermal cut plate edges. In particular the combination of varying temperatures and loads will be a major challenge for the design of structures exposed to drifting sea ice and sub-zero temperatures.

With the increasing demand for sustainable development and sources for renewable energy comes the need to constantly develop the technologies, design, and safety within the renewable energy industry. In the case of offshore wind turbines (where fatigue is one of the major design criteria), the trend follows an increase of development in areas at high latitude, where not only are the loads from wind and waves a consideration, but also that of seasonal moving and crushing sea ice causing cyclic actions.

The goal of future projects will be to develop combined load spectra for wind, waves, and ice loadings on an offshore wind turbine structure and to verify the observation made on fatigue strength at sub-zero temperatures in constant amplitude loading tests to variable amplitude loading. A first possible concept for the verification of a combined load spectra by means of variable amplitude loading tests has already been presented in Milaković et al. (2019), Braun et al. (2021c), and Høyland et al. (2021).

Furthermore, this thesis has proven that the currently available fatigue assessment methods show varying degrees of accuracy for different types of weld details. None of the typical stress-based methods are currently capable of being used for all types of weld details; however, with methods that require higher effort in preparation of the models and assessment procedure, higher accuracy can be achieved compared to more basic ap-

proaches. Due to this, there is an ongoing need to improve current fatigue assessment methods or to develop new ones.

10 | Bibliography

ABS Guide for the Fatigue Assessment of Offshore Structures (2020). Houston, Texas: American Bureau of Shipping.

Aderinola OO, Kah P, Martikainen J (2013). Efficient welding technologies applicable to HSS arctic offshore structures. *The Twenty-third International Offshore and Polar Engineering Conference*. International Society of Offshore and Polar Engineers.

Ahola A, Nykänen T, Björk T (2017). Effect of loading type on the fatigue strength of asymmetric and symmetric transverse non-load carrying attachments. *Fatigue & Fracture of Engineering Materials & Structures* 40(5):670–682. DOI: 10.1111/ffe.12531.

Ahola A (2020). Stress components and local effects in the fatigue strength assessment of fillet weld joints made of ultra-high-strength steels. PhD Thesis. Lappeenranta-Lahti University of Technology LUT.

Ahola A, Muikku A, Braun M, Björk T (2021). Fatigue strength assessment of ground fillet-welded joints using 4R method. *International Journal of Fatigue* 142:DOI: 10.1016/j.ijfatigue.2020.105916.

Akselsen OM, Ren XB, Alvaro A, Nyhus B (2017). Key Challenges in Materials and Welding for Application of Steel Structures in Arctic. *The 27th International Ocean and Polar Engineering Conference*. International Society of Offshore and Polar Engineers.

Al Zamzami I, Susmel L (2017). On the accuracy of nominal, structural, and local stress based approaches in designing aluminium welded joints against fatigue. *International Journal of Fatigue* 101:137–158. DOI: 10.1016/j.ijfatigue.2016.11.002.

Al Zamzami I, Susmel L (2018). On the use of hot-spot stresses, effective notch stresses and the Point Method to estimate lifetime of inclined welds subjected to uniaxial fatigue loading. *International Journal of Fatigue* 117:432–449. DOI: 10.1016/j.ijfatigue.2018.08.032.

Albrecht P, Yamada K (1977). Rapid calculation of stress intensity factors. *Journal of the Structural Division* 103(2):377–389.

Aleksenko E, Grinberg N, Ilushchenko K (1988). Fatigue crack growth in KhN 60 MVYu nickel alloy at 293 and 11 K (Rost ustalostnoi treshchiny v nikelevom splave KhN 60 MVIu pri temperaturakh 293 i 11 K). *Problemy Prochnosti*:25–31.

Alvaro A, Akselsen OM, Ren XB, Kane A (2014). Fundamental aspects of fatigue of steel in Arctic applications. *The 24th International Ocean and Polar Engineering Conference*.

International Society of Offshore and Polar Engineers.

Alvaro A, Akselsen OM, Ren XB, Nyhus B (2016). Fatigue Crack Growth of a 420 MPa Structural Steel Heat Affected Zone at Low Temperatures. *The 26th International Ocean and Polar Engineering Conference*. International Society of Offshore and Polar Engineers.

Alvaro A, Akselsen OM, Ren XB, Perillo G, Nyhus B (2017). On the Relation between Fatigue and Static Ductile to Brittle Transition for Weld Simulated 420 MPa Structural Steel. *The 27th International Ocean and Polar Engineering Conference*. International Society of Offshore and Polar Engineers.

Anderson TW, Darling DA (1952). Asymptotic Theory of Certain "Goodness of Fit" Criteria Based on Stochastic Processes. *The Annals of Mathematical Statistics* 23(2):193–212.

Anderson T, McHenry H (1982). *Fracture Toughness of Steel Weldments for Arctic Structures*. Boulder, Colorado: National Bureau of Standards.

Andrews RM (1996). The Effect of Misalignment on the Fatigue Strength of Welded Cruciform Joints. *Fatigue & Fracture of Engineering Materials and Structures* 19(6):755–768. DOI: 10.1111/j.1460-2695.1996.tb01320.x.

API SPECIFICATION 2W Specification for Steel Plates for Offshore Structures, Produced by Thermo-Mechanical Control Processing (TMCP) (2019). Washington, DC: American Petroleum Institute.

ASME Boiler & Pressure Vessel Code - Section 2: Materials - Part D: Properties (2017). New York: American Society of Mechanical Engineers.

Atzori B, Dattoma V (1983). A comparison of fatigue behaviour of welded joints in steel and aluminium alloys. IIW-Doc. XIII-1089-83. International Institute of Welding.

Atzori B, Lazzarin P (2001). Notch Sensitivity and Defect Sensitivity under Fatigue Loading: Two Sides of the Same Medal. *International Journal of Fracture* 107(1):1–8. DOI: 10.1023/a:1007686727207.

Atzori B, Lazzarin P, Meneghetti G (2003). Fracture mechanics and notch sensitivity. *Fatigue & Fracture of Engineering Materials & Structures* 26(3):257–267. DOI: 10.1046/j.1460-2695.2003.00633.x.

Atzori B, Lazzarin P, Meneghetti G (2005). A unified treatment of the mode I fatigue limit of components containing notches or defects. *International Journal of Fracture* 133(1):61–87. DOI: 10.1007/s10704-005-2183-0.

Atzori B, Lazzarin P, Meneghetti G (2008). Fatigue strength assessment of welded joints: From the integration of Paris' law to a synthesis based on the notch stress intensity factors of the uncracked geometries. *Engineering Fracture Mechanics* 75(3-4):364–378. DOI: 10.1016/j.engfracmech.2007.03.029.

Atzori B, Meneghetti G, Susmel L (2002). Estimation of the fatigue strength of light alloy welds by an equivalent notch stress analysis. *International Journal of Fatigue* 24(5):591–599. DOI: 10.1016/s0142-1123(01)00113-x.

Baek JH, Kim CM, Kim WS, Kho YT (2001). Fatigue crack growth and fracture toughness properties of 304 stainless steel pipe for LNG transmission. *Metals and Materials International* 7(6):579–585. DOI: 10.1007/Bf03179257.

Barsoum Z, Barsoum I (2009). Residual stress effects on fatigue life of welded structures using LEFM. *Engineering Failure Analysis* 16(1):449–467. DOI: 10.1016/j.engfailanal.2008.06.017.

Barsoum Z (2008). Residual stress analysis and fatigue assessment of welded steel structures. Doctoral Thesis. KTH Stockholm.

Basinski ZS, Korbel AS, Basinski SJ (1980). The temperature dependence of the saturation stress and dislocation substructure in fatigued copper single crystals. *Acta Metallurgica* 28(2):191–207. DOI: 10.1016/0001-6160(80)90068-1.

Baumgartner J (2014). *Schwingfestigkeit von Schweißverbindungen unter Berücksichtigung von Schweißeigenspannungen und Größeneinflüssen*. Stuttgart: Fraunhofer Verlag.

Baumgartner J (2017). Review and considerations on the fatigue assessment of welded joints using reference radii. *International Journal of Fatigue* 101:459–468. DOI: 10.1016/j.ijfatigue.2017.01.013.

Baumgartner J, Hobbacher AF, Rennert R (2020a). Fatigue assessment of welded thin sheets with the notch stress approach – Proposal for recommendations. *International Journal of Fatigue* 140:DOI: 10.1016/j.ijfatigue.2020.105844.

Baumgartner J, Ince E, Schmidt H (2013). *Erweiterung des Kerbspannungskonzepts auf Nahtübergänge von Linienschweißnähten an dünnen Blechen*. FAT-Schriftenreihe 259. Fraunhofer LBF.

Baumgartner J, Schmidt H, Ince E, Melz T, Dilger K (2015). Fatigue assessment of welded joints using stress averaging and critical distance approaches. *Welding in the World* 59(5):731–742. DOI: 10.1007/s40194-015-0248-x.

Baumgartner J, Schnabel K, Huberth F (2018). Fatigue assessment of EMPT-welded joints using the reference radius concept. *Procedia Engineering* 213:418–425. DOI: 10.1016/j.proeng.2018.02.041.

Baumgartner J, Tillmann W, Bobzin K, Öte M, Wiesner S, Sievers N (2020b). Fatigue of brazed joints made of X5CrNi18-10 and Cu110 and derivation of reliable assessment approaches. *Welding in the World* 64(4):707–719. DOI: 10.1007/s40194-020-00850-1.

Baumgartner J, Waterkotte R (2015). Crack initiation and propagation analysis at welds – assessing the total fatigue life of complex structures. *Materialwissenschaft und Werkstofftechnik* 46(2):123–135. DOI: 10.1002/mawe.201400367.

Baumgartner J, Yıldırım HC, Barsoum Z (2019). Fatigue strength assessment of TIG-dressed welded steel joints by local approaches. *International Journal of Fatigue* 126:72–78. DOI: 10.1016/j.ijfatigue.2019.04.038.

Beber VC, Schneider B, Brede M (2019). Efficient critical distance approach to predict the fatigue lifetime of structural adhesive joints. *Engineering Fracture Mechanics* 214:365–377. DOI: 10.1016/j.engfracmech.2019.03.022.

Benedetti M, Berto F, Le Bone L, Santus C (2020). A novel Strain-Energy-Density based fatigue criterion accounting for mean stress and plasticity effects on the medium-to-high-cycle uniaxial fatigue strength of plain and notched components. *International Journal of Fatigue* 133:DOI: 10.1016/j.ijfatigue.2019.105397.

Benedetti M, Fontanari V, Santus C, Bandini M (2010). Notch fatigue behaviour of shot peened high-strength aluminium alloys: Experiments and predictions using a critical distance method. *International Journal of Fatigue* 32(10):1600–1611. DOI: 10.1016/j.ijfatigue.2010.02.012.

Benedetti M, Santus C (2020). Statistical properties of threshold and notch derived estimations of the critical distance according to the line method of the theory of critical distances. *International Journal of Fatigue* 137:DOI: 10.1016/j.ijfatigue.2020.105656.

Berto F, Gallo P, Lazzarin P (2014). High temperature fatigue tests of un-notched and notched specimens made of 40CrMoV13.9 steel. *Materials & Design* 63:609–619. DOI: 10.1016/j.matdes.2014.06.048.

Berto F, Lazzarin P (2007). Relationships between J-integral and the strain energy evaluated in a finite volume surrounding the tip of sharp and blunt V-notches. *International Journal of Solids and Structures* 44(14-15):4621–4645. DOI: 10.1016/j.ijsolstr.2006.11.041.

Berto F, Lazzarin P (2009). A review of the volume-based strain energy density approach applied to V-notches and welded structures. *Theoretical and Applied Fracture Mechanics* 52(3):183–194. DOI: 10.1016/j.tafmec.2009.10.001.

Berto F, Lazzarin P, Gallo P (2013). High-temperature fatigue strength of a copper–cobalt–beryllium alloy. *The Journal of Strain Analysis for Engineering Design* 49(4):244–256. DOI: 10.1177/0309324713511804.

Bock und Polach RUF von, Kahl A, Braun M, Selle H von, Ehlers S (2019a). Analysis of governing parameters on the fatigue life of thermal cut edges. *International Conference on Ships and Offshore Structures ICSOS 2019*.

Bock und Polach RUF von, Klein M, Kubiczek J, Kellner L, Braun M, Herrnring H (2019b). State of the Art and Knowledge Gaps on Modelling Structures in Cold Regions. *ASME 2019 38th International Conference on Ocean, Offshore and Arctic Engineering*. Vol. 8: Polar and Arctic Sciences and Technology; Petroleum Technology. DOI: 10.1115/OMAE2019-95085.

Boukharouba T, Tamine T, Niu L, Chehimi C, Pluvinage G (1995). The use of notch stress intensity factor as a fatigue crack initiation parameter. *Engineering Fracture Mechanics* 52(3):503–512. DOI: 10.1016/0013-7944(94)00242-a.

Bourbita F, Remy L (2016). A combined critical distance and energy density model to predict high temperature fatigue life in notched single crystal superalloy members. *International Journal of Fatigue* 84:17–27. DOI: 10.1016/j.ijfatigue.2015.11.007.

Brandt K, Solberg JK, Akselsen OM, Østby E (2012). Initiation of Cleavage Fracture in a Weld Simuled Low Carbon Low Alloy Arctic Steel. *The Twenty-second International Offshore and Polar Engineering Conference*. International Society of Offshore and Polar Engineers.

Braun M, Fischer C, Fricke W, Ehlers S (2020a). Extension of the strain energy density method for fatigue assessment of welded joints to sub-zero temperatures. *Fatigue & Fracture of Engineering Materials & Structures* 43(12):2867–2882. DOI: 10.1111/ffe.13308.

Braun M, Grimm JH, Hoffmeister H, Ehlers S, Fricke W (2018). Comparison of fatigue

strength of post-weld improved high strength steel joints and notched base material specimens. *Ships and Offshore Structures* 13:47–55. DOI: 10.1080/17445302.2018.1425522.

Braun M, Grimm JH, Milaković AS, Hoffmeister H, Canaletti A, Ehlers S, Fricke W (2019). Bewertung der Schwingfestigkeit ausgeschliffener Schweißnähte aus hochfesten Stählen und Vergleich mit gekerbten Grundmaterialproben. *19. Tagung Schweißen in der maritimen Technik und im Ingenieurbau*. SLV Nord.

Braun M, Kahl A, Willems T, Seidel M, Fischer C, Ehlers S (2021a). Guidance for Material Selection Based on Static and Dynamic Mechanical Properties at Sub-Zero Temperatures. *Journal of Offshore Mechanics and Arctic Engineering* 143(4):1–45. DOI: 10.1115/1.4049252.

Braun M, Mayland W (2020). *Ermüdungsfestigkeit von Schweißverbindungen bei Minusgraden*. Report A 301.

Braun M, Milaković AS, Andresen-Paulsen G, Fricke W, Ehlers S (2020b). A novel approach to consider misalignment effects in assessment of fatigue tests. *Ship Technology Research* submitted for publication.

Braun M, Milaković AS, Ehlers S (2021b). Fatigue Assessment of Welded Joints at Sub-Zero Temperatures by means of Stress Averaging Approach. *Ships and Offshore Structures* 16:DOI: 10.1080/17445302.2021.1906194.

Braun M, Milaković AS, Ehlers S, Kahl A, Willems T, Seidel M, Fischer C (2020c). Sub-Zero Temperature Fatigue Strength of Butt-Welded Normal and High-Strength Steel Joints for Ships and Offshore Structures in Arctic Regions. *ASME 2020 39th International Conference on Ocean, Offshore and Arctic Engineering*. Vol. Volume 3: Materials Technology. DOI: 10.1115/OMAE2020-18892.

Braun M, Milaković AS, Renken F, Fricke W, Ehlers S (2020d). Application of Local Approaches to the Assessment of Fatigue Test results obtained for Welded Joints at Sub-Zero Temperatures. *International Journal of Fatigue* 138:DOI: 10.1016/j.ijfatigue.2020.105672.

Braun M, Müller AM, Milaković AS, Fricke W, Ehlers S (2020e). Requirements for stress gradient-based fatigue assessment of notched structures according to theory of critical distance. *Fatigue & Fracture of Engineering Materials & Structures* 43(7):1541–1554. DOI: 10.1111/ffe.13232.

Braun M, Scheffer R, Fricke W, Ehlers S (2020f). Fatigue strength of fillet-welded joints at subzero temperatures. *Fatigue & Fracture of Engineering Materials & Structures* 43(2):403–416. DOI: 10.1111/ffe.13163.

Braun M, Stange T, Ziemer G, Veer KF ter, Willems T, Kubiczek JM, Bock und Polach RUF von, Ehlers S (2021c). Einfluss von Minusgraden und variablen Lastamplituden infolge Seegangs- und Eislasten auf den Entwurf von Offshore Windenergieanlagen. *9. Fachtagung Bemessung und Konstruktion*. SLV Halle.

Braun M, Wang X (2021). A review of fatigue test data on weld toe grinding and weld profiling. *International Journal of Fatigue* 145:DOI: 10.1016/j.ijfatigue.2020.106073.

Bridges R, Riska K, Zhang S (2006). Preliminary Results of Investigation on the Fatigue of

Ship Hull Structures when Navigating in Ice. *International Conference and Exhibition on Performance of Ships and Structures in Ice (ICETECH-06)*.

Bridges R, Zhang S, Shaposhnikov V (2012). Experimental investigation on the effect of low temperatures on the fatigue strength of welded steel joints. *Ships and Offshore Structures* 7(3):311–319. DOI: 10.1080/17445302.2011.563550.

Bruder T, Störzel K, Baumgartner J, Hanselka H (2012). Evaluation of nominal and local stress based approaches for the fatigue assessment of seam welds. *International Journal of Fatigue* 34(1):86–102. DOI: 10.1016/j.ijfatigue.2011.06.002.

BS 7910:2013+A1:2015 Guide to methods for assessing the acceptability of flaws in metallic structures (2015). London, UK: British Standards Institution.

Chai G, Johansson S (2006). Fatigue Crack Propagation of Super-Duplex Stainless Steel at Different Temperatures. *16th European Conference of Fracture*. Ed. by Gdoutos EE. Springer, Dordrecht, pp. 193–194. DOI: 10.1007/1-4020-4972-2_94.

Choi HJ, Schwartz LH (1983). Fatigue crack propagation in intercritically tempered Fe-9Ni-0.1C and Fe-4Mn-0.15C. *Metallurgical Transactions A* 14(6):1089–1099. DOI: 10.1007/bf02670447.

Collmann M, Schaumann P (2018). Querbelastete Stumpfstöße als kritisches Kerbdetail bei Stahlrohrtürmen und Monopiles. *Stahlbau* 87(9):888–896. DOI: 10.1002/stab.201810016.

Coronado JJ, Cerón C (2010). Fracture mechanisms of CTOD samples of submerged and flux cored arc welding. *Theoretical and Applied Fracture Mechanics* 53(2):145–151. DOI: 10.1016/j.tafmec.2010.03.008.

DIN 50100:2016-12 Schwingfestigkeitsversuch – Durchführung und Auswertung von zyklischen Versuchen mit konstanter Lastamplitude für metallische Werkstoffproben und Bauteile (2016). Berlin, Germany: Deutsche Institut für Normung e.V. (DIN).

DNV GL Rules for Classification, Ships, Pt. 3 Hull, Ch. 9 Fatigue (2019). Høvik, Norway: DNV GL AS.

DNVGL-CG-0129: Fatigue assessment of ship structures (2018). Høvik, Norway: DNV GL AS.

DNVGL-OS-C401: Fabrication and testing of offshore structures (2018). Høvik, Norway: DNV GL AS.

DNVGL-RP-0005:2014-06: Fatigue design of offshore steel structures (2014). Høvik, Norway: DNV GL AS.

DNVGL-RP-C203: Recommended practice for Fatigue Design of offshore steel structures (2016). Høvik, Norway: DNV GL AS.

Doerk O, Fricke W, & von Selle H (2012). Validation of Different Fatigue Assessment Approaches for Thick Plate Structures Made of High Tensile Strength Steel YP47. *The Twenty-second International Offshore and Polar Engineering Conference*. International Society of Offshore and Polar Engineers.

Doerk O, Fricke W, Weissenborn C (2003). Comparison of different calculation methods for structural stresses at welded joints. *International Journal of Fatigue* 25(5):359–369. DOI: 10.1016/S0142-1123(02)00167-6.

Dong Y, Teixeira AP, Guedes Soares C (2019). Fatigue reliability analysis of butt welded

joints with misalignments based on hotspot stress approach. *Marine Structures* 65:215–228. DOI: 10.1016/j.marstruc.2019.01.006.

Efron B (1992). Bootstrap methods: another look at the jackknife. *Breakthroughs in statistics*. Springer, pp. 569–593.

Ehlers S, Østby E (2012). Increased crashworthiness due to arctic conditions - The influence of sub-zero temperature. *Marine Structures* 28(1):86–100. DOI: 10.1016/j.marstruc.2012.05.004.

Ehlers S, Polojärvi A, Vredeveldt A, Quinton B, Kim E, Ralph F, Sirkar J, Moslet P, Fukui T, Kuehnlein W, Wan Z (2018). Committee V.6: Arctic Technology. *Proceedings of the 20th International Ship and Offshore Structures Congress (ISSC 2018)*. Ed. by Kaminski ML, Rigo P. Vol. 2. Amsterdam: IOS Press, pp. 347–390. DOI: 10.3233/978-1-61499-864-8-347.

Eibl M (2003). Berechnung der Schwingfestigkeit laserstrahlgeschweißter Feinbleche mit lokalen Konzepten. Doctoral Thesis. Technische Universität Darmstadt.

Eibl M, Sonsino C, Kaufmann H, Zhang G (2003). Fatigue assessment of laser welded thin sheet aluminium. *International Journal of Fatigue* 25(8):719–731. DOI: 10.1016/s0142-1123(03)00053-7.

El Haddad MH, Topper TH, Smith KN (1979). Prediction of non propagating cracks. *Engineering Fracture Mechanics* 11(3):573–584.

EN 10225-1:2019 Weldable structural steels for fixed offshore structures – Technical delivery conditions – Part 1: Plates (2019). Brussels, Belgium: European Committee for Standardization.

EN 1993-1-8:2005 + AC:2009, Eurocode 3: Design of steel structures, Part 1-8: Design of joints (2010). Brussels, Belgium: European Committee for Standardization.

EN 1993–1–9:2005 – Eurocode 3: Design of Steel Structures – Part 1–9: Fatigue (2008). Brussels, Belgium: European Committee for Standardization.

EN ISO 19902:2018, Petroleum and natural gas industries – Fixed steel offshore structures (2018). Brussels, Belgium: European Committee for Standardization.

EN ISO 19906:2019: Petroleum and natural gas industries – Arctic offshore structures (2019). Brussels, Belgium: European Committee for Standardization.

EN ISO 26203-2:2011: Metallic materials – Tensile testing at high strain rates – Part 2: Servo-hydraulic and other test systems (2011). Brussels, Belgium: European Committee for Standardization.

EN ISO 5817:2014 Welding - Fusion welded joints in steel, nickel, titanium and their alloys (beam welding excluded) - Quality levels for imperfections (2014). Brussels, Belgium: European Committee for Standardization.

EN ISO 6892-1:2016 Metallic materials – Tensile testing – Part 1: Method of test at room temperature (2016). Brussels, Belgium: European Committee for Standardization.

EN ISO 6892-3:2015 Metallic materials – Tensile testing – Part 3: Method of test at low temperature (2015). Brussels, Belgium: European Committee for Standardization.

Erdogan F, Sih GC (1963). On the Crack Extension in Plates Under Plane Loading and Transverse Shear. *Journal of Basic Engineering* 85(4):519–525. DOI: 10.1115/1.3656897.

Esaklul KA, Yu W, Gerberich WW (1985). Effect of Low Temperature on Apparent Fatigue Threshold Stress Intensity Factors. *Fatigue at Low Temperatures*. Ed. by Stephens RI. West Conshohocken, PA: ASTM International, pp. 63–83. DOI: 10.1520/STP32747S.

Fang XY, Huang W, Yang XF, Wang JG (2020). Effects of temperature on fatigue cracks initiation and propagation for a high-speed railway wheel rim steel. *Engineering Failure Analysis* 109:DOI: 10.1016/j.engfailanal.2020.104376.

Fang XY, Cai ZB, Wang JG, Yang XF (2019). Evaluation of temperature-sensitive fatigue crack propagation of a high-speed railway wheel rim material. *Fatigue & Fracture of Engineering Materials & Structures* 42(8):1815–1825. DOI: 10.1111/ffe.13021.

Faruq NZ, Susmel L (2019). Proportional/nonproportional constant/variable amplitude multiaxial notch fatigue: cyclic plasticity, non-zero mean stresses, and critical distance/plane. *Fatigue & Fracture of Engineering Materials & Structures* 42(9):1849–1873. DOI: 10.1111/ffe.13036.

Fegredo DM, Thurston RCA (1966). The Effect of Fatigue on the Ductile-Brittle Transition Temperature of Two Mild Steels. *Canadian Metallurgical Quarterly* 5(3):181–210. DOI: 10.1179/cmq.1966.5.3.181.

Feng L, Qian X (2018). Size effect and life estimation for welded plate joints under low cycle actions at room and low ambient temperatures. *Thin-Walled Structures* 132:195–207. DOI: 10.1016/j.tws.2018.08.017.

Ferreira J, Branco C (1991). Influence of misalignment on the fatigue strength of butt welds. *International Journal of Fatigue* 13(5):405–409. DOI: 10.1016/0142-1123(91)90597-r .

Fischer C (2016). *Bewertung der Schwingfestigkeit von Schweißverbindungen mittels der Formänderungsenergiedichte*. Shaker Verlag.

Fischer C, Fricke W (2016). Effect of the stress distribution in simple welded specimens and complex components on the crack propagation life. *International Journal of Fatigue* 92:488–498. DOI: 10.1016/j.ijfatigue.2016.02.041.

Fischer C, Fricke W, Rizzo CM (2016a). Experiences and recommendations for numerical analyses of notch stress intensity factor and averaged strain energy density. *Engineering Fracture Mechanics* 165:98–113. DOI: 10.1016/j.engfracmech.2016.08.012.

Fischer C, Fricke W, Rizzo CM (2016b). Fatigue tests of notched specimens made from butt joints at steel. *Fatigue & Fracture of Engineering Materials & Structures* 39(12):1526–1541. DOI: 10.1111/ffe.12473.

Fischer C, Fricke W, Rizzo CM (2016c). Review of the fatigue strength of welded joints based on the notch stress intensity factor and SED approaches. *International Journal of Fatigue* 84:59–66. DOI: 10.1016/j.ijfatigue.2015.11.015.

FKM-Richtlinie. Rechnerischer Festigkeitsnachweis für Maschinenbauteile aus Stahl, Eisenguss- und Aluminiumwerkstoffen. (2012). Frankfurt/Main: Forschungskuratorium Maschinenbau (FKM).

Foti P, Ayatollahi MR, Berto F (2020). Rapid strain energy density evaluation for

V-notches under mode I loading conditions. *Engineering Failure Analysis* 110:DOI: 10.1016/j.engfailanal.2019.104361.

Foti P, Berto F (2020a). Evaluation of the Effect of the TIG-Dressing Technique on Welded Joints through the Strain Energy Density Method. *Procedia Structural Integrity* 25:201–208. DOI: 10.1016/j.prostr.2020.04.024.

Foti P, Berto F (2020b). Fatigue assessment of high strength welded joints through the strain energy density method. *Fatigue & Fracture of Engineering Materials & Structures* 43(11):2694–2702. DOI: 10.1111/ffe.13336.

Foti P, Razavi SMJ, Ayatollahi MR, Marsavina L, Berto F (2021). On the application of the volume free strain energy density method to blunt V-notches under mixed mode condition. *Engineering Structures* 230:DOI: 10.1016/j.engstruct.2020.111716.

Fricke W (2012). *IIW recommendations for the fatigue assessment of welded structures by notch stress analysis: IIW-2006-09*. Cambridge: Woodhead Publishing.

Fricke W (2013a). IIW guideline for the assessment of weld root fatigue. *Welding in the World* 57(6):753–791. DOI: 10.1007/s40194-013-0066-y.

Fricke W (2013b). Round-Robin Study on Stress Analysis for the Effective Notch Stress Approach. *Welding in the World* 51(3-4):68–79. DOI: 10.1007/bf03266562.

Fricke W (2014). Recent developments and future challenges in fatigue strength assessment of welded joints. *Proceedings of the Institution of Mechanical Engineers, Part C: Journal of Mechanical Engineering Science* 229(7):1224–1239. DOI: 10.1177/0954406214550015.

Fricke W, Feltz O (2013). Fatigue Tests and Numerical Analyses of Partial-Load and Full-Load Carrying Fillet Welds at Cover Plates and Lap Joints. *Welding in the World* 54(7-8):R225–R233. DOI: 10.1007/bf03263508.

Friedrich N (2020). Experimental investigation on the influence of welding residual stresses on fatigue for two different weld geometries. *Fatigue & Fracture of Engineering Materials & Structures* 43(11):2715–2730. DOI: 10.1111/ffe.13339.

Gallo P, Berto F (2016). Advanced Materials for Applications at High Temperature: Fatigue Assessment by Means of Local Strain Energy Density. *Advanced Engineering Materials* 18(12):2010–2017. DOI: 10.1002/adem.201500547.

Gallo P, Berto F, Lazzarin P (2015). High temperature fatigue tests of notched specimens made of titanium Grade 2. *Theoretical and Applied Fracture Mechanics* 76:27–34. DOI: 10.1016/j.tafmec.2014.12.007.

Garcia MAR (2020). Multiaxial fatigue analysis of high-strength steel welded joints using generalized local approaches. PhD Thesis. EPFL Lausanne. DOI: 10.5075/epfl-thesis-7394.

Gillemot LF (1976). Criterion of Crack Initiation and Spreading. *Engineering Fracture Mechanics* 8(1):239–253. DOI: 10.1016/0013-7944(76)90089-8.

Gillett HW, LePage CB, Warwick CL (1932). *Symposium on Effect of Temperature on the Properties of Metals*. West Conshohocken, PA: ASTM International. DOI: 10.1520/STP43885S.

Glinka G (1985). Energy density approach to calculation of inelastic strain-stress near

notches and cracks. *Engineering Fracture Mechanics* 22(3):485–508. DOI: 10.1016/0013-7944(85)90148-1.

Griffith AA (1921). The phenomena of rupture and flow in solids. *Philosofical Transactions of the Royal Society of London. Series A, Containing Papers of Methematical or Physical Character* 221:163–198.

Gubeljak N, Legat J, Koçak M (2002). Effect of fracture path on the toughness of weld metal. *International Journal of Fracture* 115(4):343–359. DOI: 10.1023/a:1016368019571.

Haibach E (1968). *Die Schwingfestigkeit von Schweißverbindungen aus der Sicht einer örtlichen Beanspruchungsmessung*. Report. Fraunhofer-Institut für Betriebsfestigkeit (LBF).

Haibach E (2006). *Betriebsfestigkeit: Verfahren und Daten zur Bauteilauslegung*. 3rd. Berlin, Heidelberg, New York: Springer-Verlag.

Härkegård G (1981). An effective stress intensity factor and the determination of the notched fatigue limit. *Fatigue thresholds: fundamentals and engineering applications*. Ed. by Blom AF, Beevers CJ. Vol. 2. Engineering Materials Advisory Services Ltd, pp. 867–879.

Härkegård G, Halleraker G (2010). Assessment of methods for prediction of notch and size effects at the fatigue limit based on test data by Böhm and Magin. *International Journal of Fatigue* 32(10):1701–1709. DOI: 10.1016/j.ijfatigue.2010.03.011.

Harris DJ, Benham PP (1965). Effect of High-Strain Fatigue Cycles on the Brittle-Ductile Transition of Two Mild Steels. *Journal of Mechanical Engineering Science* 7(1):93–100.

Hartmann MCN, Bock und Polach F von, Ehlers S, Hoffmann N, Onorato M, Klein M (2020). Investigation of Nonlinear Wave–Ice Interaction Using Parameter Study and Numerical Simulation. *Journal of Offshore Mechanics and Arctic Engineering* 142(2):DOI: 10.1115/1.4045625.

Hauge M, Maier M, Walters CL, Østby E, Kordonets SM, Zanfir C, Osvoll H (2015). Status update of ISO TC67/SC8/WG5: Materials for arctic applications. *The 25th International Ocean and Polar Engineering Conference*. International Society of Offshore and Polar Engineers.

Hendrikse H, Nord TS (2019). Dynamic response of an offshore structure interacting with an ice floe failing in crushing. *Marine Structures* 65:271–290. DOI: 10.1016/j.marstruc.2019.01.012.

Hensel J (2020). Mean stress correction in fatigue design under consideration of welding residual stress. *Welding in the World* 64(3):535–544. DOI: 10.1007/s40194-020-00852-z.

Hensel J, Kromm A, Nitschke-Pagel T, Dixneit J, Dilger K (2020). Capability of martensitic low transformation temperature welding consumables for increasing the fatigue strength of high strength steel joints. *Materials Testing* 62(9):891–900. DOI: 10.3139/120.111562.

Hobbacher AF (2016). *Recommendations for Fatigue Design of Welded Joints and Components*. 2nd. IIW Collection. Springer International Publishing Switzerland. DOI: 10.1007/978-3-319-23757-2.

Hobbacher AF (2017). Comparison of fatigue verification procedures at a thick-walled welded component. *Welding in the World*

61(4):801–818. DOI: 10.1007/s40194-017-0457-6.

Horn AM, Hauge M (2011). Material challenges for arctic offshore applications, a reliability study of fracture of a welded steel plate based on material toughness data at -60 °C. *The Twenty-first International Offshore and Polar Engineering Conference*. International Society of Offshore and Polar Engineers.

Horn AM, Østby E, Moslet PO, Hauge M (2016). The Fracture Resistance Approach in Order to Prevent Brittle Failure of Offshore Structures Under Arctic Environments. *ASME 2016 35th International Conference on Ocean, Offshore and Arctic Engineering*. American Society of Mechanical Engineers, V004T03A021–V004T03A021.

Horn AM, Østby E, Hauge M, Aubert JM (2012). Robust material qualification for Arctic applications. *The Twenty-second International Offshore and Polar Engineering Conference*. International Society of Offshore and Polar Engineers.

Hou CY (2007). Fatigue analysis of welded joints with the aid of real three-dimensional weld toe geometry. *International Journal of Fatigue* 29(4):772–785. DOI: 10.1016/j.ijfatigue.2006.06.007.

Høyland KV, Nord T, Turner J, Hornnes V, Gedikli ED, Bjerkås M, Hendrikse H, Hammer T, Ziemer G, Stange T, Ehlers S, Braun M, Willems T, Fischer C (2021). Fatigue damage from dynamic ice action – The FATICE project. *26th International Conference on Port and Ocean Engineering under Arctic Conditions*.

Hu Z, Berto F, Hong YS, Susmel L (2019). Comparison of TCD and SED methods in fatigue lifetime assessment. *International Journal of Fatigue* 123:105–134. DOI: 10.1016/j.ijfatigue.2019.02.009.

Hultgren G, Barsoum Z (2020). Fatigue assessment in welded joints based on geometrical variations measured by laser scanning. *Welding in the World* 64(11):1825–1831. DOI: 10.1007/s40194-020-00962-8.

IEC 61400-3-1:2019, Wind energy generation systems – Part 3-1: Design requirements for fixed offshore wind turbines (2019). International Electrotechnical Commission.

ISO/TS 35105:2018, Petroleum and natural gas industries — Arctic operations — Material requirements for arctic operations (2018). Geneva, Switzerland: International Standards Organization.

Jeong D, Lee S, Seo I, Yoo J, Kim S (2015a). Fatigue Crack Propagation Behavior of Fe24Mn Steel Weld at 298 and 110 K. *Metals and Materials International* 21(1):22–30. DOI: 10.1007/s12540-015-1004-x.

Jeong DH, Lee SG, Yoo JY, Lee JS, Kim S (2015b). Comparative studies on near-threshold fatigue crack propagation behavior of high manganese steels at room and cryogenic temperatures. *Materials Characterization* 103:28–36. DOI: 10.1016/j.matchar.2015.03.012.

Jordaan IJ (2001). Mechanics of ice–structure interaction. *Engineering Fracture Mechanics* 68(17):1923–1960. DOI: 10.1016/S0013-7944(01)00032-7.

Jung DH, Kwon JK, Woo NS, Kim YJ, Goto M, Kim S (2013). S–N Fatigue and Fatigue Crack Propagation Behaviors of X80 Steel at Room and Low Temperatures. *Metallurgical and Materials Transactions A* 45(2):654–662. DOI: 10.1007/s11661-013-2012-4.

Jung M (2018). Development and Implementing an Algorithm for Approximation and Evaluation of Stress Concentration Factors of Fillet Welds Based on Contactless 3D Measurement. Master thesis. Karlsruher Institut für Technologie.

Justo J, Castro J, Cicero S (2020). Notch effect and fracture load predictions of rock beams at different temperatures using the Theory of Critical Distances. *International Journal of Rock Mechanics and Mining Sciences* 125:DOI: 10.1016/j.ijrmms.2019.104161.

Kang KW, Goo BC, Kim JH, Kim DK, Kim JK (2009). Experimental Investigation on Static and Fatigue Behavior of Welded SM490A Steel Under Low Temperature. *International Journal of Steel Structures* 9(1):85–91. DOI: 10.1007/Bf03249483.

Karakaş Ö, Zhang G, Sonsino CM (2018). Critical distance approach for the fatigue strength assessment of magnesium welded joints in contrast to Neuber's effective stress method. *International Journal of Fatigue* 112:21–35. DOI: 10.1016/j.ijfatigue.2018.03.004.

Karakaş Ö (2017). Application of Neuber's effective stress method for the evaluation of the fatigue behaviour of magnesium welds. *International Journal of Fatigue* 101:115–126. DOI: 10.1016/j.ijfatigue.2016.10.023.

Kaufman JG (1975). Properties of Materials for Liquefied Natural Gas Tankage. Vol. ASTM STP 579. Materials, American Society for Testing and. DOI: 10.1520/STP579-EB.

Kawasaki T, Yokobori T, Sawaki Y, Nakanishi S, Izumi H (1977). Fatigue fracture toughness and fatigue crack propagation in 5.5% Ni steel at low temperature. *International Conference on Fracture (ICF4)*.

Kawasaki T, Nakanishi S, Sawaki Y, Hatanaka K, Yokobori T (1975). Fracture toughness and fatigue crack propagation in high strength steel from room temperature to −180°C. *Engineering Fracture Mechanics* 7(3):465–472. DOI: 10.1016/0013-7944(75)90047-8.

Kim JH, Kim Y (2019). Numerical simulation on the ice-induced fatigue damage of ship structural members in broken ice fields. *Marine Structures* 66:83–105. DOI: 10.1016/j.marstruc.2019.03.002.

Kim S, Jeong D, Sung H (2018). Reviews on factors affecting fatigue behavior of high-Mn steels. *Metals and Materials International* 24(1):1–14. DOI: 10.1007/s12540-017-7459-1.

Kitagawa H, Takahashi S (1976). Applicability of fracture mechanics to very small cracks or the cracks in the early stage. *Second International Conference on Mechanical Behavior of Materials. ASM, Metals Park, Ohio. 1976, 627-631*.

Kranz B, Sonsino CM (2010). Verification of FAT Values for the Application of the Notch Stress Concept with the Reference Radii Rref = 1.00 and 0.05 mm. *Welding in the World* 54(7):R218–R224. DOI: 10.1007/BF03263507.

Kubiczek J, Herrnring H, Kellner L, Ehlers S, Diewald R (2019). Simulation of temperature distribution in ship structures for the determination of temperature- dependent material properties. *12th European LS-DYNA Conference*.

Kuguel R (1961). A relation between theoretical stress concentration factor and fatigue notch factor deduced from the concept of highly stressed volume. *ASTM Proceeding*

1961. Vol. 61. ASTM International, pp. 732–748.

Lazzarin P, Berto F, Gomez FJ, Zappalorto M (2008a). Some advantages derived from the use of the strain energy density over a control volume in fatigue strength assessments of welded joints. *International Journal of Fatigue* 30(8):1345–1357. DOI: 10.1016/j.ijfatigue.2007.10.012.

Lazzarin P, Berto F, Zappalorto M (2010). Rapid calculations of notch stress intensity factors based on averaged strain energy density from coarse meshes: Theoretical bases and applications. *International Journal of Fatigue* 32(10):1559–1567. DOI: 10.1016/j.ijfatigue.2010.02.017.

Lazzarin P, Lassen T, Livieri P (2003). A notch stress intensity approach applied to fatigue life predictions of welded joints with different local toe geometry. *Fatigue & Fracture of Engineering Materials and Structures* 26(1):49–58. DOI: 10.1046/j.1460-2695.2003.00586.x.

Lazzarin P, Livieri P, Berto F, Zappalorto M (2008b). Local strain energy density and fatigue strength of welded joints under uniaxial and multiaxial loading. *Engineering Fracture Mechanics* 75(7):1875–1889. DOI: 10.1016/j.engfracmech.2006.10.019.

Lazzarin P, Meneghetti G, Berto F, Zappalorto M (2009). Practical Application of the N-Sif Approach in Fatigue Strength Assessment of Welded Joints. *Welding in the World* 53(3-4):R76–R89. DOI: 10.1007/Bf03266706.

Lazzarin P, Sonsino CM, Zambardi R (2004). A notch stress intensity approach to assess the multiaxial fatigue strength of welded tube-to-flange joints subjected to combined loadings. *Fatigue & Fracture of Engineering Materials & Structures* 27(2):127–140. DOI: 10.1111/j.1460-2695.2004.00733.x.

Lazzarin P, Tovo R (1996). A unified approach to the evaluation of linear elastic stress fields in the neighborhood of cracks and notches. *International Journal of Fracture* 78(1):3–19. DOI: Doi10.1007/Bf00018497.

Lazzarin P, Tovo R (1998). A Notch Intensity Factor Approach to the Stress Analysis of Welds. *Fatigue & Fracture of Engineering Materials and Structures* 21(9):1089–1103. DOI: 10.1046/j.1460-2695.1998.00097.x.

Lazzarin P, Tovo R, Meneghetti G (1997). Fatigue crack initiation and propagation phases near notches in metals with low notch sensitivity. *International Journal of Fatigue* 19(8-9):647–657. DOI: Doi10.1016/S0142-1123(97)00091-1.

Lazzarin P, Zambardi R (2001). A finite-volume-energy based approach to predict the static and fatigue behavior of components with sharp V-shaped notches. *International Journal of Fracture* 112(3):275–298. DOI: 10.1023/A:1013595930617.

Lefebvre F, Huther I, Parmentier G, Huther M (2019). Best practice guideline for statistical analyses of fatigue results. IIW Doc. XIII-2807-19. International Institute of Welding.

Legates DR, McCabe GJ (1999). Evaluating the use of "goodness-of-fit" measures in hydrologic and hydroclimatic model validation. *Water Resources Research* 35(1):233–241. DOI: 10.1029/1998wr900018.

Li WC, Susmel L, Askes H, Liao FF, Zhou TH (2016). Assessing the integrity of steel structural components with stress raisers using the Theory of Critical Distances.

Engineering Failure Analysis 70:73–89. DOI: 10.1016/j.engfailanal.2016.07.007.

Li ZR, Zhang DC, Wu HY, Huang FH, Hong W, Zang XS (2018). Fatigue properties of welded Q420 high strength steel at room and low temperatures. *Construction and Building Materials* 189:955–966. DOI: 10.1016/j.conbuildmat.2018.07.231.

Liao XW, Wang YQ, Qian XD, Shi YJ (2018). Fatigue crack propagation for Q345qD bridge steel and its butt welds at low temperatures. *Fatigue & Fracture of Engineering Materials & Structures* 41(3):675–687. DOI: 10.1111/ffe.12727.

Liaw PK, Logsdon WA (1985). Fatigue crack growth threshold at cryogenic temperatures: A review. *Engineering Fracture Mechanics* 22(4):585–594. DOI: 10.1016/0013-7944(85)90122-5.

Liaw PK, Logsdon WA, Attaar MH (1985). Computerized Near-Threshold Fatigue Crack Growth Rate Testing at Cryogenic Temperatures: Technique and Results. *Fatigue at Low Temperatures*. Ed. by Stephens RI. West Conshohocken, PA: ASTM International, pp. 173–189. DOI: 10.1520/STP32754S.

Liinalampi S, Remes H, Lehto P, Lillemae I, Romanoff J, Porter D (2016). Fatigue strength analysis of laser-hybrid welds in thin plate considering weld geometry in microscale. *International Journal of Fatigue* 87:143–152. DOI: 10.1016/j.ijfatigue.2016.01.019.

Livieri P, Lazzarin P (2005). Fatigue strength of steel and aluminium welded joints based on generalised stress intensity factors and local strain energy values. *International Journal of Fracture* 133(3):247–276. DOI: 10.1007/s10704-005-4043-3.

Lotsberg I (2009). Stress concentrations due to misalignment at butt welds in plated structures and at girth welds in tubulars. *International Journal of Fatigue* 31(8-9):1337–1345. DOI: 10.1016/j.ijfatigue.2009.03.005.

Lotsberg I, Fjeldstad A, Helsem MR, Oma N (2014). Fatigue life improvement of welded doubling plates by grinding and ultrasonic peening. *Welding in the World* 58(6):819–830. DOI: 10.1007/s40194-014-0161-8.

Louks R, Susmel L (2015). The linear-elastic Theory of Critical Distances to estimate high-cycle fatigue strength of notched metallic materials at elevated temperatures. *Fatigue & Fracture of Engineering Materials & Structures* 38(6):629–640. DOI: 10.1111/ffe.12273.

Lü B, Zheng X (1991). Predicting fatigue crack growth rates and thresholds at low temperatures. *Materials Science and Engineering: A* 148(2):179–188. DOI: 10.1016/0921-5093(91)90820-d.

Lü B, Zheng X (1992). A model for predicting fatigue crack growth behaviour of a low alloy steel at low temperatures. *Engineering Fracture Mechanics* 42(6):1001–1009. DOI: 10.1016/0013-7944(92)90139-6.

Lucas JP, Gerberich WW (1981). Low temperature and grain size effects on threshold and fatigue crack propagation in a high strength low alloy steel. *Materials Science and Engineering* 51(2):203–212. DOI: 10.1016/0025-5416(81)90196-8.

Luo P, Yao WX, Susmel L, Li P (2019). Prediction methods of fatigue critical point for notched components under multiaxial fatigue loading. *Fatigue & Fracture of Engineering*

Materials & Structures 42(12):2782–2793. DOI: 10.1111/ffe.13116.

MacGregor CW, Grossman N (1948). Some new aspects of the fatigue of metals brought out by brittle transition temperature tests. *The Welding Journal, Welding Research Supplement* 27.

Maddox SJ (1985). Fitness-for-purpose assessment of misalignment in transverse butt welds subject to fatigue loading. IIW document XIII-1180-85. London: International Institute of Welding.

Maddox SJ (2002). *Fatigue Strength of Welded Structures*. 2nd. Woodhead Publishing.

Mannan SL, Valsan M (2006). High-temperature low cycle fatigue, creep–fatigue and thermomechanical fatigue of steels and their welds. *International Journal of Mechanical Sciences* 48(2):160–175. DOI: 10.1016/j.ijmecsci.2005.08.004.

Martin A, Hinkelmann K, Esderts A (2011). Zur Auswertung von Schwingfestigkeitsversuchen im Zeitfestigkeitsbereich — Teil 1: Wie zuverlässig können 50 %-Wöhlerlinien aus experimentellen Daten geschätzt werden? *Materials Testing* 53(9):513–521. DOI: 10.3139/120.110256.

Marulo G, Baumgartner J, Frendo F (2017). Fatigue strength assessment of laser welded thin-walled joints made of mild and high strength steel. *International Journal of Fatigue* 96:142–151. DOI: 10.1016/j.ijfatigue.2016.11.016.

McClintock RM, Gibbons HP (1960). *Mechanical Properties of Structural Materials at Low Temperatures*. National Bureau of Standards.

Meng Xl, Rosenthal R, Rubin DB (1992). Comparing correlated correlation coefficients. *Psychological Bulletin* 111(1):172–175. DOI: 10.1037/0033-2909.111.1.172.

Merkblatt DVS 2403 Empfehlungen für die Durchführung, Auswertung und Dokumentation von Schwingfestigkeitsversuchen an Schweißverbindungen metallischer Werkstoffe (2019). Düsseldorf, Germany: DVS.

Milaković AS, Braun M, Willems T, Hendrikse H, Fischer C, Ehlers S (2019). Methodology for estimating offshore wind turbine fatigue life under combined loads of wind, waves and ice at sub-zero temperatures. *International Conference on Ships and Offshore Structures ICSOS 2019*.

Milaković AS, Gunnarsson B, Balmasov S, Hong S, Kim K, Schütz P, Ehlers S (2018). Current status and future operational models for transit shipping along the Northern Sea Route. *Marine Policy* 94:53–60. DOI: 10.1016/j.marpol.2018.04.027.

Milella PP (2012). *Fatigue and corrosion in metals*. Springer Science & Business Media.

Moody NR, Gerberich WW (1979). Fatigue crack propagation in iron and two iron binary alloys at low temperatures. *Materials Science and Engineering* 41(2):271–280. DOI: 10.1016/0025-5416(79)90148-4.

Muñiz-Calvente M, Álvarez-Vázquez A, Cicero S, Correia JAFO, Jesus AMP, Blasón S, Fernández-Canteli A, Berto F (2019). Study of the influence of notch radii and temperature on the probability of failure: A methodology to perform a combined assessment. *Fatigue & Fracture of Engineering Materials & Structures* 42(12):2663–2673. DOI: 10.1111/ffe.13082.

Necci A, Tarantola S, Vamanu B, Krausmann E, Ponte L (2019). Lessons learned from offshore oil and gas incidents in the Arctic and other ice-prone seas. *Ocean Engineering* 185:12–26. DOI: 10.1016/j.oceaneng.2019.05.021.

Neuber H (1958). *Kerbspannungslehre Grundlagen für genaue Festigkeitsberechnung mit Berücksichtigung von Konstruktionsform und Werkstoff*. 2. Springer, Berlin, Heidelberg. DOI: 10.1007/978-3-642-53069-2.

Neuber H (1968). Über die Berücksichtigung der Spannungskonzentration bei Festigkeitsberechnungen. *Konstruktion* 20(7):245–251.

Niederwanger A, Warner DH, Lener G (2020). The utility of laser scanning welds for improving fatigue assessment. *International Journal of Fatigue* 140:DOI: ARTN10581010.1016/j.ijfatigue.2020.105810.

Niemi E, Fricke W, Maddox S (2018). *Structural Hot-Spot Stress Approach to Fatigue Analysis of Welded Components*. 2nd. IIW Collection. Springer Singapore. DOI: 10.1007/978-981-10-5568-3.

NORSOK Standard M101 Structural steel fabrication (2000). Lysaker, Norway: Norwegian Standards Institution.

Nui LS, Chehimi C, Pluvinage G (1994). Stress field near a large blunted tip V-notch and application of the concept of the critical notch stress intensity factor (NSIF) to the fracture toughness of very brittle materials. *Engineering Fracture Mechanics* 49(3):325–335. DOI: 10.1016/0013-7944(94)90262-3.

Olivier R, Ritter W (1979). *Wöhlerlinienkatalog für Schweißverbindungen aus Baustählen – Teil 1: Stumpfstoß – Einheitliche statistische Auswertung von Ergebnissen aus Schwingfestigkeitsversuchen*. Düsseldorf, Germany.

Ostash OP, Kostyk EM, Levina IN (1988). Effect of Low-Temperature on the Initiation and Growth of Fatigue Cracks in 08kp Steel with Different Grain-Size. *Soviet Materials Science* 24(4):385–392.

Ostash OP, Zhmur-Klimenko VT (1987). Fatigue crack growth in metals at low temperatures (a review). *Soviet materials science : a transl. of Fiziko-khimicheskaya mekhanika materialov / Academy of Sciences of the Ukrainian SSR* 23(2):124–135. DOI: 10.1007/bf00718131.

Østby E, Hauge M, Horn A (2015). Development of materials requirement philosophies for design to avoid brittle behaviour in steel structures under Arctic conditions. *The 25th International Ocean and Polar Engineering Conference*. International Society of Offshore and Polar Engineers.

Ottersböck MJ, Leitner M, Stoschka M (2018). Impact of Angular Distortion on the Fatigue Performance of High-Strength Steel T-Joints in as-Welded and High Frequency Mechanical Impact-Treated Condition. *Metals* 8(5):302. DOI: 10.3390/met8050302.

Ottersböck MJ, Leitner M, Stoschka M, Maurer W (2019). Analysis of fatigue notch effect due to axial misalignment for ultra high-strength steel butt joints. *Welding in the World* 63(3):851–865. DOI: 10.1007/s40194-019-00713-4.

Outinen J, Makelainen P (2004). Mechanical properties of structural steel at elevated temperatures and after cooling down. *Fire and Materials* 28(2-4):237–251. DOI: 10.1002/fam.849.

Paik JK, Kim KJ, Lee JH, Jung BG, Kim SJ (2017). Test database of the mechanical properties of mild, high-tensile and stainless steel and aluminium alloy associated with cold temperatures and strain rates. *Ships and Offshore Structures* 12(sup1):S230–S256. DOI: 10.1080/17445302.2016.1262729.

Panin SV, Vlasov IV, Maruschak PO, Eremin AV, Berto F, Syromyatnikova AS, Vinogradov A (2019). Influence of long-term cold climate operation on structure, fatigue durability and impact toughness of 09Mn2Si pipe steel. *Engineering Failure Analysis* 102:87–101. DOI: 10.1016/j.engfailanal.2019.04.036.

Pattengale ND, Alipour M, Bininda-Emonds ORP, Moret BME, Stamatakis A (2009). How Many Bootstrap Replicates Are Necessary? Research in Computational Molecular Biology. Springer Berlin Heidelberg, pp. 184–200.

Pearson K (1895). Notes on Regression and Inheritance in the Case of Two Parents. *Proceedings of the Royal Society of London*. Vol. 58. Taylor & Francis, pp. 240–242.

Pedersen MM, Mouritsen OØ, Hansen MR, Andersen JG, Wenderby J (2010). Re-analysis of fatigue data for welded joints using the notch stress approach. *International Journal of Fatigue* 32(10):1620–1626. DOI: 10.1016/j.ijfatigue.2010.03.001.

Peterson R (1959). Notch Sensitivity. *Metal Fatigue*. Ed. by Sines G, Lwaisman J. McGraw-Hill, New York, pp. 293–306.

Pham H (2006). *Springer Handbook of Engineering Statistics*. London: Springer. DOI: 10.1007/978-1-84628-288-1.

Radaj D, Lazzarin P, Berto F (2013). Generalised Neuber concept of fictitious notch rounding. *International Journal of Fatigue* 51:105–115. DOI: 10.1016/j.ijfatigue.2013.01.005.

Radaj D, Sonsino CM, Fricke W (2006). *Fatigue assessment of welded joints by local approaches*. 2nd. Cambridge: Woodhead publishing.

Radaj D, Vormwald M (2007). *Ermüdungsfestigkeit: Grundlagen für Ingenieure*. 3rd. Springer Berlin Heidelberg.

Radaj D (1990). *Design and analysis of fatigue resistant welded structures*. Cambridge: Woodhead Publishing.

Ratner B (2009). The correlation coefficient: Its values range between +1/−1, or do they? *Journal of Targeting, Measurement and Analysis for Marketing* 17(2):139–142. DOI: 10.1057/jt.2009.5.

Reed RP, Durcholz RL, Schramm RE, Patrician TJ (1971). *Study of Cryogenic Storage Tank Fatigue Life. Low Temperature Mechanical Testing of AISI 304 and 310 Stainless Steels.* Report. National Bureau of Standards Cryogenic Engineering Laboratory, Boulder, Co, Cryogenics division.

Reemsnyder H (1969). Some significant parameters in the fatigue properties of weld joints. *Welding Research Supplement* 34(5):213–220.

Renken F (2020). Development of an algorithm for the statistical evaluation of weld geometries by means of laser triangulation. Master Thesis. Hamburg University of Technology.

Renken F, Bock und Polach RUF von, Schubnell J, Jung M, Oswald M, Rother K, Ehlers S, Braun M (2021). An algorithm for statistical evaluation of weld toe geometries using laser triangulation. *International*

Journal of Fatigue 149:DOI: 10.1016/j.ijfatigue.2021.106293.

Rice JR (1968). A Path Independent Integral and the Approximate Analysis of Strain Concentration by Notches and Cracks. *Journal of Applied Mechanics* 35(2):379–386. DOI: 10.1115/1.3601206.

Richard HA, Sander M (2012). *Ermüdungsrisse*. 3rd. Springer Vieweg. DOI: 10.1007/978-3-658-00087-5.

Robert C, Fricke W (2015). Assessment of quality effects on the fatigue life of laser and laser-hybrid welded specimens. *Welding and Cutting* 14(5):294–301.

Rohani Raftar H, Dabiri M, Ahola A, Björk T (2021). Re-evaluation of weld root fatigue strength for load-carrying fillet welded joints using the notch stress concept. *International Journal of Fatigue* 144:DOI: 10.1016/j.ijfatigue.2020.106076.

Rosenberg G (2003). Effect of Grain Size on the Fatigue Crack Growth in Steels at Temperatures 295 and 77 K. *ISIJ International* 43(10):1652–1657. DOI: 10.2355/isijinternational.43.1652.

Rother K, Fricke W (2016). Effective notch stress approach for welds having low stress concentration. *International Journal of Pressure Vessels and Piping* 147:12–20. DOI: 10.1016/j.ijpvp.2016.09.008.

Santus C, Taylor D, Benedetti M (2018). Experimental determination and sensitivity analysis of the fatigue critical distance obtained with rounded V-notched specimens. *International Journal of Fatigue* 113:113–125. DOI: 10.1016/j.ijfatigue.2018.03.037.

Sanz G (1980). Essai de mise au point d'une méthode quantitative de choix des qualités d'aciers vis-à-vis du risque de rupture fragile. *Revue de Métallurgie* 77(7):621–642. DOI: 10.1051/metal/198077070621.

Schmidt H, Baumgartner J, Melz T (2015). Fatigue assessment of joints using the local stress field. *Materialwissenschaft Und Werkstofftechnik* 46(2):145–155. DOI: 10.1002/mawe.201400369.

Schork B, Kucharczyk P, Madia M, Zerbst U, Hensel J, Bernhard J, Tchuindjang D, Kaffenberger M, Oechsner M (2018). The effect of the local and global weld geometry as well as material defects on crack initiation and fatigue strength. *Engineering Fracture Mechanics* 198:103–122. DOI: 10.1016/j.engfracmech.2017.07.001.

Schubnell J, Jung M, Le CH, Farajian M, Braun M, Ehlers S, Fricke W, Garcia M, Nussbaumer A, Baumgartner J (2020a). Influence of the optical measurement technique and evaluation approach on the determination of local weld geometry parameters for different weld types. *Welding in the World* 64(2):301–316. DOI: 10.1007/s40194-019-00830-0.

Schubnell J, Pontner P, Wimpory RC, Farajian M, Schulze V (2020b). The influence of work hardening and residual stresses on the fatigue behavior of high frequency mechanical impact treated surface layers. *International Journal of Fatigue* 134:DOI: 10.1016/j.ijfatigue.2019.105450.

Sedlacek G, Feldmann M, Kühn B, Tschickardt D, Höhler S, Müller C, Hensen W, Stranghöner N, Dahl W, Langenberg P, Münstermann S, Brozetti J, Raoul J, Pope R, Bijlaard F, Geradin M, Pinto VA, Dimova S (2008). *Commentary and Worked Examples to EN 1993-1-10 "Material Toughness and Through Thickness Properties" and Other Toughness Oriented*

Rules in EN 1993. EUR - Scientific and Technical Research Reports EUR 23510 EN.

Selle H von, Doerk O, Kang JK, Kim JH (2011). Fatigue tests of butt welds and plates edges of 80 mm thick plates. *Advances in Marine Structures*. Ed. by Guedes Soares C, Fricke W, pp. 511–519.

El-Shabasy AB, Lewandowski JJ (2004). Effects of load ratio, R, and test temperature on fatigue crack growth of fully pearlitic eutectoid steel (fatigue crack growth of pearlitic steel). *International Journal of Fatigue* 26(3):305–309. DOI: 10.1016/S0142-1123(03)00140-3.

ShipRight Design and construction Fatigue Design Assessment FDA ICE Fatigue Induced by Ice Loading (2011). London, UK: Limited, Lloyd's Register Group.

Shulginov B, Matveyev V (1997). Impact fatigue of low-alloy steels and their welded joints at low temperature. *International Journal of Fatigue* 19(8-9):621–627. DOI: 10.1016/s0142-1123(97)00066-2.

Sih GC (1974). Strain Energy Density Factor Applied to Mixed Mode Crack Problems. *International Journal of Fracture* 10(3):305–321. DOI: 10.1007/Bf00035493.

Silva BL da, Ferreira JLA, Araújo JA (2012). Influence of notch geometry on the estimation of the stress intensity factor threshold by considering the Theory of Critical Distances. *International Journal of Fatigue* 42:258–270. DOI: 10.1016/j.ijfatigue.2011.11.020.

Song W, Liu XS, Razavi SMJ (2018). Fatigue assessment of steel load-carrying cruciform welded joints by means of local approaches. *Fatigue & Fracture of Engineering Materials & Structures* 41(12):2598–2613. DOI: 10.1111/ffe.12870.

Sonsino CM (2009). Effect of residual stresses on the fatigue behaviour of welded joints depending on loading conditions and weld geometry. *International Journal of Fatigue* 31(1):88–101. DOI: 10.1016/j.ijfatigue.2008.02.015.

Sonsino CM, Bruder T, Baumgartner J (2013). S-N Lines for Welded Thin Joints — Suggested Slopes and FAT Values for Applying the Notch Stress Concept with Various Reference Radii. *Welding in the World* 54(11-12):R375–R392. DOI: 10.1007/bf03266752.

Sonsino CM, Fricke W, Bruyne F de, Hoppe A, Ahmadi A, Zhang G (2012). Notch stress concepts for the fatigue assessment of welded joints - Background and applications. *International Journal of Fatigue* 34(1):2–16. DOI: 10.1016/j.ijfatigue.2010.04.011.

Spaggiari A, Castagnetti D, Dragoni E, Bulleri S (2011). Fatigue life prediction of notched components: a comparison between the theory of critical distance and the classical stress-gradient approach. *Procedia Engineering* 10:2755–2767. DOI: 10.1016/j.proeng.2011.04.459.

Steiger JH (1980). Tests for comparing elements of a correlation matrix. *Psychological Bulletin* 87(2):245–251. DOI: 10.1037/0033-2909.87.2.245.

Stephens RI (1985). *Fatigue at low temperatures: a symposium*. Philadelphia, PA: ASTM International.

Stephens RI, Chung JH, Glinka G (1979). Low Temperature Fatigue Behavior of Steels - A Review. *SAE Transactions* 88(2):1892–1904. DOI: 10.4271/790517.

Stephens RI, Fatemi A, Lee HW, Lee SG, Vacas-Oleas C, Wang CM (1985).

Variable-Amplitude Fatigue Crack Initiation and Growth of Five Carbon or Low-Alloy Cast Steels at Room and Low Climatic Temperatures. *Fatigue at Low Temperatures*. Ed. by Stephens RI. West Conshohocken, PA: ASTM International, pp. 293–312. DOI: 10.1520/STP32762S.

Stonesifer FR (1978). Effect of Grain-Size and Temperature on Fatigue Crack-Propagation in A533-B Steel. *Engineering Fracture Mechanics* 10(2):305–314. DOI: 10.1016/0013-7944(78)90014-0.

Susmel L (2008). Modified Wohler curve method, theory of critical distances and Eurocode 3: A novel engineering procedure to predict the lifetime of steel welded joints subjected to both uniaxial and multiaxial fatigue loading. *International Journal of Fatigue* 30(5):888–907. DOI: 10.1016/j.ijfatigue.2007.06.005.

Susmel L, Taylor D (2007). A novel formulation of the theory of critical distances to estimate lifetime of notched components in the medium-cycle fatigue regime. *Fatigue & Fracture of Engineering Materials and Structures* 30(7):567–581. DOI: 10.1111/j.1460-2695.2007.01122.x.

Susmel L, Taylor D (2013). The Theory of Critical Distances to estimate finite lifetime of notched components subjected to constant and variable amplitude torsional loading. *Engineering Fracture Mechanics* 98:64–79. DOI: 10.1016/j.engfracmech.2012.12.007.

Suyuthi A, Leira BJ, Riska K (2013). Fatigue damage of ship hulls due to local ice-induced stresses. *Applied Ocean Research* 42:87–104. DOI: 10.1016/j.apor.2013.05.003.

Tanaka K (1983). Engineering Formulas for Fatigue-Strength Reduction Due to Crack-Like Notches. *International Journal of Fracture* 22(2):R39–R46. DOI: 10.1007/Bf00942722.

Taylor D (1999). Geometrical effects in fatigue: a unifying theoretical model. *International Journal of Fatigue* 21(5):413–420. DOI: 10.1016/S0142-1123(99)00007-9.

Taylor D (2007). *The Theory of Critical Distances: A New Perspective in Fracture Mechanics*. Elsevier.

Taylor D, Hoey D (2009). High cycle fatigue of welded joints: The TCD experience. *International Journal of Fatigue* 31(1):20–27. DOI: 10.1016/j.ijfatigue.2008.01.011.

Taylor D, Barrett N, Lucano G (2002). Some new methods for predicting fatigue in welded joints. *International Journal of Fatigue* 24(5):509–518. DOI: 10.1016/s0142-1123(01)00174-8.

Thieme A, Schröter F (2013). Modern heavy steel plates for use in offshore installations - characteristics and production processes. *Steel Construction* 6(3):186–190. DOI: 10.1002/stco.201310025.

Thurston KVS, Gludovatz B, Yu Q, Laplanche G, George EP, Ritchie RO (2019). Temperature and load-ratio dependent fatigue-crack growth in the CrMnFeCoNi high-entropy alloy. *Journal of Alloys and Compounds* 794:525–533. DOI: 10.1016/j.jallcom.2019.04.234.

Tschegg E, Stanzl S (1981). Fatigue crack propagation and threshold in b.c.c. and f.c.c. metals at 77 and 293 K. *Acta Metallurgica* 29(1):33–40. DOI: 10.1016/0001-6160(81)90084-5.

Urai A (2016). *BeautifulPlots.m*. URL: https://github.com/anne-urai/Tools/blob/master/plotting/BeautifulPlots.m (visited on 02/04/2019).

Vedernikova A, Kostina A, Plekhov O, Bragov A (2019). On the use of the critical distance concept to estimate tensile strength of notched components under dynamic loading and physical explanation theory. *Theoretical and Applied Fracture Mechanics* 103:DOI: 10.1016/j.tafmec.2019.102280.

Verreman Y, Nie B (1996). Early Development of Fatigue Cracking at Manual Fillet Welds. *Fatigue & Fracture of Engineering Materials and Structures* 19(6):669–681. DOI: 10.1111/j.1460-2695.1996.tb01312.x.

Viespoli LM, Leonardi A, Cianetti F, Nyhus B, Alvaro A, Berto F (2019). Low-temperature fatigue life properties of aluminum butt weldments by the means of the local strain energy density approach. *Material Design & Processing Communications* 1(1):e30. DOI: 10.1002/mdp2.30.

Vogt JB, Magnin T, Foct J (1993). Effective Stresses and Microstructure in Cyclically Deformed 316l Austenitic Stainless Steel: Effect of Temperature and Nitrogen Content. *Fatigue & Fracture of Engineering Materials & Structures* 16(5):555–564. DOI: 10.1111/j.1460-2695.1993.tb00766.x.

Vojvodic Tuma J, Sedmak A (2004). Analysis of the unstable fracture behaviour of a high strength low alloy steel weldment. *Engineering Fracture Mechanics* 71(9-10):1435–1451. DOI: 10.1016/s0013-7944(03)00166-8.

Wallin K (1991). Fracture Toughness Transition Curve Shape for Ferritic Structural Steels. *Fracture of Engineering Materials and Structures*. Ed. by Teoh SH, Lee KH. Springer, Dordrecht, pp. 83–88. DOI: 10.1007/978-94-011-3650-1_10.

Walters CL, Alvaro A, Maljaars J (2016). The effect of low temperatures on the fatigue crack growth of S460 structural steel. *International Journal of Fatigue* 82:110–118. DOI: 10.1016/j.ijfatigue.2015.03.007.

Walters CL, Dragt RC, Romeijn E, Weijde G van der (2014). Use of current S355 and S690 steels for arctic applications. *The 24th International Ocean and Polar Engineering Conference*. International Society of Offshore and Polar Engineers.

Wang K, Wu L, Li YZ, Qin C (2020). Experimental study on low temperature fatigue performance of polar icebreaking ship steel. *Ocean Engineering* 216:DOI: 10.1016/j.oceaneng.2020.107789.

Wang WY, Liu B, Kodur V (2013). Effect of Temperature on Strength and Elastic Modulus of High-Strength Steel. *Journal of Materials in Civil Engineering* 25(2):174–182. DOI: 10.1061/(Asce)Mt.1943-5533.0000600.

Wang YT, Liu JJ, Hu JJ, Garbatov Y, Soares CG (2021). Fatigue strength of EH36 steel welded joints and base material at low-temperature. *International Journal of Fatigue* 142:DOI: 10.1016/j.ijfatigue.2020.105896.

Weich I (2009). Ermüdungsverhalten mechanisch nachbehandelter Schweißverbindungen in Abhängigkeit des Randschichtzustands. Doctoral Thesis. TU Braunschweig.

Wilker H (2018). *Statistische Hypothesentests in der Praxis: Leitfaden zur Anwendung von Hypothesentests für die Analyse von Unterschieden, Übereinstimmungen, Zugehörigkeiten, Zufälligkeiten und Zusammenhängen*. 3. Books on Demand.

Williams ML (1956). Stress distribution at the base of a stationary crack. *Journal of Applied Mechanics* 24(1):109–114.

Williams TRG, Lawrence CC (1962). Effect of fatigue and strain aging on transition

temperature of mild steel. *The Engineer* 214:536.

Wormsen A (2007). A Fatigue Assessment Methodology for Notched Components Containing Defects. Doctoral Thesis. Norwegian University of Science and Technology.

Wormsen A, Fjeldstad A, Härkegård G (2008). A post-processor for fatigue crack growth analysis based on a finite element stress field. *Computer Methods in Applied Mechanics and Engineering* 197(6-8):834–845. DOI: 10.1016/j.cma.2007.09.012.

Wu C, Thompson ME (2020). *Sampling Theory and Practice*. ICSA Book Series in Statistics. Cham: Springer International Publishing. DOI: 10.1007/978-3-030-44246-0.

Xiao ZG, Yamada K (2004a). A method of determining geometric stress for fatigue strength evaluation of steel welded joints. *International Journal of Fatigue* 26(12):1277–1293. DOI: 10.1016/j.ijfatigue.2004.05.001.

Xiao ZG, Yamada K (2004b). Fatigue strength evaluation of root-failed welded joints based on one-millimeter stress. *Journal of Structural Engineering, A* 50(2):719–726.

Yarema SY, Krasovskii AY, Ostash OP, Stepanenko VA (1977). Development of fatigue failure of low-carbon sheet steel at room and low temperatures. *Strength of Materials* 9(3):266–272. DOI: 10.1007/bf01532476.

Yildirim HC, Marquis GB, Barsoum Z (2013). Fatigue assessment of high frequency mechanical impact (HFMI)-improved fillet welds by local approaches. *International Journal of Fatigue* 52:57–67. DOI: 10.1016/j.ijfatigue.2013.02.014.

Yin T, Tyas A, Plekhov O, Terekhina A, Susmel L (2015). A novel reformulation of the Theory of Critical Distances to design notched metals against dynamic loading. *Materials & Design* 69:197–212. DOI: 10.1016/j.matdes.2014.12.026.

Yıldırım HC (2015). Review of fatigue data for welds improved by tungsten inert gas dressing. *International Journal of Fatigue* 79:36–45. DOI: 10.1016/j.ijfatigue.2015.04.017.

Yosibash Z, Bussiba A, Gilad I (2004). Failure criteria for brittle elastic materials. *International Journal of Fracture* 125(3-4):307–333. DOI: DOI10.1023/B:FRAC.0000022244.31825.3b.

Yu W, Esaklul K, Gerberich WW (1984). Fatigue threshold studies in Fe, Fe-Si, and HSLA steel: Part II. thermally activated behavior of the effective stress intensity at threshold. *Metallurgical Transactions A* 15(5):889–900. DOI: 10.1007/bf02644563.

Zerbst U, Ainsworth RA, Beier HT, Pisarski H, Zhang ZL, Nikbin K, Nitschke-Pagel T, Munstermann S, Kucharczyk P, Klingbeil D (2014). Review on fracture and crack propagation in weldments - A fracture mechanics perspective. *Engineering Fracture Mechanics* 132:200–276. DOI: 10.1016/j.engfracmech.2014.05.012.

Zhang DY, Wang G, Yue QJ (2018a). Evaluation of ice-induced fatigue life for a vertical offshore structure in the Bohai Sea. *Cold Regions Science and Technology* 154:103–110. DOI: 10.1016/j.coldregions.2018.05.012.

Zhang D, Li Z, Wu H, Huang F (2018b). Experimental study on fatigue behavior of Q420 high-strength steel at low temperatures. *Journal of Constructional*

Steel Research 145:116–127. DOI: 10.1016/j.jcsr.2018.02.008.

Zhang G, Richter B (2000). A new approach to the numerical fatigue-life prediction of spot-welded structures. *Fatigue & Fracture of Engineering Materials & Structures* 23(6):499–508. DOI: 10.1046/j.1460-2695.2000.00316.x.

Zhang GB, Sonsino CM, Sundermeier R (2012). Method of effective stress for fatigue: Part II - Applications to V-notches and seam welds. *International Journal of Fatigue* 37:24–40. DOI: 10.1016/j.ijfatigue.2011.09.016.

Zhang S, Bridges R, Tong J (2011). Fatigue Design Assessment of Ship Structures Induced by Ice Loading - An introduction to the ShipRight FDA ICE Procedure. *The Twenty-first International Offshore and Polar Engineering Conference. International Society of Offshore and Polar Engineers*.

Zhang YH, Maddox SJ, Razmjoo R (2003). *Re-evaluation of fatigue curves for flush ground girth welds*. Cambridge.

Zhao W, Feng G, Ren H, Leira BJ, Zhang M (2019). Temperature-dependent characteristics of DH36 steel fatigue crack propagation. *Fatigue & Fracture of Engineering Materials & Structures* 43(3):617–627. DOI: 10.1111/ffe.13177.

Zhao W, Feng G, Zhang M, Ren H, Sinsabvarodom C (2020a). Effect of low temperature on fatigue crack propagation rates of DH36 steel and its butt weld. *Ocean Engineering* 196:DOI: 10.1016/j.oceaneng.2019.106803.

Zhao W, Feng G, Liu W, Ren H (2020b). Research on Fatigue Properties of Typical Welded Joints of DH36 Steel at −60 °C. *Applied Sciences* 10(11):DOI: 10.3390/app10113742.

Appendix

A | Welding procedure specifications (WPS)

Please get in contact if you are interested in the welding procedure specifications of the test specimens via: moritz.br@tuhh.de

B | S–N curves based on a free slope exponent

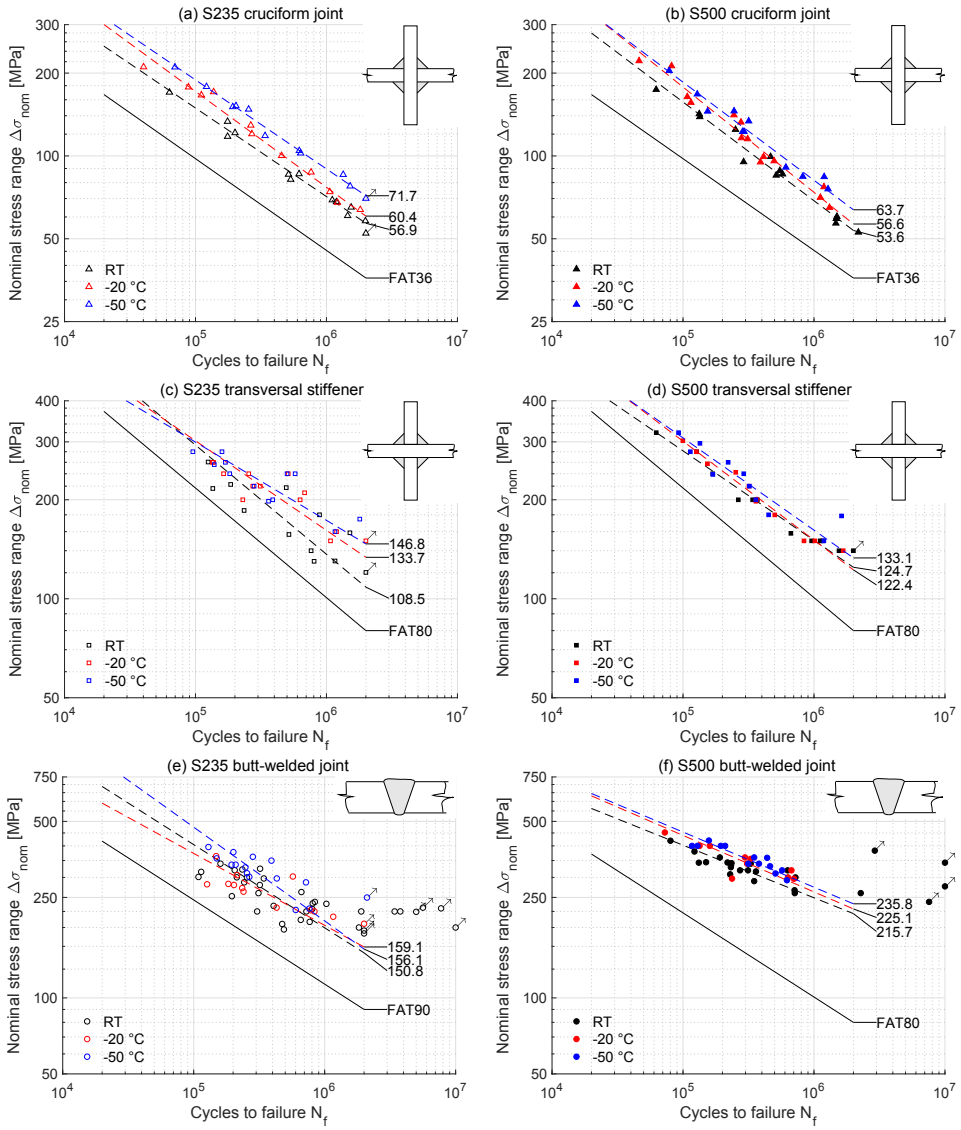

Figure 62. Fatigue test results of S235J2+N (a) and S500G1+M (b) cruciform joints, S235J2+N (c) and S500G1+M (d) transversal stiffener specimens, and S235J2+N (e) and S500G1+M (f) butt-welded joints based on a free slope exponent k

C | Fatigue test results

C.1 | S235 Butt-joints

Table 13. *S–N* test results of S235 butt-welded specimens at room temperature

Specimen-Nr.	$\Delta\sigma$ [MPa]	Number of Cycles	Temp. (RT, M20, M50)	Result
1	280.0	205609	RT	Fracture
2	217.9	5000000	RT	Run-out
3	297.1	343150	RT	Fracture
4	236.5	810333	RT	Fracture
5	180.0	5624387	RT	Run-out
6	260.0	321432	RT	Fracture
7	180.0	7744254	RT	Run-out
8	260.0	235194	RT	Fracture
9	180.0	407694	RT	Fracture
10	260.0	160151	RT	Fracture
11	220.0	243232	RT	Fracture
12	260.0	114118	RT	Fracture
13	220.0	312366	RT	Fracture
14	220.0	1902818	RT	Fracture
15	220.0	725092	RT	Fracture
16	200.0	768368	RT	Fracture
17	220.0	3781093	RT	Fracture
18	180.0	2000000	RT	Run-out
19	200.0	656954	RT	Fracture
20	180.0	488565	RT	Fracture
21	260.0	108776	RT	Fracture
22	180.0	2000000	RT	Run-out
23	220.0	803740	RT	Fracture
24	260.0	664544	RT	Fracture
25	280.0	213398	RT	Fracture
26	190.0	1826068	RT	Fracture
27	190.0	473696	RT	Fracture
28	220.0	305117	RT	Fracture
29	190.0	10000000	RT	Run-out
30	280.0	319892	RT	Fracture

Table 14. *S–N* test results of S235 butt-welded specimens at −20 °C

Specimen-Nr.	$\Delta\sigma$ [MPa]	Number of Cycles	Temp. (RT, M20, M50)	Result
1	240.0	571606	M20	Fracture
2	200.0	234684	M20	Fracture
3	280.0	148412	M20	Fracture
4	240.0	214654	M20	Fracture
5	220.0	835526	M20	Fracture
6	280.0	203002	M20	Fracture
7	180.0	2000000	M20	Run-out
8	260.0	126552	M20	Fracture
9	220.0	429544	M20	Fracture
10	260.0	240086	M20	Fracture
11	220.0	783136	M20	Fracture
12	280.0	184024	M20	Fracture
13	200.1	1162608	M20	Fracture

Table 15. *S–N* test results of S235 butt-welded specimens at −50 °C

Specimen-Nr.	$\Delta\sigma$ [MPa]	Number of Cycles	Temp. (RT, M20, M50)	Result
1	280.0	209087	M50	Fracture
2	240.0	719842	M50	Fracture
3	310.0	200989	M50	Fracture
4	280.0	392415	M50	Fracture
5	240.0	431036	M50	Fracture
6	300.0	149843	M50	Fracture
7	210.0	2105723	M50	Run-out
8	310.0	282971	M50	Fracture
9	258.1	248052	M50	Fracture
10	240.0	255448	M50	Fracture
11	320.8	129670	M50	Fracture
12	300.0	194629	M50	Fracture
13	290.1	265787	M50	Fracture
14	223.0	601768	M50	Fracture
15	220.0	763860	M50	Fracture

C.2 | S500 Butt-joints

Table 16. *S–N* test results of S500 butt-welded specimens at room temperature

Specimen-Nr.	$\Delta\sigma$ [MPa]	Number of Cycles	Temp. (RT, M20, M50)	Result
1	300.0	722026	RT	Fracture
2	419.2	80184	RT	Fracture
3	276.4	10000000	RT	Run-out
4	260.0	2274125	RT	Fracture
5	266.9	710451	RT	Fracture
6	320.0	313513	RT	Fracture
7	360.0	191116	RT	Fracture
8	260.0	713111	RT	Fracture
9	340.0	218595	RT	Fracture
10	340.0	149971	RT	Fracture
11	290.0	228992	RT	Fracture
12	300.0	231818	RT	Fracture
13	279.5	234573	RT	Fracture
14	320.0	629736	RT	Fracture
15	316.8	360445	RT	Fracture
16	240.0	7561126	RT	Run-out
17	340.0	328700	RT	Fracture
18	320.0	272590	RT	Fracture
19	290.0	349319	RT	Fracture
20	380.0	122311	RT	Fracture
21	340.0	10000000	RT	Run-out
22	380.0	2912820	RT	Run-out
23	340.0	131989	RT	Fracture

Table 17. *S–N* test results of S500 butt-welded specimens at −20 °C

Specimen-Nr.	$\Delta\sigma$ [MPa]	Number of Cycles	Temp. (RT, M20, M50)	Result
1	400.0	133737	M20	Fracture
2	360.0	297250	M20	Fracture
3	300.0	633217	M20	Fracture
4	320.0	672723	M20	Fracture
5	434.8	72671	M20	Fracture
6	340.0	327669	M20	Fracture
7	290.0	236711	M20	Fracture
8	400.0	160067	M20	Fracture
9	340.0	308737	M20	Fracture
10	290.0	702893	M20	Fracture

Table 18. *S–N* test results of S500 butt-welded specimens at −50 °C

Specimen-Nr.	$\Delta\sigma$ [MPa]	Number of Cycles	Temp. (RT, M20, M50)	Result
1	420.0	157508	M50	Fracture
2	400.0	128916	M50	Fracture
3	340.0	314754	M50	Fracture
4	400.0	194268	M50	Fracture
5	340.0	438822	M50	Fracture
6	400.0	209635	M50	Fracture
7	320.0	461843	M50	Fracture
8	360.0	349352	M50	Fracture
9	320.0	570909	M50	Fracture
10	400.0	117223	M50	Fracture
11	340.0	379852	M50	Fracture
12	300.0	508381	M50	Fracture
13	280.0	621342	M50	Fracture

C.3 | S235 Cruciform joints

Table 19. *S–N* test results of S235 cruciform joint specimens at room temperature

Specimen-Nr.	$\Delta\sigma$ [MPa]	Number of Cycles	Temp. (RT, M20, M50)	Result
1	121.29	200397	RT	Fracture
2	85.66	513308	RT	Fracture
3	170.25	63264	RT	Fracture
4	86.03	617488	RT	Fracture
5	69.15	1107726	RT	Fracture
6	117.63	175885	RT	Fracture
7	52.33	2000000	RT	Run-out
8	60.61	1450935	RT	Fracture
9	133.35	175690	RT	Fracture
10	82.11	533189	RT	Fracture
11	58.05	1983106	RT	Fracture
12	68.07	1190739	RT	Fracture
13	65.06	1542842	RT	Fracture

Table 20. *S–N* test results of S235 cruciform joint specimens at −20 °C

Specimen-Nr.	$\Delta\sigma$ [MPa]	Number of Cycles	Temp. (RT, M20, M50)	Result
1	210.45	231.96	M20	Fracture
2	67.75	79.70	M20	Fracture
3	166.32	194.67	M20	Fracture
4	100.18	124.13	M20	Fracture
5	74.04	84.67	M20	Fracture
6	63.76	73.78	M20	Fracture
7	129.19	141.63	M20	Fracture
8	177.84	191.50	M20	Fracture
9	87.25	93.37	M20	Fracture
10	120.20	128.74	M20	Fracture
11	170.84	186.05	M20	Fracture
12	210.45	231.96	M20	Fracture
13	67.75	79.70	M20	Fracture

Table 21. *S–N* test results of S235 cruciform joint specimens at −50 °C

Specimen-Nr.	$\Delta\sigma$ [MPa]	Number of Cycles	Temp. (RT, M20, M50)	Result
1	118.37	339812	M50	Fracture
2	210.15	69686	M50	Fracture
3	77.62	1515536	M50	Fracture
4	70.06	2000000	M50	Run-out
5	147.71	254516	M50	Fracture
6	151.98	203657	M50	Fracture
7	104.43	620058	M50	Fracture
8	150.78	192626	M50	Fracture
9	178.46	121347	M50	Fracture
10	102.30	635430	M50	Fracture
11	85.52	1341644	M50	Fracture

C.4 | S500 Cruciform joints

Table 22. *S–N* test results of S500 cruciform joint specimens at room temperature

Specimen-Nr.	$\Delta\sigma$ [MPa]	Number of Cycles	Temp. (RT, M20, M50)	Result
1	138.68	134308	RT	Fracture
2	85.03	514439	RT	Fracture
3	142.15	133046	RT	Fracture
4	52.78	2181756	RT	Fracture
5	174.21	62366	RT	Fracture
6	59.16	1477773	RT	Fracture
7	85.88	576098	RT	Fracture
8	60.23	1496514	RT	Fracture
9	88.37	548545	RT	Fracture
10	99.35	466503	RT	Fracture
11	124.70	251687	RT	Fracture
12	95.13	290161	RT	Fracture
13	56.93	1469382	RT	Fracture

Table 23. *S–N* test results of S500 cruciform joint specimens at −20 °C

Specimen-Nr.	$\Delta\sigma$ [MPa]	Number of Cycles	Temp. (RT, M20, M50)	Result
1	156.31	114953	M20	Fracture
2	70.63	1119176	M20	Fracture
3	115.26	311537	M20	Fracture
4	212.32	81776	M20	Fracture
5	132.55	276996	M20	Fracture
6	140.83	244758	M20	Fracture
7	77.16	1191167	M20	Fracture
8	164.04	107830	M20	Fracture
9	95.83	496190	M20	Fracture
10	64.92	1313662	M20	Fracture
11	94.95	390510	M20	Fracture
12	99.31	412030	M20	Fracture
13	221.50	46177	M20	Fracture
14	116.24	279244	M20	Fracture

Table 24. *S–N* test results of S500 cruciform joint specimens at −50 °C

Specimen-Nr.	$\Delta\sigma$ [MPa]	Number of Cycles	Temp. (RT, M20, M50)	Result
1	75.80	1280183	M50	Fracture
2	122.49	284986	M50	Fracture
3	122.65	292182	M50	Fracture
4	83.98	1195473	M50	Fracture
5	145.56	245270	M50	Fracture
6	133.81	317495	M50	Fracture
7	204.09	78425	M50	Fracture
8	167.66	128434	M50	Fracture
9	84.18	821066	M50	Fracture
10	90.90	609769	M50	Fracture
11	145.26	154210	M50	Fracture

C.5 | S235 Transversal stiffener

Table 25. *S–N* test results of S235 transversal stiffener specimens at room temperature

Specimen-Nr.	$\Delta\sigma$ [MPa]	Number of Cycles	Temp. (RT, M20, M50)	Result
1	158.73	1509639	RT	Fracture
2	130.28	1161853	RT	Fracture
3	180.00	884878	RT	Fracture
4	217.82	493274	RT	Fracture
5	120.24	2000000	RT	Run-out
6	260.52	124887	RT	Fracture
7	140.00	763297	RT	Fracture
8	216.44	135579	RT	Fracture
9	185.57	235077	RT	Fracture
10	130.00	804553	RT	Fracture
11	222.66	185544	RT	Fracture
12	156.84	516850	RT	Fracture

Table 26. *S–N* test results of S235 transversal stiffener specimens at −20 °C

Specimen-Nr.	$\Delta\sigma$ [MPa]	Number of Cycles	Temp. (RT, M20, M50)	Result
1	240.00	510210	M20	Fracture
2	260.00	137194	M20	Fracture
3	160.00	1194646	M20	Fracture
4	220.00	273922	M20	Fracture
5	240.00	163897	M20	Fracture
6	260.01	134340	M20	Fracture
7	220.00	312405	M20	Fracture
8	150.00	2000000	M20	Fracture
9	210.08	680665	M20	Fracture
10	200.00	629345	M20	Fracture
11	240.00	254828	M20	Fracture
12	200.00	229678	M20	Fracture
13	150.00	1073923	M20	Fracture

Table 27. *S–N* test results of S235 transversal stiffener specimens at −50 °C

Specimen-Nr.	$\Delta\sigma$ [MPa]	Number of Cycles	Temp. (RT, M20, M50)	Result
1	240.00	500321	M50	Fracture
2	220.01	280147	M50	Fracture
3	280.00	159305	M50	Fracture
4	260.00	169144	M50	Fracture
5	160.01	1160951	M50	Fracture
6	200.00	388773	M50	Fracture
7	174.67	1795696	M50	Fracture
8	240.00	576394	M50	Fracture
9	240.01	182489	M50	Fracture
10	198.00	361075	M50	Fracture
11	255.87	139122	M50	Fracture
12	280.01	95453	M50	Fracture

C.6 | S500 Transversal stiffener

Table 28. *S–N* test results of S500 transversal stiffener specimens at room temperature

Specimen-Nr.	$\Delta\sigma$ [MPa]	Number of Cycles	Temp. (RT, M20, M50)	Result
1	150.01	1115441	RT	Fracture
2	140.00	1552463	RT	Fracture
3	240.00	168696	RT	Fracture
4	150.01	959266	RT	Fracture
5	200.00	369667	RT	Fracture
6	140.00	2000000	RT	Run-out
7	280.00	127220	RT	Fracture
8	200.00	340001	RT	Fracture
9	150.00	1164655	RT	Fracture
10	320.00	62466	RT	Fracture
11	200.00	264277	RT	Fracture
12	158.10	666117	RT	Fracture

Table 29. *S–N* test results of S500 transversal stiffener specimens at −20 °C

Specimen-Nr.	$\Delta\sigma$ [MPa]	Number of Cycles	Temp. (RT, M20, M50)	Result
1	257.38	153744	M20	Fracture
2	197.98	359963	M20	Fracture
3	200.01	363454	M20	Fracture
4	179.89	501744	M20	Fracture
5	140.00	1671841	M20	Fracture
6	302.42	99708	M20	Fracture
7	220.00	318516	M20	Fracture
8	280.00	126662	M20	Fracture
9	149.99	838979	M20	Fracture
10	150.00	1015536	M20	Fracture
11	242.47	252670	M20	Fracture

Table 30. *S–N* test results of S500 transversal stiffener specimens at −50 °C

Specimen-Nr.	$\Delta\sigma$ [MPa]	Number of Cycles	Temp. (RT, M20, M50)	Result
1	178.63	1622199	M50	Fracture
2	320.00	92407	M50	Fracture
3	280.01	113804	M50	Fracture
4	296.97	134674	M50	Fracture
5	260.00	221062	M50	Fracture
6	240.00	290906	M50	Fracture
7	200.00	359960	M50	Fracture
8	238.82	168862	M50	Fracture
9	220.00	321248	M50	Fracture
10	180.00	450327	M50	Fracture
11	150.01	1189241	M50	Fracture